UNIVERSITAT POLITÈCNICA DE CATALUNYA
Biomedical Engineering Doctoral Programme

Optimal control prediction of assisted walking using torque-driven models

Application to active orthosis simulation to assist individuals with spinal cord injury

by Míriam Febrer Nafría

A thesis submitted for the degree of Doctor for the
Universitat Politècnica de Catalunya

Supervised by Dr. Josep Maria Font Llagunes[1]
and Dr. Benjamin Jon Fregly[2]

[1]Department of Mechanical Engineering
(Universitat Politècnica de Catalunya)
[2]Department of Mechanical Engineering & Bioengineering
(Rice University)

Barcelona, October 2020

A l'avi Ismael

Abstract

Walking impairment after spinal cord injury leads to a decreased quality of life, other serious health conditions and substantial health care costs. Consequently, gait restoration is a high priority among spinal cord-injured (SCI) subjects; and it can be partially achieved using active orthoses or exoskeletons, together with some type of external support for balance (e.g., crutches or a walker). Customisation of active orthoses control algorithms to maximise the walking ability of each patient is currently done through trial-and-error methods, making it difficult if not impossible to identify the best active control parameters for any particular patient. An objective simulation-based method that accounts for patient-specific needs would lead to a patient-tailored assistive device development process. Multibody system dynamics has been used for many years for the biomechanical analysis and simulation of human motion. Moreover, optimal control is being used to predict novel human motions, while methods to develop patient-specific neuromusculoskeletal models are currently being investigated. There are published studies that show the potential that subject-specific simulations have to improve rehabilitation treatments and assistive device adaptation to specific subjects. However, researchers have not yet fully demonstrated the effectiveness of these methods using a larger number of patients and a wider variety of treatments.

In this thesis, we have investigated the use of optimal control formulations to predict crutch-orthosis-assisted walking using torque-driven multibody dynamic models. The main objective has been to develop a simulation tool to predict crutch-orthosis-assisted walking that could serve in the future as a basis to support the design and control of an active knee-ankle-foot orthosis. The approach used involved development of a subject-specific torque-driven model based on a current available model in OpenSim, into which orthoses and crutches were incorporated. The foot-ground and crutch-ground interactions have been modelled with compliant contact models using visco-elastic force models. The different optimal control problems have been solved using a direct and simultaneous collocation method using the optimal control software GPOPS-II.

First, eight different optimal control formulations to track normal and crutch-assisted walking motions were developed and compared. Then, foot- and crutch-ground contact models were developed and calibrated to obtain dynamically consistent full walking cycles using an optimal tracking problem. Moreover, an optimal control framework for predictive simulations of normal and crutch-assisted walking patterns was implemented. Normal walking cycles were predicted using different

optimality criteria, and results were analysed and compared. Crutch-assisted walking cycles were also predicted using different optimality criteria, following different walking patterns (four-point, two-point and swing-through), and at different walking speeds. Finally, predictive simulations of crutch-orthosis-assisted walking of a healthy subject and an SCI subject using a real assistive robotic orthosis were performed, and results were evaluated against experimental data.

The original contributions from this thesis are the development and comparison of different optimal control formulations to track assisted walking motions, the analysis and comparison of different cost functions for the prediction of 3D normal walking motions, the implementation of an optimal control framework for generating predictive simulations of different 3D crutch-walking patterns, and the development and evaluation of predictive simulations of crutch-orthosis-assisted walking using a real assistive robotic orthosis. These results represent a step forward toward developing a predictive tool for the personalisation of active orthoses to specific SCI subjects, which could maximise the walking ability of each patient.

Resum

El deteriorament de la marxa després d'una lesió medul·lar disminueix la qualitat de vida del pacient, i porta com a conseqüència altres limitacions de salut i un alt cost sanitari. És per això que el restabliment de la marxa és una prioritat per a totes les persones amb lesió medul·lar. Aquest restabliment pot ser assolit parcialment utilitzant exoesquelets o ortesis actives, amb l'ajuda d'algun suport extern per mantenir l'equilibri, com crosses o un caminador. Actualment, la personalització del algorismes de control de les ortesis actives per tal de maximitzar el rendiment de la marxa de cada pacient es fa a través de mètodes de prova i error. Això fa que sigui difícil (si no pràcticament impossible) identificar els millors paràmetres de control per a cada pacient. Un mètode objectiu basat en la simulació i que tingui en compte les necessitats específiques de cada pacient podria portar-nos cap a un procés de desenvolupament de dispositius d'assistència personalitzats al pacient. La dinàmica de sistemes multisòlid s'utilitza des de fa temps per a l'anàlisi biomecànica i la simulació del moviment humà. A més, s'estan utilitzant mètodes de control òptim per predir el moviment humà, i s'estan investigant altres mètodes per desenvolupar models neuro-musculo-esquelètics adaptats al pacient. Hi ha estudis publicats que mostren el potencial que tenen les simulacions que utilitzen models personalitzats al pacient de millorar els tractaments de rehabilitació i l'adaptació dels dispositius d'assistència a pacients concrets. Tot i així, els investigadors no han demostrat encara l'efectivitat d'aquests mètodes usant un nombre gran de pacients i una varietat més gran de tractaments.

En aquesta tesi, hem investigat l'ús de formulacions de control òptim per a predir la marxa assistida amb crosses i ortesis actives mitjançant models dinàmics multisòlid a nivell esquelètic. L'objectiu principal ha estat desenvolupar una eina de simulació per tal de predir la marxa assistida amb crosses i ortesis actives que pugui servir en el futur per donar suport al disseny i el control d'una ortesi activa de genoll. La metodologia utilitzada inclou el desenvolupament d'un model adaptat al subjecte a nivell esquelètic basant en un model disponible en OpenSim, al qual se li han afegit les crosses i les ortesis. Les interaccions entre els peus i el terra i entre les crosses i el terra s'han modelat amb elements visco-elàstics. Els diferents problemes de control òptim s'han resolt utilitzant un mètode de col·locació directa amb el programari de control òptim GPOPS-II.

En primer lloc, s'han desenvolupat i comparat vuit formulacions de control òptim diferents, per tal de fer un seguiment de la marxa normal i assistida amb crosses. Després, s'han desenvolupat i calibrat els models de contacte peu-terra i

crossa-terra, i s'han utilitzat per obtenir cicles de la marxa sencers dinàmicament consistents, per mitjà d'un problema de control òptim de seguiment de dades experimentals. A més, s'ha implementat un entorn de simulació amb control òptim per a la predicció de la marxa normal i la marxa amb crosses. S'han predit cicles de marxa normals usant diferents criteris d'optimalitat, i els resultats s'han analitzat i comparat. També s'han predit cicles de marxa amb crosses usant diferents criteris d'optimalitat, seguint diferents patrons de marxa amb crosses (de quatre punts, de dos punts i d'oscil·lació), i a diferents velocitats de marxa. Finalment, s'han realitzat prediccions de la marxa assistida amb crosses i ortesis actives per a un subjecte sa i un subjecte amb lesió medul·lar, i els resultats s'han avaluat amb dades experimentals utilitzant unes ortesis actives reals.

Les contribucions originals d'aquesta tesi són el desenvolupament i la comparació de diferents formulacions de control òptim per al seguiment de moviments de marxa assistida, l'anàlisi i comparació de diferents funcions objectiu per a la predicció de la marxa normal en 3D, la implementació d'un entorn de simulació amb control òptim per a la predicció de diferents patrons de marxa assistida amb crosses en 3D, i el desenvolupament i l'avaluació de simulacions predictives de marxa assistida amb crosses i ortesis actives reals. Aquests resultats representen un pas endavant cap al desenvolupament d'una eina predictiva per a la personalització d'ortesis actives a pacients específics, que podria maximitzar el rendiment de la marxa de cada pacient.

Acknowledgements

This thesis has been possible thanks to many people. First of all, my supervisors. Thanks, Josep Maria, for your confidence in me from the beginning of this project, and for all your time spent in solving my questions and helping me to finish things until the end. Thanks, B.J., for combining so well being demanding with highlitghting always the well done work. Secondly, all my colleagues at the BIOMEC Lab that have contributed somehow to this thesis, especially Roger. Without you, this thesis would not have been possible (or at least, it would have lasted more time...). Also Alfons, Víctor and Fernando, for the crutches instrumentation; Jesús, Pau (Martínez) and Antonio, for helping during experimental captures; Daniel and Pau (Morey), for the orthoses CADs. Thanks to the students that have worked in a Bachelor's thesis related to my PhD: Natalia and David. And all the other people from the lab, with whom I have shared office, lunch times, coffee breaks, lab meeting, etc: Florian, Belén, Anna, Mireia, Douglas, Íñigo, Laura, Joan, Janet...

I want give thanks especially to you, Ivan, for being so involved and wanting to collaborate, although we had some problems with captures and we had to repeat them several times. I want to acknowledge also Dr Joan Vidal and the other professionals from Institut Guttmann, for the different meeting that we had. And all the people from who I have learnt and with who I spent great times during the conferences that I have attended in this period, especially our colleagues from the LIM Lab (Universidad de la Coruña), from the Universidad de Extremadura, and the PhD students from OpenSim.

During the PhD I had the opportunity of teaching Mechanics at ETSEIB; this has been quite challenging for me. I want to thank the other professors, Quim, Ana, Daniel, Rosa and Ernest, for your support and your patiente solving my questions, and the great shared moments. During this thesis I did two research stays. The first one, in Seville, with Dr Daniel García-Vallejo. Thanks for introducing me to the optimal control prediction, and for the warm reception. The second stay, at Houston (Texas), with my co-supervisor, Dr B.J. Fregly. Thanks to all the lab colleagues (especially Di, Marleny, Mohammad, Nick, Li, Florian) and all the friends that I did during the stay (Margarida, Lois, Jessica, Di, Fengdan, Meritxell, Anna, Erin).

Family and friends, you have been a special support during these years. Thanks, Raquel and Bianca, for our weekly lunches, talking about our theses' struggles. Thanks, dad, mom, Pau, Anna, Joan and Cris, for being glad for each small (or big) step. Thanks to all my friends and family, for being aware, for showing always

interest in what I told you, even if they were “complicated” things.

Agraïments

Hi ha moltes persones que han fet possible fer aquesta tesi. En primer lloc, els meus directors. Gràcies, Josep Maria, per haver confiat en mi des del principi, i per haver-me dedicat tant de temps, sempre atent a resoldre els meus dubtes i ajudant a treballar bé les coses fins al final. Gràcies, B.J., per saber sempre exigir però destacant alhora la feina ben feta. En segon lloc, tots els companys de BIOMEC que heu col·laborat d'alguna forma amb la tesi, especialment el Roger. Sense tu, aquesta tesi no hagués estat possible (o com a mínim, hauria durat més anys...). També l'Alfons, el Víctor i el Fernando, instrumentant les crosses; el Jesús, el Pau (Martínez) i l'Antonio, ajudant en les captures; el Daniel i el Pau (Morey), pels CADs de les ortesis. Als estudiants que heu treballat en un TFG relacionat amb la meva tesi, la Natalia i el David. I totes les altres persones del grup amb les que he compartit despatx, dinars, cafès, lab meetings, etc: Florian, Belén, Anna, Mireia, Douglas, Íñigo, Laura, Joan, Janet...

Un agraïment especial també a l'Ivan, que sempre has estat implicat i amb ganes de col·laborar, encara que haguem tingut algun problema amb les captures i les hem hagut de repetir vàries vegades. També vull donar les gràcies al Dr Joan Vidal i als altres professionals de l'Institut Guttmann, per les diferents reunions que hem tingut. I totes les persones de les que he après i amb les que ho he passat molt bé en els diferents congressos en els que he estat durant aquest temps, especialment els companys del LIM (Universidad de La Coruña), de la Universidad de Extremadura, i els doctorands d'OpenSim.

Durant la tesi he pogut donar classes de Mecànica a l'ETSEIB. Això ha estat tot un repte per mi. Agraeixo a tots els professors, Quim, Ana, Daniel, Rosa i Ernest, el vostre recolzament, el temps que m'heu dedicat, la paciència que heu tingut amb mi, i els bons moments que hem passat. Durant aquest temps també he fet dues estades de recerca. La primera, a Sevilla, amb el Dr Daniel García-Vallejo. Gràcies per haver-me introduït en la predicció amb control òptim, i per haver-me acollit tant bé. La segona estada, a Houston (Texas), amb el meu codirector, el Dr B.J. Fregly. Gràcies a tots els companys del lab (especialment la Di, la Marleny, el Mohammad, el Nick, el Li, el Florian) i les amigues que vaig fer durant l'estada (Margarida, Lois, Jessica, Di, Fengdan, Meritxell, Anna, Erin).

La família i les amigues heu sigut un recolzament molt important per mi durant aquests anys. Gràcies, Raquel i Bianca, pels nostres dinars setmanals, explicant-nos les batalletes de les nostres tesis. Gràcies, papa, mama, Pau, Anna, Joan i Cris, per alegrar-vos sempre amb cada petit (o gran) pas de la tesi. Gràcies a totes

les amigues i les persones de la família que heu estat pendents tot aquest temps, i que sempre heu mostrat tant interès en el que explicava, encara que fóssin coses “complicades”.

Contents

List of acronyms

AIS ASIA Impairment Scale

AM Angular momentum

AP Anterior-posterior

API Application Programming Interface

ASIA American Spinal Injury Association

ASIS Anterior superior iliac spines

BSP Body segment parameters

BW Body weight

BW*H Body weight times height

CAD Computer aided design

CMC Computed muscle control

CNS Central nervous system

COM Centre of mass

DC Dynamically consistent

DO Dynamic optimisation

DOF Degree of freedom

EMG Electromyography

ETSEIB Barcelona School of Industrial Engineering

FDA Forward dynamic analysis

GRF Ground reaction force

GRM Ground reaction moment

GUI Graphical user interface

HAT Head-arms-trunk

ID Inverse dynamics

IDA Inverse dynamic analysis

IK Inverse kinematics

IKA Inverse kinematic analysis

IMU Inertial measurement unit

IPOPT Interior point optimisation algorithm

KAFO Knee-ankle-foot orthosis

LCO Left crutch off

LHS Left heel strike

LTO Left toe off

ML Medio-lateral

MTP Metatarsophalangeal

MTU Muscle-tendon unit

NC Neural command

OC Optimal control

OCP Optimal control problem

PID Proportional–integral–derivative

RCO Right crutch off

RCS Right crutch strike

REA Residual Elimination Algorithm

RHS Right heel strike

RMS Root-mean-square

RMSE Root-mean-square error

ROM Range of motion

SCI Spinal cord-injured

SO Static optimisation

UPC Universitat Politècnica de Catalunya

List of relevant symbols

Optimal control problem variables

$\mathbf{x}(t)$ Vector of state variables

$\mathbf{u}(t)$ Vector of control variables

$\mathbf{s}$ Vector of static parameters

$\mathbf{m}$ Vector of marker coordinates

$\mathbf{q}$ Vector of joint coordinates

$\dot{\mathbf{q}}$ Vector of joint velocities

$\ddot{\mathbf{q}}$ Vector of joint accelerations

$\dddot{\mathbf{q}}$ Vector of joint jerks

$\boldsymbol{\tau}$ Vector of joint torques

$\dot{\boldsymbol{\tau}}$ Vector of joint torques change

$\mathbf{R}_{pelvis}$ Vector of residual forces and moments at the pelvis

$\mathbf{GRF}_{u}$ Vector of ground reaction forces and moments controls

$\mathbf{GRF}_{CM}$ Vector of ground reaction forces and moments from contact models

$\mathbf{L}$ Angular momentum of the model

T Model kinetic energy

Foot- and crutch-ground contact models

δ Penetration depth

$\dot{\delta}$ Penetration velocity

$\mathbf{K}$ Vector of spring stiffnesses

$\mathbf{y_0}$ Vector of spring resting lengths

$\mathbf{c}$ Vector of damping coefficients

$\boldsymbol{\mu}$ Vector of spring-damper units dynamic friction coefficients

v_s Spring-damper units sliding velocity norm

v_l Latching velocity

K_n Crutch tip generalised normal stiffness

χ Crutch tip hysteresis damping factor

μ_{crutch} Crutch tip coefficient of dynamic friction

R_s Crutch tip sphere radius

KAFO knee angle trajectory parameters

k_a Maximum knee flexion

k_s Peak displacement parameter

k_w Peak width parameter

t_c Cycle duration

Crutch-orthosis-assisted prediction static parameters

T_c Cycle time duration

p_{ms} Duration of multiple support phase

p_{swf} Duration of foot swing phase

p_{swc} Duration of crutch swing phase

L_s Stride length

List of Figures

List of Tables

Chapter 1

Introduction

1.1 Motivation

Each year, between 250,000 and 500,000 people worldwide suffer a spinal cord injury [1]. Walking impairment after spinal cord injury leads to a decreased quality of life, other serious health conditions (e.g., heart disease, high blood pressure), and substantial health care costs. Consequently, gait restoration is a high priority among spinal cord-injured (SCI) subjects [2]. Restoration can be partially achieved using active orthoses or exoskeletons, together with some type of external support for balance (e.g., crutches or a walker) [3]. Because SCI patients having the same clinical classification can exhibit high variability in their walking impairments, the control algorithms used in active orthoses need to be customised to maximise the walking ability of each patient. Such customisation is currently done through trial-and-error methods, making it difficult if not impossible to identify the best active control parameters for any particular patient.

Patients must be trained to learn how to use the exoskeleton together with crutches [4]. The training process is guided by a physiotherapist mainly using visual observation and easily measurable spatiotemporal parameters such as gait speed [5]. Although in some clinical practices a more detailed assessment of the patient's gait pattern is performed to improve training session outcomes [6], an objective simulation-based method that accounts for patient-specific needs could improve in the long term the adaptation of these patients to the assistive device.

This PhD thesis has been framed within the national project "Low-cost motor-FES hybrid orthosis for the gait of SCI subjects and simulation methods to support the design and adaptation" (DPI2015-65959-C3-2-R), in collaboration with researchers from University of La Coruña and University of Extremadura. One of the objectives of this national project was progressing in the use of simulation methods to support the design and adaptation of walking assistive devices, by addressing motion analysis and prediction based on subject-specific neuromusculoskeletal models. In this context, the main objective of the proposed thesis is to develop an algorithm to predict dynamically consistent (DC) assisted gait of an SCI subject using crutches and wearing active knee-ankle-foot orthoses (KAFOs)

designed by the research group [7]. This tool might serve as a support for the patient-tailored design of robotic exoskeletons and to virtually test different control strategies. It could also facilitate analysis of patient adaptation to the device and to describe the walking improvement that the patient can achieve with external assistance.

1.2 Human motion prediction

Multibody system dynamics has been used for many years for the biomechanical analysis of human motion. When studying human motion dynamics from a macroscopic point of view, the human body can be represented by rigid bodies linked by ideal joints. The dynamic analysis usually starts collecting experimental motion data to compute joint angle time histories. Knowing the evolution of these coordinates and the motion equations of the human body model allows for calculating the net joint torques that produce that movement. This first type of analysis, from motion to forces, is called inverse dynamic analysis. On the other hand, if we start from forces and torques and we want to obtain the motion that they produce, the motion ordinary differential equations have to be integrated with respect to time. This approach is known as forward dynamic analysis, and allows for investigating how motion is affected when force time histories or certain model parameters are varied.

What is more interesting is that these techniques can be used to predict novel human motions using patient-specific neuromusculoskeletal models, with many potential applications in clinical and rehabilitation practice. For this purpose, the most accepted approach consists of formulating an optimisation problem according to a certain physiological criterion, such as minimising joint torques, muscle activations, or energy consumption. Nowadays, direct collocation optimal control is the most widespread optimisation method for developing predictive simulations of human motions in rehabilitation research.

1.3 Spinal cord injury and robotic gait assistance

Spinal cord injury is produced by damage to the spinal cord that disrupts the signals from the brain to the muscles in parts of the body below the level of the lesion. The most common causes for this lesion are traffic accidents, followed by falls in elderly people [8]. Current rehabilitation includes using powered robotic exoskeletons. Lower limb exoskeletons may be devised as an ambulation device, as a rehabilitation tool, or may be aimed at allowing both objectives [5]. A systematic review of active KAFOs for gait rehabilitation can be found in [9].

1.3.1 Injury levels and classification

There are different levels of injury; depending on the location of the trauma, and whether the spinal cord is cut or pressed down. Those are classified by the American Spinal Injury Association (ASIA) and range from A (complete injury) to E (normal

motor and sensory function) [10]. A spinal cord injury is complete if the spinal cord cannot send signals below the level of the injury, and so, as a result, the patient is paralysed and has no sensory function below the injury. Conversely, it is incomplete if part of the signals can be transmitted, so the patient preserves some movement and sensory function below the injury level. The ASIA Impairment Scale (AIS) for classifying spinal cord injury determines the following levels [11]:

A. Complete injury: No motor or sensory function is preserved in the sacral segments S4 or S5.

B. Sensory incomplete: Sensory but not motor function is preserved below the level of injury, including the sacral segments.

C. Motor incomplete: Motor function is preserved below the level of injury, and more than half of muscles tested below the level of injury have a low muscle grade.

D. Motor incomplete: Motor function is preserved below the level of injury and at least half of the key muscles below the neurological level have a high muscle grade.

E. Normal: No motor or sensory deficits, but deficits existed in the past.

1.3.2 Active orthosis used in the thesis

The active orthosis simulated in this thesis is a lightweight and customised active KAFO to assist over-ground walking of SCI patients [7] (Figure 1.1, left). Specifically, target patients lack control of knee and ankle muscles, but they retain some hip muscle function, so they can initiate swing phase using these muscles. This helps to exploit the remaining physiological functions and capacities of the patient, which are not normally considered in the existing wearable exoskeletons intended for paraplegia. Moreover, since the device challenges the patients who have to initiate the step themselves, it might be helpful to encourage active participation of patients in their own care process (patient empowerment) [12].

The active KAFO provides knee flexion-extension assistance during swing phase and maintains the knee fully extended during stance phase. The ankle joint is fixed keeping the foot perpendicular to the shank. The length of the shank and the thigh links can be adjusted to fit the anthropometry of the user. The knee joint is actuated using a brushless direct current motor combined with a harmonic drive transmission. The inertial measurement units (IMUs) collected data (vertical acceleration and sagittal inclination) are used to identify the time instant when the knee flexion-extension cycle must be triggered at the initial swing. Then, a proportional–integral–derivative (PID) position control with feedforward in velocity and acceleration keeps the knee in full extension during stance (straight leg, knee locked) and performs a predefined knee flexion–extension trajectory during swing [7].

The parameters defining the knee angle trajectory are maximum knee flexion, peak displacement, peak width and cycle duration. The desired trajectory and

control of the actuated knee must be designed according to the patient's walking function after injury. One option would be to use a trial-and-error approach, which would be time consuming and fatiguing for the subject. The proposed approach is to develop a computational model of the subject to perform these trials virtually and to formulate an optimisation problem in which the orthosis control parameters are added to the design variables (Figure 1.1).

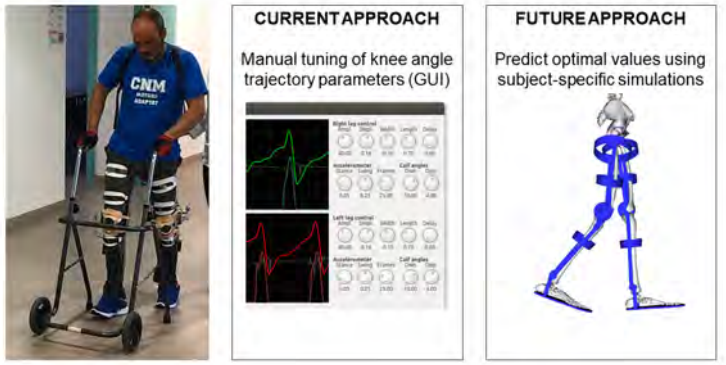

Figure 1.1: Left: The SCI subject with the active KAFO and walker. Centre: The current approach is based on trial-and-error, which is clearly fatiguing for the subject and time consuming. Right: The considered approach is to develop a computational model of the subject to perform these trials, and to state an optimisation problem in which the orthosis control parameters are added to the design variables.

The goal related to the developed active KAFO is to predict the optimal values of the knee motor control parameters for each specific SCI subject. This problem is complex, as it involves movement prediction using patient-specific 3D full-body models that include modelling of the assistive devices (crutches and orthoses) as well as foot- and crutch-ground contact. The problem also needs to define clearly what is meant for a gait cycle to be "optimal" for the patient, and what are the optimality criteria and penalty terms to be used in the optimal control problem formulation. To achieve this goal, this PhD thesis covers obtaining dynamically consistent motions tracking experimental data, developing and calibrating foot- and crutch-ground contact models, and predicting normal and assisted walking motions.

1.4 Objectives

The main objective of this thesis is to develop a simulation tool to predict crutch-orthosis-assisted walking, that could be used to support in the design and control of an active KAFO. The tool will be used to predict crutch-orthosis-assisted walking of a healthy subject and an SCI subject. To accomplish this main objective,

different specific objectives have been stated, where the complexity of simulations has been increased step by step, and within each step, methods have been applied using torque-driven models from different complexity.

The following specific objectives are proposed:

1. **To explore how optimal control problem formulation affects the ability to generate DC normal and assisted walking simulations that closely reproduce experimental data.**
   Eight different optimal control formulations, using models from different complexity (3D with head-arms-trunk (HAT) segment, 3D full-body, 3D full-body assisted by crutches) will be compared.

2. **To develop and calibrate foot- and crutch-ground contact models.**
   The foot-ground and crutch-ground contact models will be calibrated using optimal control problems that track experimental data. Different research questions associated with contact model calibration will be explored, using models from different complexity (3D with HAT segment, 3D full-body, 3D full-body assisted by crutches).

3. **To generate DC normal and crutch-assisted full gait cycles tracking experimental data (both joint coordinates and ground reactions) and having contact models to produce foot- and crutch-ground reactions.**
   Full DC gait cycles will be generated using models from different complexity (3D with HAT segment, 3D full-body, 3D full-body assisted by crutches), and will be used as initial guesses for the prediction problems. Since only two force plates are available in the motion analysis lab, it is not possible to measure foot-ground reactions (forces and moments) for a complete gait cycle. That is, the ground reaction components for one foot during the first double support have to be predicted. Therefore, this problem can be seen as a first prediction.

4. **To implement an optimal control simulation framework for predicting 3D normal walking using torque-driven models.**
   We will predict a complete gait cycle, using a 3D model with HAT segment and a 3D full-body model, without imposing symmetry and without tracking any experimental data. Different cost functions that have been used in the literature to predict normal walking will be studied and results compared against experimental data. Then, gait cycles at different speeds will be predicted.

5. **To implement an optimal control simulation framework for predicting 3D crutch-assisted walking using torque-driven models.**
   We will predict a complete gait cycle, using a 3D human body model with crutches, without imposing symmetry and without tracking any experimental data. We will study the convenience of predicting crutch-assisted walking

with different cost functions that have been used in the literature to predict normal walking. Then, crutch-assisted walking cycles following different patterns and at different speeds will be predicted.

6. **To implement an optimal control simulation framework for predicting 3D crutch-orthosis-assisted walking.**
   First, we will collect experimental walking data with locked knee and for different values of exoskeleton maximum assisted knee flexion for a healthy subject using crutches. These collected data will be employed to develop a subject-specific model of the subject, with calibrated foot- ground and crutch-ground contact models. The experimental motion with locked knee will be used to obtain a DC assisted walking cycle for the subject. Then, having the DC motion with locked knee as an initial guess, we will predict how the subject will walk with locked knee orthoses and crutches, and with active orthoses and crutches, for two different maximum knee flexion values. Finally, we will compare the simulated motion data with the experimental data of the healthy subject walking with active orthoses and crutches.

7. **To apply the crutch-orthosis-assisted walking predictive algorithm to an SCI subject.**
   First, we will collect experimental walking data with locked knee and for different values of exoskeleton maximum assisted knee flexion for an SCI subject (using a walker or crutches, depending on the case). These collected data will be employed to develop a subject-specific model of the subject, with calibrated foot-ground and crutch-ground contact models. The experimental motion with crutches and locked knee will be used to obtain a DC assisted walking cycle for the subject. Then, having the DC motion with locked knee as an initial guess, we will predict how the subject will walk with locked knee orthoses and crutches, and with active orthoses and crutches, for two different maximum knee flexion values. Finally, we will compare the simulated motion data with the experimental data of the SCI subject. More precisely, we will compare the change in spatiotemporal parameters for different levels of assistance.

1.5 Thesis contents and contributions

A chapter-by-chapter overview is given (Figure 1.2), highlighting the main contributions of each one if applicable. Moreover, in Appendix A, a list of conference abstracts and journal papers derived from this thesis is provided.

Chapter 2

In this chapter, the state of the art in human body and assistive device modelling, as well as in optimal control prediction of human motion is explained. At the end of the chapter, a critical review is done, specifying the methods that will be used for each aspect in this thesis.

Chapter 3

The general methods used in this thesis are stated, related to the development of the skeletal (or torque-driven) models and contact models, to the experimental data collection and processing, and to the implemented optimal control framework. These are the general methods that are common for all chapters; and in each section, specific methods are detailed.

Chapter 4

In this chapter, different optimal control tracking problems are developed to perform DC tracking, to calibrate foot-ground and crutch-ground contact models, and to obtain full DC cycles. The experimental data of a healthy female subject are used.

The main contribution from this chapter is the development and comparison of different optimal control formulations to track normal and assisted walking motions. These investigations have been performed for different levels of skeletal model complexity.

Chapter 5

In this chapter, optimal control problems are developed to predict human walking, using models from different complexity: normal walking with a 3D HAT model, normal walking with a 3D full-body model, and crutch-assisted walking with a 3D full-body model with crutches. The experimental data of a female healthy subject are used.

The main contributions from this chapter are the analysis and comparison of different cost functions for generating predictive simulations of 3D normal walking, and the implementation of an optimal control framework for generating predictive simulations of different 3D crutch-walking patterns.

Chapter 6

In this chapter, the methods developed in Chapters 4 and 5 are applied to predict the crutch-orthosis-assisted gait of a healthy subject and an SCI patient. In the developed formulations, the orthosis knee flexion-extension angle trajectory is imposed, and the assisted walking is predicted. The experimental data of a healthy female and an SCI male subject are used.

The main contribution from this chapter is the development and experimental evaluation of predictive simulations of crutch-orthosis-assisted walking using a real assistive robotic orthosis.

Chapter 7

In this chapter, the conclusions of the thesis are drawn, and recommendations and future research directions are outlined.

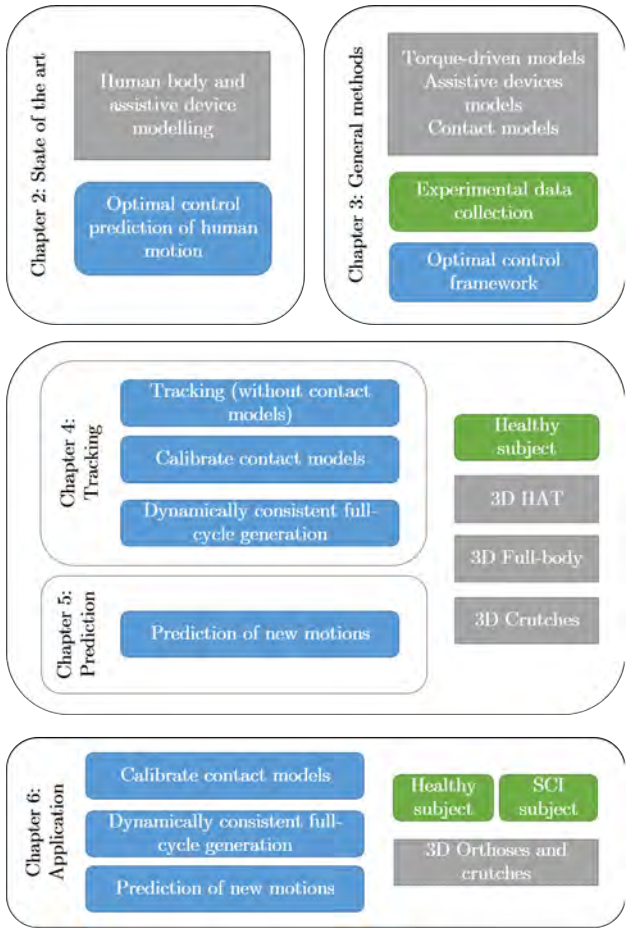

Figure 1.2: Thesis structure and chapter-by-chapter contents. Information about the different models used in this thesis are shown in grey boxes, information about the different types of optimal control problems are shown in blue boxes, and finally, information about the experimental data collected for each subject is shown in green boxes.

Chapter 2

State of the art

Neuromusculoskeletal modelling and optimal control are two fields that recently have been related for designing patient-specific treatments to improve walking function in subjects affected by neuromusculoskeletal impairments [13, 14]. In this chapter, an overview of the state of the art in human musculoskeletal modelling and assistive device modelling, as well as in optimal control prediction of human motion is given. Moreover, a brief discussion about the methods used in the literature and in this thesis is provided at the end of the chapter.

2.1 Human body and assistive device modelling

Simulation of human motion dynamics involves modelling the human neuromusculoskeletal system. Robotic devices are nowadays widely used for gait rehabilitation in subjects with neuromuscular impairments. If a subject-specific model is combined with a robotic device model, computational simulation can help to optimally design and control these assistive devices [14, 15].

2.1.1 Subject-specific musculoskeletal modelling

The human neuromusculoskeletal system can be viewed as a servo-controlled multibody dynamic system, where bones are modelled as rigid bodies connected by joints, actuated by muscles and controlled by the central nervous system (CNS) [13]. The human musculoskeletal system is a complex system, composed by about 200 bones and 300 muscles. Virtual models are always simplifications of the real system, and depending on the purpose of the study, simpler or more complex models can be used. The validity of motion prediction results highly relies on having a realistic biomechanical model, which includes body segments, joints, actuators (at joint or muscle level) and contact models to characterise body-ground interaction.

Skeletal modelling

The human skeleton is composed by several bones, with a wide range of size: from the femur (thigh) to the stapes (middle ear). There is a joint (or articulation) at any point where two bones meet, whether or not the bones are movable at that interface. There are different types of joints in the human body: cartilaginous joints permit limited movement (like intervertebral joints), whereas synovial joints allow full movement.

The skeleton is usually modelled as an open kinematic chain, with rigid bodies connected by joints. Each rigid body represents a bone (or group of bones) and the tissues that wrap it. A group of bones is usually represented using one rigid body if there is no relative motion between them or it is not relevant for the purpose of the study (e.g., motion of hand or fingers in walking). The set of parameters that describe each rigid body are basically inertial and geometric. Inertial parameters define, for each segment or body, mass, position of the centre of mass, and tensor of inertia about the centre of mass in a local coordinate system. Geometric parameters are essentially segments' length, but can include more information for visualisation purposes or for computing muscle paths. All these parameters are usually called body segment parameters (BSP).

Synovial and cartilaginous joints, that are the joints that permit relative motion between segments, can be modelled as mechanical ideal joints, with no friction and no compliance [16]. Shoulder and hip are usually defined as spherical (or ball-and-socket) joints, knee and elbow are typically modelled as revolute (or hinge) joints, and ankle and wrist, in some studies are modelled as pivot joints and in others as revolute joints.

Depending on the purpose of the study, models can be two- or three-dimensional, and can represent the whole body or only a part of it (Table 2.1). For example, for the analysis of normal gait, some studies employ 2D models of the lower limbs [17–23], because the motion is primarily contained in the sagittal plane. However, if we want to obtain more realistic results, a 3D lower-body model [24–29] or a 3D full-body model [30–37] is needed to account for off-plane components of the motion (which might be important in pathological gait patterns) or the effect of the upper-body (head, arms and trunk) on the walking dynamics in the second case. In some studies, a more detailed model of a part of the body is constructed, like for example the spine [38, 39], neck [40, 41], knee [42, 43], or hand [44].

Researchers may develop their own libraries for solving multibody system dynamics [32, 45]; or use available software for biomechanical motion analysis, like AnyBody [46, 47] or OpenSim [15, 20, 48–51]. Using an available software can help researchers to focus on the application, develop subject-specific musculoskeletal simulations and establish the desired mix between model complexity, accuracy, and performance [52].

Muscle modelling

Skeletal muscles are the ones that link to bones through tendons and cause motion. Commonly one joint is actuated by several muscles (so there is muscle redundancy for each degree of freedom, DOF). Moreover, muscles can be monoarticulated, if

Type of model	Reference	Joints	DOFs
2D HAT	Ren et al. 2007 [18]	6	7
	Ackermann and van den Bogert 2010 [19]	7	9
	Van den Bogert et al. 2011 [21]	7	9
	García-Vallejo et al. 2016 [22]	7	9
	Dorn et al. 2015 [20]	7	9
	Russell et al. 2018 [23]	9	12
3D lower	Wang et al. 2007 [24]	7	18
3D HAT	Anderson and Pandy 2001 [25]	10	23
	García-Vallejo and Schiehlen 2012 [26]	7	16
	Fluit et al. 2012 [28]	9	21
	Lin and Pandy 2017 [33]	13	21
	Koch et al. 2017 [27]	7	20
	Lin et al. 2018 [29]	13	25
3D full-body	Xiang et al. 2007 [30]	23	55
	Fregly et al. 2007 [51], Reinbolt et al. 2008 [34]	14	27
	Kim et al. 2008 [31]	16	31
	Felis and Mombaur 2013 [32]	12	31
	Felis and Mombaur 2016 [35]	14	34
	Meyer et al. 2016 [50]	16	31
	Sauder et al. 2019 [36]	20	37
	Falisse et al. 2019 [37]	14	29

Table 2.1: Type of model, number of joints and number of DOFs for some relevant references that simulate human movement. "HAT" indicates models where head, arms and trunk are considered as the same segment.

they actuate only on one joint; or biarticulated, if they actuate on two joints at a time. Several muscles may be involved in an action. The principal muscle involved is called the prime mover, or agonist; a muscle with the opposite action of the prime mover is called an antagonist. The antagonist muscle typically relaxes so as not to impede the agonist; other functions of antagonist muscles can be to slow down or stop a movement. An example of an agonist-antagonist pair are the biceps and triceps muscles: to generate elbow flexion torque, the biceps contracts and the triceps relaxes; to generate elbow extension torque, the biceps relaxes and the triceps contracts.

There are many different muscle-tendon models, the reader is referred to [53] for an extensive review. Hill-type models are widely used in muscle-driven simulations [54]. In these models, muscles and tendons are modelled as a linear actuator, which exhibits an active behavior and a passive viscoelastic one. The active behavior is produced by the muscle fibers (or contractile elements). The passive behavior is related to the tendons and the connective tissue wrapping the muscle fibers, which can be simply modelled through springs. The fiber geometry is simplified by assuming that all muscle fibers are straight, parallel, of equal length, and coplanar [54].

Regarding the muscle-tendon model parameters, researchers use muscle-tendon

parameters values from published studies [19,25,26]; use the ones included in available models implemented in musculoskeletal simulation softwares, like OpenSim or AnyBody [20, 49]; or calibrate them from experimental data via optimisation [55].

Muscles are controlled by neural excitations that produce muscle activations. Muscle activation and muscle-tendon contraction dynamics are described by differential equations [16], and by force-length-velocity curves [56], respectively. The most recent hypothesis is that the CNS activates a group of muscles together, instead of activating each muscle independently, what brings the concept of muscle synergy. Muscle synergies are represented by modules consisting of one neural command (NC), which represents the time activation of a set of muscles, and one synergy vector, which represents the weighting factor of each muscle to its NC. The number of NCs is lower than the number of muscles, so using muscle synergies reduces the number of independent time-varying activation variables [50, 57].

In some studies with skeletal-level actuation, muscles are considered in a simplified way. For example, in [32] the model contains spring-damper elements at joints to mimic the compliance and damping properties of muscles, ligaments and passive tissues at joints. Furthermore, in [58] each rotational DOF is actuated by a pair of agonist-antagonist "muscle torques", which represent the resultant torques being generated by muscle forces acting on the same DOF.

Subject-specific modelling

A musculoskeletal model of the human body can be developed using values taken from the literature for the different parameters that define the skeletal model (inertial and geometric parameters), the muscle-tendon models, and the foot-ground contact models. They are usually estimated based on experimental measures from cadaveric specimens [59]. Depending on the application, and especially for pathological cases, these parameters may be further specified towards individual characteristics, to develop patient-specific models [51, 58]. Having a subject-specific model of the patient under investigation is crucial for obtaining meaningful simulation results, and can also serve as the foundation for an objective treatment planning approach [13]. For that, it is important to accurately identify these parameter values.

Scaling

This is the first level of subject-specificity, and usually the only one done for most of the simulation studies. To adapt the values from a generic model to a specific subject model, normally regression equations are employed to adjust joint centres, segment masses and tensors of inertia. However, linear scaling has some problems, for example, how to personalise bone shape or muscle attachment, which can be relevant in some studies. To adjust these parameters to a specific subject, medical imaging can be used [14, 60].

Kinematic model

There are several characteristics that have to be adjusted specifically to the subject. Not only scaling inertial properties, but also calibrating joint axes of rotation [34, 61]. To adjust these parameters to a specific subject, kinematic measurements can be used [14, 60], together with optimisation methods [34, 50].

Muscle-tendon model

Muscle properties (e.g., insertion points, attachment locations, and muscle wrapping objects) [54] or muscle synergy parameters [55] can be adjusted for each patient. To adjust these parameters to a specific subject, electromyography (EMG) measurements and medical imaging can be used [14, 60]. In [62], muscle-tendon-related parameters are optimally identified from EMG experimental recordings.

Foot-ground contact model

The parameters of the foot-ground contact model can be calibrated (usually using an optimisation algorithm) to the values of a specific subject, using experimental kinematic and force plate data collected from that subject [63–65]. It is very interesting the work done by Remy in [66], where he identified the following three parameters as being subject-specific, after calibration using experimental data from five subjects (each performing 15 trials at different walking speeds): the overall vertical position of the visco-elastic units, the overall anterior-posterior position of the visco-elastic units, and the position of the metatarsal axis. He also obtained that damping parameters were ill suited for optimisation, and that it was easier to estimate parameters that affected the model properties in the saggital plane.

2.1.2 Assistive device modelling

The most common assistive devices are orthoses, exoskeletons, prostheses and crutches. Orthoses and exoskeletons are used to restore or augment musculoskeletal function in impaired or healthy individuals. Usually, people assisted by orthoses or exoskeletons need crutch assistance for balance. On the contrary, prostheses are used to replace anatomically or functionally missing biological limbs.

Exoskeletons and orthoses

Passive devices are usually modelled adding high-stiffness rotational springs in passive joints [67–69]. Active devices have been modelled as massless torque actuators in active joints [15, 22, 49, 70]; or embedded in the human limbs, by properly modifying mass and inertia of the corresponding body segments [22, 71]. Another option to model both passive and active devices is modelling them as independent bodies connected to the subject by using kinematic constraints, both assuming no subject-device relative motion [68, 72] or allowing relative motion [73, 74]; or by using force

constraints (prescribe force acting in parallel to residual muscle force) [75].

Prosthetic devices

Researchers have modelled prostheses following one of the approaches used for orthoses and exoskeletons: rotational springs for passive device, and torque actuator for active device [23]. A more detailed model, where the control of the prosthetic device is simulated, can be found in [75].

Crutches

Regarding crutch modelling, we can distinguish between analysis of exerimental data and simulation. In analysis studies, crutches are usually modelled as a separate link in the human-crutches model, and motion data and forces [76–78], or only forces [79] are measured experimentally. In simulation studies, 2D simple models are used when swing-through gait pattern is simulated. In [80], the arm and the crutch are modelled as the same body, and in [81] they have been modelled as separate bodies. We can also find studies where the resultant dynamic effect of arms and crutches is modelled as external forces and moments applied at the shoulders, using 2D models [82] and 3D models [67]. Moreover, three-dimensional models of a subject assisted by explicit upper limb crutches and performing a four-point gait pattern can be found in [83, 84] (Table 2.2).

Reference	Dim.	Segments	DOF	Motion	Simulation
Van der Speck et al. 2003 [82]	2D	2	2	Standing	Static and dynamic analyses
Liu et al. 2011 [80]		1	2	Swing-through	Optimal control prediction
Ackermann and Taissun 2012 [81]		3	3		
Fournier et al. 2018 [83]	3D	37	69	Four-point	Kinematic data driven
Mouzo et al. 2018 [84]		18	57		Forward dynamics

Table 2.2: Crutch-assisted models (and also exoskeleton-assisted in some cases) found in the literature. The number of segments and DOFs refer to the human body and crutches model (without considering the orthoses or exoskeleton, if considered in the study).

2.1.3 Contact modelling in human motion

In human motion analysis, different contact interactions can be considered. First of all, the contact interaction between the foot and the ground. When considering normal walking motion, ground reaction forces are, together with the gravitational forces, the only external forces applied to the body. Moreover, if the subject is assisted by crutches or by an exoskeleton (or orthosis), the contact forces acting at each of these devices may be considered, depending on the purpose of the simulation. In this subsection, we will focus on foot-ground, crutch-ground and exoskeleton-subject contact modelling.

Foot-ground contact modelling

There are basically two options for modelling such interaction: using kinematic constraints (hard contact) or a contact model (compliant or deformable contact). The first method defines the interaction between the foot and the ground using ideal kinematic constraints, which change at each phase of the gait cycle. In such case, the foot can be modelled as a single point [32], as a rigid body with two contact points [26], or as a curved plantar surface rolling on the ground without slipping [18]; and it is usually assumed that the collision is perfectly inelastic without sliding [17]. The second method establishes the physical relationship between the developed contact forces (normal and tangential) and the relative foot-ground displacements and velocities through a visco-elastic force model. Different approaches have been used in the literature: three spring-damper units per foot [28], series of spring-damper units distributed under the sole of each foot [19, 25, 85–87], grid of elastic contact elements [64], two or more spheres with a compliant Hunt-Crossley model [20, 63, 88], or a nonlinear volumetric contact model [84, 89].

Most of the published studies of gait prediction declare that their foot-ground contact model is very simplistic and has to be improved in further studies [26, 28, 32, 90]. Moreover, most studies use planar foot-ground contact models and rarely validate the results using real captures [63]. Therefore, finding a suitable foot-ground contact model for human motion simulation is currently an open research topic of great interest because in human motion analysis, the foot-ground contact model influences directly some results, like the ankle motion and torque, the ground-reaction forces and the muscle force estimates [91, 92]. A good summary of published studies that use a foot-ground contact model can be found in [64].

Normal force

Usually, the normal foot-ground contact force in human motion is modelled as a set of springs and damper units, or of deformable spheres. In the most general form, the contact force can be written in terms of its elastic (conservative) and viscous (dissipative) components as follows [93, 94]:

$$N = k\delta^n + \chi\delta^m\dot{\delta} \tag{2.1}$$

where n and m are the degrees of nonlinearity of the elastic and viscous components, respectively; k is the generalised contacting stiffness; χ is the hysteresis damping coefficient, which can be considered constant or function of the initial $\dot{\delta}$; δ is the relative penetration or deformation, and $\dot{\delta}$ is the relative normal contact velocity.

The most used models are the ones proposed by Kelvin and Voigt (where $n = 1$ and $m = 0$) and by Hunt and Crossley [95] (where $n = m$) [94]. In Table 2.3, a summary of some normal contact force models used in simulation and prediction of human motion is shown.

Reference	Type of study	Foot segm.	Elements			Model	Power	Parameter values	
			Type	n	Location				
Wojtyra 2003 [86]	Simulation	1	s+d	5	fixed	K-V	1	exp. test	equal
Peasgood et al. 2007 [87]	Simulation	1	s+d	2	fixed	own	2.2	tuned	equal
Ackermann and van den Bogert 2010 [19]	Prediction	1	s+d	10	eq. distrib.	H-C	3	tuned	equal
Moreira et al. 2012 [88]	Development	2	sph.	9	tuned	H-C	1.5	tuned	equal
Pàmies-Vilà et al. 2014 [63]	Development	2	sph.	4	calibrated	H-C	1.5	calibrated	different
Shourijeh and McPhee 2015 [65]*	Simulation	3	s+d	3	calibrated	H-C	0.89-0.95	calibrated	different
Dorn et al. 2015 [20]	Prediction	2	sph.	2	fixed	H-C	1.5	tuned	equal
Jackson et al. 2016 [64]	Development	2	s+d	38	eq. distrib.	H-C	1	calibrated	different
Meyer et al. 2016 [50]	Prediction	2	s+d	47	eq. distrib.	H-C	1	calibrated	different

Table 2.3: Normal contact force model used in the most relevant references found about foot-ground contact modelling for human motion simulation. In "Type of study" we indicate if a foot-ground contact model is developed using only a foot model without simulating the full body motion (Development), if it is used for forward dynamic simulation of the full body motion (Simulation), or it is used for predicting new full body motions (Prediction). In "Foot segm." we indicate how many segments includes the biomechanical foot model. In "Elements", we indicate the type of elements, spring and damper (s+d) or sphere (sph.); the number of elements (n); and if the location of those elements is fixed, equally distributed, manually tuned or calibrated using an optimisation procedure. In "Model", we indicate if equation of each element's normal contact force model follows a Kelving-Voigt (K-V) model or a Hunt and Crossley (H-C) model. In "Power", we indicate the values of the exponent of the indentation that appears in Eq. 3.1. In "Parameter values", we indicate if the parameter values in the normal force expression are found experimentally (exp. test), manually tuned or calibrated using an optimisation procedure; and also if the values of each parameter are equal or different for each contact element (spring, damper, or sphere). *In this reference, a comparison between three models is presented. Only information regarding the foot-ground contact model with spring-damper units is presented.

Tangential force

The tangential force is usually represented by an approximation of the Coulomb dry friction [94]:

$$T = \mu f(v, v_l)N \tag{2.2}$$

where μ is the asymptotic friction coefficient; $f()$ is usually the hyperbolic tangent or the arctangent function; v is the sliding velocity; and v_l is the latching velocity, used to avoid a numerical discontinuity at the transition through zero slip velocity. The tangential force is opposite to the sliding velocity direction.

In Table 2.4, a summary of some tangential contact force models used in simulation and prediction of human motion is shown.

Reference	Type of study	Terms of friction			Dynamic dry friction coefficient		
		static	dyn.	visc.	μ asymp.	expression	v_l (m/s)
Wojtyra 2003 [86]	Simulation		x		0.45	arctan	0.0005
Peasgood et al. 2007 [87]	Simulation	x	x		0.2	-	-
Ackermann and van den Bogert 2010 [19]	Prediction		x		1	tanh	0.05
Moreira et al. 2012 [88]	Development		x	x	0.5-1	-	-
Shourijeh and McPhee 2015 [65]	Simulation		x		0.33-0.45	arctan	0.035-0.062
Dorn et al. 2015 [20]	Prediction	x	x	x	0.8	-	0.1
Jackson et al. 2016 [64]	Development	x	x	x	0.088	tanh	0.01
Meyer et al. 2016 [50]	Prediction		x		1	tanh	0.05
Brown and McPhee 2018 [89]	Development		x		0.14	tanh	0.01
Mouzo et al. 2018 [84]	Simulation		x		(from Shourijeh and McPhee 2015 [65])		

Table 2.4: Tangential force model used in the most relevant references found about foot-ground contact modelling for human motion simulation. In "Type of study" we indicate if a foot-ground contact model is developed using only a foot model without simulating the full body motion (Development), if it is used for forward dynamic simulation of the full body motion (Simulation), or it is used for predicting new full body motions (Prediction). In "Terms of friction", we indicate if static, dynamic (dyn.) and viscous (visc.) friction terms are present in the tangential contact force model. In "Dynamic dry friction coefficient", we indicate the asymptotic friction coefficient μ value; the expression that is used in Eq. 3.2, which is usually the hyperbolic tangent (tanh) or the arctangent function (arctan); and the latching velocity v_l.

Crutch-ground contact modelling

Regarding the crutch-ground contact model, there are some studies where spring-loaded crutches are studied. In this case, the contact model is a linear spring, where the stiffness is optimised [80, 81]. For rigid crutches, some simulations are done using experimental values for crutch-ground contact forces [67,83]. In [96], an impulsive and a continuous contact model are compared in swing-through crutch gait. In [84], the crutch–ground contact is modelled as a sphere at the tip of the crutch, where the normal contact force is obtained from [97] and the tangential

force is modelled with the bristle-type approach proposed in [98]. The contact model parameters are identified by optimisation.

Exoskeleton-subject (or orthosis-subject) contact modelling

Modelling the coupling of human and wearable device dynamics is crucial to better understand the interaction between both. For that, the assistive devices should be modelled independently from the limbs that assist, and contact models between the devices and the subject should be used. There are some first works on modelling human-device contact by using springs and dampers [74, 84]. Some interesting aspects that can be investigated by modelling human-device contact are patient's comfort when wearing the assistive device [58], and also simulate the exoskeleton control based on that interaction measure.

2.2 Optimal control prediction of human motion

Advanced neuromusculoskeletal models and optimal control formulations [14] have led to a growing interest in motion prediction for clinical and sports applications. Predicting novel motions can help to anticipate the result of surgery, to design assistive devices, such as prostethics and orthoses [15, 58, 68, 99, 100], to develop rehabilitation therapies [51], and to learn how an exercise should be performed in an optimal way [90,101,102]. In Section 2.2.1, examples of works performing human motion simulation (both analysis and prediction) are presented. In Section 2.2.2, we focus on the problem formulation for human walking prediction; and finally, in Section 2.2.3 some applications in sports and rehabilitation are shown.

2.2.1 Simulation of human motion

Simulation of human motion can be carried out to better understand how one type of motion is performed [25, 90], to determine muscle forces associated to this motion [103], to study how the CNS controls the motion [104], to compare healthy motion versus pathological or impaired motion [16, 87], or to study rehabilitation outcomes [69]. Inverse dynamic simulation for a measured human motion can provide an interpretation of the forces that have produced that motion [90]; forward dynamic simulations can be used to analyse a measured motion (when using as inputs forces obtained from an inverse analysis, and tracking that measured motion) or to simulate new motions (when using as inputs, e.g., modified forces from an inverse analysis). Predictive simulations that generate new motions are usually performed by means of an optimisation problem, that is based on an inverse or forward dynamics scheme (Figure 2.1).

Inverse dynamic analysis (IDA)

IDA is the most widespread technique to analyse human motion and calculate what forces cause a certain motion. More precisely, it is used to calculate net torques that must be applied at the joints to produce a motion that is known beforehand. Input

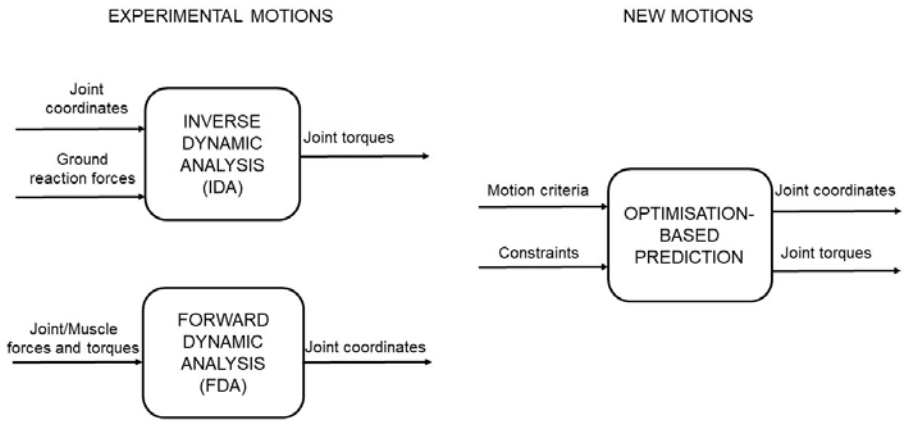

Figure 2.1: Schematic showing the main inputs and outputs considered in each method. Different approaches within each method can be considered (e.g., in IDA, having ground reaction forces as inputs or computing them from contact models; in FDA, having joint controllers to track experimental motion or not having them). Usually, IDA and FDA are used to analyse or simulate motions for which experimental data have been collected, whereas optimisation methods are used to predict new motions.

data are usually acquired kinematic data, foot-ground contact forces (or ground reaction forces, GRF) and estimated BSPs. This approach is mainly algebraic, because motion is known (i.e., coordinates, velocities and accelerations), so by replacing their values for a time range in the motion equations, joint forces and torques can be computed.

In medical applications, gait analysis is widely used. Ackermann and Schiehlen [16] studied different mechanical disturbances in gait. Based on the kinematical measurements, they used inverse dynamics (ID) and musculoskeletal models to estimate the metabolical cost, with the goal of designing orthotic and prosthetic devices. It is also interesting the work in [105], where the authors have developed a framework for solving real-time inverse kinematics (IK) and ID using personalised musculoskeletal models.

Muscle forces are difficult to be measured precisely and with non-invasive methods. For this reason, analysis and simulation of human motion are useful tools to determine muscle forces. However, once forces and torques are known for each joint, there are multiple solutions of muscle forces that yield the known joint torque. This is because the neuromusculoskeletal model is an over-actuated system, since each joint is actuated by several muscles. So, it can be exactly known the forces and torques at the joint level from the biomechanical model dynamics, but there are infinite solutions for the forces of each muscle. This is called the muscle force redundancy problem (or muscle force-sharing problem). This problem is usually solved using optimisation procedures based in physiological criteria [16, 25], where a cost function is minimised. Static Optimisation (SO) approaches solve the muscle force distribution problem for each time step, without considering the muscle activation

and contraction dynamics [25]. In this approach, the goal is to find muscle forces as optimisation variables such that an instantaneous cost function is minimised.

Usually, the biomechanical model of the human subject is actuated at each DOF, being the base-body the pelvis, which has three translations and three rotations with respect to the ground in space. When solving the equations of motion, the errors that come from model development and experimental motion capture are somehow included in the residual wrench (forces and moments acting on the pelvis segment associated with the pelvis-ground joint coordinates). Different methods have been used to minimise this residual wrench, most of them using some type of optimisation. In [106, 107] the Residual Elimination Algorithm (REA) is used to estimate dynamically consistent kinematics and kinetics for forward dynamic simulation of gait; in [108], the residual wrench is reduced using optimisation and ID; and in [109], using optimal control. A summary of some works in human walking simulation, taking into account if they ensure the dynamic consistency of the results can be found in [110].

Forward dynamic analysis (FDA)

FDA determines how a mechanical system will move when certain forces are applied. In the case of human motion, these forces might correspond to net joint torques or individual muscle forces depending on the aim of the study. Motion (evolution of joint coordinates) is then determined by integrating the differential equations of motion with respect to time. Examples of torque-driven simulations of human walking can be found in [85, 86]. FDA can be carried out with a fully actuated model, in which all the DOFs of the model are controlled, including the subject's joint DOFs and the six DOFs of the base body (usually the pelvis); or with an underactuated model, in which only the anatomical joint DOFs are controlled. In the latter case, it is necessary to account for the ground reactions, e.g., external reactions calculated from IDA or computed using foot-ground contact models. In [84], better results for full actuation have been obtained, compared to underactuation, although the underactuated case with input of the external reactions calculated from IDA yielded quite satisfactory results.

When descending to the muscular level, the forward dynamics (FD) based solution enables muscle activation and contraction dynamics to be considered, and so the obtained muscular responses are much more dynamically consistent than within the inverse-dynamics scheme. Dynamic optimisation (DO) approaches solve the muscle force distribution problem for all the simulation time range and take muscle-tendon dynamics into account. Examples of DO to solve the muscle force redundancy problem can be found in [111, 112]. Examples of simulation of human motion using musculoskeletal models can be found in [103], where jumping, pedalling and walking are analysed using this method; and in [113], where the motions of knee implants during a step-up activity are predicted from measured patterns of muscle activity, initial joint angles and velocities, and kinematics of the hip and ankle. The computed muscle control (CMC) is an algorithm that computes a set of muscle excitations (or, more generally, actuator controls) that will drive a dynamic musculoskeletal model to track a set of desired kinematics in the

presence of applied external forces [114]. In [115] a hybrid neuromusculoskeletal model that combines calibration, subject-specificity, EMG-driven and static optimisation methods together is presented. This might have important implications for studying pathological movement for which EMG recordings are limited. The same authors have presented a new approach, called neural data-driven simulation, that uses as input data electrical neuromuscular signals [75].

An interesting aspect of FDA is that it can be considered as an intermediate step towards motion prediction [116]. For example, muscle excitation patterns or other parameters of a model can be altered to determine how they affect movement. Moreover, it can also be predicted how a subject would walk when a surgical intervention or an assistive device modify some biomechanical characteristics; for instance, when a prosthesis is implanted or an orthosis is worn.

Optimal control (OC) prediction

The most accepted approach to predict how a human will move is to state an optimisation problem according to what is considered to be the optimality criterion behind such motion or task (e.g., minimising normalised torques, metabolic energy cost, joint accelerations, or muscle activations) [16,25]. The most predicted motion is normal gait in 2D [17–20] and in 3D [25, 26, 28, 30, 117]. Optimal control is nowadays widely used for applications in medical and rehabilitation technology [14]. Two main groups of methods for solving optimal control problems (OCPs) are indirect and direct methods. Indirect methods are focused on root-finding, while direct methods first convert the continuous problem into a non-linear programming problem and find the minimum of the objective function [118]. This process is called transcription, and there are mainly two classes of transcription algorithms: shooting methods and simultaneous methods [119].

Single-shooting methods work by approximating the trajectory using a single simulation. The optimisation algorithm will try to find the initial value of the states such that the defect constraint (the error committed) is driven to zero. The first prediction of muscle forces for a complete symmetric gait cycle, using a 3D model (with 23 DOF and 54 muscles), was solved using a shooting method by Anderson and Pandy [25]. Design variables were muscle excitations and initial values for muscle activations, and at each iteration, equations of motion were integrated using the predicted initial values for muscle activations. Multiple shooting breaks up the trajectory into segments and uses single shooting to solve for each segment. The end of one segment will not necessarily match with the start of the next, so there is a difference known as a defect, that it is added to the constraint vector. Felis and Mombaur [32] used the multiple shooting method to predict a 3D gait cycle, using a 31 DOF torque-driven model. State variables were joint torque controls, angles and velocities; and step length and velocity were input data.

Simultaneous methods directly represent the state trajectory using decision variables, and then satisfy the dynamics constraint only at special points in the trajectory. Direct collocation avoids integration of equations of motion. It consists on discretising the design variables (e.g., coordinates, joint torques, muscle forces) using spline functions [17], Fourier series [18] or other parameterisation methods

at specified knots (or time nodes), called collocation points [19, 24, 26, 30, 50, 69, 120]. One of the first studies using direct collocation to simulate human motion is the one of Kaplan and Heegaard [121]. They solved an OCP to find the neural excitation signals of steady-state pedalling using a 2D lower-limb musculoskeletal model. The cost function included a term minimising differences between predicted and experimental foot angles and a term minimising muscle excitations, which were the controls of the problem. A review of recent predictive simulation methods for human gait analysis can be found in [122].

2.2.2 Problem formulation for human walking prediction

In this section, we will focus on how is the optimisation problem stated (design variables, cost function, constraints) for predicting human gait, independently from the simulation method used.

Design variables

The methods for motion prediction are based in IDA and FDA. When the design variables of the optimisation problem are the coordinates (motion), at each iteration of the optimisation algorithm an inverse dynamics problem has to be solved; when the design variables are forces (joint torques or muscle forces), motion equations have to be integrated at each iteration; and finally, the design variables can be both motion and forces, and different methods are presented in the literature, referred as "predictive dynamics methods" [123] or "mixed approaches" [122].

In ID-based prediction, the motion is discretised and for each evaluation of the cost function, an ID problem has to be solved in order to obtain the joint torques. Bessonet et al. [17] predicted a complete gait cycle, with single and double support phases, for different known walking speeds. They approximated the generalised coordinates of motion using spline functions fitted at specified knots (or time nodes). The design variables were joint motion at knots and joint velocities at transition times. The dynamic model was constrained to force the motion to be cyclic and define a feasible step. By combining this approach with a method to solve the muscle force redundancy problem, muscle forces can be predicted as well. For example, Menegaldo et al. [112] proposed an hybrid methodology called Inverse Dynamics Optimal Control. It solved the ID of the multibody system and the force-sharing problem was formulated as an OCP. In this case, the cost function had two terms: a physiologically-based term for the ID-based prediction problem (e.g., minimise muscle activation or energy expenditure) and an error function between the torques calculated by inverse dynamics and the actual torque generated by the muscles.

In FD-based methods, the design variables can be joint torques, muscle forces, or muscle activations or excitations, and the equations of motion are integrated at each cost function evaluation to obtain the motion. Fluit et al. [28] described a method called forward-inverse dynamics. Their design variables were the joint torques, so their model was a torque-driven model. For each evaluation of the cost function, motion was computed integrating the motion equations. Then, when the optimal solution was found, muscle forces were computed using a musculoskeletal

analysis tool from AnyBody. A similar approach can be found in [62], where the muscle redundancy problem was solved forward in time parallel to a torque tracking between the muscle-tendon net torques and those from ID.

In predictive dynamics methods both joint angles and forces (joint torques or muscle forces) are design variables, which are discretised. Equations of motion are converted into a set of algebraic constraint equations [21,36,37,50], and the problem is transformed into a parameter optimisation algorithm, using direct collocation, or another transcription method. In an OCP, the design variables are defined either as states or controls. States are constrained to follow the differential equations prescribed by the dynamics of the problem, whereas controls are not. Using joint jerks as controls improves convergence, as reported in [50]. Ackermann and van den Bogert [19] stated an OCP to predict a complete gait cycle for a 2D model with eight muscles per leg. The design variables were generalised coordinates, generalised velocities, muscle lengths and muscle activations, and the problem was transformed into a parameter optimisation algorithm utilising direct collocation.

Cost function

It is believed that there is an optimal principle that guides human motion, although it is not clearly known which is the cost function that mathematically represents it. Some cost function terms used in human motion prediction imply minimising weighted normalised torques [27, 32, 123], minimising metabolic energy cost [25], minimising muscle activation [19], or minimising energy consumption [26,27]. Ackermann and van den Bogert [19] investigated the effects of different performance criteria (or cost functions) on predicted gait patterns. Cost functions were classified into "effort-like" and "fatigue-like", and one of the remarking conclusions was that fatigue-like cost functions produce realistic gait, with stance phase knee flexion, as opposed to energy-related cost functions which avoid knee flexion during the stance phase.

Optimal control simulations have been performed with tracking terms in the cost function [33,50], with pure prediction terms (without tracking any experimental data) [19, 20, 27, 32, 37, 117, 123], and having at the same time optimality and tracking terms [22, 26, 28, 50]. In Table 2.5 the most relevant cost functions that have been used for the prediction of normal gait are shown. Note that even if prediction is done at muscle level, there are terms that consider joint-level kinematic and dynamic magnitudes.

Constraints

When studying gait, usually some assumptions are made in order to simplify the solution. Some works assume that gait is symmetric (Table 2.5) and analyse only half of the gait cycle for both legs, or the complete cycle for only one leg. The gait cycle basically consists of two phases: stance phase and swing phase. Input gait descriptors (that usually are included in the problem formulation as constraints) can be average walking velocity [18, 30], cycle period [18], double stance duration [18], step length [30]. Giving a mean walking speed or step (or stride) length is

something widely used when predicting novel motions, because a final condition for the simulation is needed [18, 19, 26, 28, 32, 37].

2.2.3 Application of motion prediction in sports and medicine

Prediction has many applications in sport to find the most efficient way of performing a task such as running [101], rising up from squatting position [102], or kicking [90].

In rehabilitation, motion prediction can be used for gait retraining. Studies have predicted better walking patterns for a specific patient, as in [51] where gait modifications for knee osteoarthritis rehabilitation were designed. In [50] walking motions at different speeds for a post-stroke individual were predicted using a detailed subject-specific model. Moreover, in [28] a Trendelenburg gait (with weakened hip abductors) was predicted, and the model is able to predict a small increase in lateral trunk sway as a compensatory strategy.

Researchers have also predicted one-side gait disorders, as wearing an ankle-foot orthosis in one leg [69]. García-Vallejo and Schiehlen [26,124] extended the parameter optimisation approach used by Ackermann [19,125] to three-dimensional models. The 3D non-symmetrical model provides useful information of the dynamics of human gait with one-sided disorders. There are simulation-based design studies for wearable robotic systems, where the subject's assisted motion is predicted. For example, a standing long jump of a healthy subject assisted by an active orthosis was considered in [49], and the gait of an SCI subject assisted by an active orthosis in [22]. Finally, motion prediction has been used to find the optimal design parameter values for assistive devices, as in [58] where the optimal stiffness of an ankle-foot orthosis was identified.

In [23] walking with both passive and active unilateral transtibial prostheses was predicted using 2D models of 25 virtual subjects. In [37], walking with a transtibial passive prosthesis was predicted using a full 3D model. A review in emerging model-based methodologies for personalised neurorehabilitation technologies, that includes an example of designing a biomimetic variable stiffness transfemoral prosthesis, can be found in [75].

Studies predicting crutch walking motions have been done with simple models and not for patient-tailored rehabilitation purposes. There are studies based on optimal control that predict swing-through crutch walking using simple 2D models [80, 81]; or predict four point gait using 3D models [67], but modelling the crutches in an implicit way, i.e., applying the resultant dynamic effect of arms and crutches at the shoulders. Thus far, simulations having the 3D full body model and explicitly modelled crutches are driven by kinematic data [83] or track known motion data through a FD approach with torque controllers [84]. Other studies regarding crutch-assisted motions deal with studying balance when standing with crutches [82], or analysing the crutch impact in swing-through crutch gait using different contact formulations [96].

Other motions related with assistive devices have been predicted, such as wheelchair locomotion, in [126]. Motion prediction has also been used to find the optimal de-

sign parameter values for assistive devices, as in [127] where an assistive device to best support sit-to-stand transfer of geriatric patients was designed.

2.3 Discussion

The level of complexity of the musculoskeletal models used for prediction is very related with the objective of the study performed. An approach that has been widely used in the literature is to develop a subject-specific model based on a current available model in OpenSim [15, 48–51], or in AnyBody [46, 47]. In general, studies that predict walking motions with full-body models scale the model to the dimensions of the subject under study, but only few references have been found where also joint centre positions and axes have been specified for a singular subject [34, 50, 51] (Table 2.6). It has been observed that research has been first devoted to develop methods, and more recently, it has been possible to apply them for rehabilitation purposes, although a lot of work still needs to be done. While including muscle actuation in the model gives more realism to the results obtained [50], also including muscle-torque actuators in skeletal-level simulations has provided good results [32, 58, 68]. Regarding foot-ground contact models and their parameter values identification, in general many references conclude that further investigation is needed [26, 28, 32, 90]. Crutches are one of the simplest and more used assistive devices. There are some studies that analyse [76–79] or simulate [67, 80, 81, 83, 84] walking with crutches. However, none of these studies has explored predicting 3D crutch-assisted walking motions using a full body model yet (Table 2.2). Not many references that model explicitly the contact forces between orthosis and subject have been found [74, 84]. Most of the published studies do not take into account the actual physical interaction between the subject's body and the orthoses [15, 22, 49, 68, 70, 72, 73].

Compared to shooting methods, direct collocation methods have the advantage of avoiding explicit integration of the equations of motion, eliminating the need to add non-physiological stabilising controllers [84] when predicting walking motions. However, they have the challenge of being sensitive to how the OCP is formulated [120]. For human movement prediction, direct collocation problems have worked best when model dynamics is formulated implicitly rather than explicitly [21, 50]. General difficulties are to find a good initial guess [120, 122], and to be sure that the problem does not converge to a local minimum [18]. Some published studies that present prediction frameworks evaluate them simulating impaired gait (Table 2.6), such as gait with weakened muscles [28, 37] or assisted by transtibial prostheses [23, 37], and results are reasonable. Some studies go further and validate the prediction results by comparing them with experimental data from a specific patient [34, 50, 58]. All these studies show the potential that subject-specific simulations have to improve rehabilitation treatments, and assistive device development and adaptation to specific subjects [13, 14, 36, 37, 50, 52]. However, it is still needed to fully demonstrate the effectiveness of these methods using a larger number of patients and wider variety of treatments.

The approach that has been used in the present thesis is to develop a subject-

specific torque-driven model based on a current available model in OpenSim, to which orthoses and crutches are incorporated. The main reason for not incorporating muscles to the model is that it is not clear how the muscle-tendon parameter values could be identified for a specific SCI patient. This is why muscle modelling is left out of the scope of the present thesis. Therefore, muscle actuation is considered at torque level, and maximum joint torques are limited for the SCI patient taking into account his impairment level. Crutches and orthoses have been attached to the body segments without considering device-segment relative motion. The foot-ground and crutch-ground interactions have been modelled as compliant contact models, using visco-elastic force models. Orthoses-subject interaction has not been taken into account because the current prototype works with trajectory-tracking position control. It is assumed that the desired knee angle trajectory will be followed by the motor, regardless of the interaction forces.

The different OCPs have been solved using a direct and simultaneous collocation method, with the optimal control software GPOPS-II [128]. The equations of motion used for solving the ID problem in each iteration are obtained from OpenSim, through the OpenSim application programming interface (API), that defines the classes and functions in C++. The prediction framework has been developed first for simpler models than those for the final application. Moreover, different types of optimisations have been performed, first tracking optimisations to calibrate contact models and find an initial guess for prediction, and after that, predictive optimisations following an approach based on [50]. For mobility-impaired subjects, walking as close as possible to a normal gait pattern might be an additional criterion that has been taken into account [22, 122].

Reference	Type of gait	Model			Cost function terms	
		Dim.	DOFs	n musc.	Multibody model	Muscle model
Anderson and Pandy 2001 [25]	symmetric	3D	23	54	-	Muscle metabolic energy (sum of 5 terms)
Xiang et al. 2007 [30]	symmetric	3D	55	-	Squares of all joint torques	-
Ren et al. 2007 [18]	symmetric	2D	7	-	Mechanical energy expenditure	-
Kim et al. 2008 [31]	normal slope ascent	3D	31	-	Deviation of the trunk from an upright posture	-
Ackermann and van den Bogert 2010 [19]	symmetric	2D	9	16	-	Weighted muscle activations (8 different cost functions)
Van den Bogert et al. 2011 [21]	symmetric	2D	9	16	Joint coordinates tracking	Muscle activations
Fluit et al. 2012 [28]	symmetric	3D	21	-	Torque change and difference between predicted and desired kinematic outputs	-
García-Vallejo and Schiehlen 2012 [26]	non-symmetric	3D	16	28	Deviation with respect to normal walking patterns (generalised coordinates and ground reaction forces)	Total energy of transportation (energy expended per unit of length)
Felis and Mombaur 2013 [32]	symmetric	3D	31	-	Squared joint torques, head motion and impulse at touch down	-
Dorn et al. 2015 [20]	normal ground inclination backpack	2D	9	16	Head forward velocity, avoid falling, average velocity and total	Muscle metabolic energy
Felis and Mombaur 2016 [35]	symmetric	3D	34	-	Active actuation over step length, angular momentum, head angular velocities, and step time (5 different combinations)	-
Koch et al. 2017 [27]	symmetric	3D	20	-	Specific kinetic energy and jerk (combined cost function)	-
	inclined				Specific control effort, torque change, kinetic energy, and jerk (single term cost functions)	-
Lin et al. 2018 [29]	non-symmetric	3D	25	80	-	Cost of transport (metabolic rate per unit of length and mass)
Falisse at el. 2019 [37]	symmetric	3D	29	43	Joint accelerations, and passive joint torques (different combinations)	Metabolic energy rate, muscle activity, and arm excitations (different combinations)

Table 2.5: Summary of the most relevant cost functions that have been used for the prediction of normal or healthy gait, using optimisation methods (usually optimal control, but not in all cases). For each reference, information about the simulated type of gait and about the used model –dimensions (Dim.), number of degrees of freedom (DOFs), number of muscles (n musc.)– is given. Moreover, cost function terms are classified as related to the multibody model or the muscle model.

Reference	Type of model			Simulated subject			Subject-specificity			
	Dim.	Torq.-driven	Musc.-driven	Healthy	Impaired	Assisted	Scaling	Joint calib.	Musc. calib.	CM calib.
Anderson and Pandy 2001 [25]	3D HAT		x	x			x			
Xiang et al. 2007 [30]	3D full-body	x		x						
Ren et al. 2007 [18]	2D HAT	x		x						
Fregly et al. 2007 [51], Reinbolt et al. 2008 [34]	3D full-body	x			x (knee OA)		x	x		
Kim et al. 2008 [31]	3D full-body	x		x						
Ackermann and van den Bogert 2010 [19]	2D HAT		x	x						
Van den Bogert et al. 2011 [21]	2D HAT		x	x						
			x		x (trans. amp.)	x (prosth.)				
Fluit et al. 2012 [28]	3D HAT	x		x						
		x			x (Trend.)					
García-Vallejo and Schiehlen 2012 [26]	3D HAT		x	x						
			x		x (weight)					
Felis and Mombaur 2013 [32]	3D full-body	x		x						
Dorn et al. 2015 [20]	2D HAT		x	x						
García-Vallejo et al. 2016 [22]	2D HAT		x	-	x (SCI)	x (KAFO)				
Felis and Mombaur 2016 [35]	3D full-body	x		x						
Meyer et al. 2016 [50]	3D full-body	x			x (stroke)		x	x	x	x
			x		x (stroke)		x	x	x	x
Koch et al. 2017 [27]	3D HAT	x		x						
Russell et al. 2018 [23]	2D HAT		x	x						
			x		x (trans. amp.)	x (prosth.)				
Lin et al. 2018 [29]	3D HAT		x	x			x			
Falisse at el. 2019 [37]	3D full-body		x	x			x			x
			x		x (weak musc.)		x			
			x			x (prosth.)	x			
Sauder et al. 2019 [35]	3D full-body		x		x (stroke)		x	x	x	x

Table 2.6: Summary of optimisation-based predictions of normal, impaired and assisted human walking. In muscle-driven models, we include also models that are synergy-driven. When the studied subject has an impairment or wears an assistive device, the specific impairment or device is indicated. “Knee OA” stands for knee osteoarthritis, “trans. amp.” stands for transtibial amputee, “prosth.” stands for prosthesis, “Trend.” stands for Trendelenburg gait, “weight” indicates that a weight has been added to the right foot acting as a one-side disorder, “weak musc.” indicates that some muscles have been weakened in the model to emulate a gait impairment. “Scaling” indicates that the model has been scaled to a specific subject, “Joint calib.” indicates that some joint centres and axes have been calibrated using experimental data, “Musc. calib.” indicates that some muscle parameters have been calibrated using experimental data, and “CM calib.” indicates that foot-ground contact models have been calibrated using experimental data. Studies where impaired or assisted human walking has been predicted using a generic model or a model only scaled to a specific subject have been highlighted in blue. Studies where impaired or assisted human walking has been predicted using a model adapted to a specific subject, thus giving information that could be helpful for those subjects, have been highlighted in green.

Chapter 3

General methods

In this chapter, the general methods that are common in Chapters 4 to 6 are introduced. Additionally, each section from these chapters presents its own methodology according to the different studies performed. In Section 3.1, the different torque-driven models used in this work are presented. They are adapted to the subject regarding segments' dimensions and inertial parameters, and maximum joint torques. Moreover, it is explained how the assistive devices (crutches and orthoses), and the foot-ground and crutch-ground contacts are modelled. Then, the experimental data collection and processing are explained in Section 3.2. Experimental data have been collected for a healthy female and for a spinal cord-injured (SCI) male subjects. Finally, the optimal control framework, as well as the different optimal control problems that have been formulated in this work, are presented in Section 3.3.

3.1 Human body and assistive device modelling

The approach that has been used in the present thesis is to develop a subject-specific model based on a current available model in OpenSim, as in [15, 48–51]. The developed model includes the modelling of assistive devices, such as forearm crutches and the orthosis designed by the group. Contact models are needed to formulate the interaction between foot and ground, and between crutch and ground.

3.1.1 Skeletal models

The human body has been modelled as a multibody system formed by rigid bodies linked by ideal joints and controlled by torque actuators. These actuators account for the net effect of all muscle, contact, and ligament forces applied across the joints. The biomechanical models in this thesis have been developed using the simulation software OpenSim [129], which is a free software developed with the purpose of facilitating the research in biomedical applications.

All simulations have been done starting from simpler models and adding complexity step by step until reaching the model for the final application. The four

developed models are three-dimensional (Figure 3.1), and have been classified as unassisted models (3D with head-arms-trunk (HAT) segment and 3D full-body models) and models with assistive devices (assisted by crutches and by orthoses and crutches). In all cases, for the sake of simplicity, the head has been considered attached to the torso, the shoulder complex joint has been modelled by the acromial joint as a spherical joint, and the hand segment includes all the fingers attached to that segment.

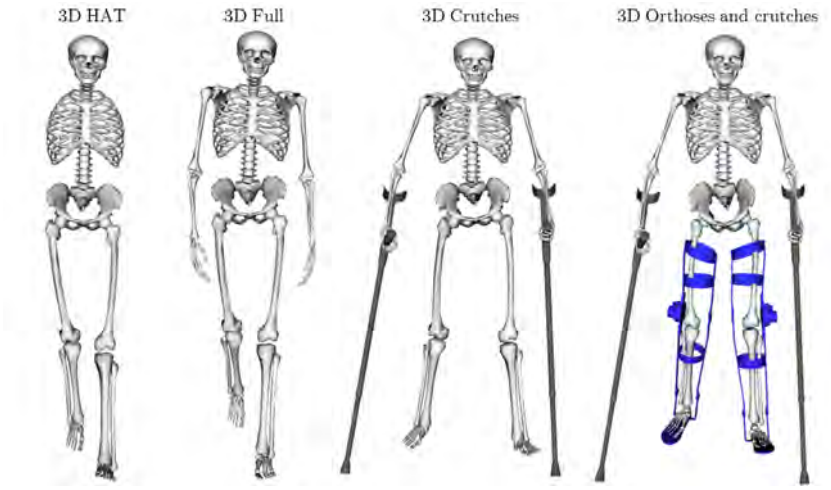

Figure 3.1: Human body models with and without assistive devices that have been adapted to a healthy subject to predict normal and assisted walking. Models are shown from less to more complexity: *3D HAT*, with head and arms attached to torso; *3D Full*, full-body model including arms; *3D Crutches*, 3D full-body model with crutches; and *3D Orthoses and cruthes*, 3D full-body model with crutches and orthoses.

3D HAT model

The first unassisted model is a 3D model with arms attached to torso. It possesses 12 bodies: pelvis, torso, humerus (right and left - r,l), tibia (r,l), talus (r,l), calcaneous (or hindfoot) (r,l), toes (or forefoot) (r,l); 12 joints: ground-pelvis, lumbar, hip (r,l), knee (r,l), ankle (r,l), subtalar (r,l), metatarsophalangeal (MTP) (r,l); and 23 degrees of freedom (DOFs): pelvis tilt, pelvis list, pelvis rotation, pelvis anterior-posterior translation, pelvis vertical translation, pelvis medio-lateral translation, lumbar extension, lumbar bending, lumbar rotation, hip flexion (r,l), hip adduction (r,l), hip rotation (r,l), knee flexion (r,l), ankle dorsiflexion (r,l), ankle rotation (r,l), MTP flexion (r,l). For hip coordinates, "adduction" instead of "abduction" is used, as the OpenSim model used to develop all the models has defined as positive the adduction angles. Moreover, coordinates for the back joint are named "lumbar", as it is the name used in the OpenSim model. Note that, for generating the *3D HAT* model, first the *3D Full* model has been developed and adapted to the subject. This model has been only developed for the healthy

subject. In the following chapters, we will refer to this model as *3D HAT* model.

3D full-body model

The second unassisted model is a 3D model with arms. It possesses 20 bodies, 20 joints and 31 DOFs. With respect to the *3D HAT* model, the additional bodies are humerus (r,l), ulna (r,l), radius (r,l) and hand (r,l); the additional joints are acromial (r,l), elbow (r,l), radioulnar (r,l) and radius-hand (r,l); and the additional DOFs are shoulder flexion (r,l), shoulder adduction (r,l), shoulder rotation (r,l), elbow flexion (r,l), pronation-supination (r,l), wrist flexion (r,l) and wrist deviation (r,l). For shoulder coordinates, "adduction" instead of "abduction" is used, as the OpenSim model used to develop all the models has defined as positive the adduction angles. A topology view of this model is shown in Figure 3.2. This model has been developed for the healthy subject, and in the following chapters, we will refer to this model as *3D Full* model. For the SCI subject, we have started from the 3D full-body model to scale it to the subject, but it has not been used for simulations, as all simulations for the healthy subject have been done for assisted motions.

3D full-body model with crutches

The first assisted model is a 3D full-body model with crutches. Crutches have been added as two new bodies, with their inertial properties. Two ways of modelling the crutches have been used in this work: attached to the forearm and attached to the hand. The first model possesses 31 DOFs (see Table 3.1), and has been used only for tracking without contact models (Section 4.1). The latter model possesses 37 DOFs (exactly the same as the *3D Full* model, as the crutches do not add any DOF), and has been used in simulations with contact models (Sections 4.2, 4.3, and 5.2). In the following chapters, we will refer to both variations of this model as *3D Crutches* model, and in each section, it is indicated which type of model is used.

3D full-body model with orthoses and crutches

The second assisted model is a 3D full-body model with orthoses and crutches. The crutches have been attached to the hand (as explained in the previous point). The orthoses have been modelled as independent bodies consisting of two segments (corresponding to thigh, and shank-foot) with dimensions and inertial properties taken from computer aided design (CAD) models of the real prototype. Each orthosis segment has been attached to the corresponding lower limb segment using a weld joint (i.e., no relative motion was permitted between bodies). The ankle, subtalar and MTP joints have been locked at 0°, due to the presence of the orthosis mechanical constraints. No joints have been defined between the orthosis links, i.e., knee orthosis joint has been considered to be perfectly aligned to the subject's knee joint. This model has been used in Chapter 6, for healthy and SCI subjects simulations, and we will refer to it as *3D Orthoses* model.

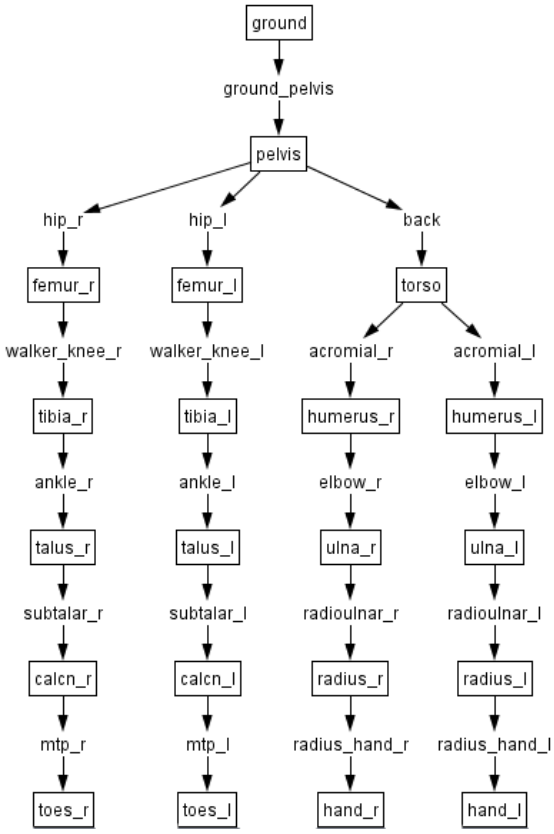

Figure 3.2: Bodies (inside boxes) and joints (out of the boxes) of the 3D full-body model. Note that the ground appears as an additional body (external to the human body model), because a joint defining the absolute movement of the base body (pelvis) needs to be added for simulation purposes. Joint coordinates of each joint are shown in Table 3.1. The figure has been extracted from the available *Topology view* in the OpenSim GUI.

Actuators

In the model, each joint coordinate is actuated by an ideal joint force or torque actuator. The inverse dynamics (ID) output gives the six residual actuator components (forces and moments acting on the pelvis), and each human joint torque, which represents the resultant actuation by muscle forces and other passive joint loads, such as friction. In all models, a three-segment foot is considered, with 3 DOFs with respect to the shank (ankle flexion/dorsiflexion, ankle rotation and MTP flexion). The only exception is the orthosis-assisted model, where feet are attached to each shank due to the orthosis constraint. Foot-ground contact is modelled through a series of spring and damper units, that are located in two foot segments (hindfoot and forefoot). The total foot-ground reactions are applied as external forces and moments to the hindfoot segment (Figure 3.3).

Joints	Coordinates	3D HAT	3D Full	3D Crutches (arm)	3D Crutches (hand)	3D Orth. and Crutch.
Ground-Pelvis	Pelvis tilt	x	x	x	x	x
	Pelvis list	x	x	x	x	x
	Pelvis rotation	x	x	x	x	x
	Pelvis AP trans.	x	x	x	x	x
	Pelvis vert. trans.	x	x	x	x	x
	Pelvis ML trans.	x	x	x	x	x
Hip (x2)	Hip flexion	x	x	x	x	x
	Hip adduction	x	x	x	x	x
	Hip rotation	x	x	x	x	x
Knee (x2)	Knee flexion	x	x	x	x	x
Ankle (x2)	Ankle dorsiflexion	x	x	x	x	-
Subtalar (x2)	Ankle rotation	x	x	x	x	-
MTP (x2)	MTP flexion	x	x	x	x	-
Back	Lumbar extension	x	x	x	x	x
	Lumbar bending	x	x	x	x	x
	Lumbar rotation	x	x	x	x	x
Shoulder (x2)	Shoulder flexion	-	x	x	x	x
	Shoulder adduction	-	x	x	x	x
	Shoulder rotation	-	x	x	x	x
Elbow (x2)	Elbow flexion	-	x	x	x	x
Radioulnar (x2)	Pro/Supination	-	x	-	x	x
Wrist (x2)	Wrist flexion	-	x	-	x	x
	Wrist deviation	-	x	-	x	x
	TOTAL DOFs	23	37	31	37	31

Table 3.1: Joints, coordinates and number of DOF of each model (*3D HAT*, *3D Full*, *3D Crutches*, and *3D Orthoses and crutches*). Two variations inside the *3D Crutches* model have been considered: attached to the forearm (arm), and attached to the hand (hand). With 'x' we indicate that the joint coordinate is included in the model, and with '-' we indicate that the joint coordinate is not included in the model. "AP trans.", "vert. trans." and "ML trans." stand for anterior-posterior, vertical and mediolateral translation, respectively.

3.1.2 Contact models

In Section 2.1.3, different approaches that have been used in the literature to model foot-ground and crutch-ground interactions have been presented. A common approach is to use compliant contact models, that establish the physical relationship between the developed contact forces (normal and tangential) and the relative foot-ground displacements and velocities through a visco-elastic force model. In this work, a set of spring and damper units have been used to model foot-ground interactions, and one sphere-plane contact model has been used to model crutch-ground interactions.

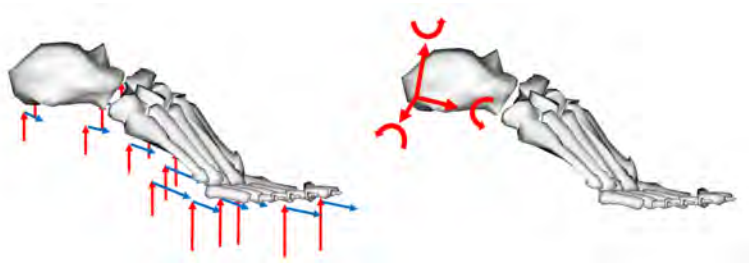

Figure 3.3: Left: For each contact point, normal and tangential components of ground reaction force are computed using a contact model. These forces are computed considering the mobility of the ankle joint, the subtalar joint and the MTP joint. Right: The total ground reaction force and moment are computed with respect to a point of the hindfoot segment, and are applied as external loads acting on this body.

Foot-ground contact model

The considered 3D foot-ground contact model consists of 16 spring and damper units, clustered in six groups per each foot (Figure 3.4). This number of springs has been defined after performing some tests, trying to find an equilibrium between tracking correctly experimental forces and moments, and finding a solution in a reasonable computation time.

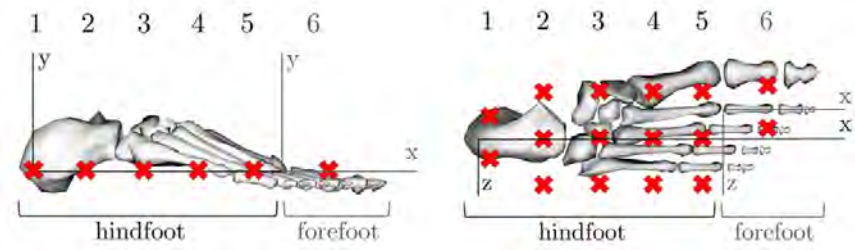

Figure 3.4: Lateral and upper view of hindfoot and forefoot segments, where each spring and damper unit is represented by a red cross. A total of 16 units are distributed in 6 groups (5 on the hindfoot and 1 on the forefoot), based on the anterior-posterior location (x). The local axes of the hindfoot are represented in black and the local axes of the forefoot are represented in grey.

The normal force in each unit (N_i) is generated using a linear spring with nonlinear damping, based on [64]:

$$N_i = K_i(\delta_i - y_{0_i})(1 + c_i\dot{\delta}_i) \tag{3.1}$$

where δ_i is the penetration depth and $\dot{\delta}_i$ is the penetration velocity of the i^{th} spring-damper unit, respectively; K_i is the spring stiffness and y_{0_i} is the spring resting length of the i^{th} spring, respectively; and c_i is the nonlinear damping coefficient of the i^{th} damper unit.

The tangential force (T_i) in each element is calculated using a simple continuous and differentiable friction model:

$$T_i = \mu_i \tanh \frac{v_s}{v_l} N_i \tag{3.2}$$

where μ_i is the coefficient of dynamic friction of the i^{th} spring-damper unit; v_s is the sliding velocity norm; and v_l is the latching velocity, used to avoid a numerical discontinuity at the transition through zero slip velocity, which has been considered to be 0.05 m/s, as in [19]. The tangential force direction is opposite to the sliding velocity direction and it is decomposed in anterior-posterior ($T_{x,i}$) and medio-lateral ($T_{z,i}$) directions.

The total force and moment are computed with respect to a certain point in the hindfoot body reference (the origin or the midpoint). For each spring, we have the three components of ground reaction force, $\mathbf{F}_i$:

$$\mathbf{F}_i = \begin{bmatrix} T_{x,i} \\ N_i \\ T_{z,i} \end{bmatrix} \tag{3.3}$$

Then, the contribution of each spring to the total moment, $\mathbf{M}_i$, is:

$$\mathbf{M}_i = \mathbf{d}_i \times \mathbf{F}_i \tag{3.4}$$

where $\mathbf{d}_i$ is the distance vector between the point where moments are computed and each spring-damper unit.

And the vector of ground reaction forces and moments, **GRF**, is computed for the right and the left foot, respectively, as the addition of the contribution of each individual spring:

$$\mathbf{GRF} = \begin{bmatrix} \sum_{i=1}^{n_e} \mathbf{F}_i \\ \sum_{i=1}^{n_e} \mathbf{M}_i \end{bmatrix} \tag{3.5}$$

where n_e is the number of spring and damper units on each foot.

Crutch-ground contact model

The crutch-ground contact model consists of a single-point contact of a sphere at the tip of the crutch that contacts the ground plane. The normal force (N_n) is obtained using a Hunt and Crossley model [95]:

$$N_n = K_n \left|\delta_n\right|^{\frac{3}{2}} + \chi \left|\delta_n\right|^{\frac{3}{2}} \dot{\delta} \tag{3.6}$$

where δ_n is the penetration depth and $\dot{\delta}$ is the penetration velocity of the centre of the sphere at the tip of the crutch, respectively; K_n is the generalised normal stiffness; and χ is the hysteresis damping factor.

The tangential force is also calculated using a simple continuous and differentiable friction model (Eq. 3.2).

3.1.3 Subject-specific models development

All models have been created starting from a published full-body OpenSim model [59]. The original model included 37 DOFs (6 DOF ground-to-pelvis joint, 3 DOF hip joints, 1 DOF knee joints, 1 DOF ankle joints, 1 DOF subtalar joints, 1 DOF toe joints, 3 DOF lumbar joint, 3 DOF shoulder joints, 1 DOF elbow joints and 2 DOF wrist joints) and 40 Hill-type muscle-tendon actuators per leg. All coordinates that were originally locked have been unlocked (subtalar angle, MTP angle, wrist flexion and wrist deviation), and muscles have been removed from the model. The original model also included a coordinate to define the patella rotation and translation, as a function of knee flexion. The patella body, as well as this coordinate, have been eliminated. It has not been necessary for the simulations performed in this thesis, as its main application is to define muscle paths of knee extensors more accurately, without modifying the full-body dynamics.

The generic models have been adapted to two differents subjects. For the healthy subject, all four models (*3D HAT*, *3D Full*, *3D Crutches* and *3D Orthoses*) have been developed and used in simulations. For the SCI subject, the *3D Full* model has been developed as an intermediate step, to develop the *3D Orthoses* model. A summary of the steps can be found in Figure 3.5.

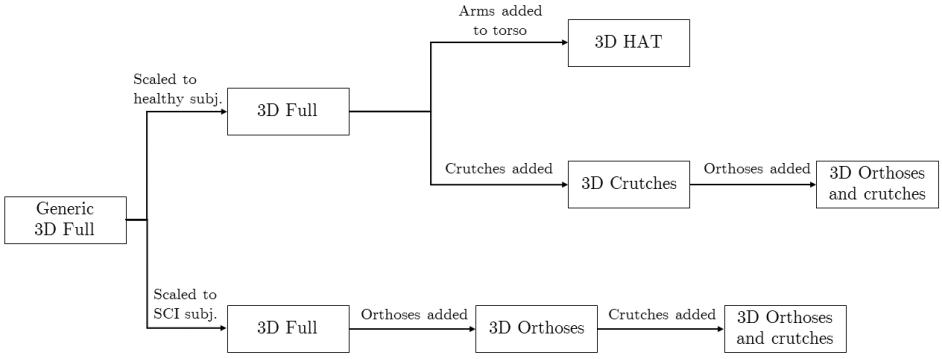

Figure 3.5: Summary of steps in the process of models construction, for the healthy and the SCI subjects, starting from a generic initial model based on a published full-body OpenSim model [59]. For the healthy subject, the four models have been shown in Figure 3.1 and described in Table 3.1. Note that for the SCI subject, first a 3D full-body model with orthoses is developed, to perform the IK of the captures with walker (as it will explained in Section 3.2). Then, crutches are added to develop a 3D full-body model with orthoses and crutches. The *3D Orthoses and Crutches* model has the same joints and DOFs for both subjects.

Model scaling

The generic model has been scaled to the healthy subject and to the SCI subject with the OpenSim "Scale Tool" using marker data from a static trial. The marker set included in the original model has been substituted by the marker set used in the experimental data collection (see Section 3.2). The original model included bony geometry and dimensions representing a 75 kg, 170 cm tall male [130, 131]. The dimensions and inertial properties of each segment in the model has been scaled according to the subject's mass and some scale factors. A body can be scaled uniformly (all directions with the same scale factor) or each direction can have its own scale factor. Moreover, scale factors can be defined manually or using experimental values. When using experimental values, a scale factor sf_i is defined according to the following expression [129]:

$$sf_i = \frac{\sum_{j=1}^{k_i} \frac{e_j}{m_j}}{k_i} \tag{3.7}$$

where e_j and m_j are the experimentally measured distance and the distance in the model between the j^{th} pair of markers included in the i^{th} measurement, respectively; and k_i is the number of pairs of markers included in the i^{th} measurement.

The scaling process is done at the same time as marker adjustment (which will be explained on Section 3.2). This process has required several steps. Firstly, we have determined manual scaling factors for pelvis and torso, as we have found that they were not correctly scaled using different measurement sets. To find these scaling factors, we have previewed in OpenSim at the same time the model markers and the experimental marker positions, and we have tried different manual scales for pelvis and torso, until distance between model and experimental markers has been found small. Secondly, we have prepared a measurement set in the OpenSim "Scale Tool" with only easy to locate markers (e.g., located on bony landmarks). Scale factors have been considered symmetric, and mean values from right and left sides have been computed. Then, using this measurement set and the scaling factors found manually, we have scaled the model. To obtain the HAT model, arms have been removed from the model (bodies and coordinates associated to their motion), and torso mass and tensor of inertia have been modified in order to include the arms mass and inertia. To obtain the assisted models, the assistive devices have been added to the human body model as explained previously (Figure 3.5).

Joint torque limits

Joint torque values have been limited considering experimental maximum values, to which a certain tolerance has been added (see Appendix C). In this way, realistic joint torques can be obtained. Moreover, to take into account the SCI subject impairment, some joint torques have been limited more restrictively according to the functional state of the subject. Following the approach applied in [58], we have assumed that the SCI subject used the 90% of his capacity during the experimental capture with passive orthoses and crutches. From the experimental values obtained

using the processed data (that will be explained in Section 3.2), the maximum values for some joint torques have been defined (Table 3.2). These limits are defined within the optimal control formulation, as bounds in the joint torque variables. No additional limits have been considered for the upper limb joints, as the subject has no impairment at that level.

	Min [Nm]		Max [Nm]	
Joint torque	**R**	**L**	**R**	**L**
Hip flexion	-40.94	-73.43	85.21	71.59
Hip adduction	-33.83	-44.38	51.33	71.13
Hip rotation	-20.63	-6.93	5.36	20.92
Knee flexion	-34		34	

Table 3.2: Joint torque limits applied to the SCI subject model with orthoses and crutches. Minimum (Min) and maximum (Max) values are shown, for both right (R) and left (L) legs. Hip torques have been limited assuming that the SCI subject used the 90% of his capacity during the experimental capture with passive orthoses and crutches [58]. Knee torque has been limited assuming that the subject has no actuation at the knee, so the total torque is only exerted by the active orthosis, and taking into account the peak torque that the electrical motor can provide.

Assistive devices models

Crutches and orthoses have been included in the model as rigid bodies, with no relative motion with respect to the body segments where they are attached (they do not introduce any additional DOF). Some assumptions have been done to find their inertial parameters, as well as to include the actuation of the orthosis in the model.

Crutches

Two pairs of forearm crutches have been used to assist the walking motion that has been captured in the laboratory: instrumented (Figure 3.6, left) and non-instrumented. The crutches centre of mass (COM) has been considered to be at half of their height. The tensor of inertia has been computed considering each crutch as a bar of negligible thickness, where mass and height have been obtained from the crutch used in the experiments (see values on Appendix B).

The two crutches have been added to the model initially with 6 DOF relative motion with respect to the forearm (or the hand) each one. To determine constant values for these generalised coordinates, we have performed an Inverse Kinematics (IK) analysis, have calculated the mean value for each translational and rotational coordinate, and finally have added a weld joint consistent with these mean values to replace each 6 DOF joint. This process has been done for each group of experimental captures, that is, if different trials have been performed sequentially, crutches position and orientation have been considered equal for all trials (using all trials for IK and calculating mean values).

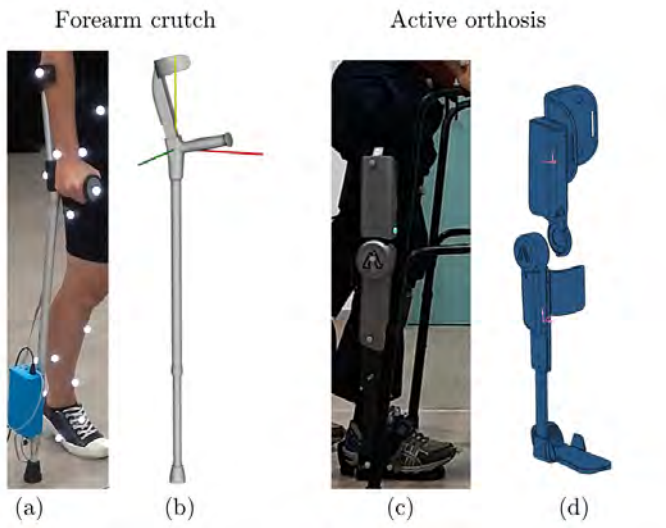

Figure 3.6: Assistive devices real prototypes and CAD models. (a) Detail from the healthy subject wearing the instrumented crutches during an experimental motion capture. (b) Crutch CAD model, with the local axes defined in OpenSim. (c) Detail from the SCI subject wearing the active orthoses during an experimental capture with the walker. (d) Active orthosis CAD model. The model consists of two segments: thigh and shank+foot.

Active orthoses

The powered knee-ankle-foot orthosis (KAFO) used in our study (Figure 3.6, right), as explained in Chapter 1, is intended for SCI patients with some remaining motor function at the hip, but who cannot control their knee and ankle muscles. These patients can walk using passive orthopaedic supports (which lock knee joint and avoid knee flexion), custom tailored to the subject, and crutches. However, in such case their gait is unnatural and exhausting. The goal of the considered assistive device is to add three modular components to a structure similar to these passive supports: an actuation system at the knee to flex and extend the joint during swing phase and lock that joint during stance phase, an inertial measurement unit (IMU) at the shank to detect user intent to take a step, and a box at the thigh containing the electronics and power supply. The knee controller locks the knee during stance, and follows a predefined knee angle trajectory during swing (Eq. 3.8). The reader is referred to [7] for more detailed information about the device.

$$\theta(t) = \frac{k_a}{2}\left[1 - cos\left(\frac{2\pi}{t_c}t - k_s sin\left(\frac{\pi}{t_c}t\right) - k_w sin\left(\frac{2\pi}{t_c}t\right)\right)\right], 0 \leq t \leq t_c \qquad (3.8)$$

where $\theta(t)$ is the predefined angle trajectory for each knee during swing phase, k_a is the maximum knee flexion, k_s is the peak displacement parameter, k_w is the peak

width parameter, and t_c is the cycle duration. Maximum and minimum values for each parameter are shown in Figure 3.7.

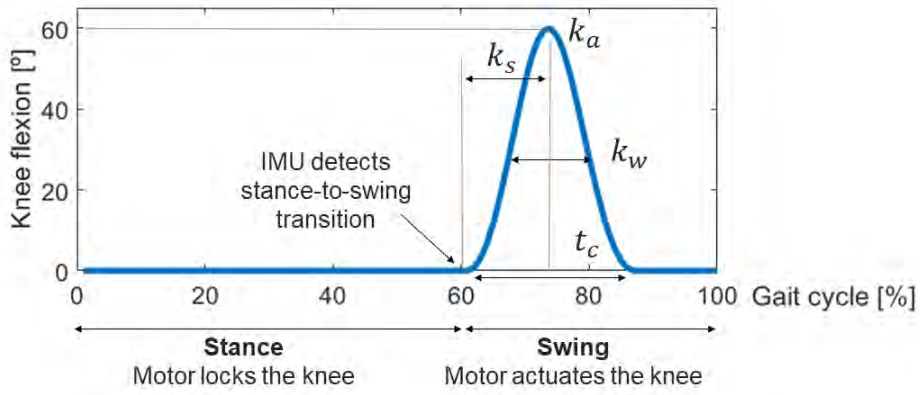

Parameter	Definition	Units	Range
k_a	Maximum knee flexion	[°]	[0.0 , 100.0]
k_s	Peak displacement parameter	[-]	[-1.0 , 1.0]
k_w	Peak width parameter	[-]	[-1.0 , 1.0]
t_c	Cycle duration	[s]	[0.0 , 2.0]

Figure 3.7: Top: Knee flexion angle obtained using Eq. 3.8. The active orthosis locks the knee during stance phase and follows a predefined knee angle trajectory during swing. An IMU located at the shank detects swing-to-stance transition. Maximum knee flexion k_a, peak displacement parameter k_s, peak width parameter k_w, and cycle duration t_c can be modified for a better adaptation to each subject. A Figure showing the effect of modifying k_s and k_w can be found in [7]. Bottom: Maximum and minimum possible values for each parameter are shown in the table.

In order to model the assistive device performance, the following assumptions have been done:

- The orthosis links move together with the correspondig lower limb segment, i.e., no relative motion between them is permitted.
- The knee orthosis joint has been considered to be perfectly aligned to the subject's knee joint.
- The knee motor is capable of following the desired knee trajectory and the knee flexion reaches the imposed maximum knee flexion. This is done in the prediction problem formulation, where the knee angle trajectory is known, and the other coordinates are predicted.
- The IMU sensors detect correctly the stance-to-swing transition event.
- For the healthy subject, the total torque acting at the knee is the sum of the subject's knee torque and the motor torque. No limit has been imposed.

- For the SCI subject the total torque acting at the knee corresponds to the motor torque, since the subject's knee muscles are not functional. This torque has been limited to 34 Nm, that is the peak torque that the electrical motor can provide.

As explained previously, the orthoses have been modelled as independent bodies consisting of two segments (corresponding to thigh, and shank-foot) with dimensions and inertial properties taken from CAD models of the real prototype (see Appendix B). Each orthosis segment has been attached to the corresponding lower limb segment using a weld joint (i.e., no relative motion is permitted between bodies). The ankle, subtalar and MTP joints have been locked at 0°, due to the presence of the orthosis mechanical constraints. No joints have been defined between the orthosis links, i.e., knee orthosis joint has been considered to be perfectly aligned to the subject's knee joint. This approach, although is a simplification, can be considered realistic as the orthoses are attached tightly with Velcro straps using a front support at the shank, a back support at the thigh, and a ratchet strap at the front and back of the foot.

For the SCI subject, some experimental captures have been performed with active orthoses and a walker. The walker has not been added to the model. To perform the inverse kinematic analysis (IKA) of these trials with walker, the orthoses have been included in the model previously to the crutches (Figure 3.5). Although it can be seen as not necessary, since the inertial properties of the orthoses do not influence on the IK solution, in that step of the process ankle, subtalar and MTP joint DOFs are eliminated.

Calibration of contact model parameter values

The following considerations have been taken into account for the calibration of contact model parameter values:

- The model has been considered symmetric, that is, right and left feet and right and left crutches have the same parameter values,
- The parameter values have been calibrated for each subject and for each capture (e.g., barefoot walking or walking with shoes),
- The calibration has been done in phases, where the previous optimal solution has been used as the initial guess for the next optimisation (see Section 4.2.1).

With the purpose of reducing the number of parameters to calibrate, some parameters have been considered fixed, and their values have been obtained by a trial-and-error process (Table 3.3). Another strategy to reduce the number of parameters to calibrate is that all the springs in the same group (see Figure 3.4) have the same value of each parameter. For the foot-ground contact model, the spring resting length y_0 has been considered zero for all cases; spring stiffnesses K_i, nonlinear damping coefficients c_i and dynamic friction coefficients μ_i have been calibrated for each group of spring-damper units. For the crutch-ground contact model, the sphere radius R_s has been considered fixed, and its value has been

manually tuned per each experimental capture (Table 3.3). The generalised normal stiffness K_n has been considered a parameter of the optimisation, as well as the hysteresis damping factor χ and the coefficient of dynamic friction μ. Initial values for these parameters have been taken from [96]. The initial guess and bounds for each parameter are show in Table 3.3; they have been obtained based on literature results and from simple calculations using experimental data.

Foot-ground contact model parameters

Fixed parameters

Symbol	Description	Units	Value
y_0	Spring resting length	[cm]	0
$pos(x,y,z)$	Spring-damper local position	[cm]	(see Table 3.4)

Calibrated parameters

Symbol	Description	Units	Min.	Guess	Max.
K	Spring stiffness	[N/m]	10^2	10^4	10^5
c	Damping coefficient	[s/m]	0.01	0.1	1
μ	Coefficient of dynamic friction	[-]	0	0.5	1

Crutch-ground contact model parameters

Fixed parameters

Symbol	Description	Units	Model	Value
Tip_y	Local position of the tip in longitudinal direction	[m]	3D Crutches	-0.77
			3D Orthoses	-0.84
R_s	Radius of the contact sphere	[cm]	3D Crutches	2
			3D Orthoses	3.5

Calibrated parameters

Symbol	Description	Units	Min.	Guess	Max.
K_n	Generalised normal stiffness	[N/m$^{3/2}$]	10^2	$3.7{\cdot}10^4$	10^5
χ	Hysteresis damping factor	[Ns/m$^{5/2}$]	10^2	10^5	10^6
μ_{crutch}	Coefficient of dynamic friction	[-]	0	0.5	1

Table 3.3: Information about foot-ground and crutch-ground contact model parameters for the healthy subject. For the fixed parameters (i.e., their value is manually tuned and fixed during calibration), the used value for each model is given (if not specified, then for all models the value is the same). For the calibrated parameters, maximum, minimum and initial guess values for each parameter are given.

3.2 Experimental data collection

Experimental data have been collected from two subjects: a healthy young female, and an SCI adult male. For each subject, different captures have been done, as it is explained later on in this section. There are many prediction problems where a tracking term is added in the cost function, to help the optimiser to find the optimal solution [22,26,132]. Other authors use experimental data to specify the initial and final states of the simulation [25], or only to validate the results [20]. In the present

Local position	Models (healthy subj.)	Spring-damper group					
		Hindfoot					Forefoot
		1	2	3	4	5	6
x [cm]	All	0.00	5.00	10.00	15.00	20.00	8.00
y [cm]	Unassisted	0.00	0.00	0.00	0.00	0.00	0.00
	3D Crutch.	-1.50	-1.50	-1.50	-1.50	0.00	0.00
	3D Orth.	-5.00	-5.00	-5.00	-5.00	-5.00	-5.00
z [cm]	All	-1.00	-3.00	-3.00	-3.00	-3.00	-1.00
		1.00	0.00	0.00	0.00	0.00	1.00
		-	3.00	3.00	3.00	3.00	-

Table 3.4: Local position of the spring and damper units for the foot-ground contact model of the healthy subject. The local axes are shown in Figure 3.4: x is the anterior-posterior direction, y is the vertical direction, and z is the mediolateral direction.

thesis, experimental measurements have been used for several purposes: skeletal models development, contact models calibration, dynamically consistent motion tracking, prediction of new motions, and results evaluation.

3.2.1 Normal and crutch walking cycles

The normal walking cycle and different crutch-walking patterns are defined. The gait patterns with orthoses and crutches are similar to the ones corresponding to gait assisted by crutches.

Normal walking cycle

The gait cycle basically consists on two phases for each leg, swing and stance. During swing, only one foot is in contact with the ground (known as single-support), but during stance, there are two periods where both feet are in contact with the ground (known as double-support phases). A walking cycle (or gait cycle) is defined from an initial event to the next same event in the same foot, e.g., right heel strike (RHS) to RHS, or left toe off (LTO) to LTO (Figure 3.8). Each phase (swing or stance) is divided in other subphases. However, in this work we will focus only in swing (no contact) and stance (contact with ground).

Some spatio-temporal parameters are used to analyse the gait cycle: cycle time, swing/stance percentage of cycle time, step length and width, stride length, speed, and cadence, among others. Also joint coordinate values are used to analyse the gait cycle, specially the ones in the sagittal plane: hip flexion, knee flexion and ankle dorsiflexion.

Crutch walking patterns

There are basically four types of cruth-walking patterns [133], with small variations within them:

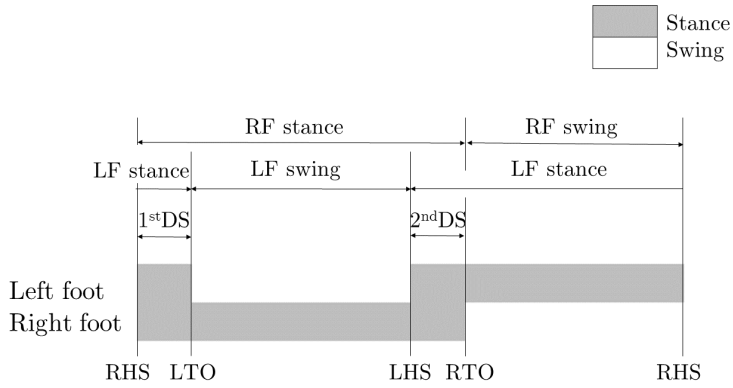

Figure 3.8: Phases of the gait cycle. During a complete gait cycle, each leg goes through two phases: stance (in grey) and swing (in white). Twice during the gait cycle, both feet are at the same time in contact with ground (in stance phase), and this is known as double support (DS). "RF" and "LF" stand for right and left foot, respectively. "RHS" and "LHS" stand for right and left heel strike, respectively; and "RTO" and "LTO" stand for right and left toe off, respectively.

- *Four-point alternating gait:* The sequence of swing phases is as follows: right crutch, left leg, left crutch, right leg.
- *Three-point gait:* This is used when the injured foot can bear some weight. Both crutches advance together, then the affected foot steps up to the crutches, and the unaffected foot steps past the crutches.
- *Two-point (or reciprocal) gait:* The sequence of swing phases is as follows: right crutch and left leg, left crutch and right leg.
- *Swing-through and swing-to gait:* The sequence of swing phases is as follows: both crutches, then both legs. In swing-through gait, both legs are placed ahead of the crutches; in swing-to gait, both legs are placed at the same position than the crutches. There is also a variation of this pattern that is used when it is not possible to bear weight on the injured leg, and only one foot is placed on the ground at each step.

3.2.2 Laboratory equipment

The experimental data have been collected at the Universitat Politècnica de Catalunya (UPC) Biomechanics Laboratory, placed in the Department of Mechanical Engineering at the Barcelona School of Industrial Engineering (ETSEIB). Experimental walking data have consisted of marker trajectories, foot-ground reaction forces and moments, and in some cases, crutch-ground reaction forces (Figure 3.9).

Surface marker motion has been recorded at 100 Hz by tracking passive reflective markers using 16 optical infrared cameras (OptiTrack V100:R2, NaturalPoint Inc.,

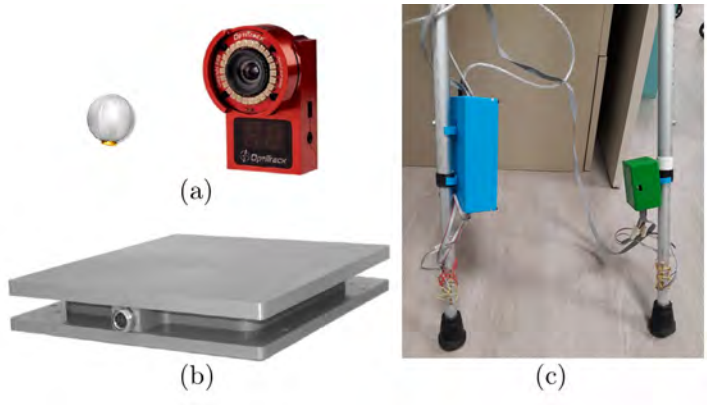

Figure 3.9: Laboratory equipment: (a) reflective marker and optical camera, (b) force plate, and (c) instrumented crutches.

Corvallis, OR, USA). Ground reaction forces and moments have been measured at the same sampling frequency by two force plates (AccuGait, AMTI, Watertown, MA, USA) located in the floor at the centre of the capture workspace. A pair of crutches have been instrumented with tri-axial load cells at the tips to measure crutch-ground contact force components at 80 Hz following the approach used in [134]. The deformation of the crutches is detected by strain gauges forming a Wheatstone bridge, thus making it possible to measure voltage variations and relate those voltage differences directly to the stresses suffered by the crutches. They have been instrumented using 12 strain gauges for each crutch, and each Wheatstone bridge is built in full bridge configuration with four gauges per bridge. Four gauges measure the axial force along the vertical axis of the crutch and the other eight gauges measure the shear stresses suffered.

All captures have been approved by the Research Committee of UPC, which handles ethical issues involved in research projects, and the subjects have given written informed consent for experimental data collection and subsequent data use for modelling purposes.

3.2.3 Healthy subject experimental captures

The experimental data of a healthy female subject (age 28 yrs., mass 55 kg, height 1.62 m) have been collected for dynamically consistent motion tracking and foot- and crutch-ground contact models calibration (Chapter 4), for normal and crutch-assisted walking prediction (Chapter 5), and for crutch-orthosis-assisted walking prediction (Chapter 6). The motion captures have been done separately in two different sessions. In the first one, normal walking (unassisted) and crutch-walking cycles using forearm crutches have been performed. In the second one, crutch-orthosis-assisted walking cycles have been performed.

Normal and crutch-assisted walking

Two types of normal walking cycles have been captured experimentally: without shoes and with shoes. The crutch walking pattern performed is a variation of the first pattern described above. It is a four-point non-alternating gait, where the sequence of swing phases is as follows: right crutch, right leg, left crutch, left leg (Figure 3.11, left). In each case, an initial static capture has been performed to scale the model and to adjust markers location. The marker protocol is based on a modified Cleveland Clinic marker protocol for the torso and lower body, and a marker protocol based on [135] for arms (Figure 3.10). There are some markers that are placed only for the static capture (that will be used for scaling the model), and are removed before dynamic captures (where the movements are performed) take place.

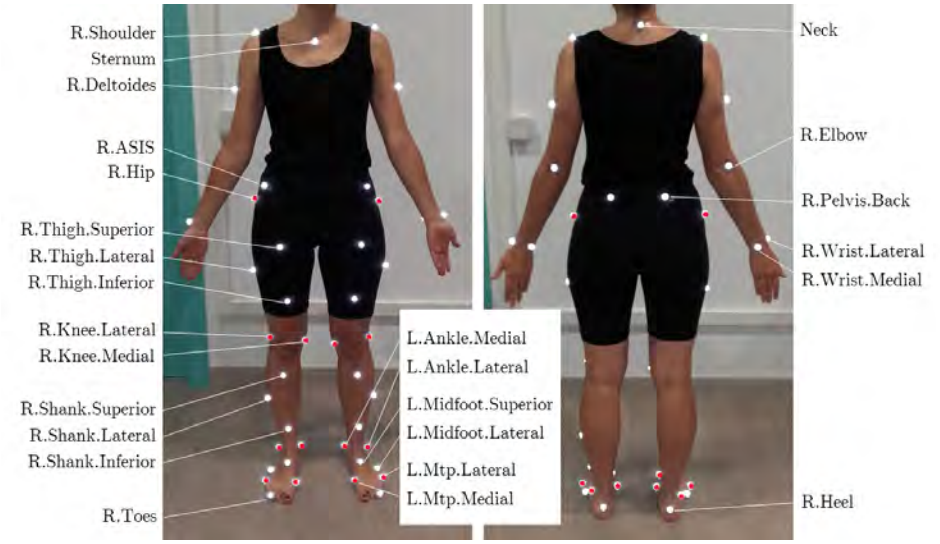

Figure 3.10: Marker protocol used for normal and crutch-assisted walking captures with the healthy subject. Marker protocol is the same for right and left sides, i.e., to each marker labelled with an R (right) or L (left) corresponds another labelled with an L or R. Static markers (those that were used only for scaling the model) are highlighted in red. For the crutch walking captures, four additional markers were placed on each crutch (see Figure 3.11, left).

The motion capture experimental process has been as follows:

1. Place markers (complete set, static + dynamic),
2. Static capture (on one force plate, to measure weight),
3. Remove static markers,
4. Walking cycles (barefoot),

5. Remove markers from feet, add shoes, add feet markers again,
6. Walking cycles (shoes),
7. Add markers to crutches,
8. Capture to calibrate crutch force measurements,
9. Static capture with crutches (only markers),
10. Crutch-walking cycles.

Crutch-orthosis-assisted walking

Crutch-orthosis-assisted walking motions have been captured. Three different maximum knee flexion angles have been imposed: 0°, 40° and 60°. The subject walked in transverse direction with respect to the force plates, in order to be able to step correctly with each foot inside each force plate (Figure 3.11, right). With this disposition of movement, the subject was not able to place the crutches out of the force plates. This fact has required an additional step in data processing, to subtract crutch-ground reactions from force plate measurements, in order to get foot-ground reactions. The marker protocol has been enhanced with more markers at the arms, and less markers at shanks and feet, since the orthoses lock relative motion between them.

Data have been collected first for a healthy subject (instead than for an SCI subject), since data collection with a healthy subject is less complicated and computational issues can be explored equally well regardless of the functional status of the subject. Moreover, orthosis performance is the same for a healthy subject or an SCI subject, as the knee control is predefined and the IMUs detect the stance-to-swing event the same way in both cases.

The motion capture experimental process has been as follows:

1. Place markers on the crutches,
2. Capture to calibrate crutch force measurements,
3. Put orthoses on the subject,
4. Place markers on subject and orthoses (complete set, static + dynamic),
5. Static capture,
6. Remove static markers,
7. Assisted-walking cycles with 0° knee flexion,
8. Assisted-walking cycles with 40° maximum knee flexion,
9. Assisted-walking cycles with 60° maximum knee flexion.

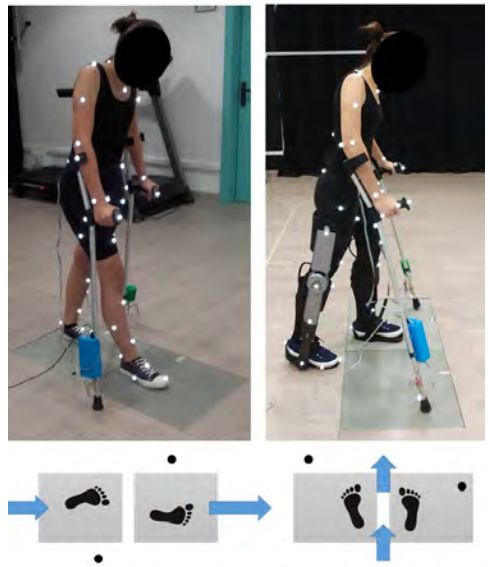

Figure 3.11: Experimental captures of crutch-assisted walking (left) and crutch-orthosis-assisted walking (right) with the healthy subject. Below each picture, a diagram shows conceptually the movement direction and how the subject placed feet and crutches with respect to the force plates. In the case of crutch-assisted walking, the subject walked along the laboratory longitudinal direction and placed the crutch tips outside of the force plates. In the case of crutch-orthosis-assisted walking, the subject walked along the laboratory transverse direction and placed the crutch tips on the force plates. This required an additional step in data processing, to subtract crutch-ground reactions from force plate measurements, in order to get foot-ground reactions.

3.2.4 SCI subject experimental captures

The experimental data of an SCI subject have been used for crutch-orthosis-assisted walking prediction in Chapter 6. The patient selected for this case study is a young adult male, 38-year-old patient that suffers paraplegia after a spinal hemangioma. He has an incomplete transverse spinal cord syndrome below the 10^{th} thoracic neurological segment (T10), classified at level B in the ASIA Impairment Scale (AIS). Sensory but not motor function is preserved below the level of injury, including the sacral segments.

The patient was able to walk with passive braces that lock his knee and a pair of forearm crutches. He could also walk assisted by the active orthoses and a walker. Although the training process is intented to achieve the walking motion of the patient using crutches and active orthoses, he was not able to do so at the time of the experimental capture. For this reason, two types of captures have been done: assisted by orthoses and walker (with locked knee and with knee flexion), and assisted by orthoses and crutches (only with locked knee due to safety reasons). During the experimental capture, it was difficult for the patient to walk with the instrumented crutches (as they include wires and the electronic modules on each

crutch), and also stepping one foot on each force plate. For these reasons, the experimental capture has been done with non-instrumented crutches, thus collecting only marker trajectories. Moreover, an additional capture of the patient placing one foot on each force plate has been done to calibrate the foot-ground contact model parameters of the patient.

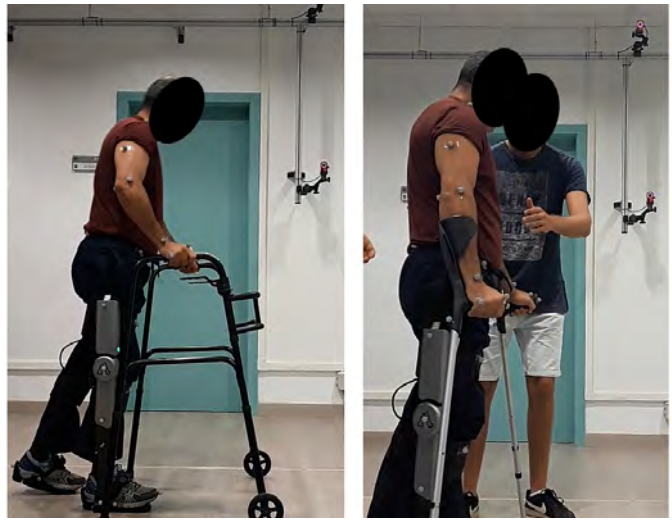

Figure 3.12: Experimental captures of walker-orthosis-assisted walking (left) and crutch-orthosis-assisted walking (right) with the SCI subject. Only marker trajectories were collected in these captures. An additional capture of the subject placing one foot on each force plate was done to calibrate the foot-ground contact model parameters of the patient.

The motion capture experimental process has been as follows:

1. Put orthoses on the subject,
2. Place markers on subject and orthoses (complete set, static + dynamic),
3. Static capture (only markers),
4. Remove static markers,
5. Assisted-walking cycles with walker with 0° knee flexion,
6. Assisted-walking cycles with walker with 20° maximum knee flexion,
7. Assisted-walking cycles with walker with 40° maximum knee flexion,
8. Place markers on the crutches,
9. Static capture with crutches,

10. Assisted-walking cycles with crutches with 0° knee flexion,
11. Capture to calibrate foot-ground contact model.

3.2.5 Data processing

Experimental data have to be processed from the raw measurements until the reference motion and force data are obtained for each capture and for each model. First of all, kinematic, force plate, and crutch load cell data have been synchronised. Data have been exported to MATLAB, where filtering has been performed. Foot-ground reaction force and moment components have been filtered using a 3rd-order zero phase lag Butterworth filter with cut-off frequency of 6 Hz. Crutch-ground reaction force components have been resampled to 100 Hz, filtered using the same filter, and transformed to the global reference frame. If the experimental capture includes crutch-ground reaction measurements, they have to be calibrated. The calibration procedure has been repeated for each group of trials, and it has been done independently per each crutch. It consists of positioning at different points of a force plate the crutch and applying different loads, while modifying the crutch orientation. Crutch marker trajectories, crutch-ground reactions from force plates and from crutches measurements are collected simultaneously. Then, an optimisation problem is solved to find the transformation matrix from crutch measurements to crutch-ground reaction forces at the tip. For the crutch-orthosis-assisted captures for the healthy subject, an additional step to substract the crutch measurements from the force plate data is needed.

Marker trajectories have been prepared in a .trc file (the format required by OpenSim). The generic full-body model has been scaled (as explained previously in Section 3.1.3), and markers that were not included in the scaling measurement set have been adjusted manually, after performing an IKA with the static motion data. The process of marker positions adjustment, without scaling the model, has been repeated for each of the different captures. For the healthy subject, for example, the model has been scaled with the experimental data of the *barefoot* motion, but feet markers have been adjusted for the *shoes* walking motion, and all markers have been adjusted for the crutch-walking motion.

Once the model has been scaled, IKA has been performed in OpenSim. All weights for tracking marker coordinates have been set to 1 for normal and crutch-assisted motions. For crutch-orthosis-assisted motions, these weights have been manually modified to give a higher weight to feet and crutch tip markers. The obtained motion has been used to translate the foot-ground reactions from the centre of the force plates to the origin (or the midpoint) of the corresponding hindfoot segment. Then, we have performed an IDA with the OpenSim C++ API to determine the initial residual loads (i.e., forces and moments) relative to the pelvis origin (Figure 3.15, left). To obtain the reference motion for the 3D HAT model, IK and ID have been done using the 3D HAT model.

Finally, walking cycles have been selected in order to use them as reference motion data for the different optimal control problems (OCPs). The event that defines the beginning of each walking cycle (normal, crutch-assisted, crutch-orthosis-assisted) depends on how the experimental motion has been performed. The ob-

jective is to use all the available measurements from the force plates, so each cycle is selected as follows: for normal walking cycles, from left heel strike (LHS) to LHS; for crutch-assisted walking, from right crutch off (RCO) to RCO; for crutch-orthosis-assisted walking for the healthy subject, from left crutch off (LCO) to LCO, and for the SCI subject, from LTO to LTO. Moreover, for contact model calibration, only the part of the cycle for which all the external forces are experimentally measured is used (Figure 3.13). For all experimental captures, the main spatiotemporal parameters, as well as maximum values for vertical ground reactions, are shown in Table 3.5.

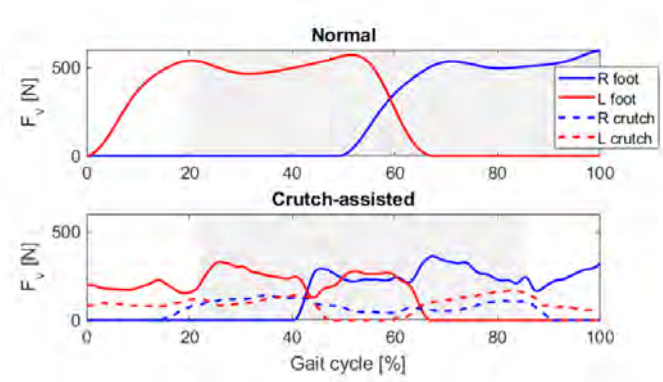

Figure 3.13: Example of normal ground reaction forces (F_v) for feet and crutches of a normal (top) and a crutch-assisted (bottom) walking cycle. Experimental data for the complete gait cycle have been used for tracking problems as reference motion and initial guess, and data for the part highlighted in grey have been used for foot- and crutch-ground contact model parameters calibration.

3.3 Optimal control framework

All the simulations performed in this work have been solved using direct and simultaneous collocation optimal control problems. Direct collocation methods guess controls and motion, discretise dynamics equations, and iterate those guesses to find motion and controls over all time frames simultaneously. They are direct methods because first convert the continuous problem into a non-linear programming problem, and then find the minimum of the objective function. They are simultaneous because states and controls trajectories are decision variables, and are solved over all time frames simultaneously. And they are collocation methods because the dynamics constraints are only satisfied at special points in the trajectory, located among different mesh intervals [119].

The main structure of the prediction algorithms is the same for the different problems. They have been written in MATLAB, since GPOPS-II is a MATLAB-based algorithm and the problem formulation can be implemented easily. The biomechanical model has been developed in OpenSim, using the GUI, previous to

the different predictions. The equations of motion used for solving the inverse dynamic problem in each iteration are obtained from OpenSim, through the OpenSim API, that defines the classes and funcions in C++. To call these functions inside MATLAB, MEX files have been used. Figure 3.14 shows a diagram representing how the different softwares have been related among them.

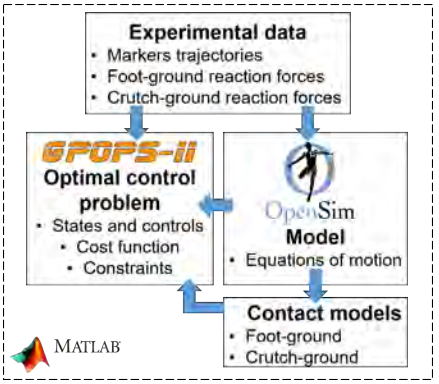

Figure 3.14: Diagram showing the relationship among the different softwares that have been used in the prediction framework. The optimal control problem is defined in GPOPS-II, and the equations of motion as well as information used as input of the contact models are obtained from OpenSim API.

3.3.1 Optimal control problem statement

A single-phase optimal control problem can be described in the following form [128]: Determine the state $\mathbf{x}(t) \in \mathbb{R}^{n_x}$, the control $\mathbf{u}(t) \in \mathbb{R}^{n_u}$, the integrals $\mathbf{p} \in \mathbb{R}^{n_p}$, the initial time t_0 and the terminal time t_f on the time interval $t \in [t_0, t_f]$, and the static parameters $\mathbf{s} \in \mathbb{R}^{n_s}$, that minimise the cost functional

$$J = \phi(\mathbf{x}(t_0), t_0, \mathbf{x}(t_f), t_f, \mathbf{p}, \mathbf{s}) \tag{3.9}$$

subject to the dynamic constraints

$$\dot{\mathbf{x}} = a(\mathbf{x}(t), \mathbf{u}(t), t, \mathbf{s}) \tag{3.10}$$

the inequality path constraints

$$\mathbf{c}_{min} \leq c(\mathbf{x}(t), \mathbf{u}(t), t, \mathbf{s}) \leq \mathbf{c}_{max} \tag{3.11}$$

the integral constraints

$$p_i = \int_{t_0}^{t_f} g_i(\mathbf{x}(t), \mathbf{u}(t), t, \mathbf{s}) \mathrm{d}t \quad (i = 1, ..., n_p) \tag{3.12}$$

and the event constraints

$$\mathbf{b}_{min} \leq b(\mathbf{x}(t_0), t_0, \mathbf{x}(t_f), t_f, \mathbf{p}) \leq \mathbf{b}_{max} \tag{3.13}$$

An optimal control problem can be formulated as a collection of N phases. For many applications, the independent variable t is time, and the phases are sequential, but neither of these assumptions is required. Many complex problem descriptions require different dynamics and/or constraints within each phase. The cost function may depend on quantities computed in each of the N phases. Furthermore, the cost function includes contributions evaluated at the phase boundaries (point functions) and over the phase (continuous functions). Similarly, some constraints must be satisfied over the entire interval $t_0 \leq t \leq t_f$ (continuous functions), whereas other constraints are imposed at a specific time, such as the boundary conditions (point functions).

3.3.2 Implementation in GPOPS-II

The transcription and solution of the optimal control problem (OCP) has been done using GPOPS-II [128]. It uses Legendre-Gauss-Radau quadrature orthogonal collocation. All simulations done in this work have been solved using the interior point optimisation algorithm (IPOPT) [136] employing the linear solver 'mumps'. In the Radau collocation method, the state of the continuous-time optimal control problem is approximated in each mesh interval. Bounds have to be defined for all variables in the problem: states, controls, static parameters, initial and final time, and integrals.

In human motion prediction, design variables of an optimal control problem can be related to motion (e.g., generalised coordinates, velocities, accelerations), forces (e.g., joint torques, muscle activations), or parameters of the predicted motion (e.g., mean speed, duration of each phase, step length) [137]. In direct collocation formulations, both controls and states are parameterised as opposed to direct shooting formulations, where only control variables are parameterised. Control variables do not need to be physical controls and are usually time varying quantities whose derivatives are not needed in the problem solution process (i.e., they do not appear in any constraint or in the cost function). Note that by definition, a state variable is a differentiated variable that appears on the left-hand side of the differential equation (Eq. 3.10). In contrast, a control variable is an algebraic variable [118]. Therefore, in our approach there is not a clear difference between state and control variables.

As mentioned in [21], implicit skeletal dynamics (e.g., F-m·a = 0) works better than explicit skeletal dynamics (e.g., a = F/m) when solving direct collocation optimal control problems involving human movement. The OCP solver used in this work, GPOPS-II [128], does not handle implicit dynamics and requires the use of explicit dynamics for dynamic constraints. We have addressed this limitation by putting an implicit form of skeletal dynamics in the path constraints, making joint acceleration or jerk additional controls, and using kinematic derivative relationships (e.g., joint jerk equals the first time derivative of joint acceleration, joint acceleration equals the first time derivative of joint velocity, etc.) for the required explicit dynamics. To make the controls unique, we have added a joint acceleration

or jerk regularisation term to the cost function. Although this term is not related to any physiological criterion, it has been employed in previous studies to improve convergence by making the solution unique [50,123]. However, it is still unknown if one type of control (joint acceleration or joint jerk) is advantageous over the other. Additional control variables in all formulations are ground reactions (foot-ground and crutch-ground reactions), as having ground reactions as controls improves the problem converge [74].

The equations of motion are included implicitly as algebraic path constraints. The equations of motion are obtained from OpenSim, which uses Simbody as its multibody dynamics engine [138]. Simbody uses a generalised coordinate formulation, so it represents the pose and motion of a multibody system using the fewest possible coordinates. The equations of motion can be written in the following matrix form:

$$[\mathbf{M}(\mathbf{q})]\ddot{\mathbf{q}} + \mathbf{C}(\mathbf{q}, \dot{\mathbf{q}}) + \mathbf{U}(\mathbf{q}) = \mathbf{F}^*, \tag{3.14}$$

where $\mathbf{q}$, $\dot{\mathbf{q}}$, $\ddot{\mathbf{q}} \in \mathbb{R}^n$ are the vectors of generalised coordinates, velocities, and accelerations, respectively; $[\mathbf{M}(\mathbf{q})] \in \mathbb{R}^{n \times n}$ is the system mass matrix; $\mathbf{C}(\mathbf{q}, \dot{\mathbf{q}}) \in \mathbb{R}^n$ is the vector of inertial terms depending on position and velocity; $\mathbf{U}(\mathbf{q}) \in \mathbb{R}^n$ is the vector associated with gravitational forces; finally, $\mathbf{F}^* \in \mathbb{R}^n$ is the vector of generalised forces that contains the unknown joint torques and residual wrench.

This system has n unknowns that appear in the terms of generalised forces F_i^*, i.e., joint torques for each generalised coordinate and the residual wrench. An inverse dynamic analysis (IDA) is performed at each iteration using the OpenSim C++ API (version 3.3), and the system kinematic state is used to calculate the net forces and torques applied at each DOF. The residual loads acting on the pelvis are limited in path constraints to be within a specific tolerance, in order to get a dynamically consistent motion.

3.3.3 Problems formulation

In this work, as it has been introduced in Chapter 1, human motion is simulated using optimal control formulations and three different approaches. The first one is to track experimental data (in Chapter 4) to obtain dynamically consistent motions and to calibrate foot- and crutch-ground contact models. The second one is to predict new motions without tracking any experimental data (in Chapter 5), for normal and crutch-assisted walking. The third one is to predict new motions tracking some quantities in the cost function (in Chapter 6), for crutch-orthosis-assisted walking. The main structure of all these problems is common for all of them, and is presented in this subsection. Then, on each section of Chapters 4, 5 and 6, the used methods for each study are specified. In Table 3.6, a summary of the problems solved, the models and experimental data used on each section is presented.

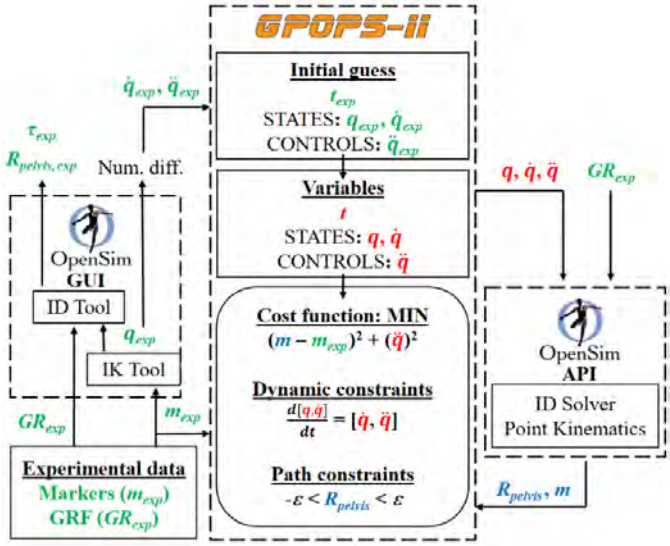

Figure 3.15: Scheme of the optimal control framework of a tracking problem without contact models, where experimental markers are tracked in the cost function, while joint accelerations are minimised. This is a particular case, but the general structure is the same for all problems and formulations. Previous to the OCP solution, IK and ID are performed in the OpenSim GUI. At each iteration, ID is solved and the model markers positions are obtained using OpenSim API. The colour legend is the following: green indicates variables that are measured experimentally or calculated directly from experimental measurements, red indicates variables of the OCP, and blue indicates magnitudes that are computed at each iteration. Variables correspond to marker coordinates ($\mathbf{m}$), joint coordinates ($\mathbf{q}$), joint velocities ($\dot{\mathbf{q}}$), joint accelerations ($\ddot{\mathbf{q}}$), ground reactions (foot-ground forces and moments and crutch-ground forces) ($\mathbf{GR}$), joint torques ($\boldsymbol{\tau}$) and residuals ($\mathbf{R}_{pelvis}$). Subscript *exp* indicates an experimental value: experimental marker coordinates and ground reactions are measured directly, while experimental joint coordinates, torques and residuals are obtained from IK and ID performed in OpenSim, respectively.

Subject	Capture	Start event	Tcycle [s]	Lstride [m]	Speed [m/s]	Support phase [%]				Max normal force [% BW]			
						RF	LF	RC	LC	RF	LF	RC	LC
Healthy	*barefoot*	LHS	1.33	1.15	0.86	69.92	66.17	-	-	107.99	103.56	-	-
	shoes	LHS	1.28	1.23	0.96	71.09	67.19	-	-	110.53	105.95	-	-
	four-point	RCO	4.80	0.84	0.18	83.48	80.25	83.84	85.46	67.07	61.21	25.72	31.71
	PASS	LCO	3.17	0.45	0.14	81.07	79.18	80.13	85.17	72.96	59.85	32.32	28.22
	ACT40	LCO	2.98	0.54	0.18	76.85	65.44	79.87	82.89	77.38	76.71	21.43	23.46
	ACT60	LCO	2.98	0.55	0.19	77.52	72.48	79.87	82.55	75.164	71.895	24.136	22.221
SCI	*PASS_W*	RTO	3.66	0.70	0.19	64.96	70.37	-	-	-	-	-	-
	ACT20_W	RTO	3.59	0.63	0.18	68.31	70.77	-	-	-	-	-	-
	ACT40_W	RTO	3.45	0.61	0.18	71.51	68.02	-	-	-	-	-	-
	PASS_C	LTO	3.99	0.41	0.10	83.46	87.47	91.98	88.47	-	-	-	-

Table 3.5: Main spatiotemporal parameters and maximum normal forces for each experimental capture performed in this work. For each capture, the start event that has been considered is indicated, as explained in the text: left heel strike (LHS), right/left crutch off (R/LCO), right/left toe off (R/LTO). The spatiotemporal parameters are cycle duration (Tcycle), stride length (Lstride), speed, and % of cycle duration of each stance phase (RF: right foot, LF: left foot, RC: right crutch, LC: left crutch). The maximum value of normal ground reaction force for each foot and crutch is given in % of body weight (BW). With '-' we indicate that a measurement is not available (it does not apply or it was not measured).

Subject	Captures		Measurements			Model	OC Problems				Exp. eval.	Chapter		
	Name	Description	Mark.	FPL	Crut.		Track. wo	Calib. CM	Track.	Pred.		4	5	6
Healthy	*barefoot*	Normal walking with and without shoes	x	x		3D HAT		x	x	x	x	x	x	
	shoes		x	x		3D Full	x	x			x			
	four-point non-alternate	Crutch-assisted walking (four-point pattern)	x	x	x	3D Crutch. (arm)	x				x	x	x	
						3D Crutch. (hand)		x	x	x	x			
	PASS	Crutch-orthosis-assisted walking with different knee maximum flexion	x	x	x	3D Orthoses and crutches		x	x	x	x			x
	ACT40		x	x	x					x	x			
	ACT60		x	x	x					x	x			
SCI	*PASS_W*	Walker-orthosis-assisted walking with different knee maximum flexion	x			3D Orthoses					x			x
	ACT20_W		x								x			
	ACT40_W		x								x			
	PASS_C	Crutch-orthosis-assisted walking with locked knees	x			3D Orthoses and crutches			x	x	x			x
	CALIB_CM	Place one foot on each force plate to calibrate foot-ground contact model	x	x				x						

Table 3.6: Summary of experimental data collected for both subjects: name of each capture that will be used during the thesis, brief description, measurements, models, optimal control problems, and chapter where it appears. For the measurements, "Mark" stands for marker trajectories, "FPL" stands for force plate measurements, and "Crut" stands for instrumented crutches measurements. For the optimal control (OC) problems, "Track.wo" stands for tracking without contact models, "Calib. CM" stands for calibration of contact models, "Track." stands for tracking with contact models, and "Pred.," stands for prediction. "Exp. eval." stands for experimental evaluation. With 'x' we indicate that those measurements or OCP are considered.

Variables

States

The state vector, $\mathbf{x}$, can be formed by several of the following quantities:

- The vector of generalised coordinates, $\mathbf{q} \in \mathbb{R}^{n_q}$
- The vector of generalised velocities, $\dot{\mathbf{q}} \in \mathbb{R}^{n_q}$
- The vector of generalised accelerations, $\ddot{\mathbf{q}} \in \mathbb{R}^{n_q}$
- The vector of net joint torques, $\boldsymbol{\tau} \in \mathbb{R}^{n_q-6}$

where n_q is the number of generalised coordinates in the model (see Section 3.1.1). Note that the vector of net joint torques is $n_q - 6$ dimensional. This is due to the fact that the other six components of the generalised force vector are those of the residual wrench applied to the pelvis (three forces and three moments).

Controls

The control vector, $\mathbf{u}$, can be formed by several of the following quantities:

- The vector of generalised accelerations, $\ddot{\mathbf{q}} \in \mathbb{R}^{n_q}$
- The vector of generalised jerks, $\dddot{\mathbf{q}} \in \mathbb{R}^{n_q}$
- The vector of net joint torques, $\boldsymbol{\tau} \in \mathbb{R}^{n_q-6}$
- The vector of joint torque change, $\dot{\boldsymbol{\tau}} \in \mathbb{R}^{n_q-6}$
- The vector of ground reaction controls, $\mathbf{GRF}_u \in \mathbb{R}^{12}$ for unassisted models (6 components per each foot), and $\mathbf{GRF}_u \in \mathbb{R}^{18}$ for crutch-assisted models (6 components per each foot and 3 components per each crutch)

Parameters
There are only two sections where a parameter vector, $\mathbf{s}$, is included in the prediction. The first one is for the calibration of contact model parameters (Section 4.2), where this vector can be formed by several of the following quantities:

- The vector of spring stiffnesses, $\mathbf{K} \in \mathbb{R}^{n_e}$
- The vector of damping coefficients, $\mathbf{c} \in \mathbb{R}^{n_e}$
- The vector of coefficients of dynamic friction, $\boldsymbol{\mu} \in \mathbb{R}^{n_e}$
- The generalised normal stiffness, K_n
- The hysteresis damping factor, χ
- The coefficient of dynamic friction, μ_{crutch}

where each one of the parameters is described in Section 3.1.2, and n_e is the number of contact elements (spring and damper units) in the human model.

For crutch-orthosis-assisted predictions in Chapter 6, the following quantities are included as parameters in the prediction problem:

- The cycle time duration, T_c
- The duration of multiple support phase (percentage of cycle time), p_{ms}
- The duration of foot swing phase (percentage of cycle time), p_{swf}
- The duration of crutch swing phase (percentage of cycle time), p_{swc}
- The stride length, L_s

Each variable in the problem (state, control and parameter) is bounded by a minimum and a maximum value, that in the case of state and control correspond to the minimum and maximum value of the experimental quantity, respectively, ± a tolerance value. State and control tolerances for each problem formulation are given in Appendix C. Bounds for parameters are given in each chapter where they are used (Chapters 4 and 6). Moreover, variables are scaled to facilitate the problem solution. The scaling factors are applied to basic magnitudes: mass, length, angle, time. And from them, all the other magnitudes are scaled consistently: e.g., linear velocity scaling factor = length scaling factor / time scaling factor (see Appendix D).

Cost function

The general cost function (Eq. 3.15) is formed by four types of terms, that are function of the state $\mathbf{x}$ and the control $\mathbf{u}$ of the problem: (1) tracking terms, $J_{track,i}(\mathbf{x},\mathbf{u})$, that minimise the error between a magnitude of the simulation and the corresponding experimental value; (2) optimality terms, $J_{opt,j}(\mathbf{x},\mathbf{u})$, that minimise a magnitude that is considered an optimality criterion in human walking; (3) regularisation terms, $J_{reg,k}(\mathbf{x},\mathbf{u})$, that may not be related to a physiologic criterion, but help the problem to converge to an optimal solution; and (4) penalty terms, $J_{pen,l}(\mathbf{x},\mathbf{u})$, that avoid undesirable features. The cost function can include none, one or more terms of each type:

$$J = \int_{t_0}^{t_f} \Big(\sum_i w_i J_{track,i}(\mathbf{x},\mathbf{u}) + \sum_j w_j J_{opt,j}(\mathbf{x},\mathbf{u}) + \sum_k w_k J_{reg,k}(\mathbf{x},\mathbf{u}) + \sum_l w_l J_{pen,l}(\mathbf{x},\mathbf{u}) \Big) \mathrm{d}t \tag{3.15}$$

where t_0 and t_f are the initial and final times of the simulation; and w_i, w_j, w_k and w_l are weights that multiply each one of the terms in the cost function (equal to one if it is not specified any other value). Each term is scaled before being multiplied by each weighting factor (see Appendix D).

In pure tracking problems (Chapter 4), tracking and regularisation terms are included; in pure prediction problems (Chapter 5), optimality and regularisation terms are included; and in prediction with tracking (Chapter 6), all types of terms are included.

Dynamic constraints

Since the implicit form of the dynamics is used (equations of motion are introduced as path constraints), dynamic constraints are simple time derivative relations of the optimal control problem variables:

$$\frac{\mathrm{d}\mathbf{x}}{\mathrm{d}t} = \dot{\mathbf{x}} \tag{3.16}$$

For instance, if the state vector, $\mathbf{x}$, is formed by the vector of generalised coordinates, $\mathbf{q}$, and the vector of generalised velocities, $\dot{\mathbf{q}}$, the dynamic constraints are the following:

$$\frac{\mathrm{d}\mathbf{q}}{\mathrm{d}t} = \dot{\mathbf{q}}, \quad \frac{\mathrm{d}\dot{\mathbf{q}}}{\mathrm{d}t} = \ddot{\mathbf{q}}. \tag{3.17}$$

Path constraints

In order to introduce equations of motion as path constraints, an IDA is performed at each iteration, and the system kinematic state is used to calculate the net forces and torques applied to each DOF. The inputs of this IDA are the variables of the optimal control problem ($\mathbf{q}, \dot{\mathbf{q}}$ and $\ddot{\mathbf{q}}$), and also the ground reaction forces (that can be the experimentally measured ground reactions, $\mathbf{GRF}_{exp}$, the control variables ground reactions, $\mathbf{GRF}_u$, or the ground reactions computed through the contact models, $\mathbf{GRF}_{CM}$). The residual wrench in the pelvis $\mathbf{R}_{pelvis} = [F_x \quad F_y \quad F_z \quad M_x \quad M_y \quad M_z]^{\mathrm{T}}$ is constrained to be close to zero. Moreover, if joint torques $\boldsymbol{\tau}$ are variables of the optimal control problem, they are forced to be the same as joint torques obtained from OpenSim, $\boldsymbol{\tau}_{IDA}$. Finally, if ground reactions are used as controls in the problem, $\mathbf{GRF}_u$, they are forced to be zero during swing. This is done by multiplying each control variable by a vector of zeros and ones that defines the swing (0) and stance (1) phase for each foot (and crutch).

The different path constraints considered in this work are the following:

- Residual forces and moments: To obtain a dynamically consistent motion, the residual forces and moments acting on the pelvis, $\mathbf{R}_{pelvis}$, are limited within a specific tolerance.

  $$-\boldsymbol{\varepsilon}_R \leq \mathbf{R}_{pelvis}(\mathbf{q}, \dot{\mathbf{q}}, \ddot{\mathbf{q}}) \leq \boldsymbol{\varepsilon}_R, \tag{3.18}$$

  being $\boldsymbol{\varepsilon}_R \in \mathbb{R}^6$ the vector defining the specific tolerance.

- Joint torques: If joint torques are variables (states or controls) of the optimal control problem, $\boldsymbol{\tau}$, they are forced to be the same as joint torques obtained

from IDA in OpenSim, $\boldsymbol{\tau}_{IDA}$.

$$-\boldsymbol{\varepsilon}_{\tau} \leq \boldsymbol{\tau} - \boldsymbol{\tau}_{IDA}(\mathbf{q}, \dot{\mathbf{q}}, \ddot{\mathbf{q}}) \leq \boldsymbol{\varepsilon}_{\tau}, \tag{3.19}$$

being $\boldsymbol{\varepsilon}_{\tau} \in \mathbb{R}^{n_q-6}$ the vector defining the specific tolerance.

- Ground reaction forces: If a contact model is used, ground reactions controls, $\mathbf{GRF}_u$, are forced to be the same as ground reactions calculated using the contact models, $\mathbf{GRF}_{CM}$.

$$-\boldsymbol{\varepsilon}_{GRF} \leq \mathbf{GRF}_u - \mathbf{GRF}_{CM}(\mathbf{q}, \dot{\mathbf{q}}) \leq \boldsymbol{\varepsilon}_{GRF}, \tag{3.20}$$

  being $\boldsymbol{\varepsilon}_{GRF} \in \mathbb{R}^{n_{GRF}}$ the vector defining the specific tolerance, where n_{GRF} is the number of components of ground reactions that are included in these path constraints. Since ground reactions controls define when each foot (or crutch) is either in swing phase or stance phase, ground reactions calculated using the contact model fulfil the condition of being zero during swing, so that no contact of the foot (or crutch) with the ground is possible during swing.

- Feet crossing: To avoid feet lateral crossing, the lateral distance between the midpoint of each foot is bounded.

- Non-sliding: To avoid sliding during stance, the value of the velocity of the midpoint of the foot is bounded during stance phase.

The values given to each tolerance ($\boldsymbol{\varepsilon}_R$, $\boldsymbol{\varepsilon}_{\tau}$ and $\boldsymbol{\varepsilon}_{GRF}$) are specified in each section. Note that these tolerances permit a difference between zero and residuals, between joint torques controls and joint torques from IDA, and between ground reaction controls and ground reactions computed from the contact model. In any case, the real values of residual loads, joint torques, and ground reactions are the ones obtained from the contact model and from the ID analysis using those ground reactions.

Endpoint constraints

The endpoint constraints evaluate state values at the initial and final times of the simulation. The different endpoint constraints considered in this work are the following:

- Initial feet position: The initial and/or final feet (and crutch, if applies) position can be imposed (within a certain tolerance), to help the problem to converge with a natural initial pose.

- Stride length: The total traveled distance in a cycle in anterior-posterior direction of the midpoint of each foot (and crutch, if applies) is imposed to be equal to the stride length (within a certain tolerance). The stride length can be a known value or a parameter of the optimisation.

- Periodicity: Periodicity can be imposed to the coordinates and the ground reactions computed from the model.

In each section, it is specified which constraints are used and what tolerances are considered in each case.

Boundary conditions

Initial and terminal times, as well as states evaluated at initial and terminal times, are bounded within a minimum and a maximum values. Therefore, boundary conditions are:

$$t_{0,min} \leq t_0 \leq t_{0,max} \tag{3.21}$$

$$t_{f,min} \leq t_f \leq t_{f,max}, \tag{3.22}$$

$$\mathbf{x}_{exp_0} - \boldsymbol{\varepsilon}_x \leq \mathbf{x}(t_0) \leq \mathbf{x}_{exp_0} + \boldsymbol{\varepsilon}_x, \tag{3.23}$$

$$\mathbf{x}_{exp_f} - \boldsymbol{\varepsilon}_x \leq \mathbf{x}(t_f) \leq \mathbf{x}_{exp_f} + \boldsymbol{\varepsilon}_x, \tag{3.24}$$

where $\mathbf{x}_{exp_0}$ and $\mathbf{x}_{exp_f}$ are the initial and final values of the experimental quantities that correspond to the states of the problem, and $\boldsymbol{\varepsilon}_x \in \mathbb{R}^{n_x}$ is the vector defining the specific tolerance (see Appendix C).

For instance, if the state vector, $\mathbf{x}$, is formed by the vector of generalised coordinates, $\mathbf{q}$, and the vector of generalised velocities, $\dot{\mathbf{q}}$:

$$\mathbf{x}_{exp_0} = \begin{bmatrix} \mathbf{q}_{exp}(t_0) \\ \dot{\mathbf{q}}_{exp}(t_0) \end{bmatrix}, \quad \mathbf{x}_{exp_f} = \begin{bmatrix} \mathbf{q}_{exp}(t_f) \\ \dot{\mathbf{q}}_{exp}(t_f) \end{bmatrix} \tag{3.25}$$

Chapter 4

Dynamically consistent tracking of motion

This thesis focuses on implementing a predictive optimal control framework to obtain dynamically consistent (DC) assisted walking motions. However, before we are able to predict new motions, a first step is to develop a framework using a 3D full-body model with technical assistive devices that tracks experimental data using an optimal control formulation and ensures dynamic consistency. For such complex system, this optimal control problem (OCP) formulation is challenging and needs to be explored before we can move forward to generating novel motion predictions.

We understand for dynamically consistent walking motion a movement with all residual loads acting on the pelvis being below a small tolerance [36, 37, 50]. This is important because, due to error introduced during the experimental data collection and modelling assumptions, the total external reactions computed from motion equations do not coincide with the experimental ground reaction forces; and thus, the external wrench applied to the pelvis (base body) is not zero. By tracking an experimental walking motion, and allowing small variations in motion and forces, the residuals can be reduced to obtain a dynamically consistent motion. Then, this movement will be used as an initial guess for the prediction problem.

In this chapter, an optimal control framework that tracks experimental data and ensures dynamic consistency is developed and applied to three models, from less to more complexity: two unassisted models (3D with head-arms-trunk (HAT) segment, and 3D full-body), and a 3D full-body model assisted by crutches. In Section 4.1, we have as a main objective to determine the best formulation that generates dynamically consistent walking motions by solving a tracking problem, without foot- or crutch-ground contact models. In Section 4.2, foot- and crutch-ground contact models are calibrated tracking experimental motions. Finally, in Section 4.3, results obtained in Sections 4.1 and 4.2 are used to generate full dynamically consistent walking cycles, using previously calibrated foot- and crutch-ground contact models.

4.1 Comparison of formulations for dynamically consistent tracking of motion

As a first step toward prediction of novel walking motions, in this section we explore how optimal control problem formulation affects the ability to generate dynamically consistent normal and assisted walking simulations that closely reproduce experimental data. To identify the most efficient and robust optimal tracking problem formulation for walking, we have addressed the following research questions related to the problem formulation:

1. Is it possible to achieve tracking joint coordinates a solution with better convergence and similar accuracy than tracking experimental marker coordinates?
2. Should both motion and ground reaction forces be adjusted to obtain a dynamically consistent solution or only motion is enough?
3. Is it joint acceleration advantageous over joint jerk as control variable in the problem formulation?

4.1.1 Methods

Models and data

Three different models from different complexity have been used in this section: 3D HAT model (*3D HAT*), 3D full-body model (*3D Full*), and 3D full-body model assisted by crutches (*3D Crutches*). All models have been described in Section 3.1.1. In the *3D Crutches* model, crutches have been modelled attached to forearm segment. For the unassisted models (i.e., without crutches), the *shoes* experimental capture (described in Section 3.2) has been used. For the crutch-assisted model, the non-alternating four-point capture has been used (see Section 3.2).

Optimal control problem formulation

To find the best formulation for dynamically consistent tracking of motion, eight different optimal control problem formulations have been studied (see Table 4.1). All problems involve combinations of tracking marker coordinates versus tracking joint coordinates, tracking ground reactions (foot-ground reaction forces and moments, and crutch-ground reaction forces, if applies) versus not tracking them, and minimising joint acceleration versus joint jerk. Minimising joint acceleration or jerk were employed in previous works that predicted human walking motions [27, 50, 123].

Variables
States and controls depend on the formulation and case used (see Table 4.1). For instance, in formulations C1 and D1, where joint acceleration is minimised, and ground reactions are included as controls, the state vector $\mathbf{x} \in \mathbb{R}^{2n_q}$ is formed

by the vector of generalised coordinates $\mathbf{q}$ and the vector of generalised velocities $\dot{\mathbf{q}}$, being n_q the number of joint coordinates in the model. The control vector $\mathbf{u} \in \mathbb{R}^{n_q+n_{GRF}}$ is formed by the vector of generalised accelerations $\ddot{\mathbf{q}}$ and the vector of ground reaction forces and moments $\mathbf{GRF}_u$, being n_{GRF} the number of ground reactions in the model:

$$\mathbf{x} = \begin{bmatrix} \mathbf{q} \\ \dot{\mathbf{q}} \end{bmatrix} \tag{4.1}$$

$$\mathbf{u} = \begin{bmatrix} \ddot{\mathbf{q}} \\ \mathbf{GRF}_u \end{bmatrix} \tag{4.2}$$

Formulation	Track	Minimise	States	Controls
A1	Marker coordinates	Joint acc.	$\mathbf{q}$, $\dot{\mathbf{q}}$	$\ddot{\mathbf{q}}$
A2		Joint jerk	$\mathbf{q}$, $\dot{\mathbf{q}}$, $\ddot{\mathbf{q}}$	$\dddot{\mathbf{q}}$
B1	Joint coordinates	Joint acc.	$\mathbf{q}$, $\dot{\mathbf{q}}$	$\ddot{\mathbf{q}}$
B2		Joint jerk	$\mathbf{q}$, $\dot{\mathbf{q}}$, $\ddot{\mathbf{q}}$	$\dddot{\mathbf{q}}$
C1	Marker coordinates + Ground reactions	Joint acc.	$\mathbf{q}$, $\dot{\mathbf{q}}$	$\ddot{\mathbf{q}}$, GRF_u
C2		Joint jerk	$\mathbf{q}$, $\dot{\mathbf{q}}$, $\ddot{\mathbf{q}}$	$\dddot{\mathbf{q}}$, GRF_u
D1	Joint coordinates + Ground reactions	Joint acc.	$\mathbf{q}$, $\dot{\mathbf{q}}$	$\ddot{\mathbf{q}}$, GRF_u
D2		Joint jerk	$\mathbf{q}$, $\dot{\mathbf{q}}$, $\ddot{\mathbf{q}}$	$\dddot{\mathbf{q}}$, GRF_u

Table 4.1: Description of the eight different formulations that have been compared in this study. Variables correspond to joint coordinates ($\mathbf{q}$), joint velocities ($\dot{\mathbf{q}}$), joint accelerations ($\ddot{\mathbf{q}}$), joint jerks ($\dddot{\mathbf{q}}$) and ground reactions (foot-ground forces and moments and crutch-ground forces, if applies) ($\mathbf{GRF}_u$).

Cost function

The general cost function can be described as the addition of one or two tracking terms and a regularisation term:

$$J_{F,c} = \int_{t_0}^{t_f} \Big(J_{track,F}(\mathbf{x}, \mathbf{u}) + J_{reg,c}(\mathbf{x}, \mathbf{u}) \Big) \mathrm{d}t \tag{4.3}$$

where t_0 and t_f are the initial and final times of the simulation; $F = [A, B, C, D]$ a subscript to indicate tracking terms and $c = [1, 2]$ a subscript to indicate the regularisation term used.

Formulations A track marker coordinates, formulations B track joint coordinates, formulations C track marker coordinates and ground reactions, and formulations D track joint coordinates and ground reactions. Thus, the possible tracking terms to be considered in the cost function are:

$$J_{track,A}(\mathbf{x},\mathbf{u}) = \sum_{i=1}^{3n_m}(m_i - m_{exp_i})^2 \tag{4.4}$$

$$J_{track,B}(\mathbf{x},\mathbf{u}) = \sum_{i=1}^{n_q}(q_i - q_{exp_i})^2 \tag{4.5}$$

$$J_{track,C}(\mathbf{x},\mathbf{u}) = \sum_{i=1}^{3n_m}(m_i - m_{exp_i})^2 + \sum_{i=1}^{n_{GRF}}(GRF_{u_i} - GRF_{exp_i})^2 \tag{4.6}$$

$$J_{track,D}(\mathbf{x},\mathbf{u}) = \sum_{i=1}^{n_q}(q_i - q_{exp_i})^2 + \sum_{i=1}^{n_{GRF}}(GRF_{u_i} - GRF_{exp_i})^2 \tag{4.7}$$

being n_m the number of markers; m_i the i^{th} component of the vector of marker coordinates $\mathbf{m}$; q_i the i^{th} component of the vector of generalised coordinates $\mathbf{q}$; GRF_{u_i} is the i^{th} component of the vector of ground reactions $\mathbf{GRF}_u$. Subscript *exp* indicates an experimental value: experimental marker coordinates and ground reactions are measured directly, while experimental joint coordinates are obtained from an IK analysis performed in OpenSim using experimental marker coordinates as inputs of the problem.

For each of the four problem formulations (A to D), we study two cases: one case uses joint accelerations as controls and minimise them in the cost function (case 1), while the other case uses joint jerks as controls, minimise them in the cost function, and adds joint accelerations as an additional state (case 2). Thus, the possible regularisation terms to be considered in the cost function are:

$$J_{reg,1}(\mathbf{x},\mathbf{u}) = \sum_{i=1}^{n_q}\ddot{q}_i^2 \tag{4.8}$$

$$J_{reg,2}(\mathbf{x},\mathbf{u}) = \sum_{i=1}^{n_q}\dddot{q}_i^2 \tag{4.9}$$

being $\ddot{q}_i$ and $\dddot{q}_i$ the i^{th} component of the vector of generalised accelerations $\ddot{\mathbf{q}}$ and joint jerk $\dddot{\mathbf{q}}$, respectively.

Dynamic constraints

Dynamic constraints are the ones described in Eq. 3.16, adapted to the states of the problem in each case (see Table 4.1).

Path constraints

Only one type of path constraint is considered for all formulations. It is to reduce residual forces and moments, as shows Eq. 3.18, being $\boldsymbol{\varepsilon}_R \in \mathbb{R}^6$ a vector of a specific tolerance, that has been defined as the ±5% or ±50% of the root

mean square (RMS) of the experimental (or initial) residual loads components. The problems where the first tolerance value is imposed are considered as "full residual reduction" (95% residual reduction) and the problems where the second tolerance value is imposed are considered as "half residual reduction" (50% residual reduction).

An inverse dynamic analysis (IDA) is performed at each iteration, and the system kinematic state is used to calculate the net forces and torques applied to each degree of freedom (DOF). In formulations A and B, the experimentally measured ground reactions are applied directly to the model. In formulations C and D, additional controls representing the ground reactions are applied to the model, and these controls track the experimental ground reaction measurements. This approach allows for slight adjustments in the ground reactions to account for measurement errors and to facilitate obtaining a dynamically consistent walking motion.

Boundary conditions

The initial and final time of the simulation are imposed from the experimental values:

$$t_0 = t_{exp_0}, \quad t_f = t_{exp_f}, \tag{4.10}$$

Boundary conditions are the ones described in Eq. 3.23.

Considered results

To compare the different formulations, we have calculated several metrics for each level of pelvis residual reduction. These metrics include the number of iterations and the computational time needed to reach each optimal solution, and the root-mean-square error (RMSE) between predicted values (marker coordinates, joint coordinates, and ground reaction forces and moments) and corresponding experimental values. Experimental marker coordinates and ground reactions are measured directly, while experimental joint coordinates are obtained from an inverse kinematic analysis (IKA) performed in OpenSim using the experimental marker coordinates. RMSE are computed resampling experimental data to the solution time steps.

4.1.2 Results

The optimal control formulations without ground reactions adjustment (A and B), have converged for models *3D HAT* and *3D Full*, but have not for model *3D Crutches*. This is why two residual reduction tolerances have been considered for this latter model: half ($\varepsilon_R = \pm 50\%$) and full ($\varepsilon_R = \pm 5\%$) residual reduction. Results for all formulations and residual reduction tolerances that have converged can be found in Tables E.1 to E.4 in Appendix E. In general and for all models, less iterations are needed when tracking joint coordinates compared with tracking marker coordinates, when ground reactions are not adjusted compared with when they are, and when residuals are reduced to the half of the experimental root-mean-square (RMS) compared with when they are totally reduced (see Table 4.2). For

the optimisations that have converged, residual forces and moments are lower for formulations that tracked joint coordinates and minimised joint jerk (B2 and D2) in *3D HAT* and *3D Full* models. However, this does not hold for the *3D Crutches* model. Apart from this, there is no remarkable difference in the reduction of residuals among formulations, that is, they are reduced to the imposed tolerance levels in all cases.

Model		3D HAT	3D Full	3D Crutches	
Number of markers		28	36	44	
Marker coordinates		84	108	132	
Joint coordinates		23	37	31	
Residual reduction		Full	Full	Half	Full
Number of iterations (time |s|)	A1	202 (57)	243 (129)	393 (354)	-
	A2	120 (45)	255 (182)	266 (326)	-
	B1	18 (6)	18 (11)	59 (60)	-
	B2	44 (17)	43 (32)	46 (63)	-
	C1	864 (302)	943 (661)	540 (585)	1895 (1920)
	C2	452 (202)	569 (466)	584 (816)	1533 (1973)
	D1	61 (22)	80 (51)	66 (79)	100 (116)
	D2	157 (71)	149 (123)	66 (102)	158 (231)

Table 4.2: Number of markers, marker coordinates (x, y, z components per each marker) and joint coordinates of each model; and number of iterations and time in seconds for each formulation and case to converge to an optimal solution. Results for unassisted models are shown for the case of full residual reduction, and results for the *3D Crutches* model are shown for half and full residual reduction. Note that the *3D Full* model has more joint coordinates than the *3D Crutches* model; this is because the model used in these simulations has the crutches attached to forearm, so there is no pronation-supination, wrist flexion and wrist deviation motion.

Tracking marker coordinates or joint coordinates

For the *3D HAT* model, convergence is better for formulations B than A (18-44 iterations compared to 120-202 iterations), and it is also better for formulations D than C (61-157 iterations compared to 452-864 iterations). This trend can be observed also in results for models *3D Full* and *3D Crutches*, for the latter both in the half and full residual reduction cases (see Table 4.2).

Mean RMSE are in general lower for those (marker or joint) coordinates that are tracked (see Table 4.3). For *3D HAT* model, mean RMSE for linear joint coordinates vary from 0.49 to 0.61 cm when they are tracked (formulations B and D), and vary from 0.68 to 1.04 cm when they are not tracked (formulations A and C). Mean RMSE for angular joint coordinates vary from 2.61 to 3.42° when they are tracked, and vary from 6.78 to 8.14° when they are not tracked. This trend can be also observed in results for models *3D Full* (Figure 4.2 and Table 4.3) and *3D Crutches*, both in the half and full residual reduction cases (Tables E.3 and E.4).

For *3D Crutches* model, mean RMSE for marker coordinates when they are tracked (formulations A and C) are lower than when they are not tracked (formulations B and D); being always these errors higher when ground reactions are not adjusted. On the contrary, for *3D HAT* and *3D Full* models, mean RMSE of marker coordinates is slightly higher when tracking marker coordinates compared to tracking joint coordinates (A vs B, and C vs D) (Figure 4.1 and Table 4.3). Regarding ground reactions, when they are adjusted (formulations C and D), errors are in general larger when tracking marker coordinates (for *3D HAT* model, 2.37-2.80 N and 0.46-0.70 Nm) compared to tracking joint coordinates (for *3D HAT* model, 0.85-2.03 N and 0.32-0.70 Nm). This trend is also observed in models *3D Full* and *3D Crutches* (Table 4.4).

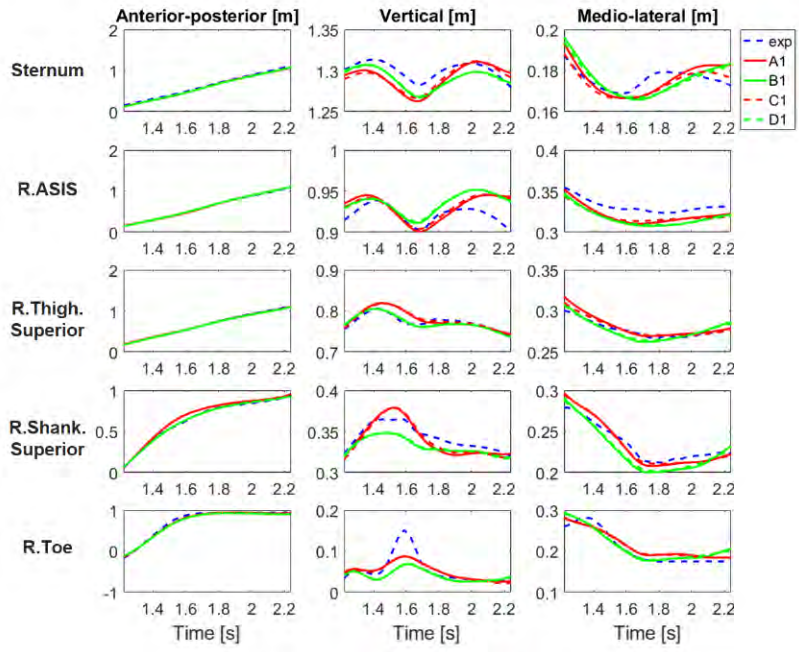

Figure 4.1: Representative marker coordinates – anterior-posterior (x), vertical (y), and medio-lateral (z) – for the *3D HAT* model. In dashed blue, measured marker trajectories (exp); in red, formulations that track marker coordinates (A1 and C1) and in green, formulations that track joint coordinates (B1 and D1). In solid line, formulations without ground reaction adjustments (A1 and B1) and in dashed line, formulations with ground reaction adjustments (C1 and D1). Only results for case 1 (minimise joint acceleration) are shown.

Minimising joint acceleration or joint jerk

Comparing minimising joint jerk versus minimising joint accelerations, differences in terms of number of iterations and computation time depend on whether

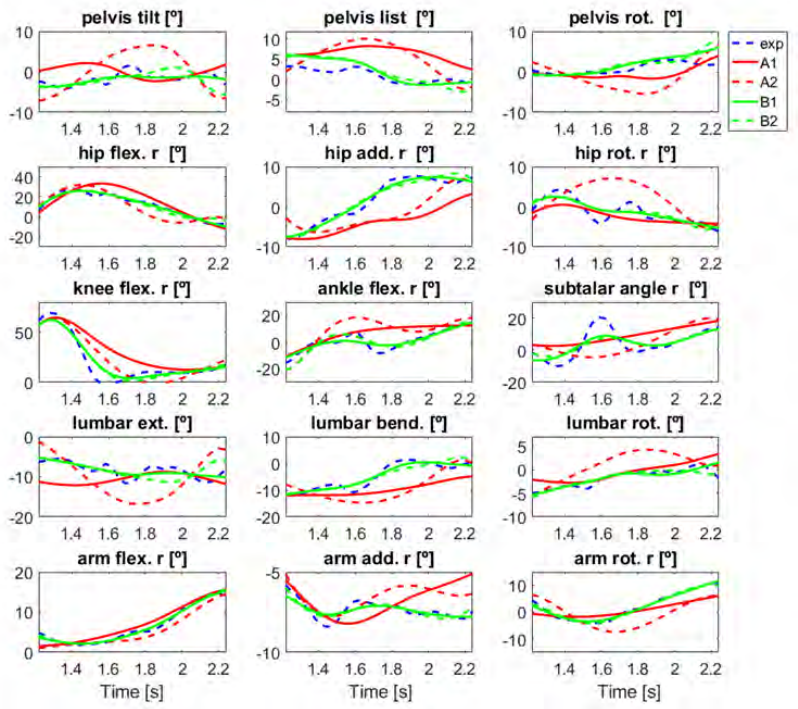

Figure 4.2: Evolution of representative coordinates of the *3D Full* model. In dashed blue, measured marker trajectories (exp); in red, formulations that track marker coordinates (A1 and A2) and in green, formulations that track joint coordinates (B1 and B2). In solid line, formulations that minimise joint acceleration (A1 and B1) and in dashed line, formulations that minimise joint jerk (A2 and B2). "Subtalar angle" refers to ankle dorsiflexion. "Arm" flexion (flex.), adduction (add.) and rotation (rot.) are shoulder flexion, adduction, and rotation, respectively. Only results for formulations without ground reaction adjustments are shown.

marker coordinates or joint coordinates are tracked. When tracking marker coordinates, minimising joint jerk requires in general less iterations and computation time than minimising joint accelerations. When tracking marker coordinates, minimising joint jerk requires more iterations and computation time (see Table 4.2). This is true for the cases with and without ground reaction adjustment, and the trend is more evident for unassisted models (*3D HAT* and *3D Full*).

Adjusting ground reactions or not

For the three models, adjusting ground reactions requires more iterations and computation time than not adjusting them (Table 4.2). For the *3D HAT* model, if formulations C are compared to formulations A (that is, formulations that track marker coordinates), and formulations D are compared to B (that is, formulations

		3D HAT		3D Full	
Formulation	RMSE	Min acc. (1)	Min jerk (2)	Min acc. (1)	Min jerk (2)
A (track m)	Marker coord. [cm]	1.71 ± 0.90	1.72 ± 0.82	1.58 ± 0.90	1.57 ± 0.81
	Joint coord. [cm]	0.86 ± 0.21	1.04 ± 0.34	0.79 ± 0.29	0.90 ± 0.28
	Joint coord. [°]	6.78 ± 4.06	8.14 ± 3.59	4.85 ± 4.03	5.95 ± 3.90
B (track q)	Marker coord. [cm]	1.58 ± 0.82	1.63 ± 0.74	1.46 ± 0.75	1.47 ± 0.67
	Joint coord. [cm]	0.56 ± 0.15	0.61 ± 0.09	0.55 ± 0.16	0.63 ± 0.06
	Joint coord. [°]	2.64 ± 1.94	3.42 ± 1.99	1.78 ± 1.86	2.22 ± 2.14
C (track m, adjust GRF)	Marker coord. [cm]	1.62 ± 0.90	1.60 ± 0.83	1.46 ± 0.91	1.42 ± 0.83
	Joint coord. [cm]	0.68 ± 0.29	0.96 ± 0.36	0.54 ± 0.24	0.83 ± 0.33
	Joint coord. [°]	6.88 ± 4.06	8.02 ± 3.70	5.01 ± 3.93	6.02 ± 3.85
D (track q, adjust GRF)	Marker coord. [cm]	1.51 ± 0.82	1.54 ± 0.71	1.38 ± 0.76	1.37 ± 0.67
	Joint coord. [cm]	0.49 ± 0.10	0.55 ± 0.09	0.48 ± 0.10	0.55 ± 0.08
	Joint coord. [°]	2.61 ± 1.96	3.38 ± 2.02	1.76 ± 1.87	2.20 ± 2.15

Table 4.3: Mean and standard deviation of RMSE of marker and joint coordinates for each formulation and for each unassisted model (*3D HAT*, *3D Full*). Results are shown for full residual reduction tolerance. Mean and standard deviation of RMSE of each magnitude are shown in black when this magnitude is tracked in the formulation, and in grey when it is not.

that track joint coordinates), formulations that adjust ground reactions require 3 to 4 more times of iterations (e.g., 202 iterations (A1) vs 864 iterations (C1)). For the *3D Full* model, formulations that adjust ground reactions require 2 to 4.5 more times of iterations, compared to formulations that do not adjust them (e.g., 243 iterations (A1) vs 943 iterations (C1)). And finally, for the *3D Crutches* model, formulations C and D, compared to A and B, respectively, require 1.1 to 2.2 more times of iterations (e.g., 393 iterations (A1) vs iterations 540 (C1)). As said previously, errors in ground reactions are in general larger when tracking marker coordinates compared to tracking joint coordinates (see Table 4.4), being the lowest mean RMSE for forces and moments for case D1 for all three models.

For the *3D Crutches* model, ground reaction adjustments are required if a dynamically consistent motion with residual values close to zero has to be found. In general, the number of iterations (and consequently computation time) is larger for the full residual reduction when compared with half residual reduction for the same formulation (Table 4.2). There is practically no difference in terms of mean RMSE for marker coordinates and angular joint coordinates for half residual reduction, compared to full residual reduction (Tables E.3 and E.4). For formulations D, the mean RMSE of linear joint coordinates is larger in the case of full residual reduction (0.80 cm for both cases 1 and 2) compared to half residual reduction (0.57 cm and 0.56 cm for cases 1 and 2, respectively). For the same formulations, the mean RMSE for ground reaction forces (GRFs) and ground reaction moments (GRMs) for half residual reduction are 1.30 N and 0.26 Nm for both cases 1 and 2. For full residual reduction, the mean RMSE for ground reaction forces (GRFs) are 1.62 and 1.63 N larger than those obtained for half residual reduction using the same formulation, and for GRMs, that difference is of 0.22 Nm .

		Track marker		Track joint coordinates	
Model	RMSE (mean ± std)	Min acc. C1	Min jerk C2	Min acc. D1	Min jerk D2
3D HAT	GRFs [N]	2.37 ± 0.62	2.80 ± 1.16	0.85 ± 0.28	2.03 ± 2.04
	GRMs [Nm]	0.46 ± 0.20	0.70 ± 0.39	0.32 ± 0.28	0.70 ± 0.61
3D Full	GRFs [N]	2.60 ± 0.75	2.85 ± 1.11	0.77 ± 0.31	1.96 ± 1.90
	GRMs [Nm]	0.61 ± 0.42	0.74 ± 0.45	0.35 ± 0.33	0.74 ± 0.62
3D Crutches	GRFs [N]	3.41 ± 2.21	3.39 ± 2.20	2.92 ± 1.98	2.93 ± 1.98
	GRMs [Nm]	1.00 ± 0.09	1.00 ± 0.08	0.48 ± 0.03	0.48 ± 0.02

Table 4.4: Mean and standard deviation (std) of RMSE of GRFs and GRMs for each formulation and model. Results are shown for full residual reduction tolerance.

4.1.3 Discussion

Convergence is always better when joint rather than marker coordinates are tracked. It is not surprising that tracking markers is more difficult in terms of convergence. For this case, at each optimiser iteration, values are given for all joint coordinates and then model marker coordinates are computed from these values and compared with experimental marker coordinates. Additionally, there are more marker coordinates than joint coordinates in each model (see Table 4.2). While it is true that tracking joint coordinates is easier, we also wanted to check whether accurate tracking of joint coordinates would result in accurate tracking of marker coordinates. If not, then we could consider tracking marker coordinates despite its higher computational cost. For this purpose, we have computed RMSE for coordinates that are not being tracked for each formulation (Tables Tables E.1 to E.4). Surprisingly, for *3D HAT* and *3D Full* models, mean RMSE both for marker and joint coordinates are lower when joint coordinates are tracked, whereas mean RMSE both for marker and joint coordinates are higher when marker coordinates are tracked (Table 4.3). For *3D Crutches* model, in formulations with ground reaction adjustments, mean RMSEs for marker coordinates are slightly lower when tracking marker coordinates compared to tracking joint coordinates (comparing for the same residual reduction tolerance, and for the same case (1 or 2)). In contrast, mean RMSE for angular joint coordinates is almost two times larger when tracking marker coordinates compared to tracking joint coordinates (comparing for the same residual reduction tolerance, and for the same case (1 or 2)). These results suggest that close tracking of joint coordinates results in close tracking of marker coordinates. Furthermore, since tracking joint coordinates requires fewer iterations and takes less computation time, it is preferable to track joint coordinates obtained from an IK analysis performed using experimental marker trajectories.

Our results have not produced a clear answer to whether minimising joint acceleration or joint jerk is better. Based on the number of iterations, there is no clear trend between cases 1 and 2 for each formulation. In general, for *3D HAT* and *3D Full* models, and for formulations tracking marker coordinates (A and C), fewer iterations are needed when minimising joint jerk. On the other hand, for formulations tracking marker coordinates (B and D), fewer iterations are needed

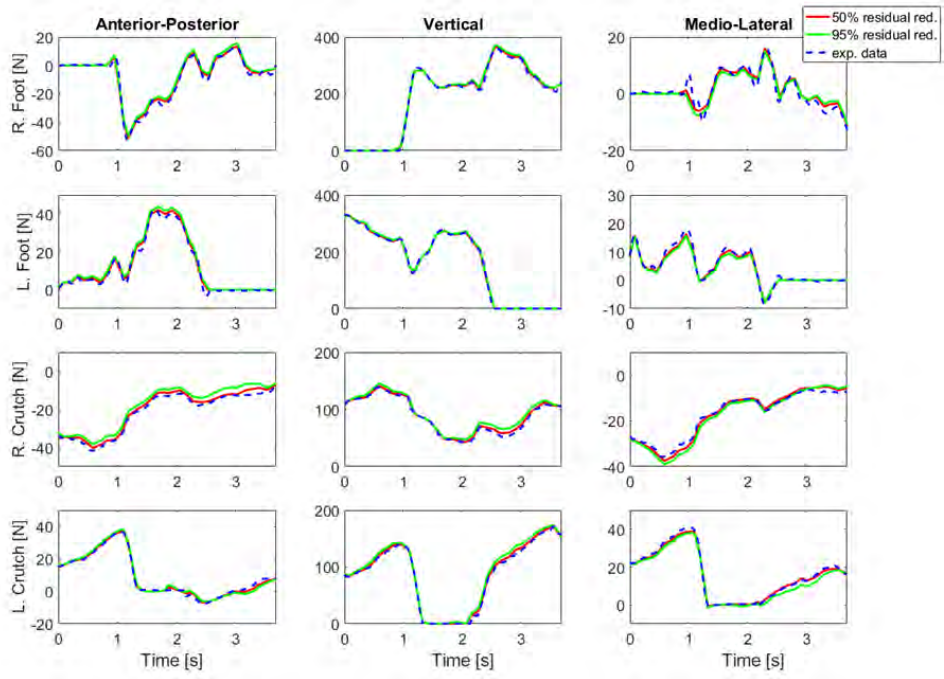

Figure 4.3: Ground reactions (control variables of the problem formulation) for formulation D2 (track joint coordinates, minimise joint jerk and adjust ground reactions), using the *3D Crutches* model. Two levels of residual reduction are shown: half reduction (50%) and full reduction (95%), with respect to the RMS of experimental residual components. "R" and "L" stand for right and left side, respectively.

when minimising joint acceleration. This is not observed for *3D Crutches* model, where we could not find a specific trend. For all models, in general mean RMSE for joint coordinates and ground reactions are lower for minimising joint accelerations, compared to minimising joint jerk. For *3D Crutches* model, these RMSE have similar values for formulations with ground reaction adjustments, both for half and full residual reduction tolerance. In terms of kinematics, simulated joint coordinates obtained from formulations that minimise joint accelerations are smoother than those obtained from formulations that minimise joint jerk (see Figure 4.2). To allow as much non-smoothness as possible, since real humans do not walk with such smooth motions, we have decided to minimise joint jerk rather than joint acceleration.

Based on our results, we suggest that ground reactions should be added as controls to the optimal control problem to maximise tracking accuracy and minimise residuals. For the *3D Crutches* model, the marker and joint coordinate tracking are both more accurate when ground reactions are adjusted (i.e., mean RMSE is lower in formulations C and D compared to formulations A and B), and problem formulations requiring full residual reduction converge only when ground reactions

are added as controls. This difference is lower for models *3D HAT* and *3D Full*, but still RMSE for marker and joint coordinates are lower for all cases (with exception of Formulation C2 for *3D Full* model, where mean RMSE for angular coordinates is slightly higher when adjusting ground reactions). Though formulations A and B without ground reaction adjustment for the *3D Crutches* model are able to converge for full residual reduction as well; they do so only when joint coordinate bounds are increased substantially, resulting in visibly unrealistic motions (e.g., the model walks without the feet contacting the ground). This observation suggests that for full residual reduction, no solution exists with joint coordinate bounds of less than 3 cm and 5° when using formulations A or B. In contrast, if both motion and ground reactions are adjusted, then an optimal solution can be obtained within realistic model coordinate error bounds.

Our computation time and RMSE for joint coordinates are consistent with results found in the literature. Our computation time for the more complex model (*3D Crutches*) varies from 1 to 33 min. In Lin et al. [33], 3 to 5 hours were required to track experimental data for a complete gait cycle using a 3D model with 25 DOFs and 80 muscle-tendon units (MTUs). In Meyer et al. [50], roughly 30 minutes were required for a torque-driven prediction using a 3D model with 37 DOFs. In Shourijeh et al. [139], 45 minutes were needed to obtain muscle forces tracking experimental data using a 3D model with 16 DOFs and 46 muscles. These published studies included muscles in their models or predicted a new motion instead of tracking experimental data, so it is not surprising that they required more time than in our study. Furthermore, the obtained joint coordinate tracking results are consistent with errors reported in the previous studies. For formulation D2 with full residual reduction, the obtained RMSE for joint coordinates are 0.5 cm and 0.8° for linear and angular coordinates, respectively. For same errors, Lin et al. [33] reported 0.5 cm and 1.2°, while Lin et al. [29] reported 0.3 cm and 2°, which are both the same order of magnitude as the computed errors in the formulations that have converged with more accurate results.

Overall, the formulation that has produced better results for all three models in terms of convergence and errors with respect to the experimental values is formulation D2, that tracks joint coordinates, minimises joint jerk and adjusts ground reactions (Table 4.5). It will be used as the starting point for Sections 4.2 and 4.3. This formulation could be improved adding tracking of representative markers (e.g., pelvis and feet markers), and adding path constraints that permit a maximum error per each coordinate and ground reaction component.

	Model		3D HAT	3D Full	3D Crutches
	Exp. motion		shoes	shoes	non-alt. four point
Conv.	Iterations		157	149	158
	Time [s]		70.52	122.80	231.18
RMS	Residual forces [N]	exp. data [N]	15.68	16.72	18.70
		solution [N]	0.30	0.43	1.09
		reduction [%]	98.09	97.43	94.17
	Residual moments [Nm]	exp. data [N]	8.46	7.40	11.68
		solution [N]	0.15	0.17	0.59
		reduction [%]	98.23	97.70	94.95
RMSE	Marker coord. [cm]		1.54	1.37	1.90
	Joint coord. [cm]		0.55	0.55	0.80
	Joint coord. [°]		3.38	2.20	1.60
	GRFs [N]		2.03	1.96	2.93
	GRMs [Nm]		0.70	0.74	0.48

Table 4.5: Results obtained using the three models and the formulation that has produced better results, D2 (track joint coordinates, minimise joint jerk and adjust ground reactions), for full residual reduction. Results shown are number of iterations, computation time, mean of RMS of residual forces and moments (values obtained with the experimental data, values obtained from the solution and percentage of reduction), mean of RMSE of marker and joint coordinates (linear and angular), GRFs (foot- and crutch-ground, if applies) and GRMs (foot-ground).

4.2 Foot-ground and crutch-ground contact model calibration

In human motion prediction, as new motions for which no experimental data is available are found, it is necessary to model the contact interaction between the foot and the ground in order to predict foot-ground contact forces. Usually, the foot-ground contact model establishes the physical relationship between the developed contact forces (normal and tangential) and the relative foot-ground displacements and velocities through a visco-elastic force model [93, 94]. Different approaches that have been used in the literature can be found in Section 2.1.3. Finding a suitable foot-ground contact model for human motion simulation is currently an open research topic [91, 92].

In this section, the foot-ground and crutch-ground contact models presented in Section 3.1.2 are calibrated using optimal control problems that track experimental data. The research questions associated with the contact models calibration are:

1. Is it possible to calibrate all parameters at the same time, or they should be optimised one by one?

2. Is it necessary to calibrate spring-damper positions or they can be previoulsy fixed?

3. Are the values of parameters capture-dependent and/or model-dependent? That is:

    a For the same subject and model, is it possible to calibrate parameter values for one experimental capture and use them for tracking another experimental capture?

    b For the same subject, is it possible to calibrate parameter values for a simpler model (i.e., the *3D HAT* model) and use them for a more complex model (i.e., the *3D Full* and *3D Crutches* models)?

4.2.1 Methods

Models and data

Three different models have been used in this section: *3D HAT*, *3D Full*, and *3D Crutches*, all them described in Section 3.1.1. In the *3D Crutches* model, crutches have been modelled attached to hands, as it has been observed that having the wrist degrees of freedom facilitates to track better the crutch motion, and to calibrate the corresponding crutch-ground contact model reproducing closely the experimental crutch-ground reactions.

Both the *barefoot* and the *shoes* experimental data (described in Section 3.2) have been tracked to calibrate the foot-ground contact parameters of the unassisted models. For the crutch-assisted model, the non-alternating four-point capture has been used (described in Section 3.2).

The foot-ground and crutch-ground contact models used are the ones described in Section 3.1.2. In Table 3.3, information about contact model parameters is summarised: for fixed parameters, the used value is given; for parameters that are optimised through a calibration process, minimum, maximum and initial guess values are also given.

Optimal control problem formulation

The foot-ground and crutch-ground contact model parameters are calibrated using an optimal control problem that tracks experimental data. The problem formulation is based on Formulation D2 presented in Section 4.1. The foot-ground and crutch-ground contact model parameters are variables of the problem, and new constraints ensuring that ground reaction controls equal ground reactions calculated using the corresponding contact model are added.

Variables

The state vector $\mathbf{x} \in \mathbb{R}^{3n_q}$ is formed by the vector of generalised coordinates of the model $\mathbf{q}$, the vector of generalised velocities $\dot{\mathbf{q}}$, and the vector of generalised accelerations $\ddot{\mathbf{q}}$. The control vector $\mathbf{u} \in \mathbb{R}^{n_q+n_{GRF}}$ is formed by the vector of generalised jerk $\dddot{\mathbf{q}}$ and the vector of ground reaction forces and moments $\mathbf{GRF}_u$, that includes foot-ground reactions (and crutch-ground reactions for the *3D Crutches* model):

$$\mathbf{x} = \begin{bmatrix} \mathbf{q} \\ \dot{\mathbf{q}} \\ \ddot{\mathbf{q}} \end{bmatrix} \tag{4.11}$$

$$\mathbf{u} = \begin{bmatrix} \dddot{\mathbf{q}} \\ \mathbf{GRF}_u \end{bmatrix} \tag{4.12}$$

The contact model parameter values have been calibrated in a process step by step (described in Table 4.6), starting from a problem where only one parameter is calibrated (for each of the spring and damper units). Then, using as initial guess that solution, a second parameter is added to the optimisation, and the process is repeated until all the contact model parameters are included in the problem. The complete parameter vector is:

$$\mathbf{s} = \begin{bmatrix} \mathbf{K} \\ \mathbf{c} \\ \boldsymbol{\mu} \\ K_n \\ \chi \\ \mu_{crutch} \end{bmatrix} \tag{4.13}$$

being each parameter described in Table 3.3. The spring stiffnesses vector $\mathbf{K}$, the generalised stiffness K_n and the hysteresis damping factor χ have a scaling factor

of 10^{-4}.

Cost function

The general cost function is based on Formulation D2 in Section 4.1:

$$J = \int_{t_0}^{t_f} \Big(\sum_{i=1}^{n_q} (q_i - q_{exp_i})^2 + \sum_{i=1}^{n_{GRF}} (GRF_{u_i} - GRF_{exp_i})^2 + \sum_{i=1}^{n_q} \dddot{q}_i^2 \Big) \mathrm{d}t \qquad (4.14)$$

being t_0 and t_f the initial and terminal times of the optimal control problem; n_q the number of joint coordinates and n_{GRF} the number of tracked ground reactions (that may not be all the ground reactions in the model); q_i and $\dddot{q}_i$ the i^{th} component of the vector of generalised coordinates $\mathbf{q}$ and joint jerk $\dddot{\mathbf{q}}$, respectively; GRF_{u_i} the i^{th} component of the vector of ground reactions $\mathbf{GRF}_u$. Subscript *exp* indicates an experimental value: experimental marker coordinates and ground reactions are measured directly, while experimental joint coordinates are obtained from an IK analysis performed in OpenSim using the experimental marker coordinates.

For *3D HAT* and *3D Full* models, only forces are tracked in the cost function (normal or all forces), depending on the parameters that are optimised (see Table 4.6). For the *3D Crutches* model, all components (foot-ground forces and moments, and crutch-ground forces) are tracked in the cost function. Moreover, when using this latter model, it is necessary to force feet and crutches to be in contact with the ground when they are in the experimental motion. This is done adding a penalty term in the cost function (Eq. 4.14) to avoid values of vertical position of foot midpoints and crutch tips larger than 5 cm during stance phase for each foot and crutch. This term has a weighting factor of 0.01 in the cost function.

Dynamic constraints

Dynamic constraints are the ones in Eq. 3.16, adapted to the states of the problem in this case. That is:

$$\frac{\mathrm{d}\mathbf{q}}{\mathrm{d}t} = \dot{\mathbf{q}}, \quad \frac{\mathrm{d}\dot{\mathbf{q}}}{\mathrm{d}t} = \ddot{\mathbf{q}}, \quad \frac{\mathrm{d}\ddot{\mathbf{q}}}{\mathrm{d}t} = \dddot{\mathbf{q}}. \qquad (4.15)$$

Path constraints

Two types of path constraints are considered in this problem:

- Residual forces and moments: Residual forces and moments are imposed to be below a specific tolerance, as shows equation 3.18. In this problem, residual tolerances are ±RMS from each component of the experimental residual values. It is important to remark that the main objective is not to produce a dynamically consistent motion, but to track as closely as possible motion and forces.

- Ground reaction forces: Ground reactions controls equal ground reactions calculated using the contact model, as shows equation 3.20. For *3D HAT* and *3D Full* models, only forces are tracked in the path constraints (normal or all forces), depending on the parameters that are optimised (see Table 4.6). For the *3D Crutches* model, all forces (foot-ground forces and crutch-ground forces) are tracked in the path constraints, and a more adjusted tolerance is given to some of them, depending on the parameters that are optimised.

  For *3D HAT* and *3D Full* models, the initial values for path constraint tolerances are 30 N for all components; and these values are used for steps 1 to 3 (Table 4.6). The last calibration step has been repeated adjusting these tolerances (from 30 N to 20 N, and then to 10 N, etc) until the last value for which the problem has converged. The optimal solution (states, control and parameters) of one step is used as the initial guess for the following step.

  For *3D Crutches* model, the general values for path constraint tolerances are 200 N for feet normal forces, 100 N for crutches normal forces, and 50 N for tangential forces. In steps 1 and 2, the tolerance values for crutches normal forces are divided by 2. In step 3, also the tolerance values for crutches tangential forces are divided by 2. Finally, in step 4, all path constraint tolerances values are divided by 2. The initial guess for foot-ground contact model parameters in step 4 are the optimal values obtained for *3D HAT* model and *shoes* experimental data. The last calibration step has been repeated adjusting at the same time all tolerances (multiplying by 0.8, 0.6, 0.4, etc) until the last value for which the problem has converged.

Model	Step	Parameters	Cost function	Path constr.
3D HAT 3D Full	1	**K**	N	N
	2	**K, c**		
	3	**K, c, μ**	N,T	N,T
3D Crutches	1	K_n	N,T,M,Nc,Tc	adj. tol. Nc
	2	K_n, χ		
	3	K_n, χ, μ_{crutch}		adj. tol. Nc, Tc
	4	**K, c, μ**, K_n, χ, μ_{crutch}		adj. tol. N, T, Nc, Tc

Table 4.6: Calibration steps for each one of the skeletal models. For each model and step, it is indicated the contact model parameters that are calibrated in the optimisation, the ground reaction components that are tracked in the cost function, and the ground reaction components that are included in path constraints (Path constr.). N and N_c stand for normal forces for feet and crutches, respectively; T and T_c stand for tangential forces for feet and crutches, respectively; and M stands for foot-ground moments. For *3D Crutches* model, all forces are included in path constraints, and tolerances are adjusted (adj. tol.) for the indicated components. The solution obtained at each step is used as the initial guess of the following step. For the *3D Crutches* model, the initial guess for foot-ground contact model parameters in step 4 are the optimal values obtained for *3D HAT* model and *shoes* experimental data.

Endpoint constraints

No endpoint constraints are considered in this problem.

Boundary conditions

Boundary conditions are the ones described in Section 4.1.

Additional tests and results

Once the contact models parameters have been calibrated per each model and data set, two additional tests have been done:

1. To check if it is necessary to calibrate spring-damper positions or they can be previoulsy fixed, two additional calibration steps have been done using the *3D HAT* model and *barefoot* experimental data. Using the results obtained for step 3 (see Table 4.6), anterior-posterior position (pos_x) per each group of springs has been calibrated tracking all forces and moments. Then, using these results, medio-lateral position (pos_z) per each spring-damper unit has been calibrated, tracking again all forces and moments.

2. To check if the values of parameters are capture-dependent and/or model-dependent, the *barefoot* experimental data has been tracked using the *3D Full* model and four different sets of calibrated parameters for foot-ground contact model: (1) *3D Full* model and *barefoot* motion, (2) *3D Full* model and *shoes* motion, (3) *3D HAT* model and *barefoot* motion, and (4) *3D HAT* model and *shoes* motion.

The considered results in this section to compare solutions and to evaluate the calibration methods have been convergence of the solution (number of iterations and computation time), mean RMS of residual loads, mean RMSE of model coordinates (linear and angular), and mean RMSE of ground reactions (forces and moments). RMSE have been computed resampling experimental data to the solution time values.

4.2.2 Results

Optimal contact model parameter values for each group of spring-damper units (1 to 6), for each model (*3D HAT*, *3D Full* and *3D Crutches*) and for each set of experimental data (*barefoot* and *shoes* for unassisted models, non-alternate four-point for *3D Crutches* model) are shown in Figure 4.4, and their exact values are reported in Appendix F. Optimal parameter values for crutch-ground contact model can be found in the same Appendix.

Foot-ground contact model parameters

Information about convergence, residual wrench components and errors with respect to experimental data can be found in Table 4.7. Total iterations (without changing spring positions) are in general lower for *3D HAT* model, compared with *3D Full* model. RMS of residual force and moments are similar for each capture (*barefoot* and *shoes*), since they are not reduced, but only maintained (i.e., it is not allowed to find a solution with residual forces and moments with higher RMS than the experimental values). Regarding mean RMSE of computed linear and angular joint coordinates with respect to their experimental counterparts, values for *barefoot* capture are in general lower than those for *shoes* capture for the same model. There is not much difference in RMSE for ground reaction forces, which vary from 11.10 to 16.84 N; and for ground reaction moments, which vary from 6.59 to 9.88 Nm.

		3D HAT		3D Full	
		Barefoot	Shoes	Barefoot	Shoes
Conv.	Total iterations	1584	1062	2056	2926
RMS	Residual forces [N]	17.69	22.77	14.13	22.27
	Residual moments [Nm]	5.37	6.88	4.05	5.61
RMSE	Joint coord. [cm]	0.28	0.61	0.24	0.50
	Joint coord. [°]	2.76	3.29	1.87	2.15
	GRFs [N]	16.84	16.36	14.82	11.10
	GRMs [Nm]	9.67	6.59	9.88	8.44

Table 4.7: Convergence and accuracy of solutions for calibrating foot-ground contact model using both unassisted models. Results are shown for the third calibration step (see Table 4.6).

Parameter values can be very different from one group to another, changing one or two orders of magnitude (e.g., stiffness value for *3D HAT* model and *barefoot* data is $5.24 \times 10^4 N/m$ for group 1, $0.37 \times 10^4 N/m$ for group 2, and $0.01 \times 10^4 N/m$ for group 3). For all three models, parameters for groups 4 to 6 remained almost equal to their initial guess value (see Figure 4.4).

Crutch-ground contact model

Foot-ground and crutch-ground contact model parameters for the *3D Crutches* model have been more difficult to calibrate than foot-ground contact model parameters for the models without crutches. As explained previously, an additional term in the cost function has been added to penalise if feet or crutches were not in contact with the ground when needed. Also, all forces and moments have been tracked in the cost function and all forces in the path constraints (as described in Table 4.6). The exact values for each crutch-ground contact model parameter can be found in Table F.2 in Appendix F. Convergence, residual RMS, and joint

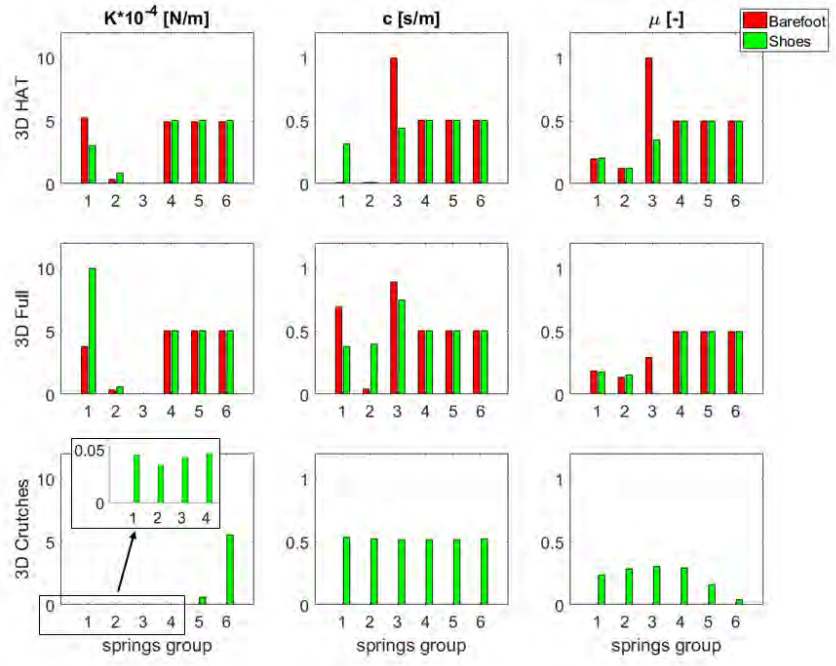

Figure 4.4: Optimal values for springs stiffness K, damping coefficient c and friction coefficient μ of each each group of springs (1 to 6), for each model (*3D HAT*, *3D Full*, *3D Crutches*) and for each set of experimental data (*barefoot* and *shoes* for unassisted models, non-alternate four-point for *3D Crutches* model). Results are shown after the last step of the calibration process, without varying spring and damper initial positions.

coordinates and ground reactions RMSE with respect to experimental data can be found in Table 4.11 (second column). In Figure 4.5, foot- and crutch-ground reaction forces once the contact models have been calibrated are shown.

Spring positions

A first additional test has been performed to check if it is necessary to calibrate spring positions or they can be previoulsy fixed. It has been compared the solution calibrating spring positions and without calibrating them, using the *3D HAT* model and *barefoot* experimental data (Figure 4.6). Exact values of anterior-posterior local position (pos_x) and medio-lateral local position (pos_z) can be found in Table F.3 in Appendix F.

Calibrated parameters for different models and/or captures

Finally, it has been tested if the parameters calibrated for a specific model and set of experimental data can be used for another model (of the same subject)

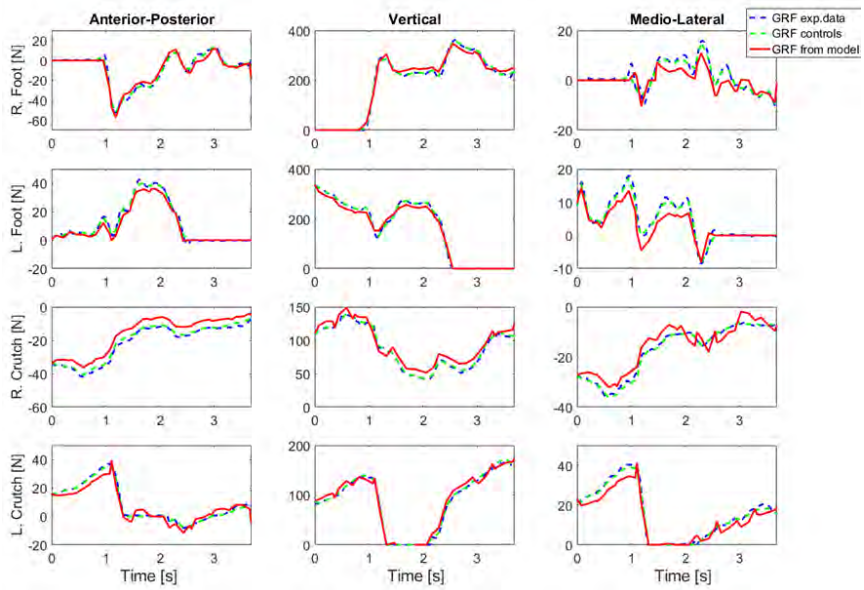

Figure 4.5: Foot- and crutch-ground reaction forces for the *3D Crutches* model once the contact models have been calibrated (after all the optimisation steps). In dashed blue, experimental data, in dashed green, control variables, in red, solution from contact model. "R" and "L" stand for right and left side, respectively.

and/or another set of experimental data. In Table 4.8 and Figure 4.7, results for dynamically consistent tracking of *barefoot* data using the *3D Full* model and four different sets of foot-ground contact model parameters are shown. The different values for foot-ground contact model parameters correspond to: (1) *3D Full* model and *barefoot* motion, (2) *3D Full* model and *shoes* motion, (3) *3D HAT* model and *barefoot* motion, and (4) *3D HAT* model and *shoes* motion.

4.2.3 Discussion

Foot-ground and crutch-ground contact model parameters have been calibrated for three different models (*3D HAT*, *3D Full* and *3D Crutches*), and three different experimental data sets (*barefoot* and *shoes* for models without crutches, and four-point gait for model with crutches), resulting in a total of five calibrated contact models. Results in terms of joint coordinates and ground reactions RMSE are consistent with results obtained in other studies that calibrate foot-ground contact models using viscoelastic elements. For example, RMSE of ground reaction forces vary from 4.55 to 10.40 N in [64], which are slightly lower than ours (11.10 to 16.84 N for unassisted models); and RMSE of normal forces are 28.8 N in [89] and 36.59 N in [63], which are higher than ours.

The proposed foot-ground contact model consists of 16 springs distributed in 6 groups. Different numbers of springs can be found in the literature (see Table 2.3).

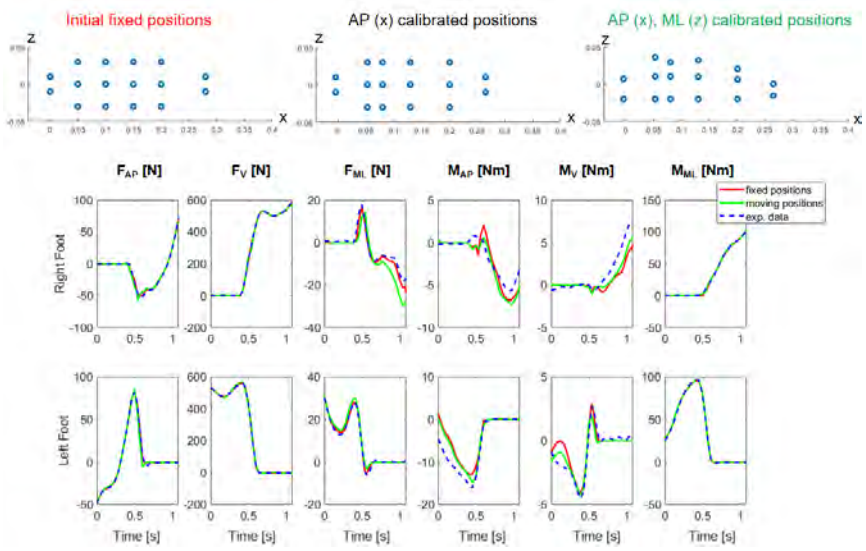

Figure 4.6: Ground reactions obtained after calibration of K, c, μ (red) compared to results after calibration of pos_x and pos_z (green) and with respect to experimental values (dashed blue). Results for *3D HAT* model and *barefoot* experimental data.

The assumption of symmetry between values of both feet is done in many other works that use contact models [50,63,64]. Having the springs distributed in groups, with the same parameter values per each group, is a way of allowing differences in parameter values, but reducing the number of variables. This has been done using different approaches in other studies. In [64] (38 spring and damper units), difference between individual spring stiffness and mean stiffness for all springs is minimised, and the same for damping coefficient values. In [50] (47 spring and damper units), the stiffness distribution across the entire shoe sole is approximated by a three-dimensional parabolic surface, which possesses only six unknown coefficients, and the damping coefficient is considered equal for all dampers. In our work, friction coefficient is different per each group of springs, as in [63], where it is calibrated for each of the 4 spheres. This is not done in other studies in literature, that calibrate friction coefficient equal for all springs [64], or set a fixed value for all springs, without optimising it [19].

In [66], contact model parameter values were calibrated using experimental data from five subjects (performing 15 trials at different walking speeds each), and it was found that the vertical and anterior-posterior position of the visco-elastic units is specific for each subject. However, in our simulations results have not change considerably when springs positions were optimised versus not (see Figure 4.6). Absolute RMSE in ground reaction moments, even when they are not tracked, are lower than errors in forces (Table 4.7). For this reason, the calibration of springs positions will not be considered in Chapters 5 and 6 for the foot-ground contact model of the human models.

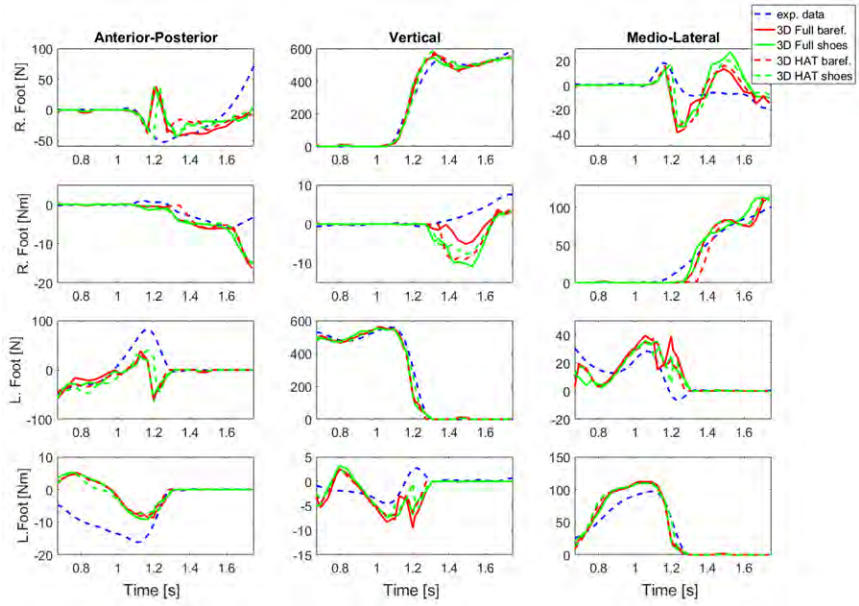

Figure 4.7: Ground reactions resulting from dynamically consistent tracking of *barefoot* motion. The *3D Full* skeletal model has been used with each one of the calibrated contact models for the *3D HAT* and *3D Full* models. In dashed blue, ground reactions from experimental *barefoot* motion. In green and red, results for *3D Full* skeletal model tracking the *barefoot* motion and using different values for foot-ground contact model parameters, corresponding to: (1) *3D Full* model and *barefoot* motion (solid green line), (2) *3D Full* model and *shoes* motion (solid red line), (3) *3D HAT* model and *barefoot* motion (dashed green line), and (4) *3D HAT* model and *shoes* motion (dashed red line). "R" and "L" stand for right and left side, respectively.

An analysis using different calibrated contact models with the same model and experimental motion data has been done to check if the result when tracking experimental motion and reducing residual wrench is sensitive to the contact model parameters. The objective is to see if, for the same model, it is possible to calibrate parameters for one experimental capture and then use them for tracking other experimental capture. Moreover, it also allows to check if it is possible to calibrate parameter values for a simpler model (*3D HAT*) and then use them for a more complex model (*3D Full* and *3D Crutches*). As results show, for *3D Full* model (see Figure 4.7 and Table 4.8), there is not much difference in terms of joint coordinates mean RMSE (0.56 to 0.67 cm, and 1.10 to 1.27°), or in ground reactions (3.34 to 6.38 N, and 0.80 to 1.30 Nm), when using contact model parameters calibrated using the *3D Full* model or the *3D HAT* model. These results may indicate that it is possible to calibrate parameter values for a simpler model and use them for a more complex model, for the same subject.

The crutch-ground contact model has been more challenging to calibrate. Having only a 6 DOF crutch model and tracking experimental global position and

Skeletal model		3D Full			
Experimental data		Barefoot			
Foot-ground contact model		Full baref.	Full shoes	HAT baref.	HAT shoes
RMS	Residual forces [N]	0.36	1.31	0.64	0.67
	Residual moments [Nm]	0.25	0.76	0.37	0.38
RMSE	Joint coord. [cm]	0.56	0.67	0.59	0.65
	Joint coord. [°]	1.10	1.25	1.16	1.27
	GRFs [N]	3.34	6.38	4.37	5.91
	GRMs [Nm]	1.30	0.88	1.26	0.80

Table 4.8: Residuals mean RMS and coordinates and ground reactions mean RMSE, resulting from dynamically consistent tracking of the *barefoot* experimental motion using the *3D Full* skeletal model with each one of the four different sets of calibrated foot-ground contact model parameters: (1) *3D Full* model and *barefoot* motion (highlighted in grey), (2) *3D Full* model and *shoes* motion, (3) *3D HAT* model and *barefoot* motion, and (4) *3D HAT* model and *shoes* motion.

orientation of the crutch, crutch-ground contact model parameters are tracked easily with good match in both motion and forces. Having a full-body model with crutches (*3D Crutches*), the number of elements (feet or crutches) in contact with the ground increases during all the cycle. There are not single support and double support phases, as in normal walking, but all the phases are multiple support phases, as three of four elements are always in contact with the ground. This is why the penalty term that ensures contact when it is supposed to be is needed. Otherwise, it is possible to find a solution that is dynamically consistent, but without contact of crutch or foot when it is supposed to be, or with more weight supported by one foot or one crutch than the contralateral foot or crutch. In [84], a similar crutch-ground contact model was calibrated and used for forward dynamic simulation; however, results of calibrated parameters and errors between experimental and simulated crutch-ground reaction forces were not reported.

4.3 Dynamically consistent full cycle generation

Once contact models are calibrated, the next step is to generate a dynamically consistent full gait cycle, that will be used as an initial guess for the prediction problems. This is done tracking experimental data (both joint coordinates and ground reactions), and having contact models to produce foot- and crutch-ground reactions. Since only two force plates are available in the motion analysis lab, we do not have foot-ground reactions (forces and moments) for a complete gait cycle. Ground reaction components for one foot during the first double support have to be predicted, as no ground reaction force data are available. In this sense, this problem can be seen as a first prediction.

The objectives of this section are the following:

1. To develop an optimal control formulation for dynamically consistent tracking of experimental motion, using calibrated contact models.
2. To generate a full dynamically consistent cycle for each model, in order to use them as initial guesses for the prediction problems.
3. To compare convergence, residual reduction, and accuracy with respect to experimental motion and forces when tracking with versus without contact models.
4. To compare convergence, residual reduction, and accuracy with respect to experimental motion and forces when tracking joint coordinates and ground reactions versus tracking only joint coordinates or only ground reactions.

4.3.1 Methods

Models and data

A full dynamically consistent gait cycle has been obtained for *3D HAT* and *3D Full* models for the *barefoot* experimental motion, and for *3D Crutches* model for the non-alternate four-point experimental motion. Models are described in Section 3.1.1, and experimental data are described in Section 3.2. The foot- and crutch-ground contact model parameters have been previously calibrated in Section 4.2.

Optimal control problem formulation

The OCP is formulated as a tracking problem, where foot- and crutch-ground reactions are obtained using the previously calibrated contact models. The formulation is based on Formulation D2 from Section 4.1.

Variables

The state vector $\mathbf{x} \in \mathbb{R}^{3n_q}$ is formed by the vector of generalised coordinates of the model $\mathbf{q}$, the vector of generalised velocities $\dot{\mathbf{q}}$, and the vector of generalised

accelerations $\ddot{\mathbf{q}}$. The control vector $\mathbf{u} \in \mathbb{R}^{n_q+12}$ (or $\in \mathbb{R}^{n_q+18}$, for the *3D Crutches* model) is formed by the vector of generalised jerk $\dddot{\mathbf{q}}$ and the vector of ground reaction forces and moments $\mathbf{GRF}_u$, that includes foot-ground and crutch-ground reactions (for the *3D Crutches* model):

$$\mathbf{x} = \begin{bmatrix} \mathbf{q} \\ \dot{\mathbf{q}} \\ \ddot{\mathbf{q}} \end{bmatrix} \tag{4.16}$$

$$\mathbf{u} = \begin{bmatrix} \dddot{\mathbf{q}} \\ \mathbf{GRF}_u \end{bmatrix} \tag{4.17}$$

Cost function

The general cost function is based on Formulation D2 from Section 4.1:

$$J = \int_{t_0}^{t_f} \Big(w_q \sum_{i=1}^{n_q} (q_i - q_{exp_i})^2 + w_{GRF} \sum_{i=1}^{n_{GRF}} (GRF_{u_i} - GR_{exp_i})^2 + w_j \sum_{i=1}^{n_q} \dddot{q}_i^2 \Big) \mathrm{d}t \tag{4.18}$$

being n_q the number of joint coordinates and n_{GRF} the number of ground reactions in the model; w_q, w_{GRF} and w_j the weights for joint coordinate errors, ground reaction errors and joint jerk, respectively; q_i and $\dddot{q}_i$ the i^{th} components of the vector of generalised coordinates $\mathbf{q}$ and joint jerk $\dddot{\mathbf{q}}$, respectively; GRF_{u_i} the i^{th} component of the vector of ground reactions $\mathbf{GRF}_u$; and finally, t_0 and t_f the initial and terminal times of the optimal control simulation. Subscript *exp* indicates an experimental value: experimental marker coordinates and ground reactions are measured directly, while experimental joint coordinates are obtained from an IK analysis performed in OpenSim using the experimental marker coordinates.

Weights for each term in the cost function have been modified manually in each problem variation to help convergence and improve the solution (see Table 4.9). When a full cycle is tracked, the error between ground reaction controls and experimental values is minimised only for the part of the cycle where experimental ground reactions are available.

Dynamic constraints

Dynamic constraints are the ones described in Section 4.2.

Path constraints

Two types of path constraints are considered in this problem:

- Residual forces and moments: Residual forces and moments are bounded below a small tolerance, as shows Eq. 3.18. Residual reduction tolerances are shown in Table 4.10.

Problem	Model	Cost function terms weights		
		q error	GRF error	jerk
Track joint coordinates and ground reactions	3D HAT 3D Full	1	0.1	1
	3D Crutches	1	0.1	0.01
Track joint coordinates	3D Full	1	-	0.1
Track ground reactions		-	0.1 Normal 1 other	0.1

Table 4.9: Weights for each term in the cost function for each problem and model. The cost function (Eq. 4.18) is formed by three terms: coordinate error (q error), ground reactions error (GRF error) and jerk. Note that when only coordinates (or only ground reactions) are tracked, there is no weight, as no error term for ground reactions (or coordinates) is considered.

- Ground reaction forces: Ground reaction controls equal ground reactions calculated using the contact model, as shows Eq. 3.20, being $\boldsymbol{\varepsilon}_{GRF} \in \mathbb{R}^{n_{GRF}}$ a vector of a specific tolerance (see Table 4.10).

Endpoint constraints

For *3D HAT* and *3D Full* models, no endpoint constraints are considered. For the *3D Cructhes* model, periodicity has been imposed in ground reactions: initial and final ground reaction forces have been imposed to be equal (with a tolerance of ± 50 N).

Several steps are followed for generating a DC full cycle for each one of the models (see Table 4.10), and the optimal solution from one step is used as the initial guess of the following step. For *3D HAT* and *3D Full* models, two steps have been considered, adjusting the path tolerances for residual reduction. For the *3D Cructhes* model, more steps are needed. Different tolerance values for residual reduction path constraints, for path constraints that minimise errors between ground reaction controls and ground reactions computed from contact models, and for endpoint constraints forcing periodicity of ground reactions have been considered.

Boundary conditions

Boundary conditions are the ones described in Section 4.1.

Additional tests and results

Once a full DC cycle has been obtained per each model and data set, two additional tests have been performed:

<table>
<tr><th rowspan="2">Model</th><th rowspan="2">Step</th><th colspan="2">Path constr.</th><th colspan="2">Endpoint constr.</th></tr>
<tr><th>Res. red.</th><th>GRF Tol. [N, Nm]</th><th>GRF comp.</th><th>Tol. [N, Nm]</th></tr>
<tr><td rowspan="2">3D HAT
3D Full</td><td>1</td><td>70%</td><td rowspan="2">1</td><td colspan="2" rowspan="2">-</td></tr>
<tr><td>2</td><td>95%</td></tr>
<tr><td rowspan="10">3D Crutches</td><td>1</td><td>50%</td><td rowspan="2">50</td><td colspan="2" rowspan="4">-</td></tr>
<tr><td>2</td><td>70%</td></tr>
<tr><td>3</td><td rowspan="8">95%</td><td rowspan="2">40</td></tr>
<tr><td>4</td></tr>
<tr><td>5</td><td rowspan="2">30</td><td rowspan="2">Normal</td><td rowspan="2">50</td></tr>
<tr><td>6</td></tr>
<tr><td>7</td><td rowspan="2">20</td><td rowspan="4">All</td><td rowspan="4">50</td></tr>
<tr><td>8</td></tr>
<tr><td>9</td><td>10</td></tr>
<tr><td>10</td><td>1</td></tr>
</table>

Table 4.10: Tolerances in path and endpoint constraints for each model and step. Residual reduction (Res. red.) tolerance is computed as the indicated percentage of reduction of the RMS of each component of the experimental residual wrench. Ground reaction tolerances (GRF Tol.) are equal in value for forces and moments. For endpoint constraints, the component where periodicty is imposed is indicated (GRF comp.), and also the tolerance value (Tol.).

1. Track only joint coordinates and predict ground reactions.
2. Track only ground reactions and predict joint coordinates.

These problems can be seen as initial predictions, because they track part of the experimental data and predict part of them. Only the part for which all experimental ground reactions were available (aproximately 80% of the cycle) has been simulated, in order to get comparable solutions.

The considered results in this section have been convergence of the solution (number of iterations and computation time), mean RMS of residual loads, mean RMSE of coordinates (linear and angular), mean RMSE of ground reactions (forces and moments). RMSE have been computed resampling experimental data to the solution time steps. Moreover, convergence and results (residual reduction, RMSEs with respect to experimental motion and forces) when tracking with and without contact models have been compared.

4.3.2 Results

A dynamically consistent cycle for each model (*3D HAT*, *3D Full* and *3D Crutches*) and cycle section (80% and 100%) has been generated. The cycle for *barefoot* capture starts at left heel strike (LHS), and for the four-point crutch gait starts at right crutch strike (RCS) (see Section 3.2).

For *3D HAT* and *3D Full* models, the optimal solution reducing 70% residual forces and moments has been used as an initial guess for reducing 95% residuals.

In Figure 4.8, the solutions for *3D HAT* model for the first step (reducing 70% residuals) and final results (reducing 95% residuals) are shown. Ground reactions for the right foot during first double support are fully predicted, as they are not available from experimental data. For *3D Full* model, results in terms of convergence, residual reduction and errors in joint coordinates and ground reactions are shown in Table 4.12 (first column, for 80% of cycle).

For *3D Crutches* model, more optimisation steps are needed (as described in Table 4.10). Foot-ground and crutch-ground reactions for a complete cycle (experimental, controls and values from contact model) are shown in Figure 4.9.

Compare tracking with and without contact models

For the *3D Crutches* model, that is the more complex model used in this section, results have been compared in terms of convergence, residual reduction, and errors in joint coordinates and ground reactions among the main different problems presented in this chapter (Table 4.11): (1) Tracking without contact models (solution of Formulation D2, Section 4.1), (2) Calibration of contact models (Section 4.2) , (3) Tracking with contact models (80% of cycle), and (4) Tracking with contact models (100% of cycle). The optimal solution obtained from the first problem (tracking without contact models) has been used as an initial guess for the three next problems (in each case, having the 80% or full cycle time). In terms of convergence, problems with contact models (calibration and tracking) require much more steps (7 to 10) than problems without contact models, and tracking with contact models require 1 or 2 mesh iterations. Comparing tracking with contact models for part of the cyle (80%) and for the full cycle, a similar number of steps is required, but much more iterations are needed in the case of full cycle tracking. Regarding residual reduction, the minimum values for residual forces and moments are obtained in the tracking problem without contact models. For tracking with contact models, these values are higher (up to 8.62 N and 11.10 Nm) than for tracking without contact models. For the contact model calibration, these values are the highest, as the tolerance is the RMS of experimental values for each residual wrench component.

Track only joint coordinates or only ground reactions

Finally, it has been compared tracking joint coordinates and ground reactions, tracking only joint coordinates, and tracking only ground reactions (for the case of 80% cycle, as not all ground reactions are available for all the cycle). In Figure 4.10, ground reaction forces are shown for these three tracking problems for the *3D Full* model. The number of iterations is similar when tracking both joint coordinates and ground reactions, or only joint coordinates (128-129 iterations), but it is higher when tracking only ground reactions (302 iterations) (Table 4.12). Residuals are reduced to lower values for the case of tracking only ground reactions, but mean RMSE for joint coordinates (linear and angular) increases with respect to the other cases. Mean RMSE for ground reactions (forces and moments) are similar for tracking joint coordinates and ground reactions and tracking only ground

3D Crutches		Track. wo. CM	CM calib.	Track. w CM (80%)	Track. w CM (Full)
Conv.	Total simulations	1	10	7	10
	Total iterations	158	1471	613	2553
	Total mesh iterations	0	0	1	2
RMS	Residual forces [N]	1.09	15.94	1.68	8.62
	Residual moments [Nm]	0.59	9.40	6.24	11.10
RMSE	Joint coord. [cm]	0.80	0.32	0.39	0.39
	Joint coord. [°]	1.60	0.60	0.35	0.36
	GRFs [N]	2.93	5.98	7.92	7.67
	GRMs [Nm]	0.48	2.76	3.57	3.20

Table 4.11: Convergence, residual RMS and joint coordinates and ground reactions RMSE with respect to experimental data for different problems using *3D Crutches* model. The problems are: (1) Tracking without contact models (solution of Formulation D2, Section 4.1), (2) Calibration of contact models (Section 4.2), (3) Tracking with contact models (80% of cycle), (4) Tracking with contact models (100% of cycle). Total simulations are the number of steps performed, using as initial guess for each problem the optimal solution from the previous one. Total mesh iterations refer to the number of mesh iterations performed in the last step, where mesh iterations are allowed in order to reach the desired interior point optimisation algorithm (IPOPT) and mesh tolerance.

reactions, and are higher when tracking only joint coordinates.

4.3.3 Discussion

Obtaining a full cycle, where part of the ground reactions are predicted, has required in general more iterations for each model, than obtaining a dynamically consistent walking motion for 80% of the cycle. This is expected, because there is an interval of the gait cycle for which experimental data are not available and, therefore, the corresponding motion has to be fully predicted. This dynamically consistent full gait cycle can be used as an initial guess of a prediction problem, that will be a starting feasible solution and may help the problem to converge.

From the comparison of results for the *3D Crutches* model, tracking data with and without contact models, it is observed that the most difficult problems in terms of number of steps and total iterations are contact model calibration and full cycle tracking with contact models. In the contact model calibration problem, it is necessary to add a penalty term in the cost function that ensures that crutches and feet are in contact with the ground when needed according to the experimental motion. For the tracking problem with previously calibrated contact models, on the contrary, this is not necessary. The fact that residuals are more difficult to be reduced in the tracking problems with contact models, may indicate that it is complicate to reach a solution by modifying motion and forces. In these cases, other approaches might be considered, such as changing mass or centre of mass position of some bodies in the model. Nevertheless, the obtained results are good enough to consider that the solution found is dynamically consistent [140].

An optimal solution has been obtained for tracking only joint coordinates or

Skeletal model		3D Full		
Experimental data		Barefoot (80% cycle)		
Track		Coords. + GRFs	Only coords.	Only GRFs
Conv.	Total iterations	128	129	302
RMS	Residual forces [N]	0.65	0.35	0.10
	Residual moments [Nm]	0.37	0.21	0.08
RMSE	Joint coord. [cm]	0.56	0.29	1.63
	Joint coord. [°]	1.10	1.03	7.06
	GRFs [N]	7.85	18.45	6.28
	GRMs [Nm]	3.38	7.05	2.08

Table 4.12: Comparison of convergence, residual RMS, and joint coordinates and ground reactions RMSE with respect to experimental data for the *3D Full* model and 80% of *barefoot* experimental capture. Three different tracking problems have been solved: (1) Track joint coordinates and ground reactions, (2) Track only joint coordinates, and (3) Track only ground reactions.

only ground reactions, for the *3D Full* model. As it is expected, mean RMSE are larger for the magnitudes that are not tracked, and residuals are lower for the case of tracking ground reactions (where more freedom is given to the coordinates to change in order to reduce residuals). These last formulations can be viewed as initial prediction problems, where there is a tracking term, but some magnitudes are predicted. In the next chapter, fully predictive predictions without any tracking term will be introduced.

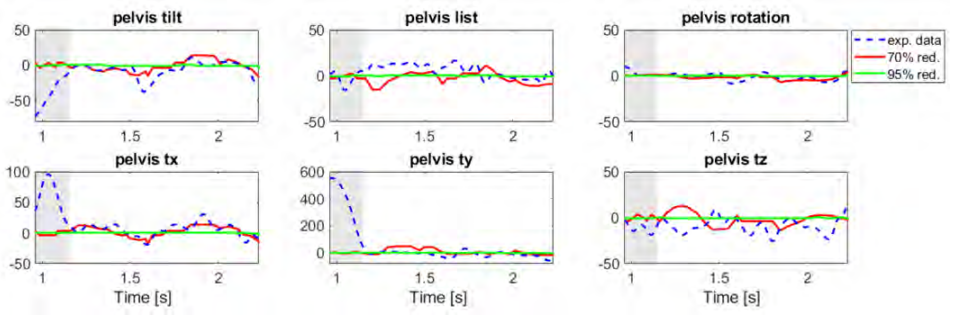

(a)

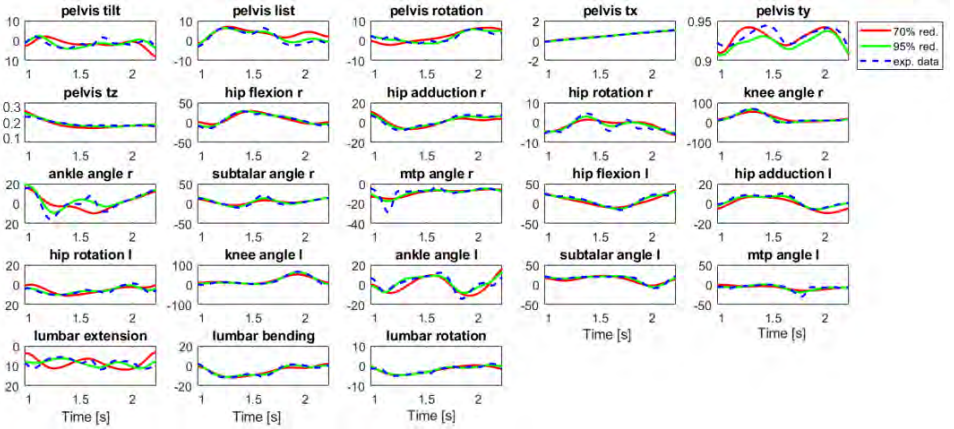

(b)

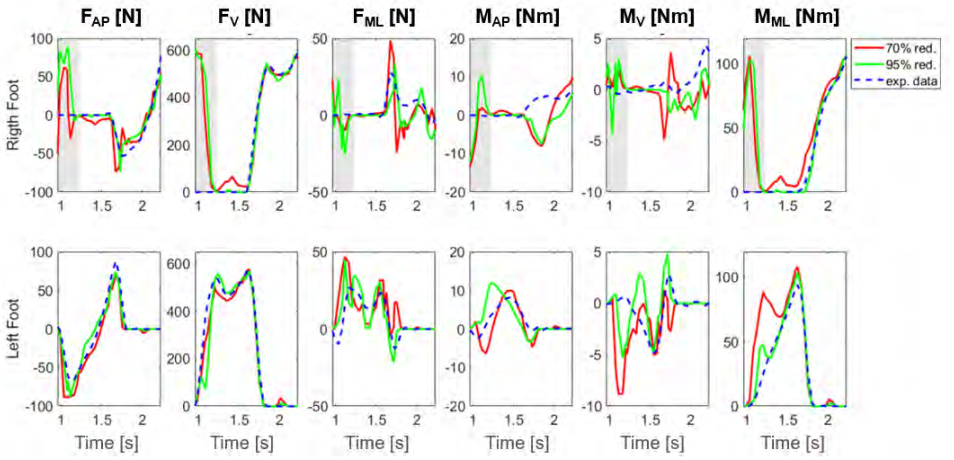

(c)

Figure 4.8: Experimental residuals (a), joint coordinates (b) and ground reactions (c) (in dashed blue) for the *3D HAT* model, compared to results obtained when reducing 70% (in red) and 95% (in green). The area in grey corresponds to the first double support were no force plate data are available. Residual forces "pelvis tx", "ty" and "tz" correspond to "pelvis anterior-posterior", "vertical" and "medio-lateral translation", respectively.

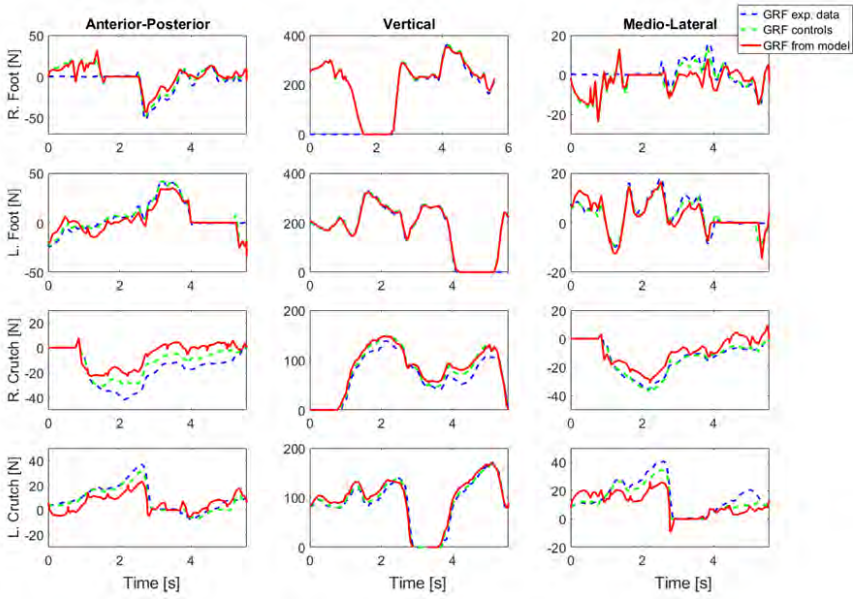

Figure 4.9: Foot-ground and crutch-ground reaction forces for a complete cycle: experimental values in dashed blue, controls in dashed green and values from contact model in red. “R” and “L” stand for right and left side, respectively. The first multiple support is predicted for right foot, and part of the last multiple support is predicted for left foot.

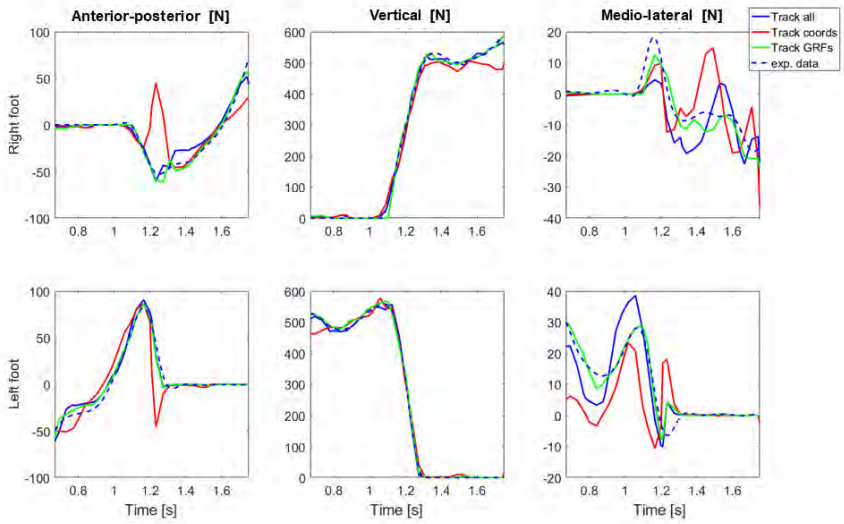

Figure 4.10: Ground reaction forces for the *3D Full* model and 80% of *barefoot* experimental capture, comparing three different tracking problems: (1) Track joint coordinates and ground reactions, (2) Track only joint coordinates, and (3) Track only ground reactions.

4.4 Conclusions

Dynamically consistent tracking of motion without contact models

- The presented problem formulations have converged with similar performance for different models and different experimental captures. This shows the robustness of the proposed optimal control problem formulations.
- Tracking marker coordinates consumes more iterations and time. Conversely, tracking joint coordinates requires less iterations and time, but the errors obtained with respect to experimental data (i.e., experimental marker trajectories) are similar to errors found when tracking markers.
- Adding crutches to the models makes it more difficult to fully reduce residuals mantaining a good tracking of experimental motion. Tracking ground reactions permits them to vary with respect to the experimental measurements, thus allowing to reduce residuals more efficiently. This can be done with ground reactions computed from contact models, or with ground reactions added as control variables to the problem.

Foot-ground and crutch-ground contact model calibration

- The calibrated parameters for foot-ground contact models have been used for different models and different data sets, showing similar results in terms of error with respect to the experimental data (both coordinates and ground reactions). Although more research needs to be done in terms of the calibration process and other issues regarding foot-ground contact modelling, we consider that the obtained results are good enough to fullfil the objectives of the present thesis.
- From the obtained results, it can be concluded that calibrating the parameters using the HAT model is easier in terms of convergence, and produces similar results in terms of accuracy (error with respect to the experimental coordinates and ground reactions) than calibrating the same parameters using a full-body model.

Dynamically consistent tracking of motion with contact models

- Having contact models (compared to having only ground reactions as controls of the problem) makes it more difficult to find the solution. For models without crutches, sometimes a two-step optimisation is needed, that is, finding first a solution for a higher residual tolerance (e.g., reducing residuals 70%), and then using this optimal solution as the initial guess for the full residual reduction simulation (e.g., reducing residuals 95%). For the model with crutches, even more steps are needed to reach the desired residual tolerance, starting from a solution with high tolerance values.

- Having a good initial guess seems to be very important to improve the problem convergence. It is not easy to distinguish when the problem is not converging because it does not have a solution, or because a suitable initial guess has not been found yet. Generating initial guesses for the same problem with high tolerances for path constraints seems to be a good approach.

Chapter 5

Prediction of normal and crutch-assisted walking

Prediction of novel motions has the potential to support personalised medicine, e.g., for developing personalised rehabilitation therapies [51], or designing personalised exoskeletons [15, 68, 99, 100]. However, it has associated large computational costs, so computationally efficient frameworks to predict human motion are needed [37], if they are to be used in real applications. It is accepted that there is a sort of optimisation criterion that the human neuromusculoskeletal system follows in order to perform motion, and it is believed that this may be related to minimising energy consumption or effort [27]. However, these criteria may change when dealing with impaired subjects' motion, or motion assisted by crutches or exoskeletons [22, 122].

This chapter investigates how to predict new motions without tracking experimental data. In Section 5.1, an optimal control problem is formulated for the prediction of normal walking, starting from a 3D model with arms attached to torso, followed by a 3D model that includes arm motion. In Section 5.2, crutch-assisted walking is considered, using a 3D model with arms and crutches. Different crutch-walking patterns are predicted with the aim of developing a methodology that can be applied for different scenarios of impairment and rehabilitation therapy.

Having an algorithm that allows to predict different crutch walking patterns is a first stepping stone toward developing a predictive tool to assist physiotherapists to choose the best crutch assisted walking pattern for a specific subject to optimise gait training. Moreover, this approach could be very useful for other researchers to study different biomechanical aspects of crutch walking, as it could overcome some limitations that existing studies of crutch walking in gait analysis laboratories declare, such as difficulty in recruiting subjects or limitation in the number of tests that can be performed [141–144].

5.1 Prediction of 3D normal walking

As it has been introduced in Chapter 2, the physiological criteria used for humans to walk may be to minimise metabolic energy (e.g., the consumed energy per unit walking distance) [25, 37] or may be related with fatigue-like cost functions [19]. From the different cost functions used in the literature (see Table 2.5), some optimality criteria related to kinematics, dynamics at torque level and energy have been considered in this study: minimise mechanical power, that is related to energy consumption when using torque-driven models [18, 123], minimise angular momentum, which has been found to be small for human walking [32, 145], minimise kinetic energy [27], minimise squared joint torques [17, 27, 32], and minimise joint acceleration, joint jerk [27, 123] or joint torque change [27, 28, 123].

When studying gait, usually some assumptions are made in order to simplify the solution. For example, some works assume that gait is symmetric and analyse only half of the gait cycle for both legs [25, 146], or impose constraints ensuring symmetry [18, 28, 32]. Conversely, other works do not impose symmetry [26, 123]. In both cases, whether symmetry is imposed or not, periodicity can be considered [28, 32]. In this work, symmetry is not imposed between left and right sides of the body, but periodicity in joint angles and ground reactions is considered.

The objectives of this section are the following:

1. To predict a complete gait cycle, using a 3D model with arms attached to torso (*3D HAT*) and a 3D model with arms (*3D Full*), without imposing symmetry, and without tracking any experimental data.
2. To study different cost functions that have been used in the literature to predict normal walking and compare results against experimental data.
3. To define a new cost function combining different terms in order to improve the predicted walking motion, in terms of convergence and similarity with normal walking.
4. To predict gait cycles at different speeds.

5.1.1 Methods

Models and data

To predict normal walking, two different models have been used: a 3D model with head-arms-trunk (HAT) segment (*3D HAT*) and a 3D model that includes arm motion (*3D Full*). Both models have been described in Section 3.1.1. The foot-ground contact model used for each model and the parameters for each spring and damper units are shown in Figure 5.1, and correspond to those obtained in Section 4.2. The *barefoot* experimental data (described in Section 3.2) have been tracked to obtain a dynamically consistent cycle that has been used as the initial guess of the predicted motion for each model (Section 4.3).

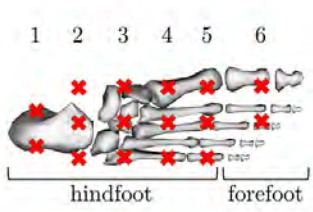

	Spring-damper group					
	Hindfoot					Forefoot
Location	1	2	3	4	5	6
x	0.00	0.05	0.10	0.15	0.20	0.08
y	0.00	0.00	0.00	0.00	0.00	0.00
z	-0.01	-0.03	-0.03	-0.03	-0.03	-0.01
	0.01	0.00	0.00	0.00	0.00	0.01
	-	0.03	0.03	0.03	0.03	-

Skeletal model	Foot-ground contact model parameter	Spring-damper group					
		1	2	3	4	5	6
3D HAT	Spring stiffness [N/m]	$5.24{\cdot}10^4$	$0.37{\cdot}10^4$	$0.01{\cdot}10^4$	$4.91{\cdot}10^4$	$4.91{\cdot}10^4$	$4.91{\cdot}10^4$
	Damping coefficient [s/m]	0.01	0.01	1.00	0.51	0.51	0.51
	Coefficient of dynamic friction [-]	0.20	0.12	0.99	0.50	0.50	0.50
3D Full	Spring stiffness [N/m]	$3.76{\cdot}10^4$	$0.31{\cdot}10^4$	$0.01{\cdot}10^4$	$5.02{\cdot}10^4$	$5.02{\cdot}10^4$	$5.02{\cdot}10^4$
	Damping coefficient [s/m]	0.69	0.04	0.89	0.51	0.51	0.51
	Coefficient of dynamic friction [-]	0.18	0.13	0.29	0.50	0.50	0.50

Figure 5.1: Top figure and top table: Local position of each of the 16 spring-damper units, that are distributed in six groups (spring-damper units of groups 1 to 5 are located on the hindfoot, and spring-damper units of group 6 are located on the forefoot). Bottom table: values of spring stiffness K, damping coefficient c and coefficient of dynamic friction μ obtained from the calibration for each one of the 6 groups of spring-damper units.

Optimal control problem formulation

Walking cycles have been predicted using an optimal control problem. The main structure of the problem has been presented in Section 3.3. The main difference with the simulations in Chapter 4 is that no experimental data are tracked in the cost function. For this reason, new terms are considered in the cost function, and additional constraints are needed.

Variables

The variables in the problem are similar to the variables used for tracking (presented in Section 4.1), and they vary depending on the regularisation term used (see Table 5.1). As an example, for the case where joint acceleration is minimised, the state vector $\mathbf{x} \in \mathbb{R}^{2n_q}$ is formed by the vector of generalised coordinates of the model, $\mathbf{q} \in \mathbb{R}^{n_q}$, and the vector of generalised velocities, $\dot{\mathbf{q}} \in \mathbb{R}^{n_q}$. The control vector $\mathbf{u} \in \mathbb{R}^{n_q+n_{GRF}}$ is formed by the vector of generalised accelerations, $\ddot{\mathbf{q}} \in \mathbb{R}^{n_q}$ and the vector of ground reaction forces and moments $\mathbf{GRF}_u \in \mathbb{R}^{n_{GRF}}$:

$$\mathbf{x} = \begin{bmatrix} \mathbf{q} \\ \dot{\mathbf{q}} \end{bmatrix} \tag{5.1}$$

$$\mathbf{u} = \begin{bmatrix} \ddot{\mathbf{q}} \\ \mathbf{GRF}_u \end{bmatrix} \tag{5.2}$$

Remember that the ground reaction controls, $\mathbf{GRF}_u$, are used to define a walking cycle. They define when each foot is either in swing phase or stance phase, that is, all reaction components are forced to be zero during swing. This is done by multiplying each control variable by a vector of zeros and ones that defines the swing (0) and stance (1) phase for each foot.

Minimise	Joint acceleration	Joint jerk	Torque change	Joint acceleration and torque change	Joint jerk and torque change
States	Joint coordinates Joint velocities	Joint coordinates Joint velocities Joint accelerations	Joint coordinates Joint velocities Joint torque	Joint coordinates Joint velocities Joint torque	Joint coordinates Joint velocities Joint accelerations Joint torque
Controls	Joint accelerations Ground reactions	Joint jerk Ground reactions	Joint accelerations Joint torque change Ground reactions	Joint accelerations Joint torque change Ground reactions	Joint jerk Joint torque change Ground reactions

Table 5.1: States and controls of the optimal control problem are different depending on the regularisation terms used. Five possible options are considered in this work: minimise joint acceleration, minimise joint jerk, minimise joint torque change, and minimise at the same time joint torque change with joint acceleration or joint jerk.

Variable bounds (minimum and maximum values for each state and control) have been described in Section 3.3.3. Since experimental data are not tracked in the predictions, the solution found can be optimal regarding the minimisation of the cost function terms, but the resulting motion might be unnatural. To avoid this issue, different bounds have been used for each joint coordinate, taking into account the experimental motion values (see more details on Appendix C).

Cost function

Different cost function terms that have been used in the literature for predicting normal gait have been used in this work. They are classified in two different groups: optimality terms, if they are minimised based on an optimality criterion, and regularisation terms, if they are minimised to help the solution converge (see Table 5.2). Simple cost functions combining one of each type of terms have been considered, and also multi-term cost functions combining three or more terms. No tracking terms have been used in the different walking predictions.

The general cost function can be described as:

$$J = \int_{t_0}^{t_f} \Big(\sum_i J_{opt,i}(\mathbf{x}, \mathbf{u}) + \sum_j J_{reg,j}(\mathbf{x}, \mathbf{u}) \Big) \mathrm{d}t \tag{5.3}$$

where t_0 and t_f are the initial and final simulation times. The different optimality terms used, $J_{opt,i}(\mathbf{x}, \mathbf{u})$, to be considered in the cost function are: (1) the sum of squared joint torques, $\sum_{i=1}^{n_q-6} \tau_i^2$, being n_q the number of generalised coordinates and τ_i the i^{th} component of the vector of joint torques, $\boldsymbol{\tau}$; (2) the squared norm of the global angular momentum, $\|\mathbf{L}\|^2$, being $\mathbf{L}$ the global angular momentum of the

model computed in the global centre of mass; (3) the sum of the squared norms of the local angular momenta, $\sum_{i=1}^{n_b} \|\mathbf{L}_i\|^2$, being n_b the number of bodies in the model and $\mathbf{L}_i$ the local angular momentum at the centre of mass of the i^{th} body of the model; (4) the sum of squared mechanical power, computed for each relative coordinate (i.e., not for the absolute pelvis translation and rotation coordinates), $\sum_{i=7}^{n_q}(\dot{q}_i\tau_{i-6})^2$, being $\dot{q}_i$ the i^{th} component of the vector of generalised velocities, $\dot{\mathbf{q}}$; and (5) the squared value of the model kinetic energy, T^2. The different regularisation terms, $J_{reg,j}(\mathbf{x},\mathbf{u})$ are: (1) the sum of squared joint accelerations, $\sum_{i=1}^{n_q} \ddot{q}_i^2$, being $\ddot{q}_i$ the i^{th} component of the vector of generalised accelerations, $\ddot{\mathbf{q}}$; (2) the sum of squared joint jerks, $\sum_{i=1}^{n_q} \dddot{q}_i^2$, being $\dddot{q}_i$ the i^{th} component of the vector of generalised jerk, $\dddot{\mathbf{q}}$; (3) the sum of squared joint torque changes, $\sum_{i=1}^{n_q-6} \dot{\tau}_i^2$, being $\dot{\tau}_i$ the i^{th} component of the vector joint change, $\dot{\boldsymbol{\tau}}$.

	Type	Term	References
Optimality terms	Dynamic	Joint torque (Torq)	Felis and Mombaur, 2013 [32] Xiang et al., 2007 [24]
		Global angular momentum (AMG)	Felis and Mombaur, 2013 [32]
		Local angular momentum (AML)	-
	Energetic	Mechanical power (MP)	Ren et al., 2007 [18]
		Kinetic Energy (KE)	Koch et al., 2017 [27]
Regularisation terms	Kinematic	Joint acceleration (Acc)	Falisse et al., 2019 [37]
		Joint jerk (Jrk)	Meyer et al., 2016 [50]
	Dynamic	Joint torque change (Tch)	Fluit et al., 2012 [28]

Table 5.2: Different cost function terms that have been used in the literature and in this work for prediction of normal walking. They are classified in two different groups: optimality terms, if they are minimised based on an optimality criteria, and regularisation terms, if they are minimised to help the solution converge. In this section, cost functions are defined initially combining one optimality term with one regularisation term, and after that, multi-term cost functions combining three or more terms are considered also.

Dynamic constraints

Dynamic constraints are the ones in Eq. 3.16, adapted to the states of the problem in each case (see Table 5.1).

Path constraints

The following path constraints are considered in this formulation:

- Residual forces and moments: Residual forces and moments are bounded below a small tolerance, as shows equation 3.18, being 0.1 N (or Nm) the tolerance for residual wrench components.

- Joint torques: Joint torques from the optimal control problem are forced to be the same as joint torques obtained from OpenSim, as shows equation 3.19,

being 30 Nm the tolerance for differences between joint torques controls and those obtained from inverse dynamics (ID).

- Ground reaction forces: Ground reaction controls equal ground reactions calculated using the contact model, as shows equation 3.20, being 50 N (or Nm) the tolerances for differences between ground reaction forces controls and those computed from the contact model.

- Feet crossing: To avoid feet lateral crossing, the lateral distance between the midpoint of each foot is bounded. This distance has been bounded between 0.1 m and 1 m.

- Non-sliding: To avoid sliding during stance, the value of the velocity of the midpoint of the foot is bounded during stance phase.

Endpoint constraints

- Initial feet position: Initial position for right and left foot with respect to the centre of the pelvis has been imposed (with a tolerance of ± 1 cm). Since the predicted gait cycle starts with left heel strike, the left foot midpoint is located half of the stride length forward (with respect to the pelvis centre) and the right foot midpoint is located half of the stride length backward.

- Stride length: Stride length has been imposed. For that, the total travelled distance in a cycle in anterior-posterior direction of the midpoint of each foot has been imposed to be equal to the stride length (with a tolerance of ± 5 cm).

- Periodicity: The predicted gait cycle has been considered cyclic. Periodicity has been imposed in three different ways. Initial position of the midpoint of each foot with respect to the center of the pelvis has been imposed to be equal to the final position (with a tolerance of ± 5 cm), initial and final angular joint coordinates have been imposed to be equal (with a tolerance of $\pm 10°$), and finally initial and final normal ground reaction forces have been imposed to be equal (with a tolerance of ± 50 N).

Boundary conditions

Boundary conditions are the ones described in Section 4.1, being bounds for joint coordinates described on Appendix C.

Studies performed and evaluation of results

With the aim of predicting full walking cycles at different speeds, different studies are performed, from a first exploration using two-term cost functions combining each optimality criterion and regularisation term, to predictions using more detailed multi-term cost functions that combine different terms.

1. First exploration.
   The goal of this first study is to compare many combinations of optimality and regularisation terms, with the aim of choosing those that will be investigated more carefully. Simulations have been performed using only the *3D HAT* model, and limiting the maximum number of interior point optimisation algorithm (IPOPT) iterations to 1000. Each optimality term has been combined with one or two regularisation terms (see Table 5.1), resulting in twenty-five cost functions compared.

   To evaluate results, the number of iterations needed to converge to an optimal solution has been taken into account. Moreover, a similarity index has been qualitatively computed, comparing each resulting motion with the experimental one. Similarity index per each cost function, S_{cf}, is computed according to:

$$S_{cf} = \sum_{i=1}^{n_q} (S_{shape,i} + S_{ROM,i}) \tag{5.4}$$

   where cf is the evaluated cost function; $S_{shape,i}$ is 1 if the shape of the simulated coordinate is close to the experimental value, and 0 if not; $S_{ROM,i}$ is 1 if the range of motion (ROM) of the simulated coordinate is close to the experimental value, and 0 if not; and nq is the number of coordinates in the model.

   From this initial study, a regularisation term has been chosen to compare all optimality criteria, using both models (*3D HAT* and *3D Full*).

2. Comparison of optimality criteria.
   Once a regularisation term has been chosen, the different optimality criteria have been studied with more detail, using both models (*3D HAT* and *3D Full*). In this case, periodicity is imposed to the predicted gait cycle.

   For the evaluation of results it has to be taken into account that a solution can be optimal mathematically (it can minimise the different terms in the cost function, and fulfil all constraints), but at the same time the resulting motion be unnatural. For this reason, convergence (time to converge and number of iterations) has been considered, but more importance has been given to the quality of the resulting motion. For that, different parameters that describe features and quality of gait have been chosen from the literature [147], and have been divided into qualitative and quantitative features (see Table 5.3). Qualitative features (correct torso motion, knee flexion and arms swing) have been observed directly from the visualisation of the motion in OpenSim. Quantitative features have been computed from the coordinates trajectories and compared against experimental results in the literature: maximum knee flexion [148, 149] and maximum hip abduction [150], lateral pelvis displacement ROM [147, 151, 152], lumbar extension and bending ROM [153, 154], and shoulder flexion ROM [155, 156]. Moreover, the trajectory of the global centre of mass has been obtained from OpenSim.

	Qualitative results		Quantitative results		
	Feature	Description	Feature	Value	References
Legs motion	Correct knee flexion?	Knee flexes and extends during swing phase	Max knee flex [°]	60 ± 10	Öberg et al., 1994 [148] Winter, 2009 [149]
			Max hip abduction [°]	9.5 ± 1	Pietraszewski et al., 2012 [150]
Torso motion	Correct torso motion?	Torso sways forward and backward, oscillating around the mean orientation twice per cycle	ROM pelvis ML trans. [cm]	4.5 ± 1	Saunders, 1953 [147] Malanga et al., 1998 [151] Dodd et al., 1998 [152]
			ROM lumbar ext. [°]	5 ± 2	Feipel et al., 2001 [153]
			ROM lumbar bend. [°]	9 ± 3	Crosbie et al., 1997 [154]
Arms motion	Correct arms swing?	Each arm swings forward during the swing phase of the opposite leg, and swings backwards during the swing phase of the corresponding leg	Shoulder flex ROM [°]	32 ± 4	Van de Walle et al., 2018 [155] Hejrati et al., 2016 [156]

Table 5.3: Different parameters that describe features and quality of gait are chosen from the literature. For the qualitative results, a description for normal gait is given. For the quantitative results, a range of reference values is obtained from experimental results in the literature. When more than one study is considered, the maximum and minimum values of all studies are used to define the minimum and maximum values of the range, and the mean value of the range is computed from them.

3. Multi-term cost function.
   With the aim of obtaining a better walking cycle, a cost function combining different terms has been developed for each one of the skeletal models (*3D HAT* and *3D Full* models). For that, results from the previous comparison study that minimised errors with respect to experimental motion have been taken into account. To validate the resulting motion, the same gait features from the previous study have been computed (see Table 5.3).

4. Prediction at different speeds.
   Using the *3D Full* model, gait cycles at different speeds ($\pm 20\%$) have been predicted. Each speed (low and high) has been achieved by modifying stride length or cycle time. In Table 5.4, the stride length and cycle time (or duration) imposed in each prediction are shown. The duration of each phase (swing and stance for each leg) is adapted from the experimental data, maintaining the percentages of each phase with respect to the total cycle time. The cost function used is minimising global angular momentum and joint torque change, that is the two-terms cost function for which arms swing has been correctly predicted.

	Initial	Low speed (-20%)		High speed (+20%)	
		Low stride length	High cycle time	High stride length	Low cycle time
Speed [m/s]	0.75	0.60		0.90	
Stride length [m]	1.00	0.80	1.00	1.20	1.00
Cycle time [s]	1.33	1.33	1.66	1.33	1.11

Table 5.4: Using the *3D Full* model, gait cycles at different speeds (±20%) are predicted. Each speed (low and high) can be achieved by modifying stride length or cycle time. In the first column, the initial values correspond to the ones obtained from the experimental data. Stride length and cycle time are imposed values in the problem formulation, and speed is computed from them. The duration of each phase (swing and stance for each leg) is adapted from the experimental data, maintaining the percentages of each phase with respect to the total cycle time.

5.1.2 Results

First exploration

Twenty-five cost functions combining each optimality term and one or two regularisation terms in Table 5.2 have been compared using the *3D HAT* model. Information about convergence (number of iterations) and similarity with respect to the experimental data is shown in Table 5.5. Minimising joint torque and joint torque change converges with the lowest number of iterations (28) and the highest similarity value (35). Minimising mechanical power and torque change also converges with a low value of iterations (106), and minimising global angular momentum (AM) has a high similarity value (23) compared with the rest of solutions. Overall, better results in terms of convergence and similarity to experimental data are obtained when minimising joint torque change: similarity values are higher for all optimality terms, and number of iterations are lower in general for all optimality terms. Therefore, from this initial exploration, joint torque change is found to be the regularisation term that provides the best performance.

Comparison of cost functions

Using the regularisation term of minimising joint torque change, five different optimality criteria have been compared for *3D HAT* and *3D Full* models: minimise mechanical power, angular momentum per each body, global angular momentum, kinetic energy and joint torque. All cost functions have converged for both models with comparable number of iterations (84 to 250) and computation time (1 to 10 min approximately) in most of the cases, being the highest number of iterations and computation time for the case of minimising kinetic energy (1506 iterations and almost an hour for the *3D Full* model, as can be seen in Table 5.6).

Roughly, it can be said that minimising the same criteria using the model with and without arms, results in a similar motion for both models. Moreover, minimising joint torque and mechanical power produces similar results for almost

	Convergence term									
	Acceleration		Jerk		Torque change		Acc. + torq. ch.		Jerk + torq. ch.	
Optimality term	n iter.	Simil.	n iter.	Simil.	n iter.	Simil.	n iter.	Simil.	n iter.	Simil.
Mechanical power	393	8	185	9	106	13	190	7	753	11
Local AM	265	11	247	12	120	10	241	5	349	12
Global AM	>1000	-	>1000	-	169	23	>1000	-	>1000	-
Kinetic energy	>1000	-	>1000	-	278	12	483	6	247	10
Joint torque	377	13	417	7	28	35	196	8	662	12

Table 5.5: Results obtained for the initial exploration using the *3D HAT* model. A total of 25 different cost functions have been tested, and number of iterations to converge (n iter.) and similarity value (Simil.) are given per each cost function. Similarity value, as explained in the methods section, is computed looking at the coordinates plots and comparing shape and ROM of each coordinate with the corresponding experimental values. Notice that for some cost functions the problem has not converged for less than 1000 IPOPT iterations, which does not mean that the problem is not able to converge with more iterations. However, as it has been said, a limit of 1000 iterations has been considered. In those cases, the similarity value is not given.

all coordinates (Figure 5.2). Regarding lower body motion in the sagittal plane, predicted hip, knee and ankle flexion angles are close to experimental values for all cost functions, being the most different results the ones obtained for kinetic energy minimisation. Regarding upper body motion, results differ for each cost function. Arm motion is only predicted correctly when minimising global angular momentum, being again minimising kinetic energy the cost function that produces less accurate results compared with experimental data. Torso motion is well predicted in sagittal and frontal planes when minimising mechanical power and joint torque, but it sways more than in the experimental motion. Regarding global centre of mass (COM) trajectory, minimising kinetic energy produces a smooth COM trajectory, while minimising local angular momentum produces some peaks at the beginning of the cycle in the sagittal plane (x-y) for the *3D Full* model (Figure 5.3).

Multi-term cost function

Once a predicted full cycle has been obtained with each optimality criteria, the possibility of combining more than one criteria to obtain a more realistic prediction has been investigated. For the *3D HAT* model, the lowest mean root-mean-square errors (RMSEs) for all angular coordinates are 5.07°, for minimising mechanical power and joint torque change, and 5.63°, for minimising global angular momentum and joint torque change. In terms of convergence, minimising mechanical power requires 84 iterations (the same as minimising joint torque), while minimising global angular momentum requires 213 iterations (4.22 min) (see Table 5.6). In the predicted motion when minimising mechanical power, torso motion is correct, and ROM of lumbar extension and bending are consistent with experimental data. In the predicted motion when minimising global angular momentum, maximum knee flexion and hip abduction are also consistent with experimental data. For this model, the considered multi-term cost function includes minimising mechan-

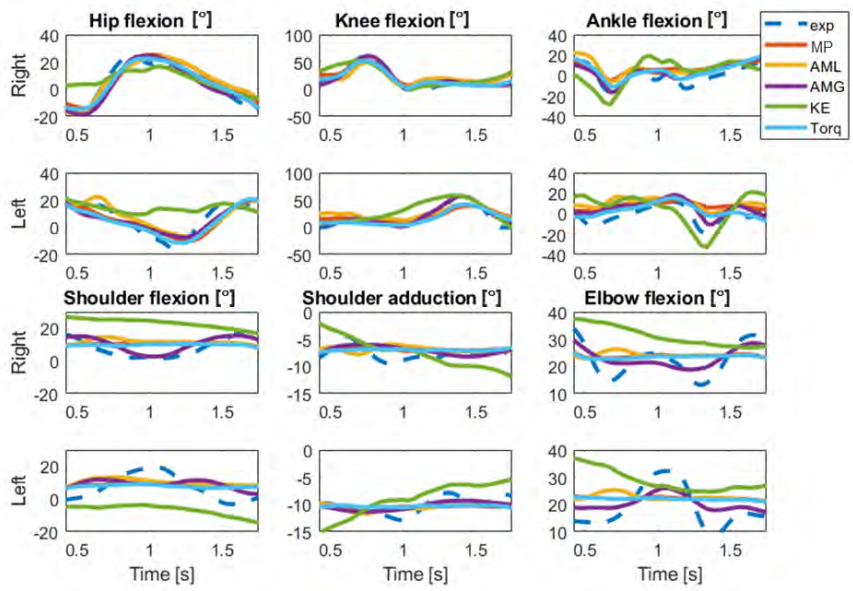

Figure 5.2: Results for the comparison of cost functions for the *3D Full* model, compared to the experimental values (exp). Values for the experimental motion are taken from the *barefoot* gait data using the *3D Full* model. A total of five cost functions have been compared, all of them minimising joint torque change (tch) and each one of the optimality criteria: mechanical power (MP), local angular momentum (AML), global angular momentum (AMG), kinetic energy (KE) and squared joint torque (Torq). Some of the main joint coordinates for lower and upper body are plotted: hip flexion, knee flexion, ankle flexion, shoulder flexion and adduction, and elbow flexion. Joint coordinates are shown for both right and left sides and for a complete gait cycle, from left heel strike to left heel strike.

ical power, global angular momentum, and joint torque change. Using this cost function, the solution has converged with 927 iterations and 21.79 min. Results have improved in general, compared to each cost function results, but lumbar extension ROM has increased to 7.5°, resulting in an abrupt torso motion, as it has been also observed when minimising global angular momentum.

For the *3D Full* model, the lowest mean RMSEs for all angular coordinates are 4.90°, for minimising global angular momentum and joint torque change, and 6.28°, for minimising joint torque and joint torque change. However, looking at mean RMSE for pelvis and torso coordinates, those values are lower for minimising mechanical power than for minimising joint torque. For this reason, minimising global angular momentum, joint torque and mechanical power have been considered for the multi-term cost function. Two combinations have been tested: (1) minimising joint torque, global angular momentum, and joint torque change; and (2) minimising mechanical power, global angular momentum, and joint torque change. The first combination presents abrupt changes in different coordinates, while the second not; and for this reason the second combination is the one with better

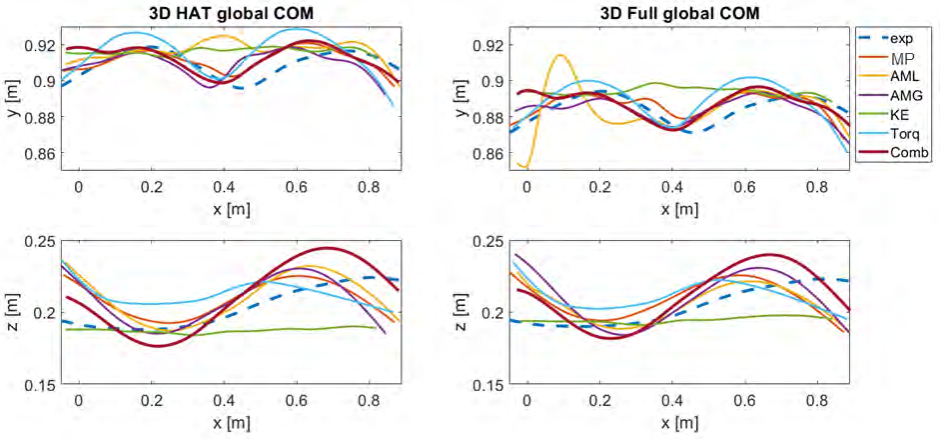

Figure 5.3: Global center of mass (COM) trajectory for the sagittal plane (x-y) and for the horizontal plane (x-z) for each model (*3D HAT* and *3D Full*), for each cost function and for the experimental motion (exp). Values for the experimental motion are taken from the *barefoot* gait data using the *3D Full* model. A total of five cost functions have been compared, all of them minimising joint torque change and each one of the optimality criteria: mechanical power (MP), local angular momentum (AML), global angular momentum (AMG), kinetic energy (KE) and squared joint torque (Torq).

performance. However, it does not predict well arm motion. This is why two additional changes have been done to improve the solution: minimise mechanical power for all the joints but arms joints, and add an additional term in the cost function that minimises difference between right and left shoulder flexion angular velocities. The latter term comes from what can be observed from the experimental values in Figure 5.2, that when right shoulder flexion increases its value, left shoulder flexion decreases it, and viceversa. Using this cost function, a walking cycle is predicted in 770 iterations and 35.82 minutes. Results are improved in general, but the arms swing is lower, i.e., shoulder flexion ROM is decreased compared to the solution that only minimises global angular momentum, and the torso motion is still abrupt.

Main coordinates and ground reactions forces for multi-term cost functions for the *3D HAT* and *3D Full* models are shown in Figures 5.4 and 5.5, respectively. In general, lower limbs motion is better predicted than torso and arms motion. ROM for lumbar extension is close to the experimental ROM, but it is lower for lumbar bending and rotation. The largest difference in ROM can be found in elbow flexion, where the predicted ROM is much lower than the experimental ROM. Ground reaction forces are well predicted in terms of shape compared to the experimental values, but can reach maximum values (in absolute values) 50 N higher (for tangential components of force) and 100 N higher (for the normal force) than the experimental ones. It can also be observed that the obtained values of the ground reactions include some peaks, and thus, they are not as smooth as the experimental curves are. The global COM trajectory for these solutions reproduces better

than the previous predictions the experimental trajectory of the global COM in the sagittal plane (x-y), but it does not follow correctly the experimental trajectory of the global COM in the horizontal plane (x-z), as it is shown in Figure 5.3. Frontal and lateral views of the experimental motion and the predicted motions using the multi-term cost functions for *3D HAT* and *3D Full* models are shown in Figures 5.6 and 5.7, respectively.

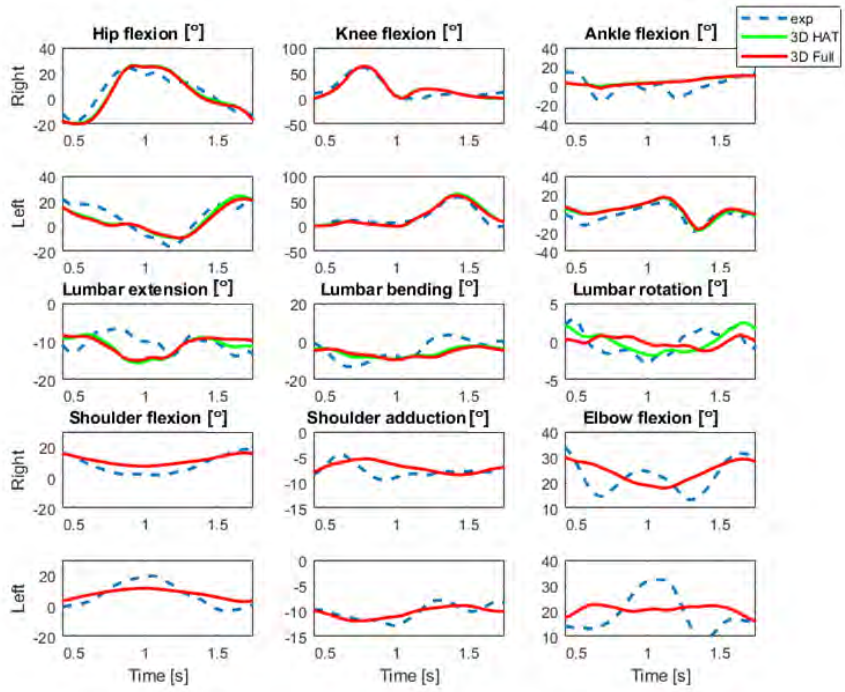

Figure 5.4: Results for the multi-term cost functions for both models (*3D HAT* and *3D Full*), compared to the experimental values (exp). Values for the experimental motion are taken from the *barefoot* gait data using the *3D Full* model. Some of the main joint coordinates for lower and upper body are plotted: hip, knee and ankle flexion; lumbar extension, bending and rotation; shoulder flexion and adduction, and elbow flexion (arms joint coordinates only for *3D Full* model). Joint coordinates are shown for both right and left sides and for a complete gait cycle, from left heel strike to left heel strike. The multi-term cost functions are: for *3D HAT* model, minimising mechanical power, global angular momentum and joint torque change; for *3D Full* model, minimising lower body and torso mechanical power, global angular momentum, joint torque change, and the difference between right and left shoulder flexion velocities.

Speed variations

Walking cycles at different speeds have been predicted. In this case, the cost function used is minimising global angular momentum and joint torque change us-

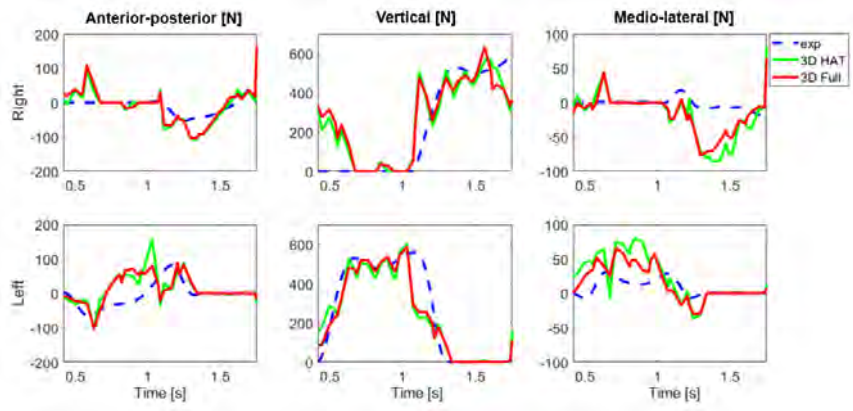

Figure 5.5: Results for the multi-term cost functions for both models (*3D HAT* and *3D Full*), compared to the experimental values (exp). Values for the experimental motion are taken from the *barefoot* gait data using the *3D Full* model. Note that there are not available ground reactions for the right foot first support. Ground reaction forces are shown for both right and left sides and for a complete gait cycle, from left heel strike to left heel strike. The multi-term cost functions are: for *3D HAT* model, minimising mechanical power, global angular momentum and joint torque change; for *3D Full* model, minimising lower body and torso mechanical power, global angular momentum, joint torque change, and the difference between right and left shoulder flexion velocities.

ing only the *3D Full* model. Four different simulations have been performed at two different speeds, according to Table 5.4, by varying stride length or cycle duration, respectively. Simulations at low speed have converged with similar number of iterations (299 and 289). Conversely, for simulations of walking at high speed, the case of low cycle duration has converged with fewer iterations (261), while a higher number of iterations is required for the case with high stride length (391). Computation time varies from 9 to 15.5 min.

Figure 5.8 shows the most relevant coordinates for each combination of cycle duration and stride length. Comparing solutions with variation of stride length, for the case of high stride length (1.2 m), ranges of motion for hip flexion, ankle flexion, lumbar joint coordinates (extension, bending and rotation), shoulder flexion and elbow flexion are the highest of all solutions. For the case of low stride length (0.8 m), ranges of motion for hip, knee, shoulder and elbow flexion are the lowest of all solutions. Comparing solutions with variation of cycle duration, for the case of high cycle duration, knee flexion ROM is the highest one, whereas lumbar bending and rotation ROM are the lowest ones. For the case of low cycle duration, lumbar extension has the lowest ROM.

5.1.3 Discussion

In this section, normal walking cycles using a model with arms attached to torso (*3D HAT*) and a full-body model with arms (*3D Full*) have been predicted without

adding any tracking term in the cost function. Different optimality criteria and regularisation terms have been compared (Table 5.2) in order to determine a cost function combining different terms, that reproduces closely experimental normal walking. This cost function has been formed basically by minimising mechanical power, global angular momentum and joint torque change, for both models *3D HAT* and *3D Full*. Computation time has varied from less than two minutes to almost an hour for cost functions with two terms, and between 20 and 35 minutes for the multi-term cost functions. Arm motion is well predicted for these cost functions, but torso motion is abrupt and it sways more than what is observed in experimental data. Finally, gait cycles performed at different speeds have been predicted, by modifying stride length or cycle duration.

The predicted motions minimising joint torque change combined with different optimality criteria generally predict a correct motion of the lower limbs. Moreover, the solutions obtained by minimising mechanical power and by minimising joint torque are similar, and are also similar the solutions minimising global and local angular momentum (see Figure 5.2). Arm motion is only well predicted in the case of minimising global angular momentum, which seems reasonable, as it has been found that whole-body angular momentum is small, and that arm motion contributes to reduce it [145]. Torso motion presents two opposite results that are similar for both analysed models: it is stiff or rigid when minimising local angular momentum and kinetic energy, and it has abrupt changes (it sways with larger ROM and higher velocity compared with torso orientation in normal walking) when minimising global angular momentum. This last aspect appears also in the multi-term cost functions (as it can be observed in Figures 5.6 and 5.7). Surprisingly, minimising kinetic energy results in the most different motion, which is not consistent with results reported in [27], where motion was predicted minimising specific kinetic energy. In the latter work, a 3D HAT model was used, and symmetry was imposed between right and left sides of the body. Maybe the fact of not imposing symmetry or having arms in our model may have led to different results compared to the literature. Cost functions where a global term has been minimised (global angular momentum or kinetic energy) have required more iterations compared to the cost functions where terms computed for each body (local angular momentum) or joint (mechanical power, joint torque) have been minimised (Table 5.6). Kinetic energy is similar in all solutions (and minimum for the case of minimising kinetic energy), local angular momentum is similar when minimising local angular momentum and when minimising kinetic energy, and surprisingly minimising joint torque produces lower mechanical power values than minimising mechanical power. Nevertheless, each term (mechanical power, joint torque, local or global angular momentum and kinetic energy) has in general the lowest values when that term is minimised in the cost function, compared with the results from the other cost functions, which seems reasonable.

Predicted ground reaction forces are close to the experimental ones, but they present some peaks (Figure 5.5). The relative error is higher in the case of medio-lateral contact forces (Fz). This could be related to a problem that has been observed regarding the constraint that imposes low velocity values of the foot middle point during stance. Since the middle point in the foot has very low value of

velocity during stance (sometimes close to zero), the foot tends to rotate around that point; and this could be the reason of having large values for medio-lateral foot-ground contact force. It seems that this condition (or a similar one) is necessary, because when not imposed, the feet slide when are in contact with ground. Three other options have been investigated to solve this issue in a different way: imposing low velocity in different points of the foot, using different bounds for velocity in anterior-posterior direction or for all velocity components; or minimising this velocity in the cost function. However, all strategies have resulted in worse results. More investigation is needed to improve this aspect. Regarding the peaks presented in the predicted ground reactions, they have also been observed in other works where motion is predicted without having any tracking term in the cost function [29, 157].

The multi-term cost functions require more computation time to converge than the addition of the computation times required for minimising each term in the cost function separately. However, the predictive simulations using these multi-term cost functions are not the ones that require more computation time. Results obtained using the multi-term cost functions for the *3D HAT* and *3D Full* have improved in general the features that define a correct gait pattern. However, there are some aspects that could be improved, since arm motion is not so realistic as when minimising only global angular momentum, and torso motion is a little bit abrupt compared to the experimental motion. Maybe adding some penalty terms in the cost function (e.g., penalising lateral movement or arms crossing) could produce a more realistic pattern. Regarding the global COM trajectory, it is closer to the experimental motion for the x-y plane (sagittal), than for the x-z plane (horizontal) (Figure 5.3). The values for each magnitude that has been minimised have been compared between experimental and predicted motions (Figure 5.9). It has been noticed that predicted motions have much lower values for each one of these terms, e.g., the solution minimising global angular momentum has global angular momentum that is much lower than that same magnitude computed using the experimental motion. This suggests that although angular momentum has found to be small for human walking [145], it may not be the only criterion for predicting walking. In the multi-term cost function, although mechanical power is minimised as well, the global angular momentum continues being much lower in the predicted motion than in the experimental motion.

Walking cycles at different velocities have been predicted and have converged with natural motion patterns. For the high stride length (1.2 m), range of motion for hip flexion is the highest of all solutions, whereas for the case of low stride length (0.8 m), it is the lowest of all solutions. These results are consistent with those reported in [158], where a longer step length is related with more hip flexion. Although imposing at the same time cycle duration and stride length could be seen as a limitation, note that stride length is not exactly imposed, as a tolerance is permitted in this magnitude (± 5 cm in all simulations, but could be increased if desired). Giving a mean walking speed or step (or stride) length is something widely used when predicting novel motions, because a final condition for the simulation is needed [18, 19, 26, 28, 32, 37]. Some of these works also consider cycle duration as a known parameter. Nevertheless, more research is needed in order to give

more freedom to walking speed and/or step (or stride) length in the predictive simulations.

Having ground reactions as controls in the optimal control formulation has worked well in Chapter 4, as it helped the problem to converge, because path constraint tolerances were tightened step by step. The main difference with those simulations is that experimental ground reactions were tracked, whereas in this chapter, they are fully predicted. It has been tested if the problem can be solved having ground reactions as controls and without having them. In the case of having them as controls, it has been compared having all components or only some of them: all components (three forces and three moments for each foot, twelve control variables), only forces (three forces for each foot, six control variables), or only normal forces (two control variables). For the *3D HAT* model and cost function minimising global angular momentum and joint torque change, having only normal forces as controls requires 724 iterations (16.75 min), compared with 213 iterations (4.22 min) that requires having all components as controls. In both cases, the predicted motion is very similar. When ground reactions controls are not included in the simulation, the path constraints ensuring that ground reactions controls and from contact models are equal, have to be replaced by other constraints that ensure that ground reactions are zero during swing phase. All tests done in this case (having all components in path constraints or only normal forces) have led to unfeasible solutions or have only converged for large tolerance values (500 N or Nm). This does not necessarily mean that it is not possible to predict walking cycles without having ground reactions as controls, but in that case, new constraints should be considered in order to define a walking cycle (remember that the ground reaction controls define the walking cycle by being zero or different from zero). Since the optimal control formulation with all ground reactions as controls is the one that has shown better performance in our simulations, this approach will be the one considered for the following sections of this work.

Although in this work the computation efficiency is not proposed as an objective, results are in concordance with the ones reported in the literature (and even better in some cases). In our work, for a 3D full-body torque-driven model, predictions have required from 4 min to 1 h. In [50], roughly 30 min have been required for a torque-driven prediction using a 3D full-body model, and 1 h for a muscle activation-driven prediction. In [37], an average 36 min is required for a direct collocation predictive simulation using a 3D full-body and muscle-driven model. This result is better than ours, since the considered model included muscles. Other simulations (both tracking and predictive simulations) using 2D and 3D models including muscles, varied their computation time from 30 min to 1 h [19,139], from 1 to 5 h [29, 48], or from 10 to 65 h [20, 26, 157]. Although these models include muscle-tendon groups, some of them are planar models or 3D models without arms, so computation times would be comparable with ours.

There are some aspects in this study that need further investigation, some of which have already been mentioned previously. Regarding the constraint of having low values for velocity in the midfoot during stance, it would be interesting to study how to avoid the problem of rotating around this point of near-zero velocity, while preventing foot from sliding at the same time. Moreover, the cost functions

developed by selecting different terms could be improved, adding more terms and weighting differently each term. Another fact that is critical and needs more study is that for different variable bounds and constraint tolerances (path and endpoint), different results have been obtained, thus changing the results in terms of RMSEs and ROMs compared with the experimental motion, and resulting in a different best multi-term cost function. Another limitation of the reported simulations is that finding solutions with more tightened tolerances than the ones presented in Section 5.1.1 (50 N (or Nm) for ground reaction forces, 30 Nm for joint torques, 50 N for normal forces periodicity, and 10° for angular coordinates periodicity) has been difficult. In order to find motions with more tightened tolerances, maybe tolerance values should be different for normal and tangential forces, for example, or for each angular coordinate (depending on their particular ROM).

		Convergence		Legs motion			Torso motion				Arms motion	
		n iter.	Time [min]	Correct knee flexion?	Max knee flex* [°]	Max hip abduction [°]	Correct torso motion?	ROM pelvis ML trans. [cm]	ROM lumbar ext. [°]	ROM lumbar bend. [°]	Correct arms swing?	Shoulder flex ROM* [°]
Reference value		-	-	-	60 ± 10	9.5 ± 1	-	4.5 ± 1	5 ± 2	9 ± 3	-	32 ± 4
Experimental motion		-	-	yes	60.20	7.46	yes	4.21	5.59	16.11	yes	19.80
3D HAT	**MP + tch**	84	1.61	yes	49.75	7.65	yes	2.49	6.91	8.01	-	-
	AML + tch	136	2.40	yes	46.72	10.43	stiff	5.85	6.34	11.33	-	-
	AMG + tch	213	4.22	yes	62.71	9.51	abrupt	5.65	7.01	5.64	-	-
	KE + tch	651	12.62	yes	56.64	6.35	stiff	1.58	10.41	13.78	-	-
	Torq + tch	84	1.68	yes	46.88	10.23	yes	3.01	4.96	8.17	-	-
	combination**	927	21.79	yes	64.21	3.64	abrupt	5.52	7.50	7.00	-	-
3D Full	**MP + tch**	100	3.91	yes	45.80	8.13	yes	3.59	4.77	5.38	no swing	3.16
	AML + tch	91	3.58	yes	45.72	16.40	stiff	5.91	10.63	5.56	no swing	5.93
	AMG + tch	250	9.71	yes	59.07	9.87	abrupt	4.96	7.99	9.49	yes	10.83
	KE + tch	1506	57.38	yes	55.51	5.08	stiff	2.03	10.15	9.98	no swing	10.46
	Torq + tch	127	4.90	yes	47.11	8.96	yes	3.25	3.55	7.91	no swing	2.63
	combination**	770	35.82	yes	62.74	5.41	abrupt	5.10	6.63	7.11	yes	8.71

Table 5.6: Results for the comparison of cost functions and the chosen multi-term cost function, for both models *3D HAT* and *3D Full*, compared to results found in the literature, and to the experimental values. Values for the experimental motion are taken from the *barefoot* gait data using the *3D Full* model. A total of five cost functions have been compared, all of them minimising joint torque change (tch) and each one of the optimality criteria: mechanical power (MP), local angular momentum (AML), global angular momentum (AMG), kinetic energy (KE) and squared joint torque (Torq). The references from which reference values are obtained have been shown in Table 5.3.
*The maximum knee flexion and the shoulder flexion ROM correspond to the mean values between right and left sides. In the case of maximum hip abduction, it is the maximum between right and left side, to obtain the most critical value.
**Multi-term cost function for *3D HAT*: minimising mechanical power, global angular momentum and joint torque change. Multi-term cost function for *3D Full*: minimising lower body and torso mechanical power, global angular momentum, joint torque change, and the difference between right and left shoulder flexion velocities.

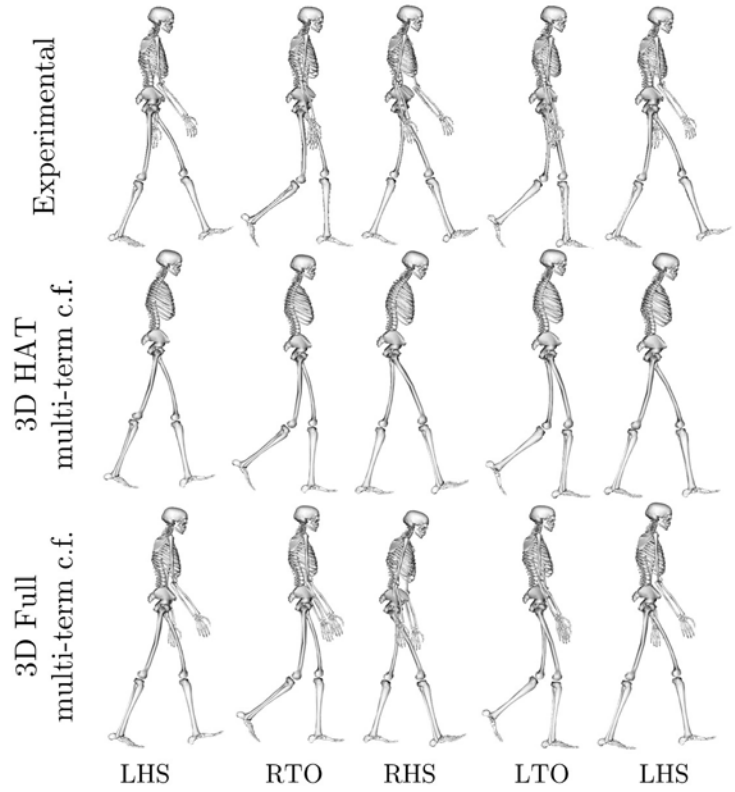

Figure 5.6: Lateral views from the experimental motion and the predicted motions using the multi-term cost function for each model. The experimental motion corresponds to the *barefoot* gait data using the *3D Full* model. Screenshots from the experimental and predicted motions are shown at the main events in the gait cycle: left heel strike (LHS), right toe off (RTO), right heel strike (RHS), left toe off (LTO), and LHS again. The multi-term cost functions are: for *3D HAT* model, minimising mechanical power, global angular momentum and joint torque change; for *3D Full* model, minimising lower body and torso mechanical power, global angular momentum, joint torque change, and the difference between right and left shoulder flexion velocities.

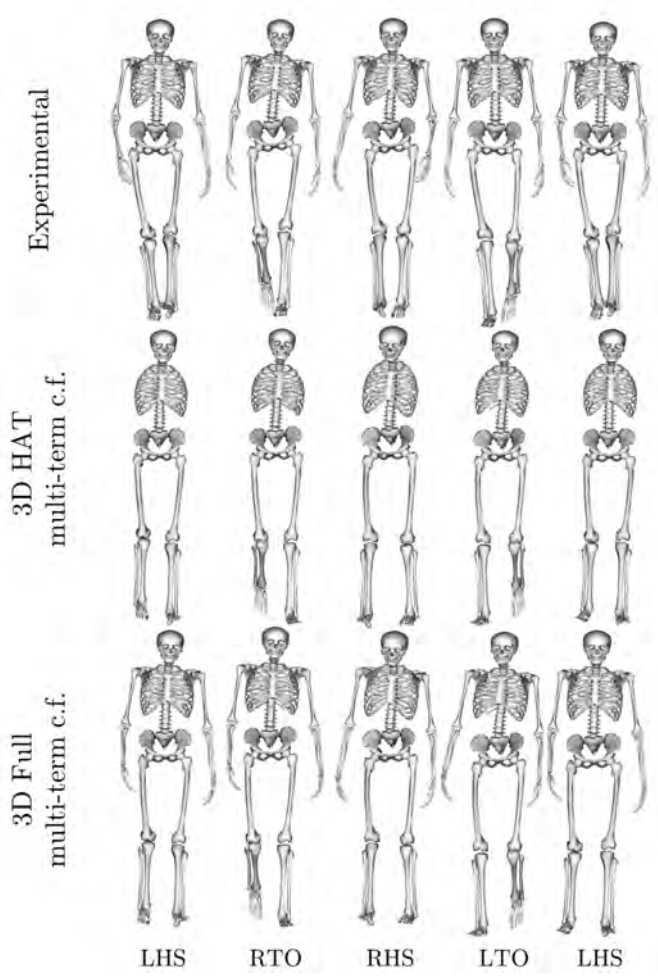

Figure 5.7: Frontal views from the experimental motion and the predicted motions using the multi-term cost function for each model. The experimental motion corresponds to the *barefoot* gait data using the *3D Full* model. Screenshots from the experimental and predicted motions are shown at the main events in the gait cycle: left heel strike (LHS), right toe off (RTO), right heel strike (RHS), left toe off (LTO), and LHS again. The multiterm cost functions are: for *3D HAT* model, minimising mechanical power, global angular momentum and joint torque change; for *3D Full* model, minimising lower body and torso mechanical power, global angular momentum, joint torque change, and the difference between right and left shoulder flexion velocities.

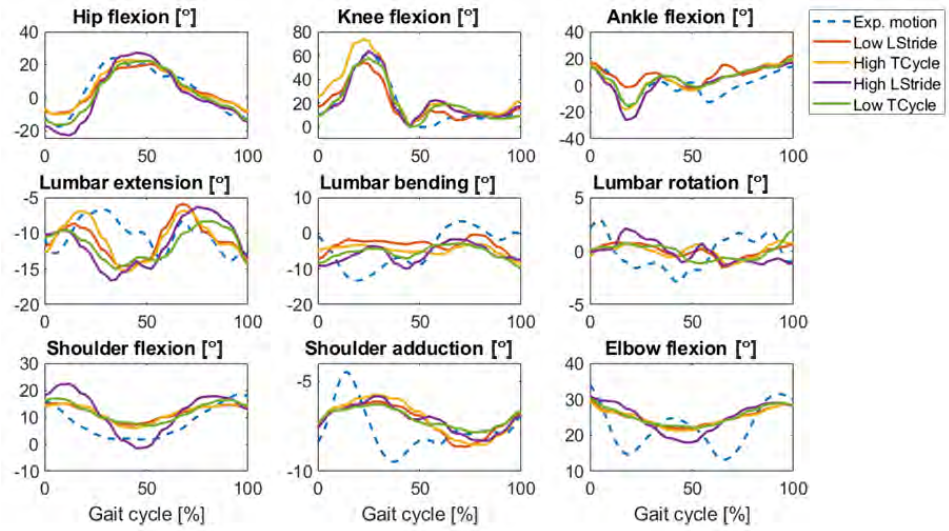

Figure 5.8: Most relevant joint coordinates for predictive simulations of walking at different speeds, using the *3D Full* model, compared to the experimental motion. The values for each stride length (LStride) and cyle duration (TCycle) are shown in Table 5.4. Results are shown for the right side of the body. Since there are different durations of gait cycle, results are shown in % of gait cycle.

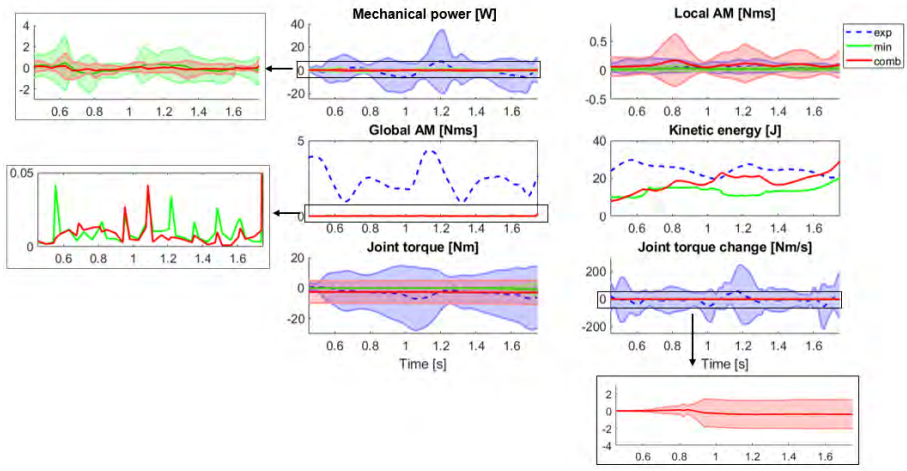

Figure 5.9: Values for the *3D Full* model of each of the terms considered in the different cost functions that have been compared in this work: mechanical power, local angular momentum (AM), global angular momentum, kinetic energy, joint torque and joint torque change. In blue, values computed from the experimental *barefoot* gait data (exp). In green, values computed from the predicted motion when each one of those terms is minimised together with joint torque change (min). In red, values computed from the predicted motion when the multi-term cost function is used (minimising lower body and torso mechanical power, global angular momentum, joint torque change, and the difference between right and left shoulder flexion velocities) (comb). For those values that are computed for each joint or body, the mean and standard deviation is plotted. Note that these values are scaled in the cost function, so they are comparable when they are minimised.

5.2 Prediction of 3D crutch-assisted walking

In this section, we seek to develop an optimal control problem formulation capable of predicting different patterns of crutch-assisted walking. Walking with crutches could induce undesirable outcomes if the achieved walking pattern has unwanted features, such as high loads on the shoulders [77–79] or high pressures in the forearm due to skin-crutch contact [76]. To avoid such issues, patients must learn how to walk with an adequate pattern using crutches, guided by the assessment of a physiotherapist. Optimal control prediction of crutch-assisted walking could be an objective method to help physiotherapists to determine the most suitable crutch-walking pattern for each patient.

The objectives of this section are the following:

1. To predict a complete gait cycle, using a 3D human body model with crutches (*3D Crutches*), without imposing symmetry and without tracking experimental data.
2. To study the convenience of predicting crutch-assisted walking with different cost functions that have been used in the literature to predict normal walking.
3. To predict crutch-assisted walking cycles following different patterns.
4. To predict crutch-assisted walking cycles at different speeds.

5.2.1 Methods

Models and data

To predict crutch-assisted walking, crutches have been added to the *3D Full* model, obtaining the *3D Crutches* model (described in Section 3.1.1). A non-alternate four-point crutch walking pattern has been captured experimentally, as described in Section 3.2. This atypical crutch-walking pattern has been chosen since it is different from the alternating four-point-crutch walking pattern chosen most frequently by patients, thereby providing a qualitative test case for optimal control walking predictions.

The foot-ground and crutch-ground contact models used in this section differ in some aspects from the contact models presented in Section 4.2. The foot-ground contact model consists of 10 spring and damper units, distributed in four groups on each foot (Figure 5.10). The local position of each spring and damper unit, x, z, and the spring resting length of each group, y_0, have been calibrated. For the crutch-contact model, the radius of the sphere has been calibrated, but not the coefficient of dynamic friction, that has been considered to be 1. Parameters have been calibrated following an approach similar to the one presented in Section 4.2, and results for each contact model parameter are shown in Table 5.7. Mean RMSE for ground reactions obtained from contact models compared to experimental measurements are 5.53 N for forces and 6.27 Nm for moments.

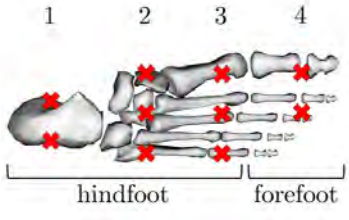

	Spring-damper group			
	Hindfoot			Forefoot
Location	1	2	3	4
x	0.03	0.11	0.15	0.02
y	0.00	0.00	0.00	0.00
z	$-0.7{\cdot}10^{-3}$	-0.04	-0.05	0.00
	0.00	0.02	-0.02	0.04
	-	0.04	0.01	-

Figure 5.10: Local position of each of the 10 spring-damper units, that are distributed in four groups. Spring-damper units of groups 1 to 3 are located on the hindfoot, and spring-damper units of group 4 are located on the forefoot.

Foot-ground contact model parameter	Group 1	Group 2	Group 3	Group 4
Spring stiffness [N/m]	2605	2886	4014	3563
Damping coefficient [s/m]	45.75	$1.45{\cdot}10^{-4}$	1.44	1.91
Spring resting length [cm]	0.75	-0.55	-1.5	-1.39
Coefficient of dynamic friction [-]	0.18	0.09	0.15	0.46

Crutch-ground contact model parameter	Tip
Generalised normal stiffness [$N/m^{3/2}$]	$9.35{\cdot}10^{3}$
Hysteresis damping factor [$Ns/m^{5/2}$]	$8.96{\cdot}10^{4}$
Sphere radius [cm]	4.3

Table 5.7: Calibrated parameters for foot-ground [64] and crutch-ground [96] contact models. Symmetry is imposed between right and left feet, and right and left crutches. Each group of springs for the foot-ground contact model is shown in Figure 5.10.

Once the foot-ground and crutch-ground contact model parameters have been calibrated, a dynamically consistent full-cycle that closely reproduces the experimentally measured motion and ground reactions has been generated following the approach presented in Section 4.3. This resulting crutch-walking motion has been used as reference data for optimal control crutch-walking predictions.

Optimal control problem formulation

Three different crutch-walking patterns have been predicted using an optimal control problem. The main structure of the problem is similar to the problem used for normal walking prediction, that has been presented in Section 5.1. Only differences with respect to that problem formulation are included here.

Variables

States and controls are the ones described in Section 5.1, and the vector of ground reaction controls, $\mathbf{GRF}_u$, includes also the crutch-ground reaction forces.

Cost function

From the different cost function terms presented in Table 5.2, six combinations have been chosen: minimising mechanical power, local angular momentum or kinetic energy, together with minimising squared joint jerk or torque change. To give more importance to the optimality criteria, a weight of 0.01 is placed on the term that minimises joint jerk or torque change.

The general cost function can be described as:

$$J_{ij} = \int_{t_0}^{t_f} \Big(J_{opt,i}(\mathbf{x}, \mathbf{u}) + 0.01 J_{reg,j}(\mathbf{x}, \mathbf{u}) \Big) \mathrm{d}t \tag{5.5}$$

where t_0 and t_f are the initial and final simulation times. The different optimality terms used, $J_{opt,i}(\mathbf{x}, \mathbf{u})$, to be considered in the cost function are: (1) the sum of the squared norms of the local angular momenta, $\sum_{i=1}^{n_b} \|\mathbf{L}_i\|^2$, being n_b the number of bodies in the model and $\mathbf{L}_i$ the local angular momentum at the centre of mass of the i^{th} body of the model; (2) the sum of squared mechanical power, computed for each relative coordinate (i.e., not for the absolute pelvis translation and rotation coordinates), $\sum_{i=7}^{n_q} (\dot{q}_i \tau_{i-6})^2$, being $\dot{q}_i$ the i^{th} component of the vector of generalised velocities, $\dot{\mathbf{q}}$; and (3) the squared value of the model kinetic energy, T^2. The different regularisation terms, $J_{reg,j}(\mathbf{x}, \mathbf{u})$ are: (1) the sum of squared joint jerks, $\sum_{i=1}^{n_q} \dddot{q}_i^2$, being $\dddot{q}_i$ the i^{th} component of the vector of generalised jerk, $\dddot{\mathbf{q}}$; and (2) the sum of squared joint torque changes, $\sum_{i=1}^{n_q - 6} \dot{\tau}_i^2$, being $\dot{\tau}_i$ the i^{th} component of the vector joint change, $\dot{\boldsymbol{\tau}}$.

Dynamic constraints

Dynamic constraints are the ones described in Section 5.1.

Path constraints

Path constraints are the ones described in Section 5.1, adding the corresponding path constraints ensuring that crutch-ground forces are equal to the forces obtained with the contact model. Moreover, lateral distance between each crutch and foot from the same side is bounded in a path constraint, and stride length and nonsliding condition (near zero velocity of the contact point during stance phase) are imposed also to the crutch tips.

Endpoint constraints

Endpoint constraints are the ones described in Section 5.1, where the feet and crutches initial position depends on the predicted crutch-walking pattern (Figure 5.11, left). Swing duration and stride length have been taken from the measured motion (0.96 s and 0.84 m, respectively), and adapted to each crutch-walking pattern.

Boundary conditions

Boundary conditions are the ones described in Section 4.1.

Studies performed and evaluation of results

With the aim of predicting crutch walking cycles following different patterns and at different speeds, different studies have been performed. First, the same crutch-walking pattern than the experimental data is followed, and then, the approach is extended to other crutch-walking patterns.

1. Cost functions comparison.
   Using the reference gait cycle as an initial guess and the different cost function formulations, new crutch-walking motions that follow the same four-point non-alternating gait pattern have been predicted without tracking any experimental data. Stride length and phase durations have been imposed from the experimental data to obtain predicted crutch-assisted walking motions comparable to the reference motion. For crutch-walking patterns, there are not so clear gait determinants as in normal walking. For this reason, to assess the results and choose the best cost function for crutch walking prediction, RMSE between predicted and reference joint coordinates and ground reactions, and differences in joint ROM have been computed.

2. Multi-term cost function.
   With the aim of obtaining a better walking cycle, and according to the previous results, a multi-term cost function has been considered, taking for each part of the body the optimisation criterion for which best results in terms of error have been achieved. To check that the resulting motion reproduces better the experimental motion, RMSE between predicted and reference joint coordinates and ground reactions, and differences in joint ROM have been computed.

3. Crutch walking patterns prediction.
   To develop a method that can predict any crutch-assisted walking pattern, we have made several modifications to the previous problem formulation. The walking cycle has been parameterised based on swing phase duration and stride length. We have assumed that swing duration is the same for feet and crutches for both the right and left sides. Duration of multiple support phases between consecutive swing phases have also been considered to be the same. Three new walking patterns have been predicted: (1) four-point alternating gait, (2) two-point (or reciprocal) gait, and (3) swing-through gait. For each walking pattern, the sequence of swing phases is as follows: (1) four-point alternating gait: right crutch, left leg, left crutch, right leg; (2) two-point gait: right crutch and left leg, left crutch and right leg; and (3) swing-through gait: both crutches, both legs ahead of the crutches [133] (Figure 5.11, right). The initial position, which has been added as an endpoint constraint, is also pattern-dependent (Figure 5.11, left). Swing duration and

stride length have been imposed, taken from the measured motion (0.96 s and 0.84 m, respectively). To assess simulation results, joint coordinates, joint torques, and ground reactions have been compared against results from literature, and ground reactions have been compared among crutch-gait patterns.

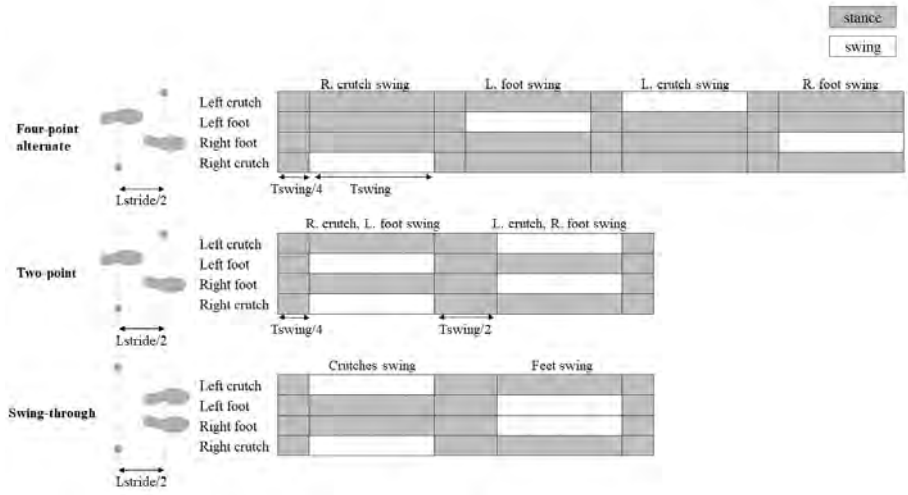

Figure 5.11: Description of each crutch-walking pattern using stride length (Lstride) and swing duration (Tswing). Initial position has been the same for four-point and two-point walking patterns. Multiple support had a duration of a quarter of swing phase duration for four-point gait pattern and of half of the swing phase duration for two-point and swing-through gait patterns. It has been split between the beginning and end of the cycle for two-point and swing-through patterns to facilitate convergence and periodicity of ground reactions. The duration of a complete gait cycle has been five times swing duration for the four-point gait pattern, and three times swing duration for the two-point and swing-through gait patterns.

4. Prediction at different speeds.
   Variations from the first new walking pattern (four-point alternating gait) have been predicted for faster and slower speeds by modifying cycle time or stride length (Table 5.8). Both quantities, cycle time and stride length, are imposed in the problem formulation: swing phases for each foot and crutch are determined from the cycle time, and this information is used to define when ground reactions are zero; and stride length has been imposed in the endpoint constraints, as explained previously. To assess the results from speed variations within the same gait pattern, joint coordinates have been compared against those obtained for the prediction with initial values of cycle time and stride length.

	Initial	Low speed (-15%)		High speed (+15%)	
		Low stride length	High cycle time	High stride length	Low cycle time
Speed [m/s]	0.18	0.15		0.20	
Stride length [m]	0.84	0.74	0.84	0.95	0.84
Cycle time [s]	4.80	4.80	5.50	4.80	4.10

Table 5.8: Values of stride length and cycle time (or duration) considered in each variation of speed for the four-point alternating gait pattern. Stride length and cycle time are imposed values in the problem formulation, and speed is computed from them.

5.2.2 Results

Cost functions comparison

All six cost functions have converged for the four-point non-alternating gait, with stride length and swing durations imposed from experimental data. Convergence is better (less number of iterations and less computation time) for the case of minimising mechanical power and joint jerk, closely followed by the case of minimising angular momentum and torque change (Table 5.9). Convergence is worse (up to 10 times more iterations and computation time) when minimising kinetic energy and joint jerk. Overall, minimising angular momentum shows less error with respect to the reference motion than minimising mechanical power or kinetic energy. Mean RMSE for all angular coordinates is lower when minimising angular momentum and joint jerk (6.30°), while mean difference of ROM for all angular coordinates is lower when minimising angular momentum and torque change (7.26°). With jerk minimisation, differences in joint coordinates ROM with respect to reference values are larger (7° to 18°) than with torque change minimisation (5° to 15°). In all cases, ROMs are lower for the solution than for the reference motion, so the larger the difference in ROM, the smaller the ROM is for that group of coordinates in the solution. In the case of torso coordinates (i.e., lumbar joint), RMSE is lower for minimisation of mechanical power and joint jerk (5.96°), and ROM difference is lower for minimisation of kinetic energy and torque change (7.30°). Regarding ground reactions, minimising mechanical power and joint jerk is the cost function with lowest mean RMSE for normal forces (40.2 N), while minimising angular momentum and torque change is the cost function with lowest mean RMSE for tangential forces (12.67 N). Qualitatively, minimising joint jerk leads to smoother coordinates than minimising torque change, while minimising torque change leads to smoother ground reactions than minimising joint jerk.

Multi-term cost function

According to these results, a multi-term cost function has been considered, taking for each part of the body the optimisation criterion for which best results in terms of error have been achieved. The proposed cost function is minimising angular momentum of upper and lower limb segments, mechanical power of lumbar and

		Joint jerk			Torque change			Multi-term
		Mechanical power	Angular momentum	Kinetic energy	Mechanical power	Angular momentum	Kinetic energy	
Convergence	Iterations	**91**	199	952	134	96	310	758
	Time [min]	**2.92**	6.4	35.84	4.99	3.64	17.51	35.04
Mean RMSE coordinates	Full body [°]	6.65	**6.3**	9.19	7.69	8.21	7.51	***6.69***
	Torso [°]	**5.96**	6.18	9.83	7.63	7.32	7.89	**5.72**
	Upper limbs [°]	8.84	**8.22**	10.29	9.25	8.66	8.98	***8.57***
	Lower limbs [°]	**5.21**	4.89	8.09	6.39	8.29	6.12	***5.49***
Mean absolute difference of ROM	Full body [°]	12.41	12.14	11.24	9.71	**7.26**	9.61	11.08
	Torso [°]	11.22	12.92	12.02	10.13	8.65	**7.3**	***10.3***
	Upper limbs [°]	18.21	17.12	16.55	14.3	**9.43**	15.61	15.89
	Lower limbs [°]	8.9	8.38	7.22	6.01	**5.57**	5.75	8.03
Mean RMSE ground reactions	Normal [N]	**40.2**	44.15	58.09	48.65	58.42	52.06	51.55
	Tangential [N]	15.41	16.65	28.28	13.62	**12.67**	14.13	**12.62**
	Moments [Nm]	4.76	**4.71**	7.6	5.18	5.06	5.78	***5.18***

Table 5.9: Number of iterations, computation time, and mean RMSE of coordinates, mean difference in ROM, and mean RMSE of ground reactions with respect to the dynamically consistent reference data. Coordinates are grouped for torso (lumbar joint), upper limbs (shoulder, elbow and wrist), and lower limbs (hip, knee, ankle, subtalar and metatarsal). The best result of the six initial cost functions for each magnitude is highlighted in bold text. In the last columns, results for the multi-term cost function are shown. This cost function involves minimisation of lumbar and lower body mechanical power, upper and lower limbs angular momentum, joint jerk (0.01 weight) and torque change (0.01 weight). In bold and underlined, results that are better than all the six initial cost functions are highlighted; in bold and italics, results that are better than the mean of all the six initial cost functions are highlighted.

lower limb joints, and both joint jerk and torque change. In this case, states are joint coordinates, joint velocities, joint accelerations and joint torques; and controls are joint jerk and joint torque change (Table 5.1). Using the multi-term cost function, the computation time and number of iterations increase when compared to the previous formulations, but the results in terms of RMSE and differences in ROM with respect to the reference motion are the best overall (Table 5.9, last column). Pelvis tilt, pelvis rotation, lumbar extension and hip flexion are well predicted, both in shape and in ROM, and RMSEs for these coordinates are between 3.3° and 6.4° (Figure 5.12). On the other hand, hip rotation, lumbar bending, arm flexion and wrist flexion follow the tendency of experimental data, but ROMs have reduced (e.g., 30° less ROM for arm flexion). Regarding ground reactions, normal forces follow the tendency of reference data, but the computed forces are smoother than the experimental ones, especially foot-ground reactions (Figure 5.13).

Crutch walking patterns prediction

Having the walking cycle parameterised based on the swing phase duration and stride length, three new walking patterns (for which no experimental data are available) have been predicted: four-point alternating, two-point and swing-through crutch gait patterns. Four-point alternating pattern has converged when using the multi-term cost function, but two-point and swing-through patterns have not.

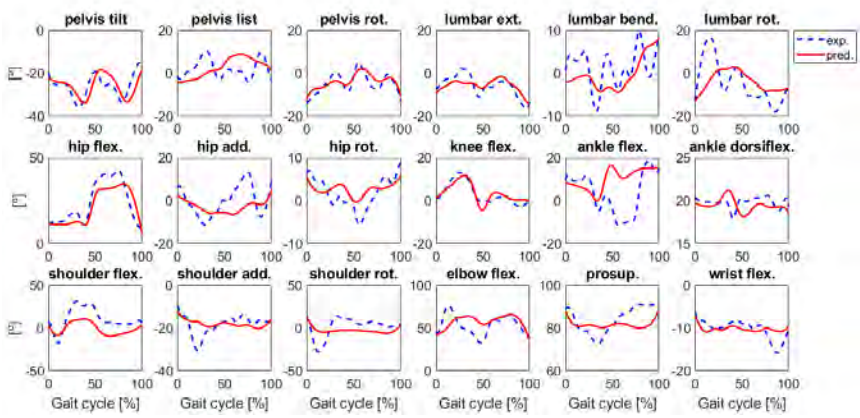

Figure 5.12: Joint coordinates for the multi-term cost function (minimisation of lumbar and lower body mechanical power, upper and lower limbs angular momentum, joint jerk, and torque change). Predicted curves (pred.) are shown in solid red lines, and reference curves (exp.) are shown in dashed blue lines. Note that scales of vertical axes are different for each coordinate. Only the right side of the body is shown. Tracking errors are comparable on the left side.

For that reason, the cost functions for which convergence was better –minimising mechanical power and joint jerk, and minimising angular momentum and torque change (Table 5.9)– have been used to predict these new patterns. It has been found that the three new patterns converge when minimising angular momentum and torque change. The results obtained using the latter cost function have been used to compare the three new crutch-assisted walking patterns. Maximum values for vertical foot-ground reactions are around 50-60% body weight (BW) for four-point gait, almost 80% BW for two-point gait, and around 50% BW for swing-through gait (Figure 5.14). In the case of crutches, the maximum values for vertical reactions are 35% BW for four-point gait, 30% BW for two-point gait, and 50% BW for swing-through gait (Figure 5.14). Shoulder angles are similar for four-point gait and two-point gait patterns, in terms of ROM and maximum and minimum values (Figure 5.15, top). Regarding swing-through gait pattern, shoulder flexion-extension presents higher symmetry than the other shoulder coordinates. Shoulder flexion and adduction torques are higher for the swing-through gait pattern. For example, maximum value for shoulder flexion torque is 5.4 %BW*H (i.e., percentage of body weight times height), compared to 1.38 %BW*H for two-point gait and 2.9 %BW*H for four-point gait (Figure 5.15, bottom).

Prediction at different speeds

The presented formulation allows to predict crutch walking cycles at different speeds. For the four-point alternating crutch gait pattern, predictions at higher and lower speeds have been obtained by modifying initial stride length or cycle duration values (Table 5.8). The cost function used in these predictions has been

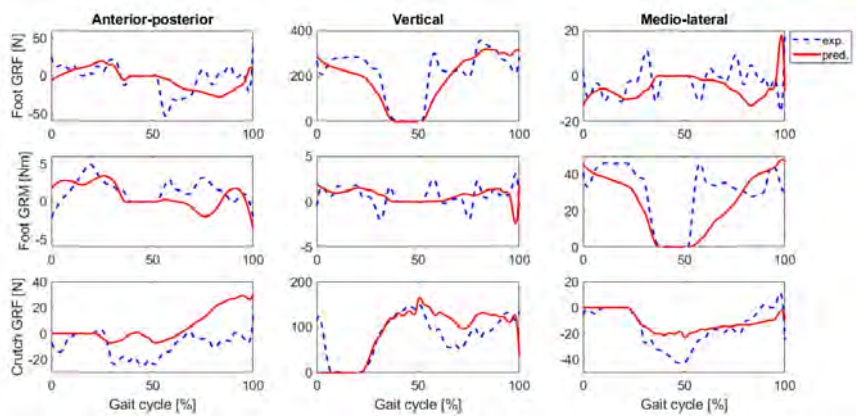

Figure 5.13: Foot- and crutch-ground reactions for the multi-term cost function (minimisation of lumbar and lower body mechanical power, upper and lower limbs angular momentum, joint jerk and torque change). Moments are computed at the origin of the calcaneous body. Predicted force or moment components (pred.) are shown in red, and their reference values (exp.) are shown in dashed blue. Note that scales of vertical axes are different for each force or moment. Only the right reactions (foot and crutch) are shown.

the multi-term cost function. Convergence is better when only cycle duration is modified, without varying stride length (36-39 iterations); while varying stride length, without varying cycle duration, requires much more iterations (298-363). Considering differences for all angular coordinates with respect to the movement at initial speed, the closest solution is the one with low cycle time and initial stride length (mean RMSE is 2.4°), while the solution with larger differences is the one with high stride length and initial cycle time (mean RMSE of 5.9°). For constant cycle time, differences in some coordinates are observed when stride length is modified (Figure 5.16). For the case of low speed (that is, low stride length), the larger difference is found in lumbar joint (mean RMSE of 5.71°). In this case, the torso is less inclined (i.e., sum of pelvis tilt and lumbar extension is lower in absolute value) and hip flexion is lower during all cycle compared to the movement at initial speed. For the case of high speed (that is, high stride length), the larger difference is obtained for lower limb joints (mean RMSE of 6.6°). In this case, hip flexion is lower during swing phase for right leg and higher during swing phase for left leg compared to the movement at initial speed. Moreover, elbow flexion is higher during almost all cycle time.

5.2.3 Discussion

The aim of this section is to generate a method to predict three-dimensional crutch-assisted walking motions following different patterns without tracking any experimental data. For that, different cost functions have been tested, comparing the obtained predictive simulations with experimental data (joint coordinates and ground

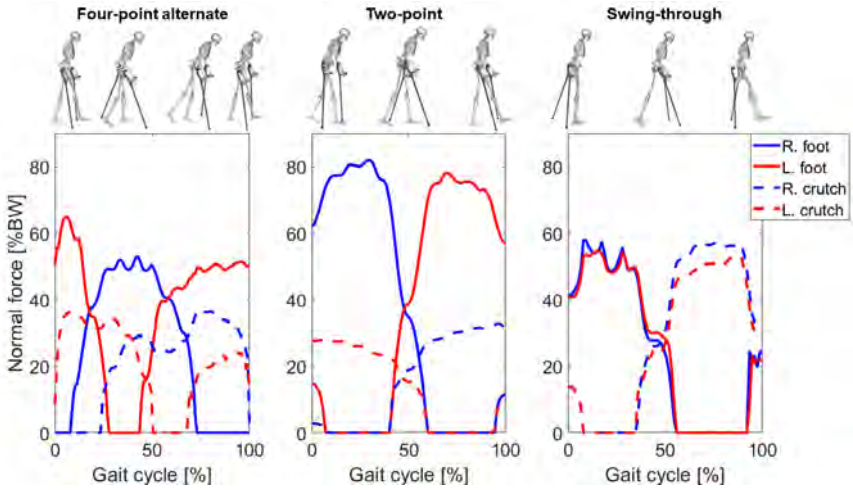

Figure 5.14: Sagittal views and normal ground reactions for the three different walking patterns. The cost function used for the prediction is minimising angular momentum and torque change. Normal reactions are shown in %BW (i.e., percentage of body weight).

reactions) from a healthy subject following a four-point non-alternating crutch gait pattern. To reduce errors with respect to reference data, a cost function combining minimisation terms of angular momentum, mechanical power, joint jerk and torque change has been chosen. This cost function has been used to predict four-point alternating crutch gait at the same speed as the experimental conditions and at a higher and lower speeds. However, this cost function has not converged for two-point and swing-through crutch gait patterns, which have been predicted minimising angular momentum and torque change. The fact that not all patterns have converged for the cost function that has given better results for four-point non-alternating gait may indicate that the optimality criteria are pattern-dependent. A key aspect of the presented algorithm is that having ground reactions as additional controls allows to define phases inside the cycle without the need of formulating a multiple phase problem, and facilitating the definition of different crutch walking patterns. Small variations of the problem to predict more weight bearing on one side than the other or having only one crutch are easy to implement, giving a wide margin of applications to this formulation. To our knowledge, no studies have yet predicted three-dimensional full-cycle crutch walking patterns using a full-body model. Moreover, there are few studies where novel gait motions are predicted without tracking any experimental data [122]. The developed predictive approach could be applied to study different biomechanical aspects of crutch walking in virtual subjects, to assist physiotherapists to choose the optimal crutch walking pattern for a specific subject, and to help in the design and control of exoskeletons, when crutches are needed for balancing.

The combination of terms chosen for the cost function (minimising angular momentum of upper and lower limbs, mechanical power of lumbar and lower limbs joints, and both joint jerk and torque change) presents overall better results in

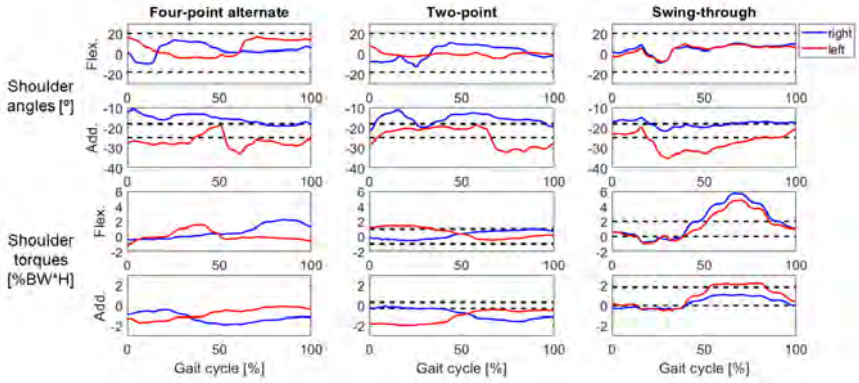

Figure 5.15: Shoulder coordinates in degrees and torques in %BW*H (i.e., percentage of body weight times height) for each walking pattern. In blue, results for right side and in red, results for left side. In black dashed lines, maximum and minimum values from experimental studies have been taken for comparison. Values for four-point gait pattern have been taken from [76] (only angles), and values for two-point and swing-through gait patterns have been taken from [77] (angles and torques). Values for shoulder angles are positive for flexion and adduction.

error terms when compared to the six initial cost functions for the four-point non-alternating crutch gait pattern (Table 5.9). However, there are not large differences in errors among cost functions and some solutions are very similar. For instance, regarding ground reaction normal forces, the difference between the lowest and the largest RMSE is 18 N, that is, only a 3% of the maximum value for experimental normal forces. As different optimality criteria lead to similar solutions, it seems that the solution depends more on how the problem is formulated (in terms of constraints and initial guess, for example) than on the particular criterion used in each case. It is not clear how these criteria are related among them or with the task of crutch walking [137, 157]. The fact that the proposed formulation has predicted correctly four-point gait (alternating and non-alternating) does not imply that it corresponds to the physiological criteria that humans follow when walking with crutches. More research is needed to find these criteria. In our predictive simulations, we have found that qualitatively joint jerk minimisation produces smoother joint coordinates, while torque change minimisation produces smoother ground reactions. The minimisation of both variables at a time produces coordinates and ground reactions that are not as smooth as when they have been minimised separately, and they look qualitatively more realistic. We have not found studies that minimise at the same time joint jerk and torque change, as they are considered to be comparable criteria [123, 159], although they produce different motions for gait [27] or arm reaching tasks [160–162].

Results for the three new crutch walking patterns (four-point alternating, two-point, swing-through) are consistent with experimental results from previous studies on crutch locomotion. Regarding ground reactions, in swing-through gait pattern the weight is distributed in a similar way between feet and crutches, while in

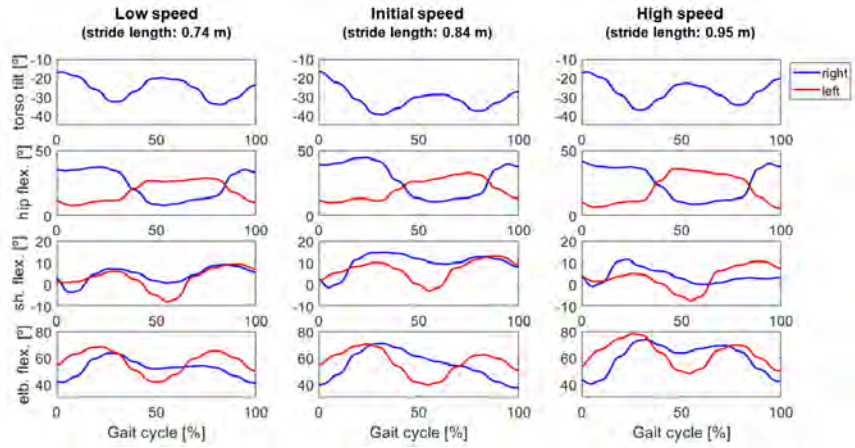

Figure 5.16: Some joint coordinates for predictions at different speeds for four-point alternating pattern. All simulations have been done with the same cycle time (4.80 s). In blue, right coordinates, in red, left coordinates. Torso tilt is the torso inclination (sum of pelvis tilt and lumbar extension), positive backwards. "sh. flex." stands for shoulder flexion, and "elb. flex" stads for elbow flexion.

four-point and two-point gait patterns, more weight is supported by the feet [133]. Two-point and four-point patterns have similar values for normal forces, being the ones in two-point gait a little bit higher. This result is in agreement with [163], where plantar pressures in normal walking, four-point crutch walking and two-point crutch walking were measured and compared. Regarding shoulder coordinates, shoulder flexion-extension curves for all patterns are inside the maximum and minimum values extracted from [76, 77], and follow a similar tendency for four-point and two-point gaits. In the case of swing-through gait, the results are almost symmetric, although symmetry has not been imposed, which indicates that the movement of the legs is parallel [164, 165]. Conversely, the ROM and mean value for shoulder abduction-adduction, though similar for all three walking patterns, are not inside the maximum and minimum values extracted from [76, 77]. These differences may be due to the large variability presented in crutch walking among subjects [76]. Regarding shoulder torques, swing-through gait presents higher values for shoulder flexion and abduction moments, which is consistent with the fact that this pattern requires considerable upper body strength to support the entire body weight [133, 164]. However, the values obtained in our simulations are higher than those reported in [77].

Results for the different variations of four-point alternating gait are reasonable. The initial guess used has been the solution with initial stride length (0.84 m) and initial cycle time (4.80 s). It was expected that much less iterations are needed for the simulations with the initial stride length, that only vary the cycle duration, compared with the simulations with modified stride length, because coordinates need to change in order to adapt to the new stride length. For the initial cycle duration and lower stride length, the strategy followed by the solution to reduce

stride length is to incline less the torso and to reduce shoulder flexion and elbow flexion. Conversely, for the initial cycle duration and higher stride length, the strategy followed by the solution to increase step length is to increase hip flexion. Although this is not done symmetrically, as hip flexion increases for the left leg but decreases for the right leg, the variations of both at the same time produce a higher stride length. A longer step length is related with more hip flexion [158] and, in crutch walking, step length is also related with shoulder and elbow flexion. This is in agreement with our predictive crutch walking simulations, where reducing shoulder and elbow flexion produces gaits with reduced stride length, and increasing hip flexion produces gaits with increased stride length.

This study possesses some limitations regarding the experimental data used, the initial guess generation for each pattern, and the global optimality of the solutions. Only a single walking cycle for one subject and one type of walking pattern has been collected, and we have used manual tuning of each term in the cost function [32, 157], instead of solving an inverse optimal control problem to find the weights for each term [166, 167]. Moreover, we have investigated only terms that are used for normal walking prediction, that may not be exactly the ones representing the physiological criteria for crutch locomotion prediction. Therefore, more research is needed regarding the cost function formulation for crutch-assisted locomotion. Another limitation is that the process of generating a first initial guess for each crutch walking pattern has been manual. For the different walking patterns, the same formulation (cost function and constraints) has converged or not depending on the initial guess. Since this is a common limitation in direct collocation methods, as the convergence relies on having good initial guesses [122], more research is needed on how to objectively define this initial guess. Finally, the obtained solutions could be local minima, because for different combinations of IPOPT and mesh tolerances that we have tested (for the four-point non-alternating gait pattern), each cost function has converged to different solutions.

5.3 Conclusions

Prediction of 3D normal walking

- Minimising mechanical power, global angular momentum and joint torque change are the cost function terms that have provided better results for both models (with and without arm motion).
- Results obtained using the multi-term cost functions for the *3D HAT* and *3D Full* models have improved in general the features that define a correct gait cycle. However, there are some aspects that could be improved (e.g., arm swing, torso sway). A more detailed study regarding the different cost function terms is needed to find a multi-term cost function that predicts better normal walking.
- Having ground reactions as controls (three forces and three moments for each foot, twelve control variables) helps the problem to converge, and this is the option for which we have obtained most accurate results.
- Having a final condition for the simulation (e.g., imposing stride length or periodicity) helps the problem to converge.
- Limiting the value of velocity for contact points avoids sliding, but it has some problems associated, like the foot trying to rotate around that point. More research is needed to find other ways to avoid sliding during stance phase for each foot.
- Walking cycles at different velocities have been predicted and have converged with natural motion patterns. Nevertheless, more research is needed in order to give more freedom to walking speed and/or step (or stride) length in the predictive simulations.

Prediction of 3D crutch-assisted walking

- Having ground reactions as additional controls allows to define phases inside the cycle without the need of formulating a multiple phase problem, thus facilitating the definition of different crutch walking patterns in the same problem formulation.
- The combination of terms chosen for the cost function (minimising angular momentum of upper and lower limbs, mechanical power of lumbar and lower limbs joints, and both joint jerk and torque change) presents overall better results in error terms when compared to the six simple cost functions for the initial four-point non-alternating crutch gait pattern.
- The fact that not all patterns have converged for the cost function that has given better results for four-point non-alternating gait may indicate that the optimality criteria are pattern-dependent.

- We have investigated only terms that are used for normal walking prediction, which may not be exactly the ones representing the physiological criteria for crutch locomotion prediction. Therefore, more research is needed regarding the cost function formulation for crutch-assisted locomotion.
- A critical aspect of this study is that the convergence of the simulations can depend on the chosen initial guess, and it is not clear how to objectively define the initial guess for each crutch walking pattern.

Chapter 6

Application to crutch-orthosis-assisted walking

The main objective of this thesis is to contribute to the development of methods to predict assisted walking and provide support to the design and control of assistive devices, such as exoskeletons and orthoses. As a future goal, we want to use the developed methods in this thesis to computationally predict the optimal crutch-orthosis- assisted walking pattern for spinal cord-injured (SCI) patients, with the aim of personalising an active knee-ankle-foot orthosis (KAFO) controller to the unique needs of individual SCI subjects [7]. In this chapter, the crutch-orthosis-assisted walking pattern is predicted for a healthy young female and a young male with spinal cord injury. For that, the methods developed in Chapters 4 and 5 are used as the starting point. The selected cost function includes tracking terms [22, 50], and gait cycle duration and stride length are added as free parameters of the optimal control problem formulation.

6.1 Objectives

To achieve the goal of this chapter, some specific objectives are stated:

1. Collect experimental walking motions at different values of active orthosis maximum knee flexion for a healthy subject (using crutches) and an SCI subject (using a walker or crutches, depending on the case).
2. Analyse and compare experimental data:
    a For the healthy subject, extended knee motion versus active motion (at different maximum knee flexion values).
    b For the SCI subject, extended knee motion versus active motion, with walker.

   c For the SCI subject, walking with walker versus walking with crutches, for the extended knee motion.

   d Healthy subject change in spatiotemporal parameters versus SCI subject change in spatiotemporal parameters, comparing assisted motion with locked knee and assisted motion with knee flexion-extension.

3. Use the collected data to develop a subject-specific model of both subjects, with calibrated foot-ground and crutch-ground contact models.

4. Use the collected extended knee motion with crutches to obtain a dynamically consistent (DC) assisted walking cycle for both subjects.

5. Having the DC extended knee motion as an initial guess, predict how both subjects will walk with active orthoses and crutches, first with locked knee, and for two different maximum knee flexion values.

6. Evaluate the obtained results comparing them with the experimental data of both subjects:

   a For the healthy subject, compare predicted motions with experimental motions with crutches. Compare joint coordinates, ground reaction forces, and change in spatiotemporal parameters between motions with extended knee and with knee flexion.

   b For the SCI subject, compare change in spatiotemporal parameters between motions with extended knee and with knee flexion, comparing the change in experimental motions with walker with the change in predicted motions with crutches.

6.2 Methods

The methods studied in Chapters 4 and 5 have been used to develop a subject-specific model of a healthy and an SCI subject, to find a dynamically consistent motion for a complete crutch-walking cycle, and to predict different motions assisted by active KAFOs. Since methods have been presented previously, in this section they will be introduced briefly, remarking the difference (if necessary) with the methods used in the previous chapters.

6.2.1 Data collection and models development

As it has been explained in Section 3.2, several assisted walking cycles have been collected for a healthy young female and an SCI young male. The functioning of the active orthoses, as well as the assumptions done in the model, have been explained in Section 3.1.3. In Table 6.1, the knee angle trajectory parameter values for the 7 different type of trials are given. The crutch gait pattern followed by both subjects has been an alternating four-point pattern. For the SCI subject, it has been challenging to walk using the active orthoses and crutches, and he has needed to perform two additional crutches steps, in order to maintain balance. The captures

will be named in this chapter as PASS, for the motions with locked knee (as this pattern is comparable to the gait pattern using passive orthoses), and ACTXX, for the motions with assisted knee flexion, where "XX" is the maximum knee flexion (20°, 40° or 60°).

Parameter	Definition	Unit	Healthy	SCI (W)	SCI (C)
k_a	Maximum knee flexion	[°]	0, 40, 60	0, 20, 40	0
k_s	Peak displacement parameter	[-]	-0.1	-0.1	-0.1
k_w	Peak width parameter	[-]	0.12	0.12	0.12
t_c	Cycle duration	[s]	0.8	0.8	0.8

Table 6.1: Experimental values for each parameter that define the assisted knee flexion, following Eq. 3.8. The healthy subject performed three trials assisted by the active orthoses and crutches, the SCI subject performed three trials assisted by active orthoses and a walker (W), and one trial assisted by active orthoses and crutches (C). Values for peak displacement parameter k_s, peak width parameter k_w, and cycle duration t_c where set equal for both subjects and all captures. Maximum knee flexion k_a was the only parameter that was modified from one capture to another.

The healthy subject model is the one used in Chapters 4 and 5, with two small variations: (1) the crutches have been again attached to hands using all experimental captures (with locked knee and with knee flexion), having more relative weight for the tip crutches in the inverse kinematic analysis (IKA) in OpenSim; and (2) the foot- and crutch-ground contact models have been calibrated again using the locked knee motion capture. The optimal control problem (OCP) for contact models calibration is based on the one presented in Section 4.2, using as parameters initial guess the values obtained for the *3D Crutches* model in that section. An additional term in the cost function minimises the error between experimental and simulated positions for heels, metatarsal joint centres, and crutch tips (differently than the penalty term used in Section 4.2).

The SCI subject model has been developed as explained in Section 3.1.3. Joint torques acting at hip have been limited assuming that the patient used the 90% of his capacity during the experimental capture with locked knee and crutches [58]. The foot-ground contact model parameters have been calibrated using an additional capture of the patient placing one foot on each force plate (explained with more detail in Section 3.2). The crutch-ground contact model parameters have been taken from the healthy subject results, since the instrumented and non-instrumented crutches are the same type of crutches.

6.2.2 Data analysis

The main objective of the experimental data analysis is twofold: to find evidences to develop the cost function and constraints in the prediction problem, and to evaluate results from prediction. For each subject and capture, the more representative walking cycles have been used to compute different spatio-temporal parameters. For the healthy subject, one cycle has been used, corresponding to the cycle for

which more force plates data were available. For the SCI subject with walker, three cycles have been used, and for the SCI subject with crutches, one cycle has been used.

For crutch walking motion, spatiotemporal parameters and other magnitudes used to study kinematics and dynamics are not so commonly defined as in normal walking [168,169]. For instance, from 31 different variables (kinematics, forces and energy consumption) analysed in 18 references [168], the most commonly used variables were speed (12 references), step or stride length (7 references), swing/stance phase ratio (6 references) and ground reaction forces (6 references). Other variables were used only in less than or equal to 4 references, and 10 variables were used only in one reference.

Spatiotemporal measures have been calculated using kinematic gait events, from the IKA motions obtained using OpenSim GUI. Spatial measurements include: stride length, step length, crutch step length, foot-crutch anterior-posterior (AP) distance, step width, crutch width, foot-crutch medio-lateral (ML) distance. Temporal measurements include: cycle duration, foot swing phase and crutch swing phase. Other magnitudes that have been computed are speed and global centre of mass (COM) displacement. From all variables that could be computed for right and left sides, the mean value and the symmetry index (following the expression used in [7]) have been computed. Joint coordinates, joint torques and ground reaction forces have also been computed (when possible). Ranges of motion (ROMs) for hip flexion-extension, hip abduction-adduction and pelvis tilt have been computed as well [7,170]. Hip hiking has been evaluated calculating the vertical displacement of the anterior superior iliac spines (ASIS) marker [171, 172], and circumduction has been evaluated computing the thigh absolute angle in frontal plane [171].

6.2.3 Prediction of crutch-orthosis-assisted gait

The first step before predicting new motions is the initial guess generation. This has been done obtaining a dynamically consistent full cycle (Full DC cycle) tracking the experimental data with locked knee and with crutches, for each subject. The used cycles start at left crutch off (LCO) for the healthy subject, and at left toe off (LTO) for the SCI subject. The cost function included terms that tracked experimental coordinates and experimental ground reaction forces and moments (GRFs) (only available for the healthy subject), and minimised joint jerk.

The prediction problems have been developed using what has been observed in experimental data analysis and findings from Chapters 4 and 5. Moreover, some improvements have been applied to overcome some of the limitations found and discussed in Chapter 5. With these inputs, an initial formulation has been developed, and a walking cycle with locked knee (PASS) has been predicted for the healthy subject. Results have been compared against experimental data, and different iterations have been performed, until a final formulation has been reached. This formulation has been used to predict PASS and ACT motions for both subjects, and it is the one that is presented below.

As a remind, some assumptions that have been presented in Chapter 3 are that the inertial measurement units (IMUs) sensors detect correctly the stance-to-swing

transition event, that the knee motor is capable of following the desired knee trajectory, and that the knee flexion reaches the imposed maximum knee flexion value. In the problem formulation, the latter is done differently for PASS and ACT predictions: in the first case, knee angle is bounded within 0° and 2°; in the second case, knee angle is imposed from the expression of the predefined knee flexion-extension trajectory (Eq. 3.8 in Section 3.1.3), and the rest of coordinates are predicted.

Variables

The state vector $\mathbf{x} \in \mathbb{R}^{4n_q-6}$ is formed by the vector of generalised coordinates of the model, $\mathbf{q} \in \mathbb{R}^{n_q}$, the vector of generalised velocities, $\dot{\mathbf{q}} \in \mathbb{R}^{n_q}$, the vector of generalised accelerations, $\ddot{\mathbf{q}} \in \mathbb{R}^{n_q}$, and the vector of net joint torques, $\boldsymbol{\tau} \in \mathbb{R}^{n_q-6}$. Remember that n_q is the number of generalised coordinates in the model (see Section 3.1.1), and that the vector of net joint torques is $n_q - 6$ dimensional, as the 6 first generalised forces and moments are those associated with the residual wrench applied to the pelvis.

$$\mathbf{x} = \begin{bmatrix} \mathbf{q} \\ \dot{\mathbf{q}} \\ \ddot{\mathbf{q}} \\ \boldsymbol{\tau} \end{bmatrix} \tag{6.1}$$

Some joint torques have been limited for the SCI subject with more restrictive bounds, as explained in Section 3.1.3, and knee torque has been limited to be within ±34 Nm, that is the motor peak torque value. Knee torque has not been limited so restrictively for the healthy subject, as she has full actuation at knee joint, so in this case the general joint torque limits explained in Appendix C have been used.

The control vector $\mathbf{u} \in \mathbb{R}^{2n_q-6+n_{GRF}}$ is formed by the vector of generalised jerks, $\dddot{\mathbf{q}} \in \mathbb{R}^{n_q}$, the vector of joint torque change, $\dot{\boldsymbol{\tau}} \in \mathbb{R}^{n_q-6}$, and the vector of foot-ground reaction forces and moments and crutch-ground reaction forces $\mathbf{GRF}_u \in \mathbb{R}^{n_{GRF}}$:

$$\mathbf{u} = \begin{bmatrix} \dddot{\mathbf{q}} \\ \dot{\boldsymbol{\tau}} \\ \mathbf{GRF}_u \end{bmatrix} \tag{6.2}$$

Remember that the ground reaction controls, $\mathbf{GRF}_u$, are used to define a walking cycle. They define when each foot and crutch is either in swing phase or stance phase, that is, all reaction components are forced to be zero during swing. This is done by multiplying each control variable by a vector of zeros and ones that defines the swing (0) and stance (1) phases for each foot and crutch.

In this formulation, cycle duration and stride length are free variables. The parameter vector, $\mathbf{s}$, is formed by the cycle time duration (T_c), the duration of multiple support phase (p_{ms}), of foot swing phase (p_{swf}), and of crutch swing phase (p_{swc}) in percentage of cycle time, and the stride length (L_s):

$$\mathbf{s} = \begin{bmatrix} T_c \\ p_{ms} \\ p_{swf} \\ p_{swc} \\ L_s \end{bmatrix} \tag{6.3}$$

The initial guess, and minimum and maximum values per each parameter have been obtained from the experimental data, and minimum and maximum values have been computed according to those values (Table 6.2). A scale factor of 0.01 has been used for the percentages of cycle duration: duration of multiple support phase (p_{ms}), of foot swing phase (p_{swf}), and of crutch swing phase (p_{swc}).

	Healthy subject			SCI subject		
	Min	Max	Guess	Min	Max	Guess
Cycle duration [s]	2.95	3.20	3.08	3.56	4.56	4.06
Multiple support [%]	0.00	8.92	3.92	6.67	16.67	11.67
Foot swing [%]	17.55	27.55	22.55	11.75	21.75	16.75
Crutch swing [%]	12.65	22.65	17.65	4.85	14.85	9.85
Stride length [m]	0.38	0.60	0.51	0.50	0.75	0.65

Table 6.2: Minimum and maximum bounds, and initial guess for each predicted parameter and for each subject. Initial guess has been obtained from the experimental data, and minimum and maximum values have been computed according to those values.

Cost function

The cost function includes tracking terms, optimisation terms, regularisation terms and penalty terms (each one with a different relative weight, which have not been included in the following expression to make it simpler):

$$J = \int_{t_0}^{t_f} \Big(\sum_i J_{track,i}(\mathbf{x},\mathbf{u}) + \sum_j J_{opt,j}(\mathbf{x},\mathbf{u}) + \sum_k J_{reg,k}(\mathbf{x},\mathbf{u}) + \sum_l J_{pen,l}(\mathbf{x},\mathbf{u}) \Big) \mathrm{d}t + \frac{0.01}{L_s} \tag{6.4}$$

Tracking terms $J_{track,i}$ have been included in the cost function following the approach in [50]. Tracking terms include:

- Arm coordinates tracking,
- Hip and lumbar joint torques tracking.

It has been checked in the experimental data that arm coordinates are similar in all different captures for the same subject. Moreover, it has been found that hip and lumbar joint torques are the joint torques that look more similar in all different captures for the same subject. As the main goal of these terms is to help the problem to converge, but not to track exactly those joint coordinates and torques,

both tracking terms have a relative weight of 0.1.

Optimality terms $J_{opt,j}$ are based on the ones obtained in Section 5.2, and include:

- Local angular momentum for lower limbs and upper limbs, for both subjects,
- Mechanical power for lumbar joints and lower limb joints, for the healthy subject,
- Mechanical power for lumbar and shoulder joints, for the SCI subject.

Minimising mechanical power for lumbar and lower limb joints has been found in Section 5.2 to work correctly for crutch-assisted walking. In the case of an SCI subject who has no actuation at lower limbs, it makes no sense to minimise lower limbs mechanical power. For this reason, it has been changed this term by minimising shoulder joints mechanical power, that seems more reasonable for an SCI subject, that bears more weight on crutches than a healthy subject does.

Regularisation terms $J_{reg,k}$ are the ones obtained in Section 5.2, and include:

- Joint jerk, with a relative weight of 0.01,
- Joint torque change, with a relative weight of 0.01.

Penalty terms $J_{pen,l}$ have been added to improve motion and avoid undesirable effects, and include:

- The inverse value of crutch tips mediolateral distance, with a relative weight of 0.001. This helps to increase the crutches base of support,
- The difference between crutch tip and foot mediolateral distance in right and left sides, with a relative weight of 0.01 for the SCI subject (1 for the healthy subject). This helps to improve symmetry between right and left sides,
- The torso COM velocity in ML direction, with a relative weight of 0.1, for the SCI subject (only ACT motions). This helps to minimise torso lateral motion and improves balance.

Each term is squared in the cost function. Note that in this case the cost function includes stride length maximisation, which is done minimising the inverse of stride length, with a relative weight of 0.01. This is only included for the ACT motions predictions.

Dynamic constraints

Dynamic constraints are:

$$\frac{\mathrm{d}\mathbf{q}}{\mathrm{d}t} = \dot{\mathbf{q}}, \quad \frac{\mathrm{d}\dot{\mathbf{q}}}{\mathrm{d}t} = \ddot{\mathbf{q}}, \quad \frac{\mathrm{d}\ddot{\mathbf{q}}}{\mathrm{d}t} = \dddot{\mathbf{q}}, \quad \frac{\mathrm{d}\boldsymbol{\tau}}{\mathrm{d}t} = \dot{\boldsymbol{\tau}}. \tag{6.5}$$

Path constraints

Path constraints are based on the ones described in Section 5.1, and new path constraints are added:

- Residual forces and moments are reduced, being 1 N (or Nm) the tolerance for residual wrench components,
- Joint torques from the optimal control problem are forced to be the same as joint torques obtained from OpenSim, being 5 Nm the tolerance for differences between joint torque controls and those obtained from inverse dynamics (ID),
- Ground reaction control forces equal ground reaction forces calculated using the contact model, being 50 N the tolerance for normal forces and 25 N the tolerance for tangential forces,
- The lateral distance between the midpoint of each foot and between the crutch tips is bounded. Maximum and minimum values have been obtained from experimental data,
- To avoid sliding during stance, the value of the velocity of the midpoint of the foot and of each crutch tip are bounded during stance phase,
- Align crutches with forearm. This is done bounding the distance between the crutch cuff and one point at the forearm at the corresponding height,
- Impose crutch in contact with ground during stance. This is done bounding the vertical position of the crutch tip during stance.

Endpoint constraints

Endpoint constraints are the following:

- Residuals at the end of simulation are bounded as they are during all simulation,
- The final simulation time equals the cycle duration parameter,
- Initial feet and crutch tips position is imposed within a tolerance. This position is adapted for each subject and motion, and it is obtained from the experimental data,
- Stride length for each foot and crutch tip equals the stride length parameter,
- Periodicity is imposed to joint coordinates with a tolerance of ±20% ROM (different value for each coordinate),

- Periodicity is imposed to normal ground reaction forces with a tolerance of ±100 N,
- Mean speed is imposed to be the same as in the experimental motions, only for the healthy subject.

6.2.4 Evaluation of prediction results

To evaluate predicted results, parameters and magnitudes described in Section 6.2.2 have been computed for each solution and compared to experimental motions.

Healthy subject

For the healthy subject, joint coordinates, joint torques and ground reaction forces have been compared between the experimental data and the predicted results. Changes in spatiotemporal parameters and symmetry indices (following the expression used in [7]) have been computed and also compared. Moreover, two different studies have been performed: to check how having different initial guesses affects the results, and also to compare different cycle duration, stride length and speed conditions.

SCI subject

For the SCI subject, joint coordinates, joint torques and ground reaction forces have been compared between experimental data when using crutches and predicted results. Changes in spatiotemporal parameters have been computed and compared between experimental data when using the walker and predicted results using crutches.

6.3 Results

6.3.1 Data analysis and comparison

Spatiotemporal parameters, joint angles and ROMs, forces and other magnitudes have been analysed for each subject and each level of assistance. In general, more variation has been detected among the different captures for the healthy subject with active orthoses and crutches than for the different captures for the SCI subject with active orthoses and walker, as can bee observed in Figure 6.1. The walking motion of the SCI subject with active orthoses and crutches (only PASS motion) is more unstable, which can be observed also in Figure 6.1 (bottom plot), as he does not walk following a straight line. Moreover, there are two crutch steps added to the typical four-point alternating pattern.

Joint coordinates, joint torques and ground reaction forces (feet and crutches) of the three motions for the healthy subject (PASS, ACT40, ACT60) can be found in Appendix G. Regarding joint coordinates (Figure G.1), a similar tendency is found for all coordinates in PASS, ACT40 and ACT60 motions, with increased ROMs in

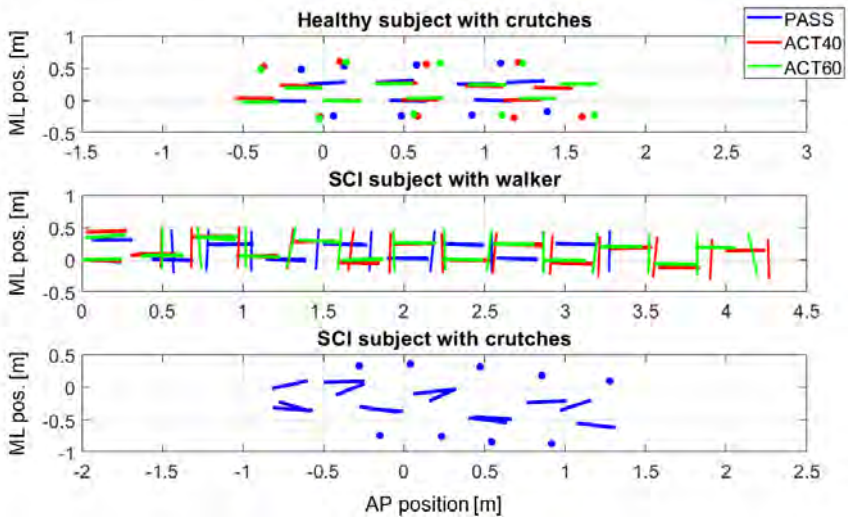

Figure 6.1: Feet and crutches (or walker) positions in the transverse plane for each subject and each assistance condition. A line from heel to toe tip is plotted to show the foot position during stance (in the case of SCI subject with crutches, foot position is plotted at heel strike and toe off, as feet moved with respect to the ground during stance). A point is plotted to show crutch tip position during stance. A line from right wrist centre to left wrist centre is plotted to show the position of the walker during phases where it was static with respect to the ground.

general in ACT motions compared to PASS. Some of the largest differences are 13° for lumbar bending (in both ACT motions, compared to PASS), and 12-11 cm for pelvis lateral displacement (in ACT40 and ACT60 motions, respectively, compared to PASS). Arm coodinates present in general larger ROMs in ACT motions compared to PASS (e.g., for shoulder flexion up to 33° for ACT60 left arm and elbow flexion up to 32° for ACT40 right side), although they follow also a similar tendency. This is why a relative weight of 0.1 has been given to the term in the cost function that tracks arm coordinates from PASS experimental motion. Regarding joint torques (Figure G.2), the most significant changes are observed in hip adduction and hip rotation torques (right and left sides). Similar to what has been said for the arm coordinates, as the tendency in the lumbar and hip joint torque curves was similar for the three motions, a relative weight of 0.1 has been given to the corresponding cost function tracking term. Regarding ground reaction forces (Figure G.3), normal feet contact forces have increased in ACT motions compared with PASS motion, while normal crutch contact forces have decreased. This has increased the symmetry between right and left values for feet and crutches normal forces.

Regarding spatiotemporal parameters for the healthy subject, stride length increases from PASS (0.45 m) to ACT40 (0.54 m) and ACT60 (0.55 m), while cycle duration decreases sligthly, so walking speed increases as well (Table 6.3). The relative swing phase duration for feet increases from PASS (almost 20%) to ACT

motion (28% and 25% for ACT40 and ACT60, respectively), while the swing phase duration for crutches stays almost the same; and the duration of all the multipple supports (where both feet and both crutches are in contact with ground) decreases form PASS to ACT (Figure 6.2, left). Step width decreases from PASS to ACT, and crutch width increases; but at the same time the global COM displacement in vertical and mediolateral (ML) directions increases (up to 172% in ML direction for ACT40), and hip flexion, hip adduction and pelvis tilt ROMs increase as well (Table 6.3).

	Experimental values			Variation [%]	
	PASS	ACT40	ACT60	ACT40	ACT60
Stride [m]	0.45	0.54	0.55	19.09	22.79
Duration [s]	3.17	2.98	2.98	-5.99	-5.99
Speed [m/s]	0.14	0.18	0.19	26.68	30.62
Step width [m]	0.27	0.24	0.22	-10.31	-15.70
Crutch width [m]	0.79	0.82	0.80	4.84	2.17
COM ML disp. [cm]	5.94	16.17	14.43	172.34	142.94
COM vert. disp. [cm]	1.84	2.39	2.37	30.12	29.13
Hip flex-ext ROM [°]	20.95	26.10	34.40	24.54	64.16
Hip abd-add ROM [°]	14.03	20.23	17.41	44.21	24.17
Pelvis tilt ROM [°]	16.62	22.23	23.51	33.74	41.44

Table 6.3: Most relevant spatiotemporal and kinematic parameters for each experimental trial of the healthy subject (PASS, ACT40 and ACT60), and variation for each active motion (ACT40 and ACT60) with respect to the case with locked knee (PASS). "COM" refers to the model global centre of mass

Joint coordinates of the three motions for the SCI subject with active orthoses and walker (PASS, ACT20, ACT40) can be found in Appendix H, Figure H.1. In this case, arm motion is similar for the three motions, but some differences can be found in hip and lumbar joints coordinates (e.g., around 10° more of ROM for hip adduction in ACT motions compared to PASS motion). Regarding spatiotemporal parameters, almost no difference can be found in percentage of swing and support phases (Figure 6.2, right), stride length decreases from PASS (0.70 m) to ACT20 (0.63 m) and ACT40 (0.61 m), and cycle duration decreases also sligthly, so speed decreases as well (Table 6.4). Step width and global COM ML displacement increase, whil global COM vertical displacement decreases. There is not a clear tendency for hip flexion and pelvis tilt ROM, and hip adduction ROM increases (as said previously).

Joint coordinates from the experimental motion of the SCI subject with active orthoses and crutches can be found in Appendix H, Figure H.2. Joint torques and ground reaction forces obtained after ensuring dynamic consistency through the optimal control tracking algorithm can be found in Figures H.3 and H.4, respectively. These joint torques are in general higher (in %BW*H) than for the healthy subject experimental joint torques (Figure G.2), and are the ones that have been

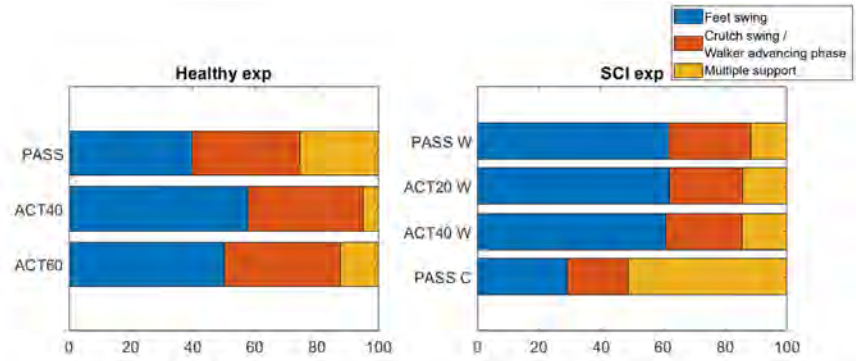

Figure 6.2: Percentage of cycle duration for each phase and experimental capture, for both healthy subject and SCI subject. In the case of the SCI subject, W stands for walker and C stands for crutches. The swing time is computed as the total time spent in swing phase for both feet or both crutches. The multiple support time is computed as the total time where both feet and crutches are in contact with ground (or both feet are in contact with the ground and the walker is at rest with respect to the ground).

used to limit the maximum values for hip and lumbar joint torques for the SCI patient predictions. Weight distribution is similar for feet and crutches (Figure H.4), which has not been observed for the healthy subject, for which more weight was supported by feet than by crutches (Figure G.3). Regarding spatiotemporal parameters, the stride length is 0.41 m, cycle duration is 3.99 s, and speed is 0.10 m/s, significantly lower than PASS motion for healthy subject and SCI subject with walker. Almost half of the cycle time is spent with both feet and both crutches in contact with the ground, and swing durations for feet and crutches are reduced considerably, especially for feet (Figure 6.2, right). Moreover, crutch width, 1.11 m, is larger than for the healthy subject captures (see Figure 6.1).

Comparing ACT motions with respect to PASS motion for the healthy and the SCI subject with walker, some parameters behave in the same way: global COM ML displacement and hip adduction ROM increase for both subjects, and cycle duration decreases for both subjects (Tables 6.3 and 6.4). At the same time, other parameters behave in the opposite way: stride length, walking speed and global COM vertical displacement increase for the healthy subject and decrease for the SCI subject; and step width decreases for the healthy subject and increases for the SCI subject. Hip hiking can be observed for both subjects (Figure 6.3, top row), but circumduction is greater for the SCI subject, for the two types of assisted motion: walker-orthosis- and crutch-orthosis-assisted motion (Figure 6.3, bottom row).

6.3.2 Healthy subject crutch-orthosis-assisted predictions

Previously to the prediction problems, the foot-ground and crutch-ground contact models have been calibrated using the PASS experimental data. Once the contact models have been calibrated, a full DC cycle has been generated, to be used as

	Experimental values			Variation [%]	
	PASS	ACT20	ACT40	ACT20	ACT40
Stride [m]	0.70	0.63	0.61	-9.95	-13.24
Duration [s]	3.66	3.59	3.45	-1.91	-5.65
Speed [m/s]	0.19	0.18	0.18	-8.19	-8.04
Step width [m]	0.22	0.25	0.25	13.46	11.82
COM ML disp. [cm]	5.19	5.40	8.09	4.14	55.97
COM vert. disp. [cm]	2.18	1.61	1.72	-26.35	-21.17
Hip flex-ext ROM [°]	51.85	53.97	49.91	4.09	-3.74
Hip abd-add ROM [°]	20.78	30.82	28.58	48.32	37.54
Pelvis tilt ROM [°]	35.68	36.09	35.47	1.14	-0.59

Table 6.4: Most relevant spatiotemporal and kinematic parameters for each experimental trial with walker of the SCI subject (PASS, ACT20 and ACT40), and variation for each active motion (ACT20 and ACT40) with respect to the case with locked knee (PASS). "COM" refers to the model global centre of mass

an initial guess for the predictions. For this tracking problem, in addition to the residuals computed using GRFs controls, residuals using the values from contact models have also been limited in path constraints, to help the problem to converge.

Three assisted motions (PASS, ACT40 and ACT60) have been predicted having as initial guess the Full DC cycle obtained from tracking PASS experimental data. Predicted joint coordinates, joint torques and ground reaction forces can be found in Appendix G. Simulations have required from 514 iterations (PASS) to 1133 iterations (ACT60), and from 32 min (PASS) to 1h 34 min (ACT60). For all three cases, the predicted cycle duration has been 2.95 s, and the predicted stride length has been 0.39 m, 0.50 m and 0.53 m, for PASS, ACT40 and ACT60, respectively (Table 6.5).

	n iter	Time	Tcycle [s]	Lstride [m]	Speed [m/s]
PASS	514	32 min	2.95	0.39	0.13
ACT40	548	45 min	2.95	0.50	0.17
ACT60	1133	1h 34 min	2.95	0.53	0.18

Table 6.5: Number of iterations (n iter), computation time (time), and main spatiotemporal parameters obtained in crutch-orthosis-assisted predictions of the healthy subject. Cycle duration (Tcycle) and stride length (Lstride) were optimised parameters in the simulations, and mean speed has been computed from them.

Stride length and step width have increased for predicted ACT motions compared to predicted PASS motion (Table 6.6). Crutch width has remained almost the same (Figure 6.4). The global COM medio-lateral displacement has also increased, and hip flexion ROM has almost duplicated the value for PASS prediction. Opposite to this, hip adduction and pelvis tilt ROMs have decreased in predicted ACT motions compared to predicted PASS. In experimental motions, symmetry

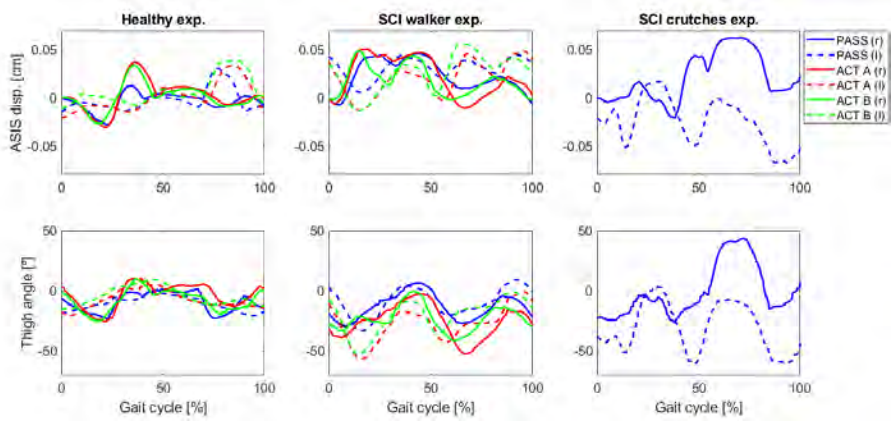

Figure 6.3: ASIS vertical displacement, which can be considered a measure of hip hiking [172], and thigh angle in frontal plane, which can be considered a measure of circumduction [171], for each subject and assistance condition, for both right (solid lines) and left (dashed lines) sides. "ACT A" refers to the lower value of maximum knee flexion (40° for the healthy subject and 20° for the SCI subject), and "ACT B" refers to the higher value of maximum knee flexion (60° for the healthy subject and 40° for the SCI subject)

improves in crutches swing duration, in foot step length and in foot-crutch ML distance (for ACT motions with respect to PASS), and these improvements are also observed in the predicted motions (Figure 6.5). For the other parameters, there is not a clear tendency of improvement, but, in general, predicted symmetry indices regarding AP and ML distances have improved with respect to their experimental values.

Regarding joint coordinates, hip angles are better predicted (that is, predicted angle trajectories are closer to the experimental ones) in sagittal and transverse plane, while lumbar angles are better predicted in frontal plane (Figure 6.6). Arm motion is practically the same for the three predicted motions (Figure G.4). ASIS vertical displacement and thigh absolute angle in frontal plane have been computed as measures of hip hiking and circumduction. Differences in maximum values with respect to PASS motion maximum values during swing for each of these magnitudes have been computed (Table 6.7). Hip hiking decreases in predicted motions with knee flexion assistance, but thigh angle increases in frontal plane for both right and left sides.

Predicted normal forces for crutches are higher than in experimental motion, and they reach maximum values of around 50% BW, compared to 20-30% BW for experimental motion (Figure 6.7). Regarding joint torques, they are in general much higher for the upper body, reaching values more than 2 times higher (e.g., 2.35 times for lumbar bending and 2.66 times for arm flexion) compared to experimental joint torques.

Two additional studies have been done. Firstly, it has been compared how imposing speed, not imposing it, and maximising stride length or not affects predicted parameters (especially cycle duration and stride length). In all cases, the predicted

	Predicted values			Variation [%]	
	PASS	ACT40	ACT60	ACT40	ACT60
Stride [m]	0.38	0.49	0.52	28.52	36.84
Duration [s]	2.94	2.94	2.94	0.00	0.00
Speed [m/s]	0.13	0.17	0.18	28.52	36.84
Step width [m]	0.19	0.23	0.21	16.73	7.73
Crutch width [m]	0.75	0.75	0.75	0.04	0.06
COM ML disp. [cm]	4.78	5.97	7.07	24.73	47.71
COM vert. disp. [cm]	1.88	1.88	2.40	-0.24	27.38
Hip flex-ext ROM [°]	14.21	28.29	28.37	99.08	99.62
Hip abd-add ROM [°]	21.25	17.18	18.19	-19.13	-14.41
Pelvis tilt ROM [°]	17.50	15.70	16.99	-10.33	-2.90

Table 6.6: Most relevant spatiotemporal and kinematic parameters for each prediction results of the healthy subject (PASS, ACT40 and ACT60), and variation for each active motion (ACT40 and ACT60) with respect to the case with locked knee (PASS). "COM" refers to the model global centre of mass

		ACT40		ACT60	
		R	L	R	L
ASIS peak [cm]	Exp.	2.45	0.25	2.12	0.69
	Pred.	0.20	-0.18	-0.73	-0.52
Thigh angle [°]	Exp.	-2.38	7.58	-1.26	9.13
	Pred.	-7.85	-18.03	-18.40	-16.44

Table 6.7: Differences in ASIS maximum vertical position and thigh maximum angle (measures of hip hiking and circumduction, respectively [171, 172]) of the ACT predicted motions with respect to PASS predicted motion for the healthy subject. The maximum values have been computed during the swing phase for each case, and for right (R) and left (L) sides.

cycle duration is the same, 2.95 s, that corresponds to the lower bound selected for this parameter (Table 6.8). Stride length varies from 0.387 m for the case where no constraints are imposed to this parameter, to 0.591 m for the case where stride length is maximised. The percentage of duration of each phase does not vary, as it has been observed in all the different predictions. Finally, more iterations (1668) are required when mean speed is imposed, while less iterations (975) are required when no conditions are imposed to stride length and cycle duration. Secondly, two additional initial guesses have been tested, and results have been compared against the predicted motion using Full DC as the initial guess. Experimental data for PASS and ACT40 have been used as the initial guess (and also as reference values for the tracking terms in the cost function) for predicting ACT40 motion. Less iterations are needed when using experimental data, and also the objective value and the maximum mesh relative error are lower (Table 6.9). Moreover, mean RMSE

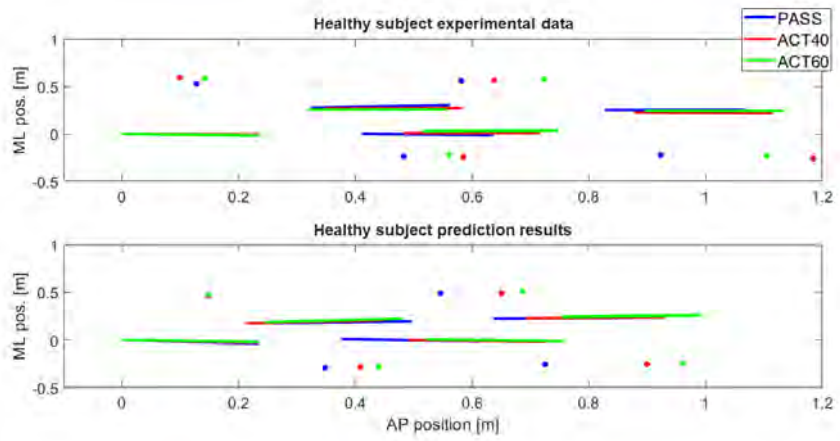

Figure 6.4: Feet and crutches positions in the transverse plane for the healthy subject experimental motion (top) and predicted motion (bottom). A line from heel to toe tip is plotted to show the foot position during stance. A point is plotted to show crutch tip position during stance.

have been computed for each solution compared to the initial solution (using as initial guess the Full DC motion), and larger errors are found for the case of using ACT40 as the initial guess (2.04 cm and 7.39°, compared to 0.53 cm and 1.63°).

Case	n iter	Tcycle [s]	% ms	% swF	% swC	Lstride [m]	Speed [m/s]
Impose speed	1668	2.950	4.460	22.550	17.650	0.560	0.190
Maximise Lstride	1420	2.950	4.460	22.550	17.650	0.591	0.200
Free Lstride	975	2.950	4.460	22.550	17.650	0.387	0.131

Table 6.8: Results obtained for imposing mean speed, maximising stride length (Lstride), and leaving stride length as a free parameter without any constraint, for the healthy subject. Number of iterations (n iter) are given first. Then, the optimised parameters are shown: cycle duration (Tcycle); percentages of each phase: multipple support (ms), foot swing (swF) and crutch swing (swC); and stride length. Mean speed has been computed from optimised cycle duration and stride length. In all cases, the maximum knee flexion has been set at 40° (ACT40).

6.3.3 SCI subject crutch-orthosis-assisted predictions

Foot-ground contact model has been calibrated for the SCI subject, following the methods previously explained. Then, using the calibrated foot-ground contact model and the crutch-ground contact model previously calibrated with the healthy subject data, a full DC cycle has been obtained for the PASS motion with crutches. In the tracking problem, no GRFs have been tracked in the cost function, as no

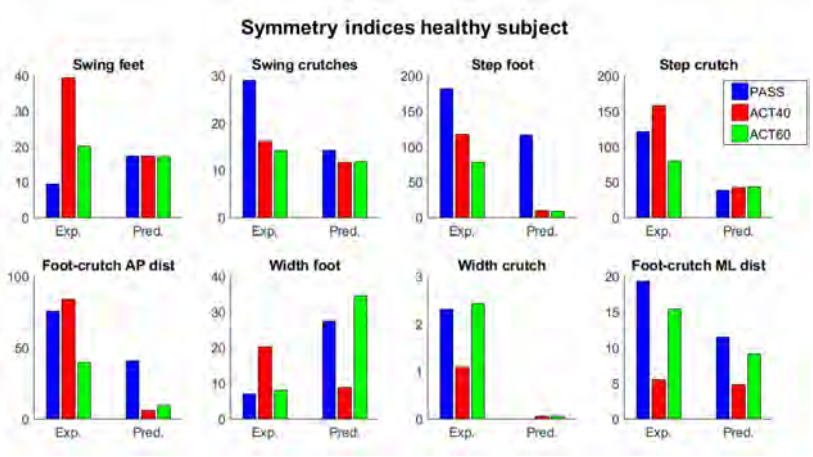

Figure 6.5: Symmetry indices (in absolute values) for different spatiotemporal parameters for the healthy subject experimental motion (Exp.) and predicted motion (Pred.). Temporal parameters are the relative duration of feet and crutch swing phases. Spatial parameters include distances between feet and crutches in anterior-posterior direction ("step"), and in mediolateral direction ("width"), and AP an ML distances between foot and crutch from the same side ("Foot-crutch AP/ML dist."). Note that the scale is different per each SI, to show more clearly all bars.

experimental measures were available.

Three assisted motions (PASS, ACT20 and ACT40) have been predicted having as initial guess the Full DC motion obtained from PASS experimental data. Predicted joint coordinates, joint torques and ground reaction forces can be found in Appendix H. As in the tracking problem for the healthy subject, in the predictions it has been needed to include as path constraints the residuals computed using the values from contact models, to help the problem to converge. Moreover, force components corresponding to the left crutch have been excluded from the path constraints that impose equality between GRFs controls and GRFs computed from contact models. Simulations have required more iterations and time than for the healthy subject: from 2010 iterations (ACT20) to 2585 iterations (ACT40), and from almost 3h (PASS and ACT20) to almost 4h (ACT40) (Table 6.10).

Regarding spatiotemporal parameters, stride length increases from PASS (0.49 m) to ACT motions (0.63 m for ACT20 and 0.62 m for ACT40), while cycle duration remains practically constant, so speed increases as well (Table 6.10). There is not much difference in the relative duration of swing phase for each foot (16-17%) and for each crutch (9-10%). Stride length, speed and step width increase for ACT motions with respect to PASS (Table 6.11). Moreover, global COM ML displacement, hip flexion ROM and pelvis tilt ROM increase for ACT motions with respect to PASS. On the contrary, hip adduction ROM decreases. In all three cases, each foot rotates around its midpoint during stance. Although this is also observed for the healthy subject predictions, this tendency is more relevant for the SCI subject.

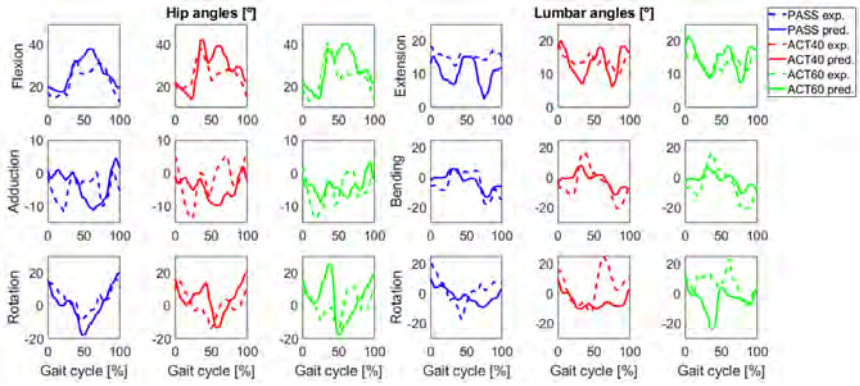

Figure 6.6: Hip flexion, adduction and rotation, and lumbar extension, bending and rotation, for each prediction (PASS, ACT40 and ACT60, in solid line) compared to the experimental values (in dashed line). Results are shown for the right hip.

	Convergence			RMSE coord.	
Initial guess	n iter	Objective	Mesh error	Linear [cm]	Angular [°]
PASS Full DC	1420	0.3345	0.0068	-	-
PASS exp.	1070	0.3298	0.0067	0.5304	1.6291
ACT40 exp.	894	0.3280	0.0057	2.0476	7.3864

Table 6.9: Results obtained after using three different initial guesses: the full cycle obtained from tracking the experimental motion with locked knee (PASS Full DC), the experimental motion with locked knee (PASS exp.), and the experimental motion with 40° of maximum knee flexion (ACT40 exp.), for the healthy subject. Results related to convergence are shown: number of iterations (n iter), cost function value (Objective), maximum relative error on mesh (Mesh error). Moreover, mean RMSEs have been computed for linear and angular coordinates with respect to the first solution (PASS Full DC initial guess). In all cases, the maximum knee flexion has been set at 40° (ACT40).

Regarding coordinates, arm coordinates are almost the same for all three predicted motions, as it has been also observed for the healthy subject (Figure H.5). Predicted joint torques are similar for PASS and ACT motions, being the higher values for lumbar bending (6.02% BW*H), hip adduction (7.62% BW*H) and shoulder adduction (8.35% BW*H) (Figure H.6). Normal ground reaction forces are slightly lower for feet in ACT motions compared PASS motion, while they are slightly higher for crutches in ACT motions compared PASS motion. This tendency is more marked for the left side (Figure H.7).

6.4 Discussion

In this chapter, the assisted motions of a healthy and an SCI subject have been collected with no knee flexion (PASS) and with active knee flexion for different

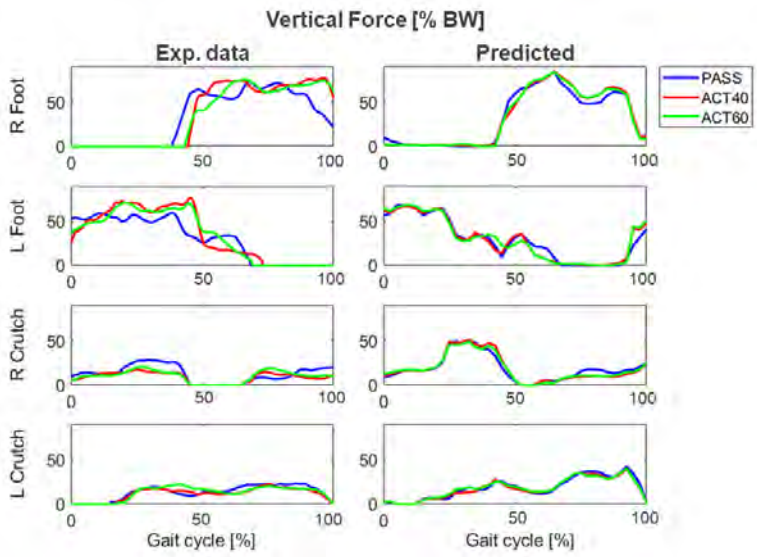

Figure 6.7: Normal forces in %BW of experimental motion (Exp. data, left) compared to predicted motions (right) for the healthy subject, and for each foot and crutch (R: right, L: left)

	n iter	n mesh	Time	Tcycle [s]	Lstride [m]	Speed [m/s]
PASS	2448	2	2h 41 min	3.96	0.50	0.13
ACT20	2010	2	2h 56 min	3.95	0.66	0.17
ACT40	2585	3	3h 47 min	3.95	0.63	0.16

Table 6.10: Number of iterations (n iter), computation time (time), and main spatiotemporal parameters obtained in crutch-orthosis-assisted predictions of the SCI subject. Cycle duration (Tcycle) and stride length (Lstride) were parameters optimised in the simulations, and mean speed has been computed from them.

angle amplitudes (ACTXX). Since the SCI subject was not able to walk with the active orthoses imposing knee flexion and with crutches, only PASS motion has been collected with crutches; and ACT motion with different knee angle amplitudes have been collected with the walker. The main goal of collecting these experimental data was to provide information to develop the OCP formulation and also to evaluate the prediction results. The observed change in spatiotemporal parameters differs in the healthy subject compared with the SCI subject (Table 6.12). For example, for the healthy subject, stride length increases in motions with knee assistance, while it decreases for the SCI subject. In the case of the healthy subject, the stride length was conditioned because she had to step correctly on the force plates, while the SCI subject did not have this constraint. Moreover, in the case of the healthy subject, it has to be taken into account that it was the first time that the subject walked with the active orthoses, both in PASS and ACT motions. This is

	Predicted values			Variation [%]	
	PASS	ACT20	ACT40	ACT20	ACT40
Stride [m]	0.49	0.63	0.62	27.96	25.77
Duration [s]	3.96	3.95	3.95	-0.25	-0.25
Speed [m/s]	0.12	0.16	0.16	28.28	26.09
Step width [m]	0.36	0.40	0.39	12.48	9.49
COM ML disp. [cm]	8.90	12.21	11.25	37.30	26.47
COM vert. disp. [cm]	2.91	3.13	2.85	7.32	-2.07
Hip flex-ext ROM [°]	33.27	44.74	41.18	34.48	23.79
Hip abd-add ROM [°]	47.96	42.82	43.69	-10.72	-8.90
Pelvis tilt ROM [°]	37.65	39.28	42.98	4.33	14.17

Table 6.11: Most relevant spatiotemporal and kinematic parameters for each prediction results (with active orthoses and crutches) of the SCI subject (PASS, ACT20 and ACT40), and variation for each active motion (ACT20 and ACT40) with respect to the case with locked knee (PASS). "COM" refers to the model global centre of mass

maybe the reason for lateral motion being more remarkable for the healthy subject, especially in ACT motions (increase of global COM ML displacement, increase of hip adduction ROM). The change in cycle duration is small for both subjects. Step width decreases for the healthy subject in ACT motions compared to PASS motions, but it increases for the SCI subject. Moreover, it is not clear in the captured motions that compensatory movements as hip hiking and circumduction are reduced, as it is observed in other references [7, 172, 173].

For the healthy subject, joint coordinates are more similar between predicted motions, than comparing each prediction with the corresponding experimental data. This could be because the only difference in all problem formulations is the imposed knee flexion, being the cost function, constraints, and the initial guess equal for all cases. In the experimental data, this difference in knee flexion produces more changes in the rest of coordinates than in the predicted motions. In general, the improvements in symmetry indices observed in the experimental captures are also observed in the predicted motions. Regarding arm motion tracking, it seems that although a low relative weight (0.1) has been considered, it is not a good option to track those coordinates, as predicted arm coordinates do not vary from one solution to another, while they do in experimental motions.

The number of iterations and computation time for healthy subject crutch-orthosis-assisted predictions are larger than for crutch-assisted walking predictions (Section 5.2), but it seems reasonable, as the cost function is much more complex in this chapter and also more constraints (path and endpoint) are imposed. One improvement with respect to the predictions in Chapter 5 is that stride length and cycle duration are free parameters of the optimisation. They have been bounded using the information of the experimental motion, and in general, cycle duration has been close to the minimum, while stride length has been close to the maximum. Moreover, the initial position of crutch tips and feet midpoints is imposed, with a certain tolerance. The percentages of each phase have converged to the same values

	Healthy subject variations [%]				SCI subject variations [%]			
	Experimental		Predicted		Experimental (W)		Predicted (C)	
	ACT40	ACT60	ACT40	ACT60	ACT20	ACT40	ACT20	ACT40
Stride [m]	19.09	22.79	28.52	36.84	-9.95	-13.24	27.96	25.77
Duration [s]	-5.99	-5.99	0.00	0.00	-1.91	-5.65	-0.25	-0.25
Speed [m/s]	26.68	30.62	28.52	36.84	-8.19	-8.04	28.28	26.09
Step width [m]	-10.31	-15.70	16.73	7.73	13.46	11.82	12.48	9.49
Crutch width [m]	4.84	2.17	0.04	0.06	-	-	-4.03	-3.85
COM ML disp. [cm]	172.34	142.94	24.73	47.71	4.14	55.97	37.30	26.47
COM vert. disp. [cm]	30.12	29.13	-0.24	27.38	-26.35	-21.17	7.32	-2.07
Hip flex-ext ROM [°]	24.54	64.16	99.08	99.62	4.09	-3.74	34.48	23.79
Hip abd-add ROM [°]	44.21	24.17	-19.13	-14.41	48.32	37.54	-10.72	-8.90
Pelvis tilt ROM [°]	33.74	41.44	-10.33	-2.90	1.14	-0.59	4.33	14.17

Table 6.12: Summary of variations of relevant spatiotemporal and kinematic parameters for each active motion with respect to the case with locked knee, for both subjects and for experimental and predicted motions. "COM" refers to the global centre of mass. When the variation is well predicted, results are highlighted in green. When the tendency (increasing or decreasing) is well predicted, but values are considerably different, results are highighted in yellow.

for all solutions. For foot and crutch swing, the optimal value is the provided initial guess; for multiple support duration, the optimal value is higher than the provided initial guess (Table 6.2). It has been also observed that stride length value depends more on how the problem is formulated (e.g., if mean speed is imposed or not, if stride length or speed are maximised, etc.) than on the maximum knee flexion angle provided by the orthosis. Regarding the initial guess comparison, it can be concluded that it is not strictly necessary to have as an initial guess a dynamically consistent motion, as the algorithm also converges to an optimal solution when the initial guess is not dynamically consistent (e.g., the experimental data without any modification). In future work, if the optimal assisted walking of a patient wants to be predicted, the initial guess will be the experimental motion with locked knee, as experimental data of at least this motion will be needed to develop and calibrate the model. But if we want to avoid local minima solutions, then different initial guesses could be used, e.g., these experimental data and random variations of these data.

Results for the SCI subject are preliminary, as many aspects need to be improved, and the experimental validation has not been performed totally (as no data were available for the SCI patient walking with crutches and knee assistance). In this case, all predictions have required more iterations and time than for the healthy subject. The maximum values for joint torques have been obtained assuming that the patient was walking using the 90% of his capacity, following the approach in [58]. To obtain these torque constraints, we have used the best available information, that is, joint torques obtained for the dynamically consistent tracking of PASS motion with crutches, which has been done using a contact model calibrated without having experimental GRFs data. In the future, it would be better to perform a clinical exploration of the patient, and measure or quantify those val-

ues experimentally (with a Biodex device or similar). For the SCI subject, a cycle starting with LTO has been predicted, while for the healthy subject the cycle has been predicted starting with LCO. This has been necessary due to the available experimental data; the best crutch walking cycle (in the case of the SCI subject), or the cycle for which more information was available (for the healthy subject) have been chosen. The problem formulation has been adapted to predict walking cycles starting from these two different gait events, and it could predict cycles starting from any instant of the walking cycle.

Different problems and issues have been found during simulations performed in this chapter. Obtaining the Full DC motion for the healthy subject has been difficult, and it has been necessary to add residuals computed using the GRFs from the contact models. This could be due to the fact that experimentally measured crutch-ground reaction forces might contain some errors (from the measurement and/or the data processing), and this could have made it difficult to closely track those values. Other possible reasons could be that crutches simulated motion was limited because of the crutch-hand weld joint (which is better than having them attached to the forearm, as in Section 4.1, but does not exactly represent the reality); and that the shoulder joint modelling did not capture the complexity of the real anatomical joint. Regarding the SCI subject, as the Full DC motion has been obtained without tracking experimental GRFs, these issues have not been observed. For the predictive simulations of the SCI subject, left crutch-ground contact forces have been removed from path constraints, in order to help the problem to converge. Other ways to fulfill the condition of GRFs controls equal to GRFs from contact models have been needed to be found, which also happened in other predictions from previous chapters. One possible reason could be that the predicted reaction forces are sensitive to the crutch tip radius, and it might be difficult to have both feet and both crutches in contact with the ground simultaneously. This has been solved by limiting residuals obtained using ground reaction controls as inputs, and residuals obtained having GRFs from contact models as inputs, which is not consistent with the purpose of having GRFs controls. Nevertheless, more research is needed regarding this aspect.

This study possesses some limitations. Regarding the experimental captures, a previous training should have been done by the healthy subject, as the capture day was the first time that she used the active orthoses. The patient could not walk with crutches and active orthoses with knee assistance, so captures using walker have been used instead for results evaluation. Moreover, no foot- and crutch-ground contact forces were available for the PASS motion with crutches. Regarding the biomechanical model, the shoulder joint modelling should be improved as it has been detected that shoulder and scapular motion is large for this type of assisted gait. For the SCI subject, the model has been scaled following the same process as for the healthy subject, without taking into account the impairment and how it could affect the results. Moreover, for the SCI subject, the foot-ground contact model has been calibrated using a short period of data, and crutch-ground contact model has not been possible to calibrate. Regarding the active orthoses modeling, some assumptions and simplificactions have been done, which may not correspond exactly to the real device performance. For example, the knee angle trajectory

has been imposed exactly, and in the experimental captures it was observed that the maximum knee flexion was not reached. This option has been chosen because from the different tests performed (tracking knee angle in the cost function, or in a path constraint), it was the option that worked better. Regarding the problem formulation, it remains unknown the optimal criteria that follow impaired subjects when walking with crutches and active orthoses. The cost function has been developed from what has been found in Section 5.2 (which has not been fully proved yet), and some suggestions from different references that did not predict the same type of assisted gait as in this chapter. Finally, it must be remarked that although the obtained results represent an important step toward our final goal stated in Chapter 1 (to predict the optimal values of the knee motor control parameters for each specific SCI subject), more research is needed before they could be applied to find the optimal knee motor control parameters to assist a specific patient.

Future work is needed to improve the problem formulation for predicting crutch-orthosis-assisted walking. First, more experimental captures should be done, with more patients, and with different parameter values defining the orthosis knee angle trajectory. In addition, the model should be improved with some aspects that have been highlighted in the previous paragraph: enhance shoulder joint modelling, and adapt better the scaling process to the specific aspects of the SCI subject. Moreover, the problem formulation could be improved considering how the distribution of ground reactions between feet and crutches is done. As it has been pointed out, the SCI subject did not perform exactly a four-point alternating crutch walking pattern. Therefore, it should be included in the algorithm the possibility of modifying a little bit the pattern, if needed. Another interesting aspect would be investigating how to include the training process and motor learning of the patient in the predictions, identifying at each stage of the process the optimal parameter values defining the knee angle trajectory that should be used. Finally, it is also important to improve the efficiency of the algorithm, since for the SCI subject predictions the computation time has been around 3-4 h.

6.5 Conclusions

- Crutch-orthosis-assisted walking cycles have been predicted having stride length and cycle duration as free parameters of the optimisation.

- The number of iterations and computation time have been higher than for crutch walking predictions (Section 5.2). However, it seems reasonable, as the cost function is much more complex in this chapter and also more constraints (path and endpoint) are imposed. More research is needed to check if the cost function could be simplified, or if it should include other terms.

- Some simulations have not converged with the initial formulation (e.g., obtaining the Full DC motion for the healthy subject and predicting the assisted gait for the SCI subject). In these cases, it has been necessary to add in path constraints the residuals computed using GRFs from contact models. One possible reason could be that predicted reaction forces are sensitive to the

crutch tip radius (which is a parameter of the crutch normal force), and it might be difficult to have both feet and both crutches in contact with the ground simultaneously, while fulfiling residual constraints.

- Experimental validation for the healthy subject has not been as succesful as expected. In general, the improvements in symmetry indices observed in the experimental captures are also observed in the predicted motions. However, joint coordinate evolution is more similar between predicted motions, than between each prediction compared with the corresponding experimental capture.

- The active orthosis predefined knee angle trajectory has been imposed in the prediction problems. This is a simplified problem compared to the goal of this research, which is to predict the optimal parameter values of the knee angle trajectory for a specific patient. The obtained results represent a first step toward this final goal, but more research is needed before these methods could be applied to find the optimal knee motor controller parameters to assist a specific patient.

- Results for the SCI subject are preliminary, as many aspects need to be improved. Moreover, the experimental validation has not been performed thoroughly, as no data were available for the SCI patient walking with crutches and knee assistance. More experimental captures should be done, with more patients, and selecting different parameter values defining the orthosis knee angle trajectory.

Chapter 7

Conclusions

In this thesis, we have investigated optimal control formulations to predict crutch-orthosis-assisted walking using torque-driven multibody dynamic models. Firstly, foot- and crutch-ground contact models were developed and calibrated and dynamically consistent full walking cycles were obtained using an optimal tracking problem. Secondly, normal and crutch-assisted walking were predicted comparing different cost functions. Finally, the crutch-orthosis-assisted gait of a healthy subject and an SCI subject were predicted. The knee angle trajectory, which is predefined in the real active orthosis prototype, was imposed in the prediction algorithm. Results were evaluated with respect to collected experimental data.

In this last thesis chapter, results are discussed especially referring to the final application of this work, contributions and general conclusions are stated, and some recommendations for future work are outlined.

7.1 General conclusions

A remarkable aspect of this work is that the level of complexity of simulations was increased from one chapter to the next and, inside each chapter, more or less detailed models were used. In this way, the obtained results and extracted conclusions are more general and may not depend on a specific model, experimental data, or simulation. It is interesting that the same base problem formulation worked well for tracking problems and for prediction problems (for both with and without tracking terms in the cost function). The main structure of all optimal control problems used in the different simulations was the same. However, many times "manual tuning" (e.g., adjusting variable bounds, preparing a suitable initial guess, adding or removing some constraints, etc.) was needed, and it was not clear whether the tuning depended on the specific model or motion data. Another aspect to note is that improvements were included from one section or chapter to the following ones. For example, crutches were attached to the forearm in Section 4.1, and they were attached to hands from Section 4.2 until the end, as this permitted better simulation of crutch walking patterns. Inverse kinematic analysis was done using the same weight for all markers in Chapters 4 and 5 but different weights were used

in Chapter 6, which allowed us to improve the results. Cycle duration and step length were imposed in predictions in Chapter 5, and they were free parameters in Chapter 6.

Some results in this thesis do not represent a new contribution, but it was necessary to obtain them in order to develop all the previous steps and reach the final goal. For example, foot- and crutch-ground contact models were developed and calibrated for predicting new motions in Chapters 5 and 6. Different research questions were explored, but many aspects remain open and could be further explored. However, it is beyond the scope of this thesis to study in more detail foot- and crutch-ground contact models; they have been developed as a required tool for our simulations.

Eight different optimal control formulations to track normal and assisted walking motions were developed and compared: track marker coordinates vs joint coordinates, minimise joint acceleration vs joint jerk, and adjust ground reactions vs not adjusting them. Three different models (3D HAT, 3D full-body, 3D full-body with crutches) were used to compare these formulations. A novel contribution of this thesis is that, overall, it was found that small adjustments to ground reactions are required to achieve convergence, tracking of joint instead of marker coordinates significantly improves convergence, and minimising joint jerks or joint accelerations have similar effects on convergence. Based on these results, foot- and crutch-ground contact forces were included as controls in all optimal control problem formulations (tracking, calibration of contact models, prediction of new motions).

An optimal control framework was implemented for generating predictive simulations of 3D normal and crutch-assisted walking patterns. Normal walking was predicted using 3D HAT and 3D full-body models, and different optimality cost function terms were compared. It was found that minimising mechanical power, global angular momentum and joint torque change were the cost function terms that provided better results for both models (that is, with and without arm motion). These results are an original contribution from this thesis. Crutch-assisted walking cycles were predicted, using different optimality criteria, following different patterns (four-point, two-point and swing-through), and at different speeds. The same problem structure worked well for all patterns, and only small variations were needed in each case: modify the sequence of stance/swing phases for each foot and crutch, and adapt the initial and final conditions for each pattern. Although some aspects could be further studied, in this thesis we have performed for first time prediction of 3D crutch-assisted walking motions, using a full-body model that includes foot- and crutch-ground contact models, and without tracking experimental data.

Having ground reaction forces as controls in the optimal control formulation is not a common approach. Some positive aspects of this approach are that phases inside the normal and crutch walking cycles can be easily defined, and that the approach can be used for both tracking and predicting new motions. In Section 5.1, different formulations (having all ground reactions as controls, having only forces, or not having them at all) were compared, and the most accurate approach was the one having all ground reaction forces and moments as controls. However, some drawbacks were also encountered, especially in crutch-assisted walking simulations

where in some cases, the problem did not converge, and required modifying some path constraints. Although in general this method produced good results, it is not clear if having ground reactions as controls improves convergence both for tracking and for predicting new motions (with or without crutches), or if it makes finding an optimal solution more difficult. More research is needed regarding this aspect. Finally, it should be noted that some of the conclusions may depend on the optimal control solver used.

Some considerations about the initial guesses used and the optimal solutions found are presented next. In general, for tracking problems, the initial guess used was based on experimental data (normal walking, with shoes and barefoot; crutch-assisted walking; and crutch-orthosis-assisted walking, for each studied subject). For the prediction problems, the initial guess used was the full dynamically consistent cycle obtained for each model and each experimental data set, using the calibrated contact models. In Section 5.2, where different crutch-assisted walking patterns were predicted, it was necessary to generate a different initial guess for each pattern (e.g., predicting a walking cycle with high path constraints tolerance values). A critical aspect is that the convergence of the simulations may depend on the chosen initial guess, and it is not clear how to objectively define a suitable initial guess for each crutch walking pattern simulation. Moreover, in predictions in Chapter 5, we detected that some parameters had high influence on results; e.g., the mesh error and IPOPT tolerances, or the bounds given for the initial and final states. Finally, in Chapter 6, the solutions for different initial guesses (which included the full dynamically consistent cycle and two different experimental motions) were compared, and it was concluded that using a dynamically consistent initial guess may not be required to predict new dynamically consistent motions.

Finally, the last contribution from this thesis is that crutch-orthosis-assisted walking motions were predicted for a healthy subject and an SCI subject, for different knee flexion maximum values that emulate the active orthosis assistance. Cycle duration and stride length were free parameters. All problems converged with higher number of iterations and computation time than crutch-assisted predictions in Chapter 5. Although experimental assessment of results was not as good as expected, these simulations represent a step forward toward developing a predictive tool for the personalisation of active orthoses to specific subjects. In all these simulations, the model was scaled for each subject, foot-ground contact models were calibrated for each subject as well, and joint torques were limited for the SCI patient according to an initial experimental capture. However, the model could be further improved to be better adapted to the subject (e.g., including a more detailed model for the shoulder joint complex, including neck motion, or calibrating positions and orientations of joint axes), in order to get more accurate predictions that could be used to make some clinical decisions for the specific subject.

7.2 Recommendations for future work

Future work could be done to improve models and methods presented in this thesis. Moreover, future steps are needed to reach the final goal presented in the intro-

duction of this thesis: the development of a tool to support patient-tailored design of lower limb robotic assistive devices, to test different control strategies virtually, to simulate patient adaptation to the device, and to predict the mobility improvement that the patient could achieve with external assistance. Next, we outline future improvements that could be performed regarding the models and methods presented in this work for crutch-orthosis-assisted walking prediction, and the next steps to be done toward developing a predictive tool to test different device control strategies virtually.

Improvements that could be done regarding the crutch-orthosis-assisted models presented in this thesis:

- To develop a more detailed model for the shoulder joint complex and add neck motion,
- To improve the level of subject-specificity by calibrating position and orientation of joint centres and axes, and limiting joint torques using more accurate experimental measures of joint torque maximum values,
- To model the orthosis-subject interaction through calibrated compliant contact models.

Improvements that could be done regarding the methods presented in this thesis:

- To add a joint torque error term in the tracking formulations for calibrating contact models and finding a full dynamically consistent cycle,
- To check if having an error term for arm angles tracking is necessary or not,
- To test other optimality terms in the cost function, as they could be different than the ones used for normal walking prediction,
- To improve the non-sliding foot condition, in order to avoid foot rotation around its midpoint,
- To perform sensitivity analyses to study the influence on the results of contact model parameters and other parameters in the optimal control problem formulation,
- To include in the problem formulation conditions about how feet and crutches ground contact is distributed along the cycle.

Possible future steps (in addition to the previous recommendations) in order to develop the predictive tool to test different control strategies virtually:

- To collect new experimental data with a higher number of SCI subjects using different combinations of parameters that define the orthosis knee flexion trajectory,

- To include in the problem formulation different knee flexion parameters as free parameters of the problem,
- To validate results and perform an iterative process, where at each step model and problem formulation are improved,
- To include in the algorithm the possibility of slightly modifying the crutch walking pattern (e.g., placing crutch tips in new positions before taking another step) if needed,
- To explore how to model and include in the formulation the patient's motor learning process.

Appendices

Appendix A

Publications

The methods generated in this work, and the results and conclusions obtained have been published in several conference abstracts and journal articles (at the time of submitting this manuscript, two journal articles have been accepted and one is in preparation). Moreover, this thesis (or the work derived from this thesis) has obtained two awards: Best PhD Thesis Proposal in Industrial Engineering Award 2017, Official Association of Industrial Engineers of Catalonia, Barcelona; and an OpenSim Outstanding Researcher Award 2017, from the NIH National Center for Simulation in Rehabilitation Research (NCSRR), Stanford University, in collaboration with the Rice Computational Neuromechanics Lab (Houston, Texas, USA).

Journal papers

Febrer-Nafría, M., Pallarès-López, R., Fregly, B.J., Font-Llagunes, J.M. Comparison of different optimal control formulations for generating dynamically consistent crutch walking simulations using a torque-driven model. Mechanism and Machine Theory, vol. 154, December 2020, 104031.[1]

Febrer-Nafría, M., Pallarès-López, R., Fregly, B.J., Font-Llagunes, J.M. Prediction of three-dimensional crutch walking patterns using a torque-driven model. Multibody System Dynamics (2020). Published online.

Febrer-Nafría, M., Fregly, B.J., Font-Llagunes, J.M. Prediction of crutch-orthosis-assisted walking for the personalisation of an active orthosis. Journal of Biomechanical Engineering. In preparation.

Conference abstracts

Febrer-Nafría, M., Mouzo, F., Lugrís, U., Fregly, B.J., Font-Llagunes, J.M. Op-

[1] In this paper, the experimental captures were performed using a previous active orthosis prototype, not the one used for all the captures in Chapter 6. For this reason, these results have not been included in the thesis.

timal control prediction of a dynamically consistent walking motion for a spinal cord-injured subject assisted by orthoses. Proceedings of the ECCOMAS Thematic Conference on Multibody Dynamics, June 19-22, Prague, Czech Republic, 2017

Font-Llagunes, J.M., Febrer-Nafría, M., Fregly, B.J. Design of personalised active orthoses for spinal cord-injured subjects based on optimal control prediction of assisted walking motions. Proceedings of the IUTAM Symposium on Intelligent Multibody Systems: Dynamics, Control, Simulation, Sept. 11-15, Sozopol, Bulgaria, 2017. Invited talk

Febrer-Nafría, M., Pallarès-López, R., Font-Llagunes, J.M., Fregly, B.J. Personalised active orthoses for SCI subjects based on optimal control prediction. Proceedings of the Conference on Dynamic Walking, May 21-24, Pensacola, FL, USA, 2018

Febrer-Nafría, M., Font-Llagunes, J.M.,Pàmies-Vilà, R. Foot-ground contact modelling for computational prediction of human walking motion. Proceedings of the 4th Joint International Conference on Multibody System Dynamics, June 24-28, Lisbon, Portugal, 2018

Pallarès-López, R., Febrer-Nafría, M., Font-Llagunes, J.M., Fregly, B.J. Evaluation of optimal control formulations for obtaining dynamically consistent walking motions. Proceedings of the 8th World Congress of Biomechanics, July 8-12, Dublin, Ireland, 2018

Febrer-Nafría, M., Font-Llagunes, J.M., García-Vallejo, D. Influence of robotic orthosis dynamic parameters on optimization-based prediction of assisted walking. Proceedings of the 8th World Congress of Biomechanics, July 8-12, Dublin, Ireland, 2018

Febrer-Nafría, M., Pallarès-López, R., Font-Llagunes, J.M. Simulación predictiva de la marcha asistida para la personalización de ortesis activas para lesionados medulares. Actas de la VIII Reunión del Capítulo Español de la Sociedad Europea de Biomecánica, Nov. 22-23, Castellón de la Plana, Spain, 2018

Febrer-Nafría, M., Pallarès-López, R., Font-Llagunes, J.M. Calibration of Foot-Ground and Crutch-Ground Contact Models for Optimal Control Prediction of Crutch-Assisted Walking Motions. ECCOMAS Thematic Conference on Multibody Dynamics, Duisburg (Germany), 2019

Appendix B

Crutch and orthosis inertial properties

Crutches

Two different crutches have been used for the experimental captures: instrumented (healthy subject) and non-instrumented (SCI subject). For each capture (or group of captures), the crutch height has been adjusted. The tip location has been used for computing indentation and crutch-ground reaction forces. The COM of the crutches has been considered to be at half of their height. The tensor of inertia has been computed considering each crutch as a bar of negligible thickness, where mass and height have been obtained from the crutch used in the experiments (Figure B.1).

Orthoses

The orthoses have been modelled as independent bodies consisting of two segments (corresponding to thigh, and shank-foot) with dimensions and inertial properties taken from CAD models of the real prototype (Figure B.2).

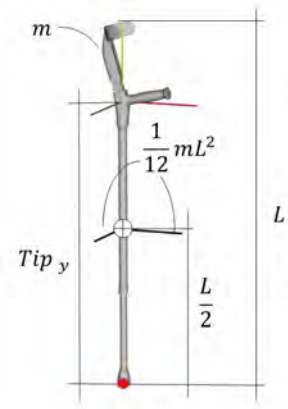

Subject	Capture	Crutches	m [kg]	L [m]	Tip_y [m]
Healthy	Crutches	Instr.	0.62	1.00	-0.77
	Orthoses and crutches	Instr.	0.62	1.07	-0.84
SCI	Orthoses and crutches	Non-instr.	0.50	1.14	-0.89

Figure B.1: Left: Crutch CAD model and expression of the moments of inertia in the orthogonal directions. Right: Crutch mass, height and tip location for each subject and capture.

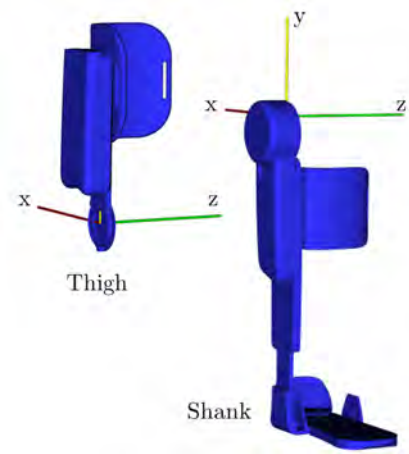

		Thigh	Shank
Mass [kg]		1.41	2.87
Mass centre [cm]	x	0.0098	-0.0067
	y	0.1587	-0.1894
	z	-0.0032	0.0028
Moments of inertia [kg·m^2]	x	0.0073	0.1474
	y	0.0032	0.0081
	z	0.0069	0.1471
Products of inertia [kg·m^2]	x	$5.45 \cdot 10^{-4}$	0.0045
	y	$9.79 \cdot 10^{-4}$	-0.0010
	x	$5.48 \cdot 10^{-4}$	-0.0178

Figure B.2: Left: Right orthosis CAD model. Right: Mass, centre of mass local position and tensor of inertia components for the right orthosis. Values for the left orthosis are the same, with the corresponding sign change in products of inertia.

Appendix C

Variable bounds

In the optimal control formulations, state $\mathbf{x}$ and control $\mathbf{u}$ variables are bounded during the entire simulation. These bounds are defined as the minimum and maximum value of the experimental quantity, respectively, $\pm$ a tolerance value $\boldsymbol{\varepsilon}_x$ or $\boldsymbol{\varepsilon}_u$:

$$\min(\mathbf{x}_{exp}) - \boldsymbol{\varepsilon}_x \leq \mathbf{x} \leq \max(\mathbf{x}_{exp}) + \boldsymbol{\varepsilon}_x, \tag{C.1}$$

$$\min(\mathbf{u}_{exp}) - \boldsymbol{\varepsilon}_u \leq \mathbf{u} \leq \max(\mathbf{u}_{exp}) + \boldsymbol{\varepsilon}_u, \tag{C.2}$$

Moreover, initial and final state values are bounded, using a similar expression as the previous one, but using initial and final values of the experimental quantities that correspond to the states of the problem:

$$\mathbf{x}_{exp_0} - \boldsymbol{\varepsilon}_x \leq \mathbf{x}(t_0) \leq \mathbf{x}_{exp_0} + \boldsymbol{\varepsilon}_x, \tag{C.3}$$

$$\mathbf{x}_{exp_f} - \boldsymbol{\varepsilon}_x \leq \mathbf{x}(t_f) \leq \mathbf{x}_{exp_f} + \boldsymbol{\varepsilon}_x, \tag{C.4}$$

Tolerance values $\boldsymbol{\varepsilon}_x$ and $\boldsymbol{\varepsilon}_u$ are defined for each state and control variables in Table C.1.

In Section 5.1, joint coordinate tolerances have been defined in a different way. Since experimental data are not tracked in the predictions, the solution found can be optimal regarding the minimisation of the cost function terms, but the resulting motion might be unnatural. To avoid this issue, it is necessary to define correctly the variable bounds, especially for joint coordinates. Each coordinate, q, is bounded by a minimum, min_q, and a maximum, max_q, value:

Chapter/Section	4.1	4.2	4.3	5.1	5.2	6
Problem	Track. wo CM	Calib. CM	Full DC track.	Normal pred.	Crutch pred.	Orth. Pred.
Joint coordinate [°]	5	10	10	0.5*ROM	5	10
Joint coordinate [cm]	3	3	3		5	5
Joint velocity [rad/s, m/s]	0.5	1	0.5	1	1	5
Joint acceleration [rad/s^2, m/s^2]	5	10	5	10	10	50
Joint jerk [rad/s^3, m/s^3]	10	100	10	100	100	100
Joint torque [Nm]	5	50	5	50	50	50
Joint torque change [Nm/s]	-	-	-	500	500	500
Foot-ground reaction force [N]	10	100	10	100	100	100
Foot-ground reaction moment [Nm]	10	100	10	100	100	100
Crutch-ground reaction force [N]	10	100	10	100	100	100

Table C.1: Tolerance values used in each problem formulation to define the minimum and maximum bounds for states (initial, final, and entire simulation) and controls (entire simulation). For the optimal control problems, "Track. wo CM" stands for tracking without contact models, "Calib. CM" stands for calibration of contact models, "Full DC track." stands for full cycle dynamically consistent tracking with contact models; and "Normal pred.", "Crutch pred. ", and "Orth. Pred." stand for normal, crutch-assisted, and crutch-orthosis-assisted walking prediction, respectively.

$$min_q \leq q \leq max_q \tag{C.5}$$

where min_q and max_q are defined using the experimental motion and the maximum and minimum values for each coordinate in the OpenSim model ($\min(q_{model})$ and $\max(q_{model})$, respectively), using as tolerance ε_x the 50% of the coordinate ROM, according to the following expressions:

$$min_q = \max[\min(q_{exp}) - 0.5ROM(q_{exp}), \min(q_{model})] \tag{C.6}$$

$$max_q = \min[\max(q_{exp}) + 0.5ROM(q_{exp}), \max(q_{model})] \tag{C.7}$$

Appendix D

Scale factors

All variables in optimal control problems have been scaled using a canonical transformation of units. This approach creates a new system of units with the goal of making the variables and their derivatives all of a similar magnitude. Only the scale factors for time, mass, length, and angle have been manually assigned (Table D.1). The other scale factors are calculated so as to keep the units consistent, e.g., the scale factor for velocity is equal to the length scale divided by the time scale (Table D.2).

Magnitude	Value
Time	10
Mass	0.25
Length	2
Angle	1

Table D.1: Basic units scale factors.

Magnitude	Value
Linear velocity	0.2
Angular velocity	0.1
Linear acceleration	0.02
Angular acceleration	0.01
Linear jerk	0.002
Angular jerk	0.001
Force	0.005
Torque	0.01
Torque change	0.001
Kinetic energy	0.01
Angular momentum	0.1

Table D.2: Other units scale factors.

Appendix E

Comparison of formulations for dynamically consistent tracking of motion. Additional results

This appendix shows additional results of the comparison of tracking formulations performed in Section 4.1 for *3D HAT*, *3D Full* and *3D Crutches* models. Results include number of iterations, computation time, mean and standard deviation of RMSE of marker and joint coordinates, GRFs and GRMs. Results are shown for full residual reduction tolerance for *3D HAT* (Table E.1) and *3D Full* (Table E.2) models, and for half (Table E.3) and full (Table E.4) residual reduction tolerance for *3D Crutches* model. Mean and standard deviation (SD) of RMSE of each magnitude are shown in black when they are tracked in the formulation, and in grey when they are not.

3D HAT - Full reduction					
Without ground-reactions adjustment		Track marker coordinates		Track joint coordinates	
		Min acc. **A1**	Min jerk **A2**	Min acc. **B1**	Min jerk **B2**
Conv.	Iterations	202	120	18	44
	Time [s]	56.74	45.02	5.75	17.05
RMS	Residual forces [N]	0.69 ± 0.30	0.77 ± 0.30	0.77 ± 0.30	0.60 ± 0.29
	Residual moments [Nm]	0.39 ± 0.19	0.40 ± 0.21	0.41 ± 0.21	0.33 ± 0.15
RMSE	Marker coord. [cm]	1.71 ± 0.90	1.72 ± 0.82	1.58 ± 0.82	1.63 ± 0.74
	Joint coord. [cm]	0.86 ± 0.21	1.04 ± 0.34	0.56 ± 0.15	0.61 ± 0.09
	Joint coord. [°]	6.78 ± 4.06	8.14 ± 3.59	2.64 ± 1.94	3.42 ± 1.99
With ground-reactions adjustment		Track marker coordinates		Track joint coordinates	
		Min acc. **C1**	Min jerk **C2**	Min acc. **D1**	Min jerk **D2**
Conv.	Iterations	864	452	61	157
	Time [s]	301.58	201.81	21.89	70.52
RMS	Residual forces [N]	0.74 ± 0.31	0.43 ± 0.23	0.77 ± 0.30	0.30 ± 0.23
	Residual moments [Nm]	0.40 ± 0.21	0.20 ± 0.15	0.42 ± 0.21	0.15 ± 0.09
RMSE	Marker coord. [cm]	1.62 ± 0.90	1.60 ± 0.83	1.51 ± 0.82	1.54 ± 0.71
	Joint coord. [cm]	0.68 ± 0.29	0.96 ± 0.36	0.49 ± 0.10	0.55 ± 0.09
	Joint coord. [°]	6.88 ± 4.06	8.02 ± 3.70	2.61 ± 1.96	3.38 ± 2.02
	GRFs [N]	2.37 ± 0.62	2.80 ± 1.16	0.85 ± 0.28	2.03 ± 2.04
	GRMs [Nm]	0.46 ± 0.20	0.70 ± 0.39	0.32 ± 0.28	0.70 ± 0.61

Table E.1: Results for *3D HAT* model and full residual reduction, with and without ground-reactions adjustment, with and without ground-reactions adjustment.

3D Full - Full reduction					
Without ground-reactions adjustment		Track marker coordinates		Track joint coordinates	
		Min acc. **A1**	Min jerk **A2**	Min acc. **B1**	Min jerk **B2**
Conv.	Iterations	243	255	18	43
	Time [s]	129.39	182.49	10.89	32.42
RMS	Residual forces [N]	0.84 ± 0.31	0.82 ± 0.30	0.83 ± 0.31	0.39 ± 0.27
	Residual moments [Nm]	0.37 ± 0.16	0.35 ± 0.16	0.36 ± 0.15	0.19 ± 0.06
RMSE	Marker coord. [cm]	1.58 ± 0.90	1.57 ± 0.81	1.46 ± 0.75	1.47 ± 0.67
	Joint coord. [cm]	0.79 ± 0.29	0.90 ± 0.28	0.55 ± 0.16	0.63 ± 0.06
	Joint coord. [°]	4.85 ± 4.03	5.95 ± 3.90	1.78 ± 1.86	2.22 ± 2.14
With ground-reactions adjustment		Track marker coordinates		Track joint coordinates	
		Min acc. **C1**	Min jerk **C2**	Min acc. **D1**	Min jerk **D2**
Conv.	Iterations	943	569	80	149
	Time [s]	660.83	465.92	51.22	122.80
RMS	Residual forces [N]	0.84 ± 0.31	0.83 ± 0.31	0.82 ± 0.28	0.43 ± 0.26
	Residual moments [Nm]	0.37 ± 0.16	0.36 ± 0.15	0.36 ± 0.16	0.17 ± 0.07
RMSE	Marker coord. [cm]	1.46 ± 0.91	1.42 ± 0.83	1.38 ± 0.76	1.37 ± 0.67
	Joint coord. [cm]	0.54 ± 0.24	0.83 ± 0.33	0.48 ± 0.10	0.55 ± 0.08
	Joint coord. [°]	5.01 ± 3.93	6.02 ± 3.85	1.76 ± 1.87	2.20 ± 2.15
	GRFs [N]	2.60 ± 0.75	2.85 ± 1.11	0.77 ± 0.31	1.96 ± 1.90
	GRMs [Nm]	0.61 ± 0.42	0.74 ± 0.45	0.35 ± 0.33	0.74 ± 0.62

Table E.2: Results for *3D Full* model and full residual reduction, with and without ground-reactions adjustment, with and without ground-reactions adjustment.

3D Crutches - Half reduction					
Without ground-reactions adjustment		Track marker coordinates		Track joint coordinates	
		Min acc. **A1**	Min jerk **A2**	Min acc. **B1**	Min jerk **B2**
Conv.	Iterations	393	266	59	46
	Time [s]	353.92	326.47	59.67	63.28
RMS	Residual forces [N]	10.99 ± 9.75	10.92 ± 9.75	11.02 ± 9.83	10.90 ± 9.59
	Residual moments [Nm]	5.77 ± 3.01	5.39 ± 2.90	5.56 ± 2.99	5.11 ± 2.70
RMSE	Marker coord. [cm]	3.64 ± 1.38	4.71 ± 1.98	5.13 ± 2.75	6.42 ± 3.38
	Joint coord. [cm]	3.09 ± 0.92	3.39 ± 1.40	3.20 ± 1.85	3.20 ± 1.97
	Joint coord. [°]	7.14 ± 2.96	8.00 ± 3.53	2.64 ± 2.15	3.22 ± 2.32
With ground-reactions adjustment		Track marker coordinates		Track joint coordinates	
		Min acc. **C1**	Min jerk **C2**	Min acc. **D1**	Min jerk **D2**
Conv.	Iterations	540	584	66	66
	Time [s]	585.19	816.31	79.27	101.69
RMS	Residual forces [N]	10.10 ± 9.05	9.82 ± 8.87	10.56 ± 9.30	10.34 ± 9.09
	Residual moments [Nm]	5.22 ± 2.92	5.19 ± 2.99	5.14 ± 2.84	5.10 ± 2.77
RMSE	Marker coord. [cm]	1.25 ± 0.82	1.23 ± 0.82	1.65 ± 0.93	1.65 ± 0.93
	Joint coord. [cm]	0.61 ± 0.26	0.62 ± 0.24	0.57 ± 0.33	0.56 ± 0.35
	Joint coord. [°]	3.32 ± 2.13	3.22 ± 2.24	1.60 ± 1.80	1.57 ± 1.80
	GRFs [N]	1.83 ± 0.82	1.84 ± 0.80	1.30 ± 0.80	1.30 ± 0.78
	GRMs [Nm]	0.51 ± 0.06	0.51 ± 0.06	0.26 ± 0.01	0.26 ± 0.01

Table E.3: Results for *3D Crutches* model and half residual reduction, with and without ground-reactions adjustment, with and without ground-reactions adjustment.

3D Crutches - Full reduction					
With ground-reactions adjustment		Track marker coordinates		Track joint coordinates	
		Min acc. **C1**	Min jerk **C2**	Min acc. **D1**	Min jerk **D2**
Conv.	Iterations	1895	1533	100	158
	Time [s]	1920.34	1973.26	115.68	231.18
RMS	Residual forces [N]	1.02 ± 1.02	1.11 ± 1.00	1.10 ± 0.97	1.09 ± 0.95
	Residual moments [Nm]	0.54 ± 0.30	0.59 ± 0.30	0.58 ± 0.29	0.59 ± 0.30
RMSE	Marker coord. [cm]	1.34 ± 0.81	1.31 ± 0.82	1.90 ± 0.92	1.90 ± 0.92
	Joint coord. [cm]	0.74 ± 0.25	0.77 ± 0.19	0.80 ± 0.56	0.80 ± 0.57
	Joint coord. [°]	3.44 ± 2.18	3.38 ± 2.25	1.63 ± 1.79	1.60 ± 1.79
	GRFs [N]	3.41 ± 2.21	3.39 ± 2.20	2.92 ± 1.98	2.93 ± 1.98
	GRMs [Nm]	1.00 ± 0.09	1.00 ± 0.08	0.48 ± 0.03	0.48 ± 0.02

Table E.4: Results for *3D Crutches* model and half residual reduction, with ground-reactions adjustment.

Appendix F

Contact models results

This Appendix presents additional results from simulations for calibrating contact model parameter values performed in Section 4.2: Foot-ground (Table F.1) and crutch-ground (Table F.2) contact model parameter values after calibration, and values of anterior-posterior and medio-lateral local position before and after calibration (Table F.3).

Skeletal model	Exp. motion	Foot-ground CM parameter	Spring-damper group					
			1	2	3	4	5	6
3D HAT	barefoot	K [N/m]	$5.24{\cdot}10^4$	$0.37{\cdot}10^4$	$0.01{\cdot}10^4$	$4.91{\cdot}10^4$	$4.91{\cdot}10^4$	$4.91{\cdot}10^4$
		c [s/m]	0.01	0.01	1.00	0.51	0.51	0.51
		μ [-]	0.20	0.12	0.99	0.50	0.50	0.50
	shoes	K [N/m]	$3.05{\cdot}10^4$	$0.83{\cdot}10^4$	$0.01{\cdot}10^4$	$5.00{\cdot}10^4$	$5.00{\cdot}10^4$	$5.00{\cdot}10^4$
		c [s/m]	0.32	0.01	0.44	0.50	0.50	0.50
		μ [-]	0.20	0.12	0.35	0.50	0.50	0.50
3D Full	barefoot	K [N/m]	$3.76{\cdot}10^4$	$0.31{\cdot}10^4$	$0.01{\cdot}10^4$	$5.02{\cdot}10^4$	$5.02{\cdot}10^4$	$5.02{\cdot}10^4$
		c [s/m]	0.69	0.04	0.89	0.51	0.51	0.51
		μ [-]	0.18	0.13	0.29	0.50	0.50	0.50
	shoes	K [N/m]	$9.99{\cdot}10^4$	$0.59{\cdot}10^4$	$0.01{\cdot}10^4$	$5.01{\cdot}10^4$	$5.01{\cdot}10^4$	$5.01{\cdot}10^4$
		c [s/m]	0.38	0.39	0.75	0.51	0.51	0.51
		μ [-]	0.18	0.15	0.00	0.50	0.50	0.50
3D Crutches	non-alt. four-point	K [N/m]	$0.45{\cdot}10^3$	$0.36{\cdot}10^3$	$0.43{\cdot}10^3$	$0.47{\cdot}10^3$	$6.10{\cdot}10^3$	$5.50{\cdot}10^4$
		c [s/m]	0.54	0.52	0.52	0.51	0.51	0.52
		μ [-]	0.24	0.28	0.30	0.29	0.16	0.04

Table F.1: Foot-ground contact model parameter values after calibration per each spring-damper group (see Figure 3.4) and for each model.

Skeletal model	Exp. motion	Crutch-ground CM parameter	
3D Crutches	non-alt. four-point	K_n [N/m$^{3/2}$]	$6.80 \cdot 10^4$
		χ [Ns/m$^{5/2}$]	$50.19 \cdot 10^4$
		μ_{crutch} [-]	0.05

Table F.2: Crutch-ground contact model parameter values after calibration.

	Spring-damper group					
Initial	**Hindfoot**					Forefoot
location	**1**	**2**	**3**	**4**	**5**	6
x [cm]	0.00	5.00	10.00	15.00	20.00	8.00
z [cm]	-1.00	-3.00	-3.00	-3.00	-3.00	-1.00
	1.00	0.00	0.00	0.00	0.00	1.00
	-	3.00	3.00	3.00	3.00	-

Calibrated	**Hindfoot**					**Forefoot**
location	**1**	**2**	**3**	**4**	**5**	**6**
x [cm]	-0.43	5.27	8.00	13.00	20.07	6.51
z [cm]	-2.00	-2.00	-2.00	-2.00	-2.00	-1.56
	0.68	1.00	1.00	0.95	0.60	0.01
	-	3.60	2.89	3.18	2.00	-

Table F.3: Values of anterior-posterior local position (x) and medio-lateral local position (z) of the spring-damper groups in the foot-ground contact model before and after calibration. These results have been obtained for the *3D HAT* model and tracking *barefoot* normal walking data.

Appendix G

Healthy subject orthosis-assisted walking experimental and predicted motions

This appendix shows experimental joint coordinates (Figure G.1), joint torques (Figure G.2) and foot- and crutch-ground reaction forces (Figure G.3), and predicted joint coordinates (Figure G.4), joint torques (Figure G.5) and foot- and crutch-ground reaction forces (Figure G.6) of the three crutch-orthosis-assisted motions for the healthy subject (PASS, ACT40, ACT60).

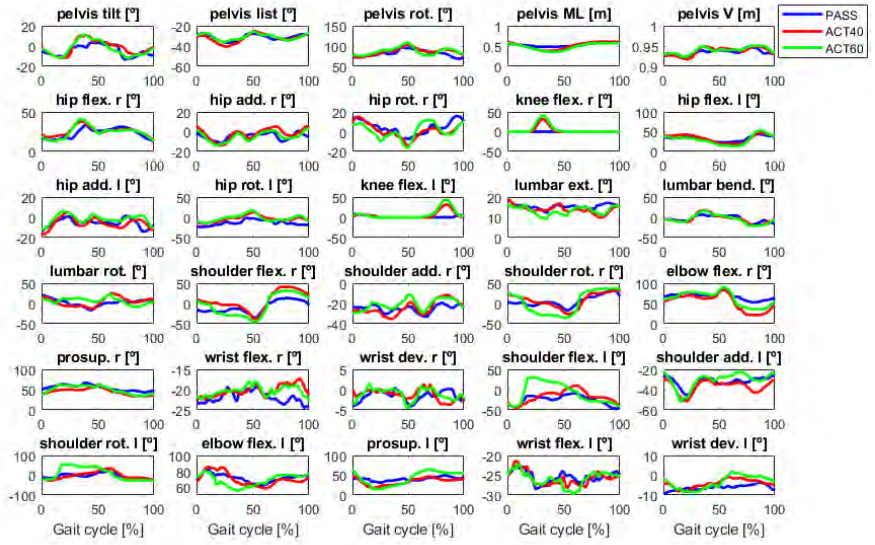

Figure G.1: Experimental joint coordinates for the healthy subject crutch-orthosis-assisted motions.

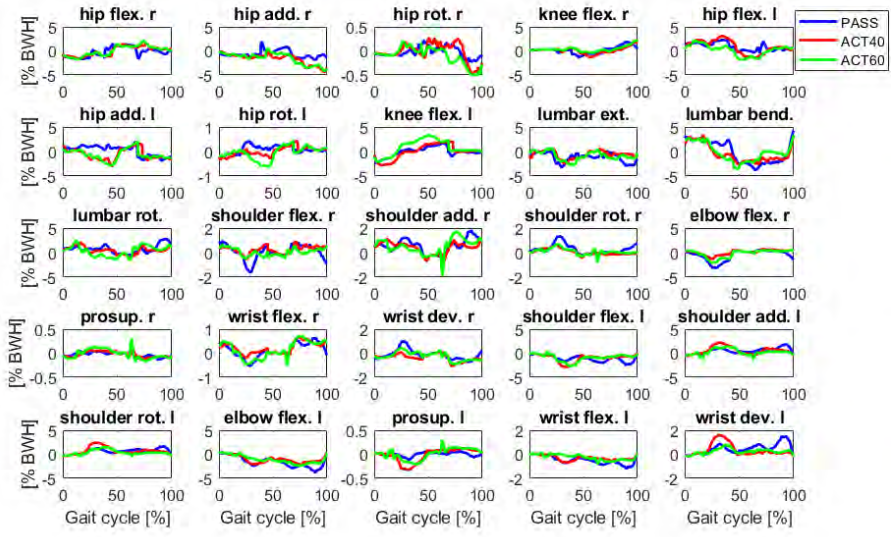

Figure G.2: Experimental joint torques (in [% BW*H]) for the healthy subject crutch-orthosis-assisted motions.

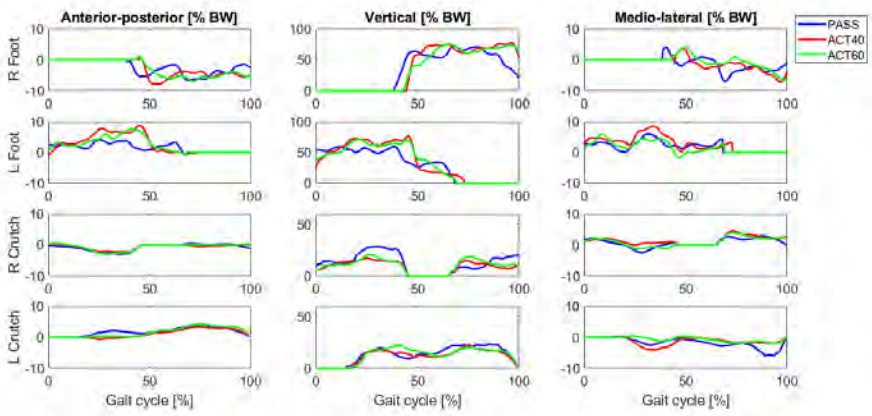

Figure G.3: Experimental foot- and crutch-ground reaction forces (in [% BW]) for the healthy subject crutch-orthosis-assisted motions. "R" and "L" refer to the right and left side, respectively.

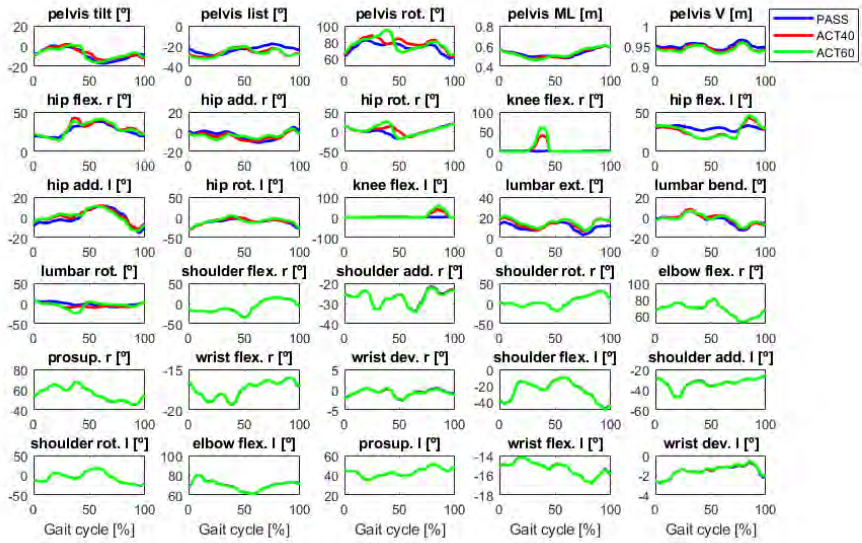

Figure G.4: Predicted joint coordinates for the healthy subject crutch-orthosis-assisted motions.

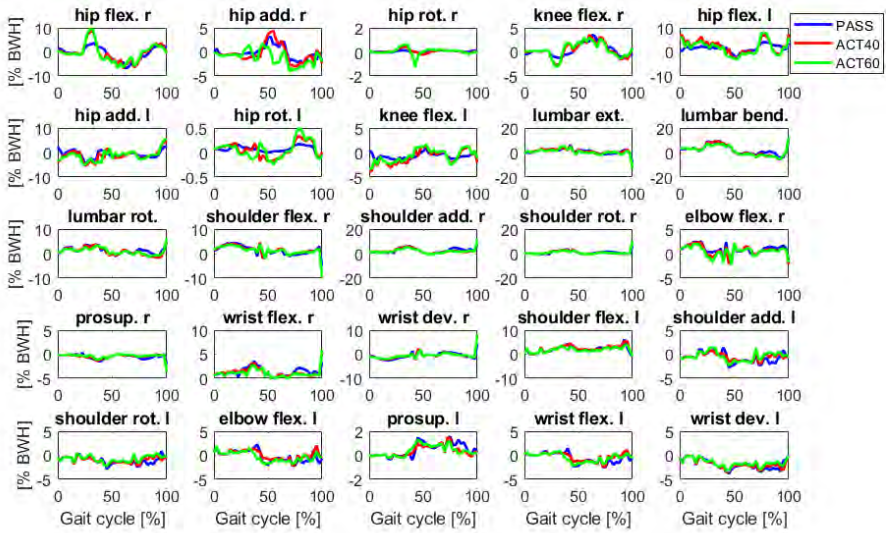

Figure G.5: Predicted joint torques (in [% BW*H]) for the healthy subject crutch-orthosis-assisted motions.

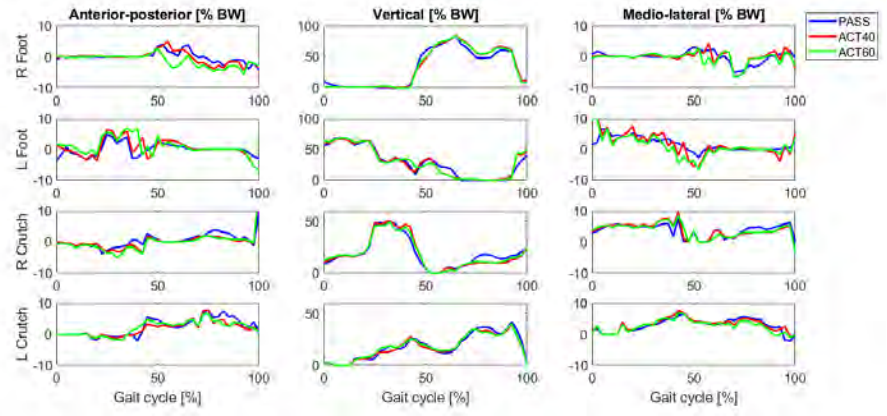

Figure G.6: Predicted foot- and crutch-ground reaction forces (in [% BW]) for the healthy subject crutch-orthosis-assisted motions. "R" and "L" refer to the right and left side, respectively.

Appendix H

SCI subject orthosis-assisted walking experimental and predicted motions

This appendix shows experimental joint coordinates (Figure H.1) of the three walker-orthosis-assisted motions for the SCI subject (PASS, ACT20, ACT40), and the experimental joint coordinates (Figure H.2) of the PASS crutch-orthosis-assisted motion for the SCI subject. Moreover, it shows the dynamically consistent joint torques (Figure H.3) and foot- and crutch-ground reaction forces (Figure H.4) after tracking of experimental joint coordinates of PASS crutch-orthosis-assisted motion for the SCI subject. Finally, it shows predicted predicted joint coordinates (Figure H.5), joint torques (Figure H.6) and foot- and crutch-ground reaction forces (Figure H.7) of the three crutch-orthosis-assisted motions for the SCI subject (PASS, ACT20, ACT40).

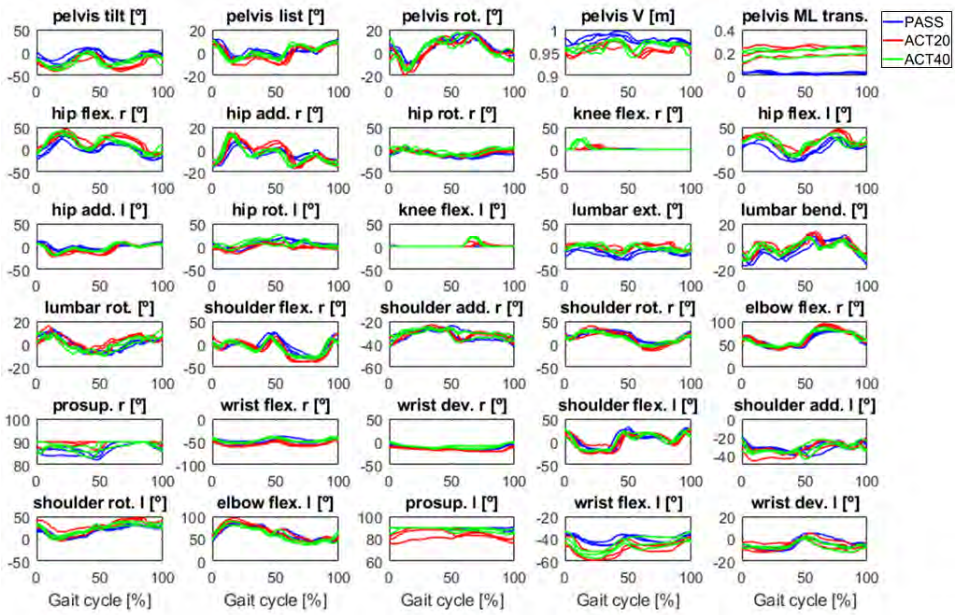

Figure H.1: Experimental joint coordinates for the SCI subject walker-orthosis-assisted motions.

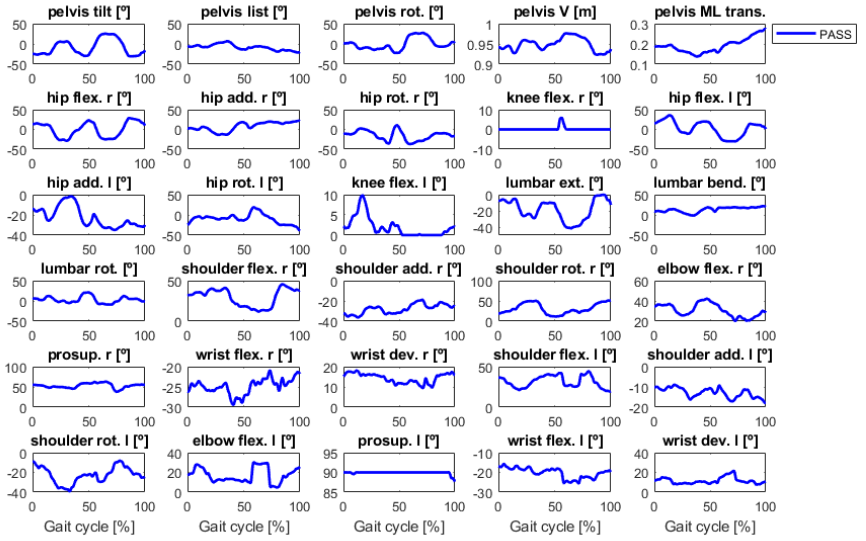

Figure H.2: Experimental joint coordinates for the SCI subject crutch-orthosis-assisted motion.

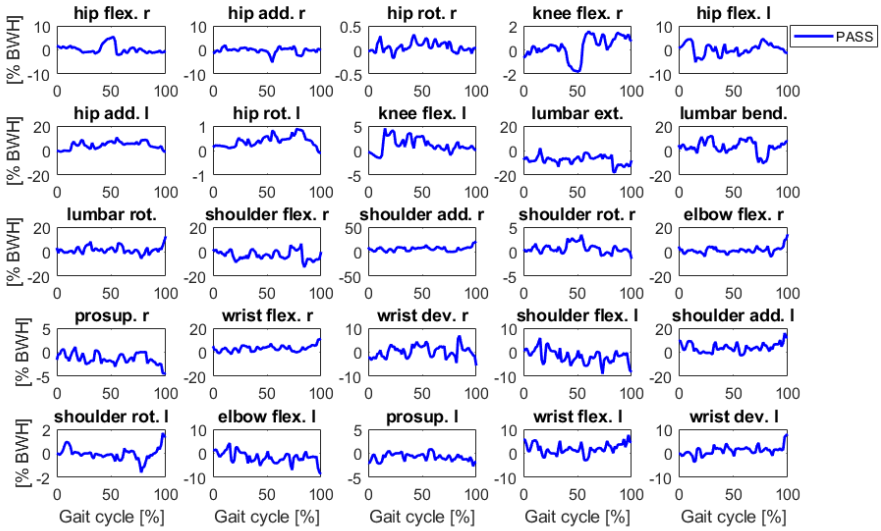

Figure H.3: Dynamically consistent joint torques (in [% BW*H]) after tracking of experimental joint coordinates for the SCI subject crutch-orthosis-assisted motion.

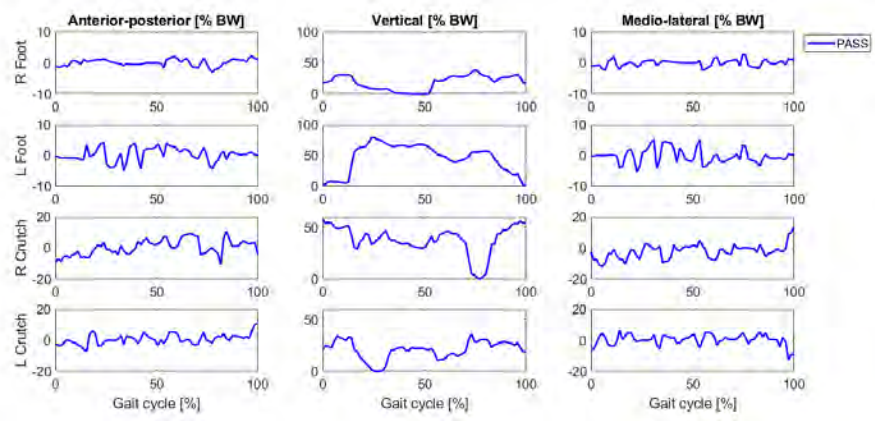

Figure H.4: Dynamically consistent foot- and crutch-ground reaction forces (in [% BW]) after tracking of experimental joint coordinates for the SCI subject crutch-orthosis-assisted motion. “R” and “L” refer to the right and left side, respectively.

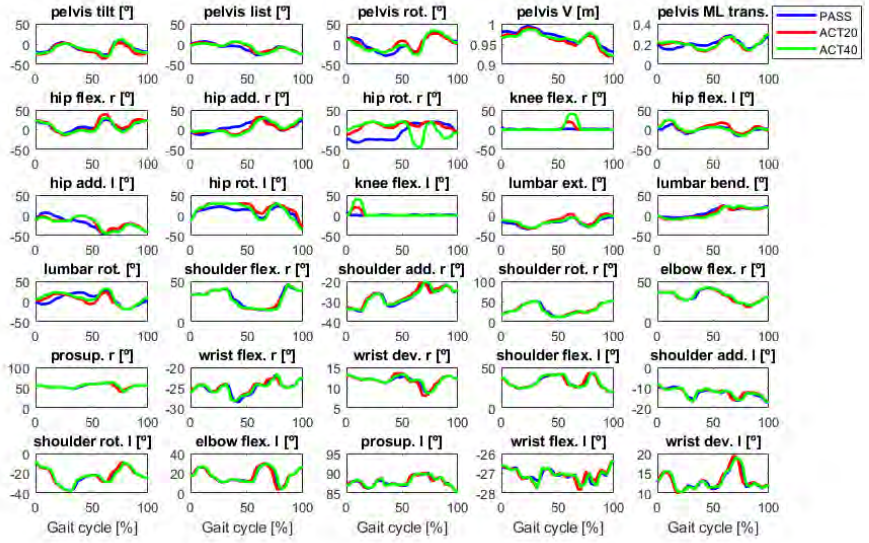

Figure H.5: Predicted joint coordinates for the SCI subject crutch-orthosis-assisted motions.

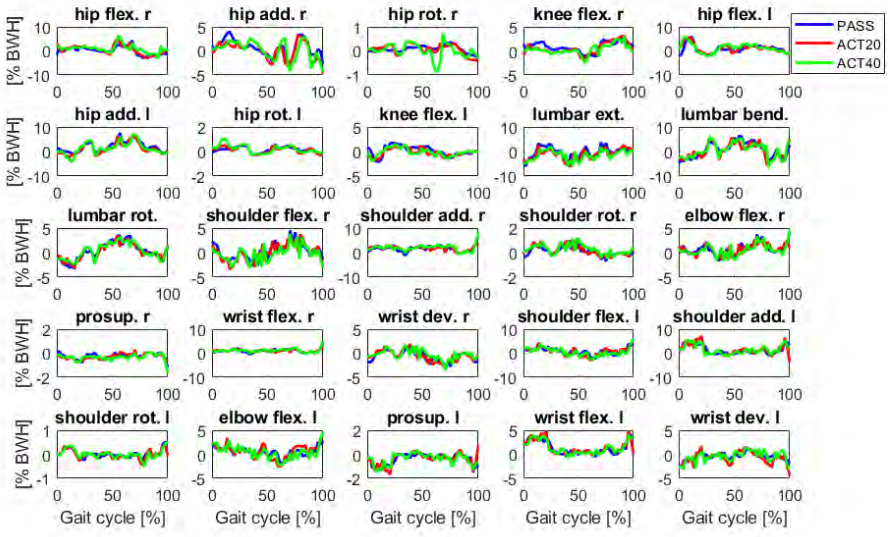

Figure H.6: Predicted joint torques (in [% BW*H]) for the SCI subject crutch-orthosis-assisted motions.

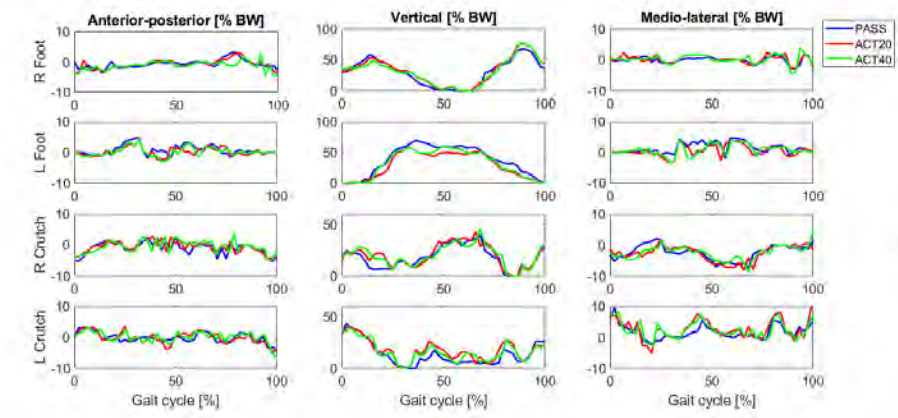

Figure H.7: Predicted foot- and crutch-ground reaction forces (in [% BW]) for the SCI subject crutch-orthosis-assisted motions. "R" and "L" refer to the right and left side, respectively.

Bibliography

[1] World Health Organization et al. Who global disability action plan 2014-2021: Better health for all people with disability. 2015.

[2] Antonio J Del-Ama, Aikaterini D Koutsou, Juan C Moreno, Ana De-Los-Reyes, Ángel Gil-Agudo, and José L Pons. Review of hybrid exoskeletons to restore gait following spinal cord injury. *Journal of Rehabilitation Research & Development*, 49(4), 2012.

[3] Josep M Font-Llagunes, Daniel Clos, Urbano Lugrís, F Javier Alonso, and Javier Cuadrado. Design and experimental evaluation of a low-cost robotic orthosis for gait assistance in subjects with spinal cord injury. In *Wearable Robotics: Challenges and Trends*, pages 281–285. Springer, 2017.

[4] Larry E Miller, Angela K Zimmermann, and William G Herbert. Clinical effectiveness and safety of powered exoskeleton-assisted walking in patients with spinal cord injury: systematic review with meta-analysis. *Medical devices (Auckland, NZ)*, 9:455, 2016.

[5] Dennis R Louie, Janice J Eng, and Tania Lam. Gait speed using powered robotic exoskeletons after spinal cord injury: a systematic review and correlational study. *Journal of neuroengineering and rehabilitation*, 12(1):82, 2015.

[6] Matteo Lancini, Ileana Bodini, and Giovanna Sansoni. Upper limb loads during robotic assisted gait: A measuring system to guide training. In *Human-Centric Robotics: Proceedings of the 20th International Conference on CLAWAR 2017*, pages 613–620. World Scientific, 2017.

[7] Josep M Font-Llagunes, Urbano Lugrís, Daniel Clos, F Javier Alonso, and Javier Cuadrado. Design, control, and pilot study of a lightweight and modular robotic exoskeleton for walking assistance after spinal cord injury. *Journal of Mechanisms and Robotics*, 12(3), 2020.

[8] Anoushka Singh, Lindsay Tetreault, Suhkvinder Kalsi-Ryan, Aria Nouri, and Michael G Fehlings. Global prevalence and incidence of traumatic spinal cord injury. *Clinical epidemiology*, 6:309, 2014.

[9] Bing Chen, Bin Zi, Zhengyu Wang, Ling Qin, and Wei-Hsin Liao. Knee exoskeletons for gait rehabilitation and human performance augmentation: A state-of-the-art. *Mechanism and Machine Theory*, 134:499–511, 2019.

[10] Steven C Kirshblum, Stephen P Burns, Fin Biering-Sorensen, William Donovan, Daniel E Graves, Amitabh Jha, Mark Johansen, Linda Jones, Andrei Krassioukov, MJ Mulcahey, et al. International standards for neurological classification of spinal cord injury (revised 2011). *The journal of spinal cord medicine*, 34(6):535–546, 2011.

[11] Timothy T Roberts, Garrett R Leonard, and Daniel J Cepela. Classifications in brief: American spinal injury association (asia) impairment scale, 2017.

[12] Peppino Tropea, Benedetta Cesqui, Vito Monaco, Sara Aliboni, Federico Posteraro, and Silvestro Micera. Effects of the alternate combination of "error-enhancing" and "active assistive" robot-mediated treatments on stroke patients. *IEEE journal of translational engineering in health and medicine*, 1:2100109–2100109, 2013.

[13] Benjamin J Fregly. Design of optimal treatments for neuromusculoskeletal disorders using patient-specific multibody dynamic models. *International journal for computational vision and biomechnanics*, 2(2):145, 2009.

[14] Katja Mombaur. Optimal control for applications in medical and rehabilitation technology: challenges and solutions. In *Advances in Mathematical Modeling, Optimization and Optimal Control*, pages 103–145. Springer, 2016.

[15] Thomas K Uchida, Ajay Seth, Soha Pouya, Christopher L Dembia, Jennifer L Hicks, and Scott L Delp. Simulating ideal assistive devices to reduce the metabolic cost of running. *PloS one*, 11(9):e0163417, 2016.

[16] Marko Ackermann and Werner Schiehlen. Dynamic analysis of human gait disorder and metabolical cost estimation. *Archive of Applied Mechanics*, 75(10-12):569–594, 2006.

[17] Guy Bessonnet, Pascal Seguin, and Philippe Sardain. A parametric optimization approach to walking pattern synthesis. *The International Journal of Robotics Research*, 24(7):523–536, 2005.

[18] Lei Ren, Richard K Jones, and David Howard. Predictive modelling of human walking over a complete gait cycle. *Journal of biomechanics*, 40(7):1567–1574, 2007.

[19] Marko Ackermann and Antonie J Van den Bogert. Optimality principles for model-based prediction of human gait. *Journal of biomechanics*, 43(6):1055–1060, 2010.

[20] Tim W Dorn, Jack M Wang, Jennifer L Hicks, and Scott L Delp. Predictive simulation generates human adaptations during loaded and inclined walking. *PloS one*, 10(4):e0121407, 2015.

[21] Antonie J van den Bogert, Dimitra Blana, and Dieter Heinrich. Implicit methods for efficient musculoskeletal simulation and optimal control. *Procedia Iutam*, 2:297–316, 2011.

[22] Daniel García-Vallejo, Josep Maria Font-Llagunes, and Werner Schiehlen. Dynamical analysis and design of active orthoses for spinal cord injured subjects by aesthetic and energetic optimization. *Nonlinear dynamics*, 84(2):559–581, 2016.

[23] Elizabeth Russell Esposito and Ross H Miller. Maintenance of muscle strength retains a normal metabolic cost in simulated walking after transtibial limb loss. *PloS one*, 13(1):e0191310, 2018.

[24] Qian Wang, Yu-Jiang Xiang, Jasbir Arora, and Karim Abdel-Malek. Alternative formulations for optimization-based human gait planning. In *48th AIAA/ASME/ASCE/AHS/ASC Structures, Structural Dynamics, and Materials Conference*, page 1909, 2007.

[25] Frank C Anderson and Marcus G Pandy. Dynamic optimization of human walking. *J. Biomech. Eng.*, 123(5):381–390, 2001.

[26] Daniel García-Vallejo and Werner Schiehlen. 3d-simulation of human walking by parameter optimization. *Archive of Applied Mechanics*, 82(4):533–556, 2012.

[27] MW Koch, M Ringkamp, and S Leyendecker. Discrete mechanics and optimal control of walking gaits. *Journal of Computational and Nonlinear Dynamics*, 12(2):021006, 2017.

[28] René Fluit, MM Van der Krogt, Herman van der Kooij, N Verdonschot, and Hubertus FJM Koopman. A simple controller for the prediction of three-dimensional gait. *Journal of biomechanics*, 45(15):2610–2617, 2012.

[29] Yi-Chung Lin, Jonathan P Walter, and Marcus G Pandy. Predictive simulations of neuromuscular coordination and joint-contact loading in human gait. *Annals of biomedical engineering*, 46(8):1216–1227, 2018.

[30] Yujiang Xiang, HJ Chung, A Mathai, S Rahmatalla, J Kim, T Marler, S Beck, J Yang, JS Arora, K Abdel-Malek, et al. Optimization-based dynamic human walking prediction. 2007.

[31] Hyung Joo Kim, Qian Wang, Salam Rahmatalla, Colby C Swan, Jasbir S Arora, Karim Abdel-Malek, and Jose G Assouline. Dynamic motion planning of 3d human locomotion using gradient-based optimization. *Journal of biomechanical engineering*, 130(3):031002, 2008.

[32] Martin Felis and Katja Mombaur. Modeling and optimization of human walking. In *Modeling, Simulation and Optimization of Bipedal Walking*, pages 31–42. Springer, 2013.

[33] Yi-Chung Lin and Marcus G Pandy. Three-dimensional data-tracking dynamic optimization simulations of human locomotion generated by direct collocation. *Journal of biomechanics*, 59:1–8, 2017.

[34] Jeffrey A Reinbolt, Raphael T Haftka, Terese L Chmielewski, and Benjamin J Fregly. A computational framework to predict post-treatment outcome for gait-related disorders. *Medical Engineering & Physics*, 30(4):434–443, 2008.

[35] Martin L Felis and Katja Mombaur. Synthesis of full-body 3d human gait using optimal control methods. In *2016 IEEE International Conference on Robotics and Automation (ICRA)*, pages 1560–1566. IEEE, 2016.

[36] Nathan R Sauder, Jessica L Allen, Lena H Ting, Trisha M Kesar, and Benjamin J Fregly. Computational design of fastfes treatment to improve propulsive force symmetry during post-stroke gait: A feasibility study. *Frontiers in Neurorobotics*, 13:80, 2019.

[37] Antoine Falisse, Gil Serrancolí, Christopher L Dembia, Joris Gillis, Ilse Jonkers, and Friedl De Groote. Rapid predictive simulations with complex musculoskeletal models suggest that diverse healthy and pathological human gaits can emerge from similar control strategies. *Journal of The Royal Society Interface*, 16(157):20190402, 2019.

[38] Alexander G Bruno, Mary L Bouxsein, and Dennis E Anderson. Development and validation of a musculoskeletal model of the fully articulated thoracolumbar spine and rib cage. *Journal of biomechanical engineering*, 137(8):081003, 2015.

[39] Marco Senteler, Bernhard Weisse, Dominique A Rothenfluh, and Jess G Snedeker. Intervertebral reaction force prediction using an enhanced assembly of opensim models. *Computer methods in biomechanics and biomedical engineering*, 19(5):538–548, 2016.

[40] Dario Cazzola, Timothy P Holsgrove, Ezio Preatoni, Harinderjit S Gill, and Grant Trewartha. Cervical spine injuries: A whole-body musculoskeletal model for the analysis of spinal loading. *PloS one*, 12(1):e0169329, 2017.

[41] Jonathan D Mortensen, Anita N Vasavada, and Andrew S Merryweather. The inclusion of hyoid muscles improve moment generating capacity and dynamic simulations in musculoskeletal models of the head and neck. *PloS one*, 13(6):e0199912, 2018.

[42] Hang Xu, Donald Bloswick, and Andrew Merryweather. An improved opensim gait model with multiple degrees of freedom knee joint and knee ligaments. *Computer methods in biomechanics and biomedical engineering*, 18(11):1217–1224, 2015.

[43] Jeremy Suggs, Conrad Wang, and Guoan Li. The effect of graft stiffness on knee joint biomechanics after acl reconstruction—-a 3d computational simulation. *Clinical biomechanics*, 18(1):35–43, 2003.

[44] Jong Hwa Lee, Deanna S Asakawa, Jack T Dennerlein, and Devin L Jindrich. Finger muscle attachments for an opensim upper-extremity model. *PloS one*, 10(4):e0121712, 2015.

[45] Urbano Lugrís, Jairo Carlín, Alberto Luaces, and Javier Cuadrado. Gait analysis system for spinal cord-injured subjects assisted by active orthoses and crutches. *Proceedings of the Institution of Mechanical Engineers, Part K: Journal of Multi-body Dynamics*, 227(4):363–374, 2013.

[46] Michael Damsgaard, John Rasmussen, Søren Tørholm Christensen, Egidijus Surma, and Mark De Zee. Analysis of musculoskeletal systems in the anybody modeling system. *Simulation Modelling Practice and Theory*, 14(8):1100–1111, 2006.

[47] Anthony Petrella, John Rasmussen, Amir Al-Munajjed, Michael Damsgaard, Morten Lund, and Arne Kiis. How good is good enough? lessons in musculoskeletal model validation with the anybody modeling system. *Journal of Medical Devices*, 7(4), 2013.

[48] Leng-Feng Lee and Brian R Umberger. Generating optimal control simulations of musculoskeletal movement using opensim and matlab. *PeerJ*, 4:e1638, 2016.

[49] Carmichael F Ong, Jennifer L Hicks, and Scott L Delp. Simulation-based design for wearable robotic systems: an optimization framework for enhancing a standing long jump. *IEEE Transactions on Biomedical Engineering*, 63(5):894–903, 2015.

[50] Andrew J Meyer, Ilan Eskinazi, Jennifer N Jackson, Anil V Rao, Carolynn Patten, and Benjamin J Fregly. Muscle synergies facilitate computational prediction of subject-specific walking motions. *Frontiers in bioengineering and biotechnology*, 4:77, 2016.

[51] Benjamin J Fregly, Jeffrey A Reinbolt, Kelly L Rooney, Kim H Mitchell, and Terese L Chmielewski. Design of patient-specific gait modifications for knee osteoarthritis rehabilitation. *IEEE Transactions on Biomedical Engineering*, 54(9):1687–1695, 2007.

[52] Ajay Seth, Michael Sherman, Jeffrey A Reinbolt, and Scott L Delp. Opensim: a musculoskeletal modeling and simulation framework for in silico investigations and exchange. *Procedia Iutam*, 2:212–232, 2011.

[53] Felix E Zajac. Muscle and tendon: properties, models, scaling, and application to biomechanics and motor control. *Critical reviews in biomedical engineering*, 17(4):359–411, 1989.

[54] Matthew Millard, Thomas Uchida, Ajay Seth, and Scott L Delp. Flexing computational muscle: modeling and simulation of musculotendon dynamics. *Journal of biomechanical engineering*, 135(2):021005, 2013.

[55] Gil Serrancolí, Allison L Kinney, Benjamin J Fregly, and Josep M Font-Llagunes. Neuromusculoskeletal model calibration significantly affects predicted knee contact forces for walking. *Journal of biomechanical engineering*, 138(8):081001, 2016.

[56] Darryl G Thelen. Adjustment of muscle mechanics model parameters to simulate dynamic contractions in older adults. *Journal of biomechanical engineering*, 125(1):70–77, 2003.

[57] Gil Serrancolí Masferrer. Optimization and muscle synergy approaches for studying muscle redundancy during walking. 2015.

[58] Manish Sreenivasa, Matthew Millard, Martin Felis, Katja Mombaur, and Sebastian I Wolf. Optimal control based stiffness identification of an ankle-foot orthosis using a predictive walking model. *Frontiers in computational neuroscience*, 11:23, 2017.

[59] Apoorva Rajagopal, Christopher L Dembia, Matthew S DeMers, Denny D Delp, Jennifer L Hicks, and Scott L Delp. Full-body musculoskeletal model for muscle-driven simulation of human gait. *IEEE transactions on biomedical engineering*, 63(10):2068–2079, 2016.

[60] Giordano Valente, Gianluigi Crimi, Nicola Vanella, Enrico Schileo, and Fulvia Taddei. nmsbuilder: Freeware to create subject-specific musculoskeletal models for opensim. *Computer methods and programs in biomedicine*, 152:85–92, 2017.

[61] Jeffrey A Reinbolt, Jaco F Schutte, Benjamin J Fregly, Byung Il Koh, Raphael T Haftka, Alan D George, and Kim H Mitchell. Determination of patient-specific multi-joint kinematic models through two-level optimization. *Journal of biomechanics*, 38(3):621–626, 2005.

[62] Mohammad S Shourijeh, Kenneth B Smale, Brigitte M Potvin, and Daniel L Benoit. A forward-muscular inverse-skeletal dynamics framework for human musculoskeletal simulations. *Journal of biomechanics*, 49(9):1718–1723, 2016.

[63] Rosa Pàmies-Vilà, Josep M Font-Llagunes, Urbano Lugrís, and Javier Cuadrado. Parameter identification method for a three-dimensional foot–ground contact model. *Mechanism and Machine Theory*, 75:107–116, 2014.

[64] Jennifer N Jackson, Chris J Hass, and Benjamin J Fregly. Development of a subject-specific foot-ground contact model for walking. *Journal of biomechanical engineering*, 138(9):091002, 2016.

[65] Mohammad S Shourijeh and John McPhee. Foot-ground contact modeling within human gait simulations: from kelvin–voigt to hyper-volumetric models. *Multibody System Dynamics*, 35(4):393–407, 2015.

[66] C David Remy. Integration of an adaptive ground contact model into the dynamic simulation of gait. *University of Wisconsin-Madison, Madison, WI*, 2006.

[67] S Tashman, FE Zajac, and I Perkash. Modeling and simulation of paraplegic ambulation in a reciprocating gait orthosis. *Journal of biomechanical engineering*, 117(3):300–308, 1995.

[68] Matthew Millard, Manish Sreenivasa, and Katja Mombaur. Predicting the motions and forces of wearable robotic systems using optimal control. *Frontiers in Robotics and AI*, 4:41, 2017.

[69] Marko Ackermann and Antonie J van den Bogert. Predictive simulation of gait in rehabilitation. In *2010 Annual International Conference of the IEEE Engineering in Medicine and Biology*, pages 5444–5447. IEEE, 2010.

[70] B Samadi, S Achiche, A Parent, L Ballaz, U Chouinard, and M Raison. Custom sizing of lower limb exoskeleton actuators using gait dynamic modelling of children with cerebral palsy. *Computer methods in biomechanics and biomedical engineering*, 19(14):1519–1524, 2016.

[71] Pei-Chun Kao, Cara L Lewis, and Daniel P Ferris. Joint kinetic response during unexpectedly reduced plantar flexor torque provided by a robotic ankle exoskeleton during walking. *Journal of biomechanics*, 43(7):1401–1407, 2010.

[72] Francesco Ferrati, Roberto Bortoletto, and Enrico Pagello. Virtual modelling of a real exoskeleton constrained to a human musculoskeletal model. In *Conference on Biomimetic and Biohybrid Systems*, pages 96–107. Springer, 2013.

[73] Diego Torricelli, Camilo Cortés, Nerea Lete, Álvaro Bertelsen, Jose E Gonzalez-Vargas, Antonio J del Ama, Iris Dimbwadyo, Juan C Moreno, Julian Florez, and Jose L Pons. A subject-specific kinematic model to predict human motion in exoskeleton-assisted gait. *Frontiers in neurorobotics*, 12:18, 2018.

[74] Gil Serrancolí, Antoine Falisse, Christopher Dembia, Jonas Vantilt, Kevin Tanghe, Dirk Lefeber, Ilse Jonkers, Joris De Schutter, and Friedl De Groote. Subject-exoskeleton contact model calibration leads to accurate interaction force predictions. *IEEE Transactions on Neural Systems and Rehabilitation Engineering*, 27(8):1597–1605, 2019.

[75] Massimo Sartori, David G Llyod, and Dario Farina. Neural data-driven musculoskeletal modeling for personalized neurorehabilitation technologies. *IEEE transactions on biomedical engineering*, 63(5):879–893, 2016.

[76] Jonas Fischer, Corina Nüesch, Beat Göpfert, Annegret Mündermann, Victor Valderrabano, and Thomas Hügle. Forearm pressure distribution during ambulation with elbow crutches: a cross-sectional study. *Journal of neuroengineering and rehabilitation*, 11(1):61, 2014.

[77] Enrique Perez-Rizo, Fernando Trincado-Alonso, Soraya Perez-Nombela, Antonio del Ama-Espinosa, Fernando Jimenez-Diaz, Vicente Lozano-Berrio, and

Angel Gil-Agudo. Application of a model to analyze shoulder biomechanics in adult patients with spinal cord injury when walking with crutches in two different gait patterns. *NeuroRehabilitation*, 40(1):129–140, 2017.

[78] Lisa Lighthall Haubert, Dee D Gutierrez, Craig J Newsam, JoAnne K Gronley, Sara J Mulroy, and Jacquelin Perry. A comparison of shoulder joint forces during ambulation with crutches versus a walker in persons with incomplete spinal cord injury. *Archives of physical medicine and rehabilitation*, 87(1):63–70, 2006.

[79] P Westerhoff, F Graichen, A Bender, A Halder, A Beier, A Rohlmann, and G Bergmann. In vivo measurement of shoulder joint loads during walking with crutches. *Clinical Biomechanics*, 27(7):711–718, 2012.

[80] Guangyu Liu, Sheng-Quan Xie, and Yanxin Zhang. Optimization of spring-loaded crutches via boundary value problem. *IEEE transactions on neural systems and rehabilitation engineering*, 19(1):64–70, 2010.

[81] Marko Ackermann and Bruno Augusto Taissun. A computational study of the swing phase of the gait with standard and spring-loaded crutches. In *2012 4th IEEE RAS & EMBS International Conference on Biomedical Robotics and Biomechatronics (BioRob)*, pages 1476–1481. IEEE, 2012.

[82] Jaap H van der Spek, Peter H Veltink, Hermie J Hermens, Bart FJM Koopman, and Herman BK Boom. A model-based approach to stabilizing crutch supported paraplegic standing by artificial hip joint stiffness. *IEEE transactions on neural systems and rehabilitation engineering*, 11(4):443–451, 2003.

[83] Brandon N Fournier, Edward D Lemaire, Andrew JJ Smith, and Marc Doumit. Modeling and simulation of a lower extremity powered exoskeleton. *IEEE Transactions on Neural Systems and Rehabilitation Engineering*, 26(8):1596–1603, 2018.

[84] Francisco Mouzo, U Lugris, Rosa Pàmies-Vilà, and J Cuadrado. Skeletal-level control-based forward dynamic analysis of acquired healthy and assisted gait motion. *Multibody System Dynamics*, 44(1):1–29, 2018.

[85] Matthew Millard, Eric Kubica, and John McPhee. Forward dynamic human gait simulation using a slip target model. *Procedia IUTAM*, 2:142–157, 2011.

[86] Marek Wojtyra. Multibody simulation model of human walking. 2003.

[87] Mike Peasgood, Eric Kubica, and John McPhee. Stabilization of a dynamic walking gait simulation. *Journal of computational and nonlinear dynamics*, 2(1):65–72, 2007.

[88] Pedro Moreira, Paulo Flores, and Miguel Silva. A biomechanical multibody foot model for forward dynamic analysis. In *2012 IEEE 2nd Portuguese Meeting in Bioengineering (ENBENG)*, pages 1–6. IEEE, 2012.

[89] Peter Brown and John McPhee. A 3d ellipsoidal volumetric foot–ground contact model for forward dynamics. *Multibody System Dynamics*, 42(4):447–467, 2018.

[90] Maximilian Stelzer and Oskar Von Stryk. Efficient forward dynamics simulation and optimization of human body dynamics. *ZAMM-Journal of Applied Mathematics and Mechanics/Zeitschrift für Angewandte Mathematik und Mechanik: Applied Mathematics and Mechanics*, 86(10):828–840, 2006.

[91] Tim W Dorn, Yi-Chung Lin, and Marcus G Pandy. Estimates of muscle function in human gait depend on how foot-ground contact is modelled. *Computer methods in biomechanics and biomedical engineering*, 15(6):657–668, 2012.

[92] Farnood Gholami, Rosa Pàmies-Vilà, József Kövecses, and Josep M Font-Llagunes. Effects of foot modelling on the human ankle kinematics and dynamics. *Mechanism and Machine Theory*, 93:175–184, 2015.

[93] Margarida Machado, Pedro Moreira, Paulo Flores, and Hamid M Lankarani. Compliant contact force models in multibody dynamics: Evolution of the hertz contact theory. *Mechanism and Machine Theory*, 53:99–121, 2012.

[94] Paulo Flores and Hamid M Lankarani. *Contact force models for multibody dynamics*, volume 226. Springer, 2016.

[95] Kenneth H Hunt and Frank R Erskine Crossley. Coefficient of restitution interpreted as damping in vibroimpact. 1975.

[96] Josep M Font-Llagunes, Ana Barjau, Rosa Pàmies-Vilà, and József Kövecses. Dynamic analysis of impact in swing-through crutch gait using impulsive and continuous contact models. *Multibody system dynamics*, 28(3):257–282, 2012.

[97] Paulo Flores, Margarida Machado, Miguel T Silva, and Jorge M Martins. On the continuous contact force models for soft materials in multibody dynamics. *Multibody system dynamics*, 25(3):357–375, 2011.

[98] Daniel Dopico, Alberto Luaces, Manuel Gonzalez, and Javier Cuadrado. Dealing with multiple contacts in a human-in-the-loop application. *Multibody System Dynamics*, 25(2):167–183, 2011.

[99] Andres F Hidalgo Romero, Sergio Lerma-Lara, and Eduardo Rocon. A predictive simulation approach suitable for gait control strategies design to be used on lower limbs assistive devices. *Gait & Posture*, 57:85–86, 2017.

[100] Matthew L Handford and Manoj Srinivasan. Robotic lower limb prosthesis design through simultaneous computer optimizations of human and prosthesis costs. *Scientific reports*, 6:19983, 2016.

[101] Hyun-Joon Chung, Yujiang Xiang, Anith Mathai, Salam Rahmatalla, Joo Kim, Timothy Marler, Steve Beck, Jingzhou Yang, Jasbir Arora, Karim Abdel-Malek, et al. A robust formulation for prediction of human running. Technical report, SAE Technical Paper, 2007.

[102] Luciano Luporini Menegaldo, Agenor de Toledo Fleury, and Hans Ingo Weber. Biomechanical modeling and optimal control of human posture. *Journal of biomechanics*, 36(11):1701–1712, 2003.

[103] Felix E Zajac. Understanding muscle coordination of the human leg with dynamical simulations. *Journal of biomechanics*, 35(8):1011–1018, 2002.

[104] RR Neptune, SA Kautz, and ML Hull. The effect of pedaling rate on coordination in cycling. *Journal of biomechanics*, 30(10):1051–1058, 1997.

[105] C Pizzolato, M Reggiani, L Modenese, and DG Lloyd. Real-time inverse kinematics and inverse dynamics for lower limb applications using opensim. *Computer methods in biomechanics and biomedical engineering*, 20(4):436–445, 2017.

[106] Darryl G Thelen and Frank C Anderson. Using computed muscle control to generate forward dynamic simulations of human walking from experimental data. *Journal of biomechanics*, 39(6):1107–1115, 2006.

[107] C David Remy and Darryl G Thelen. Optimal estimation of dynamically consistent kinematics and kinetics for forward dynamic simulation of gait. *Journal of biomechanical engineering*, 131(3):031005, 2009.

[108] Herre Faber, Arthur J Van Soest, and Dinant A Kistemaker. Inverse dynamics of mechanical multibody systems: An improved algorithm that ensures consistency between kinematics and external forces. *PloS one*, 13(9):e0204575, 2018.

[109] Roger Pallarès-López, Felipe Costa Alvim, Míriam Febrer-Nafría, Luciano Luporini Menegaldo, and Josep M Font-Llagunes. Assessment of residual reduction procedures for high-speed tasks. *Gait & posture*, 73:116–119, 2019.

[110] Jennifer N Jackson, Chris J Hass, and Benjamin J Fregly. Residual elimination algorithm enhancements to improve foot motion tracking during forward dynamic simulations of gait. *Journal of biomechanical engineering*, 137(11):111002, 2015.

[111] Brian R Umberger, Karin GM Gerritsen, and Philip E Martin. Muscle fiber type effects on energetically optimal cadences in cycling. *Journal of biomechanics*, 39(8):1472–1479, 2006.

[112] Luciano Luporini Menegaldo, Agenor de Toledo Fleury, and Hans Ingo Weber. A 'cheap' optimal control approach to estimate muscle forces in musculoskeletal systems. *Journal of biomechanics*, 39(10):1787–1795, 2006.

[113] Stephen J Piazza and Scott L Delp. Three-dimensional dynamic simulation of total knee replacement motion during a step-up task. *Journal of biomechanical engineering*, 123(6):599–606, 2001.

[114] Darryl G Thelen, Frank C Anderson, and Scott L Delp. Generating dynamic simulations of movement using computed muscle control. *Journal of biomechanics*, 36(3):321–328, 2003.

[115] Massimo Sartori, Dario Farina, and David G Lloyd. Hybrid neuromusculoskeletal modeling to best track joint moments using a balance between muscle excitations derived from electromyograms and optimization. *Journal of biomechanics*, 47(15):3613–3621, 2014.

[116] Javier Cuadrado, Urbano Lugrís, Rosa Pamies-Vila, and Josep Maria Font-Llagunes. Forward dynamics for gait analysis as an intermediate step to motion prediction. In *Proceedings of the 1st Int. and 16th National Conference on Machines and Mechanisms, iNaCoMM*, 2013.

[117] Martin L Felis, Katja Mombaur, and Alain Berthoz. An optimal control approach to reconstruct human gait dynamics from kinematic data. In *2015 IEEE-RAS 15th International Conference on Humanoid Robots (Humanoids)*, pages 1044–1051. IEEE, 2015.

[118] John T Betts. *Practical methods for optimal control and estimation using nonlinear programming*, volume 19. Siam, 2010.

[119] Matthew P Kelly. Transcription methods for trajectory optimization. *Tutorial, Cornell University, Ithaca, New York*, 2015.

[120] Friedl De Groote, Allison L Kinney, Anil V Rao, and Benjamin J Fregly. Evaluation of direct collocation optimal control problem formulations for solving the muscle redundancy problem. *Annals of biomedical engineering*, 44(10):2922–2936, 2016.

[121] Matthew L Kaplan and Jean H Heegaard. Predictive algorithms for neuromuscular control of human locomotion. *Journal of Biomechanics*, 34(8):1077–1083, 2001.

[122] Mahdokht Ezati, Borna Ghannadi, and John McPhee. A review of simulation methods for human movement dynamics with emphasis on gait. *Multibody System Dynamics*, pages 1–28, 2019.

[123] Yujiang Xiang, Jasbir S Arora, and Karim Abdel-Malek. Optimization-based prediction of asymmetric human gait. *Journal of Biomechanics*, 44(4):683–693, 2011.

[124] Werner Schiehlen and Daniel García-Vallejo. Walking dynamics from mechanism models to parameter optimization. *Procedia IUTAM*, 2:199–211, 2011.

[125] Marko Ackermann. *Dynamics and energetics of walking with prostheses*. 2007.

[126] Marko Ackermann, F Leonardi, HR Costa, and AT Fleury. Modeling and optimal control formulation for manual wheelchair locomotion: The influence of mass and slope on performance. In *5th IEEE RAS/EMBS International Conference on Biomedical Robotics and Biomechatronics*, pages 1079–1084. IEEE, 2014.

[127] Katja Mombaur and Khai-Long Ho Hoang. How to best support sit to stand transfers of geriatric patients: Motion optimization under external forces for the design of physical assistive devices. *Journal of biomechanics*, 58:131–138, 2017.

[128] Michael A Patterson and Anil V Rao. Gpops-ii: A matlab software for solving multiple-phase optimal control problems using hp-adaptive gaussian quadrature collocation methods and sparse nonlinear programming. *ACM Transactions on Mathematical Software (TOMS)*, 41(1):1, 2014.

[129] Scott L Delp, Frank C Anderson, Allison S Arnold, Peter Loan, Ayman Habib, Chand T John, Eran Guendelman, and Darryl G Thelen. Opensim: open-source software to create and analyze dynamic simulations of movement. *IEEE Transactions on Biomedical Engineering*, 54(11):1940–1950, 2007.

[130] Edith M Arnold, Samuel R Ward, Richard L Lieber, and Scott L Delp. A model of the lower limb for analysis of human movement. *Annals of biomedical engineering*, 38(2):269–279, 2010.

[131] Samuel R Hamner, Ajay Seth, and Scott L Delp. Muscle contributions to propulsion and support during running. *Journal of biomechanics*, 43(14):2709–2716, 2010.

[132] Jason P Halloran, Marko Ackermann, Ahmet Erdemir, and Antonie J Van den Bogert. Concurrent musculoskeletal dynamics and finite element analysis predicts altered gait patterns to reduce foot tissue loading. *Journal of biomechanics*, 43(14):2810–2815, 2010.

[133] Patricia L Lane and Richard LeBlanc. Crutch walking. *Orthopedic nursing*, 9(5):31–38, 1990.

[134] Emilio Sardini, Mauro Serpelloni, and Matteo Lancini. Wireless instrumented crutches for force and movement measurements for gait monitoring. *IEEE Transactions on Instrumentation and Measurement*, 64(12):3369–3379, 2015.

[135] Ge Wu, Frans CT Van der Helm, HEJ DirkJan Veeger, Mohsen Makhsous, Peter Van Roy, Carolyn Anglin, Jochem Nagels, Andrew R Karduna, Kevin McQuade, Xuguang Wang, et al. Isb recommendation on definitions of joint coordinate systems of various joints for the reporting of human joint motion—part ii: shoulder, elbow, wrist and hand. *Journal of biomechanics*, 38(5):981–992, 2005.

[136] Andreas Wächter and Lorenz T Biegler. On the implementation of an interior-point filter line-search algorithm for large-scale nonlinear programming. *Mathematical programming*, 106(1):25–57, 2006.

[137] Brian R Umberger and Ross H Miller. Optimal control modeling of human movement. *Handbook of Human Motion*, pages 327–348, 2018.

[138] Michael A Sherman, Ajay Seth, and Scott L Delp. Simbody: multibody dynamics for biomedical research. *Procedia Iutam*, 2:241–261, 2011.

[139] Mohammad S Shourijeh, Kenneth B Smale, Brigitte M Potvin, and Daniel L Benoit. A forward-muscular inverse-skeletal dynamics framework for human musculoskeletal simulations. *Journal of biomechanics*, 49(9):1718–1723, 2016.

[140] Jennifer L Hicks, Thomas K Uchida, Ajay Seth, Apoorva Rajagopal, and Scott L Delp. Is my model good enough? best practices for verification and validation of musculoskeletal models and simulations of movement. *Journal of biomechanical engineering*, 137(2):020905, 2015.

[141] A Gil-Agudo, E Pérez-Rizo, A Del Ama-Espinosa, B Crespo-Ruiz, S Pérez-Nombela, and A Sánchez-Ramos. Comparative biomechanical gait analysis of patients with central cord syndrome walking with one crutch and two crutches. *Clinical Biomechanics*, 24(7):551–557, 2009.

[142] Marco Freddolini, Francesco Esposito, Massimiliano Marcucci, Andrea Corvi, Palmina Braccio, and Leonardo Latella. Does crutch length influence gait parameters after total hip replacement surgery? *Gait & posture*, 60:262–267, 2018.

[143] Adriana Segura and Stephen J Piazza. Mechanics of ambulation with standard and spring-loaded crutches. *Archives of physical medicine and rehabilitation*, 88(9):1159–1163, 2007.

[144] Guangyu Liu, Yanxin Zhang, and Tiejun Zhang. Biomechanics of innovative spring-loaded axillary crutches. In *Proceedings 2011 International Conference on Human Health and Biomedical Engineering*, pages 503–506. IEEE, 2011.

[145] Hugh Herr and Marko Popovic. Angular momentum in human walking. *Journal of experimental biology*, 211(4):467–481, 2008.

[146] Marko Ackermann and Antonie J van den Bogert. Predictive simulation of gait at low gravity reveals skipping as the preferred locomotion strategy. *Journal of biomechanics*, 45(7):1293–1298, 2012.

[147] J. B. dec. M. Saunders, Verne T Inman, and Howard D Eberhart. The major determinants in normal and pathological gait. *JBJS*, 35(3):543–558, 1953.

[148] Tommy Oberg, Alek Karsznia, and Kurt Oberg. Joint angle parameters in gait: reference data for normal subjects, 10-79 years of age. *Journal of rehabilitation research and development*, 31(3):199–213, 1994.

[149] David A Winter. *Biomechanics and motor control of human movement*. John Wiley & Sons, 2009.

[150] Bogdan Pietraszewski, Slawomir Winiarski, and Sebastian Jaroszczuk. Threedimensional human gait pattern–reference data for normal men. *Acta of Bioengineering and Biomechanics*, 14(3):9–16, 2012.

[151] Gerard Malanga and Joel A DeLisa. Clinical observation. *Gait Analysis In The Science Of Rehabilitation*, 2:1, 1998.

[152] KJ Dodd, TV Wrigley, PA Goldie, ME Morris, and CD Grant. Quantifying lateral pelvic displacement during walking. *Clinical Biomechanics*, 13(4-5):371–373, 1998.

[153] Véronique Feipel, Thibaut De Mesmaeker, Paul Klein, and Marcel Rooze. Three-dimensional kinematics of the lumbar spine during treadmill walking at different speeds. *European Spine Journal*, 10(1):16–22, 2001.

[154] Jack Crosbie, Roongtiwa Vachalathiti, and Richard Smith. Patterns of spinal motion during walking. *Gait & Posture*, 5(1):6–12, 1997.

[155] Patricia Van de Walle, Pieter Meyns, Kaat Desloovere, Jente De Rijck, Julie Kenis, Evi Verbecque, Tamaya Van Criekinge, and Ann Hallemans. Age-related changes in arm motion during typical gait. *Gait & posture*, 66:51–57, 2018.

[156] Babak Hejrati, Sam Chesebrough, K Bo Foreman, Jake J Abbott, and Andrew S Merryweather. Comprehensive quantitative investigation of arm swing during walking at various speed and surface slope conditions. *Human movement science*, 49:104–115, 2016.

[157] Ross H Miller. A comparison of muscle energy models for simulating human walking in three dimensions. *Journal of biomechanics*, 47(6):1373–1381, 2014.

[158] Brian W Schulz, James A Ashton-Miller, and Neil B Alexander. The effects of age and step length on joint kinematics and kinetics of large out-and-back steps. *Clinical Biomechanics*, 23(5):609–618, 2008.

[159] Manindra Kaphle and Anders Eriksson. Optimality in forward dynamics simulations. *Journal of biomechanics*, 41(6):1213–1221, 2008.

[160] Yoji Uno, Mitsuo Kawato, and Rika Suzuki. Formation and control of optimal trajectory in human multijoint arm movement. *Biological cybernetics*, 61(2):89–101, 1989.

[161] Eri Nakano, Hiroshi Imamizu, Rieko Osu, Yoji Uno, Hiroaki Gomi, Toshinori Yoshioka, and Mitsuo Kawato. Quantitative examinations of internal representations for arm trajectory planning: minimum commanded torque change model. *Journal of Neurophysiology*, 81(5):2140–2155, 1999.

[162] Yasuhiro Wada, Yuichi Kaneko, Eri Nakano, Rieko Osu, and Mitsuo Kawato. Quantitative examinations for multi joint arm trajectory planning—using a robust calculation algorithm of the minimum commanded torque change trajectory. *Neural networks*, 14(4-5):381–393, 2001.

[163] Jeong-Uk Lee, Mee-Young Kim, Ju-Hyun Kim, Jeong-A Lee, Na-Mi Yoon, Byong-Yong Hwang, Bokyung Kim, and Junghwan Kim. Analysis of plantar foot pressure during the non-crutch, two-point, and four-point crutch gait performed by healthy volunteers. *Journal of Physical Therapy Science*, 23(3):489–493, 2011.

[164] Anne Griffin Perry, Patricia A Potter, and Wendy Ostendorf. *Nursing Interventions & Clinical Skills-E-Book*. Elsevier Health Sciences, 2015.

[165] Luc Noreau, Carol L Richards, François Comeau, and Daniel Tardif. Biomechanical analysis of swing-through gait in paraplegic and non-disabled individuals. *Journal of biomechanics*, 28(6):689–700, 1995.

[166] Bastien Berret, Enrico Chiovetto, Francesco Nori, and Thierry Pozzo. Evidence for composite cost functions in arm movement planning: an inverse optimal control approach. *PLoS computational biology*, 7(10):e1002183, 2011.

[167] Katja Mombaur, Anh Truong, and Jean-Paul Laumond. From human to humanoid locomotion—an inverse optimal control approach. *Autonomous robots*, 28(3):369–383, 2010.

[168] Fatemeh Rasouli and Kyle B Reed. Walking assistance using crutches: A state of the art review. *Journal of Biomechanics*, 98:109489, 2020.

[169] Mary Roberts, David Mongeon, and Francois Prince. Biomechanical parameters for gait analysis: a systematic review of healthy human gait. *Phys Ther Rehabil*, 4:6, 2017.

[170] Virginia L Little, Theresa E McGuirk, Lindsay A Perry, and Carolynn Patten. Pelvic excursion during walking post-stroke: A novel classification system. *Gait & posture*, 62:395–404, 2018.

[171] D Casey Kerrigan, Elizabeth P Frates, Shannon Rogan, and Patrick O Riley. Hip hiking and circumduction: quantitative definitions. *American journal of physical medicine & rehabilitation*, 79(3):247–252, 2000.

[172] Louis N Awad, Jaehyun Bae, Pawel Kudzia, Andrew Long, Kathryn Hendron, Kenneth G Holt, Kathleen O'Donnell, Terry D Ellis, and Conor J Walsh. Reducing circumduction and hip hiking during hemiparetic walking through targeted assistance of the paretic limb using a soft robotic exosuit. *American journal of physical medicine & rehabilitation*, 96(10):S157–S164, 2017.

[173] Fumihiro Matsuda, Masahiko Mukaino, Kei Ohtsuka, Hiroki Tanikawa, Kazuhiro Tsuchiyama, Toshio Teranishi, Yoshikiyo Kanada, Hitoshi Kagaya, and Eiichi Saitoh. Biomechanical factors behind toe clearance during the swing phase in hemiparetic patients. *Topics in stroke rehabilitation*, 24(3):177–182, 2017.